A COMPUTER SIMULATION OF COMBUSTION IN A SPARK IGNITION ENGINE

by

E. H. JAMES

THESIS Submitted in fulfillment of the requirements for the award of Master of Science of Loughborough University of Technology.

Supervisor: Mr. G.G. Lucas

November, 1969

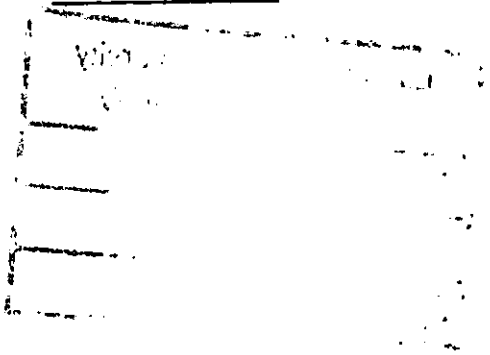

SUMMARY

A mathematical model of the compression, combustion and expansion phases of the I.F.P. Renault Variable Compression Ratio Research Engine has been developed which meets more of the basic requirements of actual engine combustion than any other model here tofore.

An attempt is made to incorporate a realistic flame pattern development across the combustion chamber from some experimental observations. Finite rates of flame propagation and heat release are considered and the Semenov laminar flame propagation theory is the determining factor in these considerations. To cater for the effects of turbulence, the laminar burning velocity from the Semenov expression is multiplied by a term derived from some flame speed measurements in the engine. It is shown, however, that this term only gives a general indication of the manner in which the turbulence varies with engine speed - allowances for the inclusion of turbulence variation with piston motion, throttling, compression ratio etc. are not made.

Dissociation of the burnt gases is catered for from chemical equilibrium considerations and heat transfer between the charge and its surroundings is included. The parameters which can be varied are mixture composition, compression ratio, engine speed, spark and valve timing, charge temperature and pressure at inlet valve closure and the mass fractions of exhaust residuals and injected water

(if any) in the unburnt charge. Three fuels are considered viz. propane, iso-octane and benzene.

Comparisons of computed and experimental results indicate that the flame travel times for iso-octane and benzene are in reasonable agreement from weak mixtures up to equivalence ratios of 1.2 and 1.3 respectively. This agreement is reflected in the corresponding pressure-crankangle diagrams. At very rich mixtures, on the other hand, large discrepancies between the flame travel times are apparent and this is again indicated on the pressure-crankangle diagrams.

A large deviation is noted between the computed and experimental equivalence ratios for minimum flame travel times for iso-octane and benzene. The computed results are well to the weak side of the experimental results. Possible reasons for this are discussed in some detail. The computed flame travel times for the three fuels used do, however, occur in the order observed from experiments and from the literature.

Experimental CO concentrations in the exhaust at rich mixtures are observed to correspond, in the equilibrium model, to a composition between the concentrations at the end of combustion and at the point of exhaust valve opening. The experimental exhaust NO concentrations at rich mixtures, on the other hand, tend to reflect the peak cycle temperature concentrations. For both CO and NO, equilibrium is seen to be a useless criterion on which to base predictions of such emissions at weak mixtures.

Since the application and further development of such a program must be towards more accurate predictions of the obnoxious exhaust

emissions CO and NO_x, a most comprehensive survey is included of the manner in which such emissions are formed in the combustion chamber, how they vary with engine operating conditions and some possible means for their control.

The computer program is written in FORTRAN 4 for use on an I.C.T. 1905 computer. Execution times vary with the length of the flame propagation period. Typically, however, they are between 25 and 50 mins.

ACKNOWLEDGEMENTS

The author gratefully acknowledges the encouragement and advice given by Mr, G.G. Lucas (Loughborough University).

Thanks are also due to Mr. K. Pawley and the technicians of the Transport Technology Department at Loughborough University for assisting with the experimental side of the work.

The help of the punch card and computer operators at the Loughborough University of Technology Computer Centre is also acknowledged.

Finally, the author thanks the Science Research Council for supporting this work.

NOTATION

a	fugacity of a substance in any given state of temperature and pressure
A	Avogadro's number (6.025×10^{23} molecules/gm-mole) : surface area (cm^2 or $metres^2$).
A_T	area of turbulent flame front
A_H	surface area of cylinder head across which heat transfer occurs (cm^2)
A_P	surface area of piston across which heat transfer occurs (cm^2)
A_C	surface area of cylinder wall across which heat transfer occurs (cm^2)
A.T.D.C.	after top dead centre
b	bore of engine cylinder (cm)
b_A	base area of a cone
b_h	value in unsteady heat transfer analysis
b.m.e.p.	brake mean effective pressure
b.s.f.c.	brake specific fuel consumption
B.D.C.	bottom dead centre

D_T ..... coefficient of turbulent diffusion

e ..... specific internal energy (cal/gm)

e_L ..... laminar flame front thickness

e_T ..... turbulent flame front thickness

e_c ..... $\sigma \times \gamma \times F_g$

E ..... internal energy (cal/gm-mole) : activation energy (cal/gm-mole)

f ..... fluctuating frequency of flow (c/s) : ($\pm \frac{a}{a_o}$) activity in the non-standard state.

F(f) ..... kinetic energy of a turbulent field at a frequency f.

F ..... molal free energy of a substance in any given state of temperature and pressure

F.T.T. ..... flame travel time (crankangle degrees or millisecs)

F_g ..... a geometric factor in radiative heat transfer considerations

g ..... mole ratio of nitrogen to oxygen in dry air

G_k ..... equilibrium constants for reactions in weak mixtures for k th constituent

h ..... height of a cone (cm) : heat transfer coefficient (cal/cm^2 sec ^oC) or ($kcal/m^2$ hr ^oC) or ($c.h.u./ft^2$

h_r ^{o}C : specific enthalpy (cal/gm)

H ..... enthalpy (cal)

HC ..... hydrocarbons

HF ..... heat of formation at 298.15^{o}K (cal/mole)

i.m.e.p ..... indicated mean effective pressure

I ..... minimum ignition energy (cals) : ionization current

I.V.O. ..... inlet valve opening

I.V.C. ..... inlet valve closure

k_i ..... specific rate constant for reaction between molecule and $i,^{th}$ active particle (cc/molecule sec)

k_r ..... specific reaction rate constant (cc/mole sec)

k_{r1} ..... forward specific reaction rate constant

k_{r2} ..... reverse specific reaction rate constant

K_T ..... correction factor in turbulent burning velocity expression

K_k ..... equilibrium constants for reactions in rich and stoichiometric mixtures for $k,^{th}$ constituent

K_{P_k} ..... equilibrium constants for $k,^{th}$ constituent

l	length of engine connecting rod (cm)
L	scale of turbulence : characteristic linear dimension in convective heat transfer analysis
L_{EU}	Eulerian scale of turbulence
L_L	Lagrange scale of turbulence
m	mass (gm) : number of atoms of carbon in a molecule of a general hydrocarbon fuel
M	mass flow rate (gm/cm^2 sec) : molecular weight
M_a	molecular weight of dry air
n	engine speed (rev/min) : number of atoms of hydrogen in a molecule of a general hydrocarbon fuel
n_k	moles of k^{th} constituent in burnt mixture (rich and stoichiometric mixtures).
n_T	total number of moles of species in burnt mixture (rich and stoichiometric mixtures)
n_B	moles of products of combustion by stoichiometric equation
n_u	moles of reactants
NO_x	oxides of nitrogen
NU	Nusselt number
p	partial pressure

p_i ..... mole fraction (partial pressure) of i^{th} active particle in burnt gas

p.p.m..... parts per million

P ..... pressure (atm)

Pr ..... prandtl number

q ..... reaction order : overall heat transfer rate (cal/sec)

q_{RAD} ..... radiative heat transfer rate (cal/sec)

q_{CON} ..... convective heat transfer rate (cal/sec)

q_k ..... parameters of equilibrium composition calculations in rich and stoichiometric mixtures

Q ..... heat transfer (cals)

Q_v ..... heat of reaction (cal/mole)

r ..... crank throw (cm) : distance of hot-wire anemometer probe from cylinder axis (mm)

r_T ..... distance of flame travel in turbulent flow

r_L ..... distance of flame travel in laminar flow

r_w ..... value in unsteady heat transfer analysis

R ..... Universal gas constant (cal/mole ^oK)

Re ..... Reynolds Number

s ..... specific entropy (cal/gm ^{o}K)

S ..... entropy (cal/gm-mole ^{o}K) : engine stroke (cm or ft.)

SF ..... entropy at 298.15^{o}K and 1 ATM pressure (cal/gm-mole ^{o}K)

t ..... time (seconds) : time of contact between an eddy and the flame front (seconds)

t_{re} ..... reaction time (seconds)

t_{i} ..... autoignition delay period (seconds)

t_{L} ..... characteristic time defining the Lagrange scale of turbulence

t_{1} ..... ionization current rise-time in a laminar flame (secs.)

t_{2} ..... fall-off time in a laminar flame ionization current (secs.)

t_{str} ..... time for piston to travel from B.D.C. to T.D.C.

t_{b1}, t_{b2} .... mean flame travel times to ionization probes 1 and 2 (milliseconds)

T ..... temperature (^{o}K)

T_{m} ..... mean temperature (^{o}K)

T_{i} ..... ignition temperature (^{o}K)

T.D.C. ..... top dead centre

T_o^1 ..... apparent delay period (seconds)

T_g ..... charge temperature (^oK)

T_w ..... combustion chamber wall temperature (^oK)

T_{gM} ..... time averaged value of the charge temperature over a complete engine cycle (^oK)

T_v ..... maximum deviation of T_g from T_{gM} in an engine cycle (^oK)

T_s ..... steady state combustion chamber wall temperature (^oK)

T_p ..... periodic combustion chamber wall temperature : piston temp (^oK)

T_c ..... coolant temperature (^oK) : cylinder wall temperature (^oK)

T_H ..... cylinder head temperature (^oK)

u_i, v_i, w_i ... instantaneous flow velocities in the x, y and z directions

$\bar{u}$, $\bar{v}$, $\bar{w}$ ..... time averaged components of the instantaneous flow velocities u_i, v_i, w_i.

u^1, v^1, w^1 ... momentary fluctuation components of u_i, v_i, w_i.

$\sqrt{u^{12}}$ ..... root mean square value of the flow fluctuation components i.e. turbulence intensity

u ..... a directional flow velocity

$\bar{u}$ ..... an average flow velocity

u_x ..... velocity fluctuations

U ..... mean flow velocity (cm/sec) or (metres/sec)

U_g ..... unburnt gas velocity (cm/sec)

U_T ..... turbulent burning velocity (cm/sec)

$U_{T_{micro}}$ ..... burning velocity due to microcsopic turbulence

U_L ..... laminar burning velocity (cm/sec)

U_T^1 ..... turbulent movement velocity

U_c ..... flame generated turbulence

v ..... specific volume (cc/gm)

V ..... volume (cc)

V_{FS}^1 ..... apparent flame speed i.e. velocity of flame front relative to combustion chamber (cm/sec)

V_L ..... laminar flame speed (cm/sec)

V_f ..... fluid velocity in convective heat transfer analysis

V_p ..... mean piston speed (cm/sec) or (metres/sec) or (ft/sec)

w_b ..... fraction of charge mass burnt

w_r ..... mass fraction of exhaust residuals in unburnt mixture

w_a ..... mass fraction of air in unburnt mixture

w_f ..... mass fraction of fuel in unburnt mixture

W ..... steric or probability factor

x ..... distance in reaction zone (cm) : distance into cylinder wall (cm) : fraction of chemically correct air entering a particular reaction

x_1, x_2 ..... distances from the spark plug to the ionization probes 1 and 2 (cm)

$\overline{x}^2$ ..... average displacement of element in flame front under influence of turbulent fluctuations

y_c ..... distance from piston instantaneous position to the top of the cylinder block (cm)

$\sqrt{\overline{y}^2}$ ..... root mean square displacement of a flame element from the mean flame front position

z_k ..... parameter of equilibrium composition calculations in weak mixtures

Z ..... an impact coefficient (No. of collisions/cm^3 sec)

Δm ..... element of mass burnt during a specified stage (gm)

Δs ..... change in specific entropy (cal/gm ^oK)

ΔQ ..... heat transferred during a specified stage (calories)

ΔF ..... change in free energy in any given state of temperature and pressure

λ ..... thermal conductivity (cal/cm sec ^{o}K)

θ ..... crankangle (degrees)

$\Delta\theta$ ..... change in crankangle during a particular stage (degrees)

θ_1 ..... microturbulent fluctuation period (sec)

θ_2 ..... macroturbulent fluctuation period (sec)

ϕ ..... equivalence ratio

η_v ..... volumetric efficiency

η ..... value in unsteady heat transfer analysis

ρ ..... density (gm/cc)

ϵ ..... eddy diffusivity

ν ..... kinematic viscosity (cm^2/sec)

ω ..... reaction rate (molecules/cc-sec) : angular frequency (c/s)

μ ..... viscosity (gm/cm sec)

σ ..... Stefan - Boltzmann constant (1.36×10^{-12} cal/cm^2 sec $^{o}K^4$)

γ ..... emissivity factor

ϵ_t ..... value in unsteady heat transfer analysis

Subscripts

(when not used in symbols above)

b ..... relating to products of combustion

B ..... conditions at computed equilibrium flame temperature

f ..... relating to fuel

i ..... relating to i^{th} active particle

j ..... j^{th} estimate within step iteration

k ..... k^{th} constituent of gas mixture

O_2 ..... relating to oxygen

u ..... relating to unburnt charge

0 ..... initial conditions : properties at start of stage : standard conditions

1 ..... properties after combustion step

2 ..... properties at end of stage

Superscripts

— ..... average or mean

LIST OF FIGURES

All figures and graphs etc. for a particular chapter or Appendix are given in numerical order at the end of the Chapter or Appendix in which they occur.

INDEX OF CONTENTS

CHAPTER 1.

INTRODUCTION.

CHAPTER 1.

INTRODUCTION.

1.1. GENERAL COMMENTS.

Computer simulations of internal combustion engine cycles are desirable because of the aid they provide in design studies, in predicting trends, in serving as diagnostic tools, in giving more complete data than is normally available from experiments and in helping to understand the complex processes which occur. The advent of high speed computers in the 1950's facilitated the detailed study of both spark ignition and diesel engine combustion processes. Most of the effort, however, has been confined to simulations of diesel engine combustion, mainly because the heat release patterns in such engines can be predicted fairly accurately from considerations of the characteristics of the fuel injection equipment.

In spark ignition engine combustion, on the other hand, the heat release pattern is not so easy to define since it is a function primarily of the rate at which the flame from the ignition point propagates outwards across the combustion chamber. The speed of this propagation is, in practice, determined by many variables including the temperatures of the burnt and unburnt fractions of charge and the degree of turbulence and swirl existent in the combustion space.

No analytical model has yet been devised which accurately simulates actual spark ignition engine combustion over the complete range of operating conditions. The requirement for such a model has accelerated in recent years because of the aid it might provide in the study and control of the obnoxious exhaust emission gases.

The purpose of this work was, therefore, to study the

compression, combustion and expansion phases of the 4-stroke, spark ignition engine cycle from a fundamental viewpoint. To this end, an analytical model was developed and programmed for use on a digital computer which incorporates the salient features of the above mentioned phases of the engine cycle. It, thus, allows for the varying effects of mixture composition, dissociation according to chemical equilibrium considerations, finite rates of flame propagation, heat transfer, spark and valve timing, compression ratio, charge temperature and pressure at inlet valve closure, engine speed, piston motion, exhaust residuals and the presence of injected water as a possible means of controlling certain obnoxious exhaust emissions. Allowance is also made for the use of three different types of fuel, viz. propane, iso-octane and benzene. The investigation was performed for one particular engine only - the Renault Variable Compression Ratio Research Engine.

This work is primarily concerned with the development of the model and the subsequent evaluation of the individual effects of some of the variables. A comparison is made between experimental and computer predicted results with regard to both flame speed and pressure-time diagrams in order to test the reliability of the model. Its ability to estimate trends in the obnoxious emissions CO and NO_x according to chemical equilibrium considerations is observed over a range of engine operating conditions and means of reducing these emissions are studied.

1.2 HISTORICAL

Prior to the appearance of high speed digital computers, attempts to predict the performance of spark ignition engines suffered from the difficulties of great arithmetical complexity and tedious repetitive calculations. The development of

thermodynamic charts eliminated many of these tedious calculations especially with regard to the thermal dissociation of the burnt gases. Such charts have been widely used in the analysis of the otto cycle engine from the time of their introduction in 1935 by Hershey, Eberhardt and Hottel.[1] They have additionally been revised a number of times to allow for improvements in fundamental data.[2,3,4] While they allow a considerable reduction in the mathematical difficulties of the otto cycle analysis however, they are not general as they are invariably presented for a particular fuel and a selected number of air/fuel ratios. Also, a constant volume combustion is considered so that the effect of engine design parameters cannot be effectively determined without great difficulty.

Attempts to consider the effects of the progressive burning of the charge were first made in connection with thermodynamic studies of combustion in constant volume bombs. Among the earliest was the study of Nagel[5] in 1908. Similar analyses were made by Flamm and Mache[6] in 1917 and Rosecrans[7] in 1926 which made use of some equilibrium studies.[8] Endres was among the first to consider the effects of piston motion whilst Hottel and Eberhardt,[9] in 1937, proposed a method for calculating the temperature gradients in an engine considering both piston motion and spark advance. These workers also took account of mixture composition, variable specific heats and dissociation.

Rassweiler and Withrow[10] and Rassweiler, Withrow and Cornelius[11] suggested a method for treating the combined effects of flame propagation and piston motion in engines from photographs taken through a quartz window installed in a cylinder head and in 1940, Withrow and Cornelius[12]

proposed a method of calculating the pressure rise in an internal combustion engine utilising the thermodynamic charts of Hershey et al.[1]

Rabezzana, Kalmar and Candelise[13] in 1939 conceived of a method for the analysis of flame propagation and expansion during combustion which took account of combustion chamber geometry, spark advance and piston motion. Although this analysis considered the thermodynamics of the working fluid in an uncomplicated manner, pressure-time diagrams could be calculated from measured flame propagation rates.

These analyses were hindered because fundamental data about flame propagation was not available. However, even if such data had been available, the sheer magnitude of the calculations involved would have precluded any extensive analysis.

The problem of considering the combined effects of mixture composition, variable specific heats, dissociation, flame propagation, heat transfer and piston motion simultaneously presented such a formidable mathematical obstacle that not until the widespread use of digital computers was such an analysis contemplated. In this context, Edson,[14] in 1960, proposed an analytical model for combustion in the spark ignition engine which was suitable for programming on a digital computer. His analysis included the effects of flame propagation, dissociation and piston motion but did not include heat transfer. No computed results have been reported from his analysis. Edson visualizes three separate subsystems existing in the combustion chamber during combustion viz. the burnt, the unburnt and the small segment of mass being transferred from the unburnt to the burnt condition. The combustion process itself was assumed

to consist of three separate, successive steps:

i) a combustion step - the constant pressure burning of a small segment of the total mass contained in the combustion chamber. This is followed by an isentropic compression of this segment and of the unburnt and previously burnt fractions to a final pressure such that the total energy and volume of the system are equal to the total energy and volume before the combustion step was initiated.

ii) a piston movement step - to the next crank angle position following the combustion step. This movement isentropically compresses (or expands) the burnt, unburnt and the newly burnt segment of mass to a new volume determined by the physical characteristics of the engine.

iii) a mixing operation - the newly burnt small mass segment and the burnt gas fraction are mixed into one burnt gas fraction. This is envisaged as a two-step process. First, a maxing at constant volume and, secondly, a simultaneous isentropic compression (or expansion) of the mixed burnt fraction and unburnt fraction to a uniform system pressure at the specified total volume.

Edson's work was followed, in 1962, by the spark ignition engine combustion simulation of Patterson.[15] A spherical flame propagation was assumed in this study and the position of the flame front relative to the ignition source was determined from the volume of the burnt gas and the length-volume distribution for the combustion chamber. The rate of flame travel was based on the laminar flame theory of

Semenov.[16] Combustion was assumed to occur in numerous small increments each of which consisted of seven steps. Each increment included the burning of some of the charge, piston motion and heat transfer according to the expression of Eichelberg.[17] The seven steps were:

i) a constant pressure combustion of a small mass increment. The total volume of burnt and unburnt gases was allowed to increase to maintain this constant pressure.

ii) a constant pressure mixing of the inflamed mass increment with the previously burnt portion.

iii) a recompression of both burnt and unburnt gas to the volume prior to combustion in step i) such that the unburnt gas followed an isentropic path.

iv) an isentropic change of state of both gaseous regions to allow for piston motion. Initially, the time required for combustion of this increment was estimated. Later, this step and the successive ones were recomputed using a more accurate time interval. This interval was computed in step vii) below.

v) a constant volume heat transfer.

vi) at the same volume, the system was allowed to attain pressure equilibrium which had been disrupted in step v). This was done adiabatically with the unburnt gas undergoing an isentropic expansion to the final uniform pressure.

vii) finally, the flame propagation velocity was computed from the initial conditions in the unburnt gas (step i) and the final conditions in the burnt gas (step vi). From this and a knowledge of the extension of the flame front into the unburnt gas during this

increment, the time interval for combustion was calculated. This was compared with the value used in step iv) and, if an appreciable difference existed, steps iv) to vii) were redone.

Patterson considered the expansion process to consist of two steps:

a) a constant volume heat transfer.

b) an isentropic change of state due to piston motion.

He went on to simulate the complete 4-stroke cycle making simplifying assumptions for the exhaust and induction processes. Results are presented of the comparison made between an experimental pressure-time diagram and a computed diagram but, however, only at one particular operating point.

Strange[18] published some work in 1964 on an analysis of an ideal otto cycle which included the effects of heat transfer, finite combustion rates, chemical dissociation and mechanical losses. During combustion, the system was assumed to comprise ten cells of equal mass. These were allowed to react one at a time to form equilibrium products. An iterative procedure was used to determine the correct system pressure and individual cell temperatures and to satisfy overall mass and energy balances. When these had been proved to be correct, heat transfer and system volume changes were considered. The expansion process was simply treated as an extension of the combustion process, the only change being that the calculations of the effects due to cell combustion were not made.

The rate of flame propagation was examined for three sets of criteria, viz:

i) a constant mass conversion rate.

ii) a constant reaction front propagation rate.

iii) a variable reaction front propagation rate of the form

$$V_R = V_{R_0} \left(\left(\frac{P_i}{P_o} \right)^{d_1} \cdot d_2 \cdot \exp \left(d_3 \cdot \frac{T_i}{T_o} \right) \right)$$

where

d_1, d_2 and d_3 are constants.

V_{R_0}, P_o and T_o are the initial values of flame speed, pressure and temperature respectively, and the subscript 'i' is an index used in the incremental calculation scheme.

The constants in this expression were chosen after some experimentation to increase the flame speed by approximately a factor of three at peak temperature and pressure.

Simplified expressions were also used to evaluate instantaneous heat transfer rates and mechanical losses due to friction effects. Despite the allowances and inclusion of many variables, Strange's model cannot be contemplated as a serious attempt at simulating actual engine combustion because too many simplifications are involved.

In 1966, Phillipps and Orman[19] proposed a completely new analytical model of spark ignition combustion. The mathematical procedures used have also been adopted in the model being developed in this work (see Chapter 3). These workers attempted to simulate the combustion in a Ricardo E6 engine and, in so doing, utilised the concept of a spherical burning pattern. The flame propagation was assumed to follow that predicted by the thermal laminar flame theory of Mallard and Le Chatelier[20] with a modification to allow for the

effects of turbulence. Heat transfer effects were catered for by the Eichelberg expression[17].

Many results are given in the Phillipps and Orman study of the influence on engine performance and flame travel times of varying many parameters including mixture composition, ignition timing, initial change temperatures and pressures, engine speed and exhaust residual fractions. It is claimed that the resulting pressure-time diagrams compare favourably with experimental ones although no comparisons are actually given. One of the major failings of the work was the inability to predict accurately and correctly the air/fuel ratio at which the flame travel time was a minimum for the three fuels they used, viz. iso-octane, benzene and di-isobutylene.

In 1969 Krieger et al[21] simulated on a computer a crank-case scavenged, two-stroke spark ignition engine and made some comparisons with experimental data. A numerical integration routine was used. The effects of dissociation were included by using empirical curve fits for the equilibrium thermodynamic properties of the combustion products of air and the fuel being examined. To describe the progress of the combustion process, a scheme proposed by Walker[22] was adopted in which the mass fraction burnt is specified by the functions:

$$w_b = C_1 . X^{N_b} \quad \text{where } 0 \leq X \leq S_y$$

$$w_b = 1 - C_2 . (1 - X)^{N_b} \quad \text{where } S_y \leq X \leq 1$$

in which

w_b = fraction of mass burnt

X = fraction of the combustion duration

N_b = exponent

S_y = some intermediate value of X called the synchronous value.

and C_1, C_2 = constants.

Krieger et al[21] converted the mass fraction burnt in the above expressions into a mass burning rate by using differentiation. The Eichelberg correlation[17] is again used in this simulation for the gas side heat transfer coefficient.

1.3. GENERAL REQUIREMENTS FOR AN ACCURATE SPARK IGNITION ENGINE COMBUSTION SIMULATION.

The computer program derived in this work endeavours to take account of the following:

i) a finite rate of combustion - this is fundamental to any realistic attempt to simulate combustion in a spark ignition engine. The rate at which the mass of charge is burnt is governed by the speed of flame propagation in the combustion space. This is determined from the temperatures and other physical properties of the burnt and unburnt gases according to the Semenov laminar theory of flame propagation. A correction factor is included to account for the effects of turbulence and swirl. Chapter 4 contains a most detailed account of the development of this section of the work along with the actual mechanisms involved in turbulent flame propagation.

ii) dissociation - thermal dissociation of the burnt gases must be allowed for in any adequate model of the combustion process. Several methods for the calculation of these effects are available in the literature. Most of these are enumerated in Chapter

6 together with an account of the development of the particular one used in this work.

iii) an accurate flame propagation pattern - Chapter 5 contains the considerations which were involved in the choice of a realistic pattern which is adjudged to resemble closely that in the actual engine.

iv) heat transfer - it is necessary to make some estimate of the quantity of heat transferred from the combustion chamber during every stage of the compression, combustion and expansion phases of the engine cycle. This is very difficult to gauge accurately as is explained in detail in Chapter 7. This Chapter also includes a review of the large amount of published literature on the subject. The various empirical equations available which attempt to depict instantaneous heat losses have been found to give widely varying results and there is no indication as to which is the best expression to use. For the reasons explained in Chapter 7, the formula proposed by Annand[23] was eventually adopted.

Other considerations which are fundamental to spark ignition engine combustion simulation are allowances for:

v) mixture composition variations.

vi) piston motion.

vii) spark and valve timing variations.

viii) compression ratio changes.

ix) variations in change temperature and pressure at inlet valve closure.

x) engine speed.

xi) changes in the mass fractions of exhaust residuals present.

xii) variable specific heats.

The constituents of all gas mixtures are assumed to behave as ideal gases. The methods of calculating the thermodynamic properties of ideal gas mixtures at a known temperature, pressure and composition are given in Appendix 7.

The resulting computer program has been written in Fortran 4 for use on an ICT 1905 computer. A listing of it is given in Appendix 8.

1.4. SCOPE.

One of the most important uses of a theoretical analysis of spark ignition engine combustion is to provide an insight into the physical processes underlying various observed phenomena. In this connection, its application to the study of the possible causes of cyclic dispersion is cited as being potentially significant. Also, the ability of such an analysis to predict trends in the obnoxious emissions carbon monoxide and the oxides of nitrogen with variation in engine operating conditions is apparent. Some means of reduction of these emissions can also be easily deduced and compared e.g. exhaust gas recirculation and water injection. From a more pragmatic viewpoint, such a facility, when developed to a sufficient degree of reliability, could provide a means of reducing the amount of engine testing required at the design stage. It, thus, should help to optimize an engine design.

C H A P T E R 2.

REVIEW OF COMBUSTION AND EXHAUST EMISSION FUNDAMENTALS IN SPARK IGNITION ENGINES.

CHAPTER 2.

REVIEW OF COMBUSTION AND EXHAUST EMISSION FUNDAMENTALS IN SPARK IGNITION ENGINES.

2.1. INTRODUCTION.

Although combustion is a chemical process, the engine specialist is interested in both its physical and its chemical consequences. Its physical consequences are concerned primarily with the development of temperature and pressure whilst its chemical consequences are of importance in obtaining better control of the combustion process and of the engine's tendency to produce certain obnoxious combustion reaction products.

The purpose of this Chapter is to define some of the fundamental processes and phenomena involved in spark ignition engine combustion and in the combustion reaction products which these processes generate. It is also intended to serve as a criterion by which the computer simulated analytical combustion model can be compared with regard to its capacity for meeting the requirements of actual combustion.

Of the three major pollutants which are of primary concern in attempted reductions of exhaust emissions from engines (i.e. carbon monoxide, the oxides of nitrogen and the unburnt hydrocarbons), only carbon monoxide and the oxides of nitrogen are considered in the computer simulation. This is because they are products of the more or less homogeneous region in the main bulk of the charge. This general review, however, also considers the unburnt hydrocarbons. The reasons for this are:

i) their generation is intimately involved with the flame propagation process in the combustion chamber.

ii) out of considerations for their effect on the com-

bustion efficiency.

iii) because it is necessary to realize the trends involved in the appearance of these emissions in engine exhausts whenever any particular variable is altered to try and reduce carbon monoxide or the oxides of nitrogen.

iv) because the continuance of this work in the future (see Chapter 9) requires an extensive background knowledge of the modes of generation and control of all the obnoxious emissions.

2.2. COMBUSTION FUNDAMENTALS.

A typical four stroke, spark ignition engine cyclic process is shown in Fig. 2-1. The combustible mixture of fuel and air is drawn into the engine during the induction process A to C i.e. from inlet valve opening to inlet valve closure. This mixes with the residual exhaust gases to form a virtually homogeneous mixture the temperature and pressure of which is raised considerably by the compression process from point C to point D. At point D, the charge is ignited by a spark discharge and a flame propagates throughout the mixture until combustion is completed at around point E. The expansion phase of the cycle then follows from E until the exhaust valve opens at F when the combustion products begin to be exhausted from the combustion chamber. This exhaust process persists until approximately point B at which time the inlet valve has already opened to begin a new cycle. The crankangle period during which both inlet and exhaust valves are open (i.e. from point A to point B) is termed the "valve overlap period." During the entire engine cycle, there is a heat exchange between the working fluid and the surroundings.

The period of the cycle under study in this work is that from inlet valve closure to exhaust valve opening (i.e. from C to F in Fig. 2-1). It thus includes the compression, combustion and expansion phases. As already stated, the compression phase increases the temperature and pressure of the charge. The extent of the increase depends upon the conditions at inlet valve closure, the compression ratio of the engine and the degree of heat exchange between the charge and the surroundings.

During this compression process, preflame reactions take place in the charge and the rates of these increase as the temperatures and pressures get higher. If conditions get severe enough, it is possible for a condition to be attained at which the entire charge ignites spontaneously. There is no control over this type of combustion at all and, in order to achieve some degree of control, the charge is forcibly ignited invariably by a spark discharge across the electrodes of a sparking plug. This discharge is usually generated externally from a high tension coil and interrupter and it usually consists of two components:[24]

i) a capacitive component which is oscillatory in nature and lasts for approximately 10^{-6} seconds.

ii) an inductive component which follows on directly from the capacitive component and lasts for about 10^{-3} seconds.

There is much controversy as to the relative importance of these two components in initiating combustion. It is unanimously agreed, however, that the spark provides the energy (in the form of heat and active particles) required to bring about the chemical reactions necessary to achieve a self-propagating flame. Such a progressive flame propa-

gation only ensues when the release of heat and the diffusion of radicals from the spark is great enough to achieve a combustion reaction in the adjoining portion of the mixture. In other words, the reaction rate has to overcome the heat losses.

It is clear that ignition processes obey the law of the conservation of energy. This means that there is a balance of energy between that provided by the external source, that released by chemical reaction and that dissipated to the surroundings by means of thermal conduction, convection, radiation and mass transfer. As a result, there must be a certain minimum quantity of energy necessary to initiate combustion under a given set of conditions. This is a function of many parameters, the most important of which are air/fuel ratio, fuel composition, charge temperature and pressure, the degree of mixture motion, the distance between the electrodes of the sparking plug, the configuration of the electrodes and the type of spark. Detailed discussions of such influences on the minimum ignition energies are given in Refs. 24, 25 and 26. Many simplified theories have been developed in attempts to predict these energy values. These have usually been derived from experiments on quiescent mixtures in constant volume bombs where conditions are not really compatible with those in highly turbulent engine combustion chambers. Typical of such expressions, however, are those of Lewis and Von Elbe[27], Spalding[28] and Weinberg and Odgers[29] whose equations are of the general form

$$I = \frac{a \cdot d^2 \cdot \lambda}{Su} \cdot \frac{(T_b - T_u)}{} \quad \ldots\ldots\ldots 2\text{-}1$$

where

I is the minimum ignition energy (calories)

λ is the charge thermal conductivity (cal/cm sec ^{o}K)

a is a constant

d is the quenching distance (cm)

Su is the burning velocity (cm/sec)

and T_b and T_u are the temperatures of the burnt and unburnt gas respectively (^{o}K).

Many authors[24, 26] have quoted results to show that, providing the energy of the spark is sufficient, it has little or no influence on the establishment of combustion. Nevertheless, it should be supplied in a relatively efficient manner, within a small volume and in a sufficiently short time to ensure that only a negligible amount is lost other than to establish the flame. Typical values of the energy per spark in conventional spark ignition engines vary within the range 10-100 millijoules[30.] In this work, the value is taken to be 20 millijoules (i.e. 0.004777 calories), all of which is assumed to be released in the chemical reaction which begins the combustion process.

The flame which is generated at ignition propagates outwards from the sparking plug through the entire charge. Two distinct gaseous regions exist in the combustion chamber at this time viz. a region of burnt gas and a region of unburnt gas. These two regions have been found to be separated by a distinctly luminous flame front. The flame does not travel at a constant speed throughout the combustion chamber but, for a normal combustion, moves very slowly at first for 1 or 2 milliseconds, then gathers speed through the main part of the chamber and finally slows down at the end of its travel. Such observations have been noted by

many workers[31,32,26,33,34]. The period of time when flame travels very slowly after ignition is often called the 'delay period' although, strictly speaking, there is no delay in spark ignition engine combustion at all.

The finite time interval during which the flame traverses the combustion chamber has an important bearing on the behaviour of the engine. In theory, the charge should burn as quickly as possible in order to minimize the heat losses and to permit the maximum expansion of the burnt gases. In practice, however, very rapid burning causes excessive combustion pressures and high rates of heat transfer to the engine structure. The result is noisy engine operation and sometimes piston failure. Very slow burning, on the other hand, is undesirable because heat is wasted during expansion and passes into the exhaust causing high fuel consumption and poor exhaust valve life. It is thus important to ensure that combustion occurs at exactly the right speed for any conditions of engine operation.

There is presently much controversy over the relationship between flame propagation and pressure development during the combustion process. On the one hand, there is the school of thought (represented by Starkman[35] and Clarke[26]) which disputes the premise that the complete chemical reaction and heat release occurs in the flame front. Starkman's objections stem from some experiments he performed on correlations between the flame travel progress (measured by ionization gap techniques) and the pressure development. He concluded that the entire charge had begun to react well before the peak pressure of the cycle was reached. In other words, the peak pressure was developed many crankangle degrees after the reaction front had completely traversed the com-

bustion space. This hypothesis is supported by Clarke who obtained direct visual information on the combustion process by fitting a quartz window into the cylinder head of a single cylinder, research engine. Clarke maintains that the advancing flame front is followed by the main heat releasing front which lasts an appreciable time after the whole charge is alight.

Opposing these contentions are those investigators who suggest that the heat release process is effectively completed at the flame front. Supporters of this theory are Rassweiler and Withrow[10] and Curry[36]. From correlations of motion pictures of flame propagation with pressure-time diagrams, Rassweiler and Withrow obtained good agreement between the combustion chamber pressure development and the volume of charge consumed by the flame at various positions of the flame front throughout the combustion process. Moreover, such correlations were found to exist at many different engine operating conditions e.g. at various mixture strengths, spark timings and throttle positions[11]. Curry also obtained good agreement between the combustion chamber pressure development and the volume of charge consumed by the flame front. His measurements of burnt gas volumes were achieved by detecting the position and progress of the flame front by ionization gap techniques. He did, in fact, use no less than 49 of these gaps in the combustion chamber. In all his measurements, the occurrence time of peak pressure was before the end of flame propagation.

In this work, the process of combustion is based on the assumption that the complete combustion reaction and heat liberation takes place in the flame front. This is probably untrue of the processes which actually occur since

the chemical reactions take place at a finite rate and equilibrium is not instantaneously established (see Chapter 6). The errors involved from this assumption will tend to vary with the speed of the flame propagation but, however, they are not considered to be very great. The flame front should really be called the "reaction" or the "combustion" zone in this context since it is the region in which the oxidation of the hydrocarbons in the fuel take place. Withrow and Boyd[37] found it to be greenish-blue in colour and the afterglow in the main body of the burnt charge behind the flame front to be bluish-white or reddish-yellow depending on the mixture ratio.

Fig. 2-2 shows the mechanism of combustion which ensues from assuming that all the heat release takes place in the flame front. Briefly, it consists of the complete burning of a small volume increment and the expansion of this into the already burnt and the still unburnt portions of the mixture until pressure equilibrium is attained. Thus, it is clear that the flame speeds, which are measured or observed in engine combustion chambers relative to the cylinder head, are the vector sums of two fundamental quantities:

i) the linear velocity of the flame front with respect to the unburnt gas. This is here called the turbulent burning velocity, U_T.

ii) the velocity of the unburnt gas itself is moving away from the flame front. This is due to the expansion of the burning gases (see Fig. 2-2) and it is conveniently called the unburnt gas velocity, U_g.

The fundamental mechanisms involved in progressive flame propagation are described in Chapter 4. Briefly, however,

it can be stated that the conduction of heat and the diffusion of active particles and radicals ahead of the flame front into the unburnt mixture are primarily involved. The condition of the charge itself is highly turbulent which enables a high rate of propagation to be achieved.

As already stated, immediately after ignition, the so-called "delay period" exists during which there is no noticeable increase in pressure due to combustion alone. Theoretically, it is most difficult to define the extent of this period since no critical point can be indicated either on pressure-time diagrams or on flame photographs. Some workers[31] have circumvented this problem by utilising the concept of an 'apparent' delay period as being proportional to the time taken for the flame to propagate a certain small distance from the sparking plug. This technique has enabled numerous investigators to observe the influence of many different engine operating conditions and variables on the magnitude of the period. Obviously, the faster the rate of burn, the less time does the period occupy and since the rate of burn has been found to increase with increases in the temperatures of the burnt and the unburnt portions of charge and with the degree of mixture motion, the "delay period":

i) is at a minimum at an equivalence ratio of 1.1 to 1.2.[31,38]

ii) decreases with increasing engine speed[31,38].

iii) is influenced slightly by spark timing variations[31].

iv) is reduced by the use of faster burning fuels.

v) is reduced by the presence of deposits in the combustion chamber[31]. The mechanism for this reduction is that the heat losses from the small flame kernel which exists just after ignition are less when deposits are

present.

At this stage of the combustion process, the expansion of the burnt gases accounts for the greater part of the flame speed i.e. the gas velocity, Ug, is much greater than the turbulent burning velocity, U_T. This is because the expansion takes place almost entirely in the direction of the unburnt portion (see the simplified analogy in Fig. 2-2).

An explanation for the generally slow flame travel during the delay period can be found in the lower temperatures of the burnt and unburnt fractions of charge and in the visualization of a "boundary layer" covering the entire combustion chamber walls and separating them from the turbulent main mass of charge. In this layer, the gas is practically stagnant and it is invariably in this that the sparking plug is positioned. Thus, until the flame has propagated out of it into the more turbulent mass, the burning velocity relative to the unburnt gas must be laminar in nature. From correlations of computed and experimental pressure-time diagrams in this study, the thickness of this layer was estimated to be approximately 3.5 mm. Obviously, this isn't a true boundary layer in the accepted sense but is the distance that the flame has to travel before the turbulent eddies of the main mass of charge act on the flame front thereby enabling the turbulent burning velocity to "take over" from the laminar burning velocity. Such an explanation accounts for the shortened delay periods found when turbulence and swirl are deliberately induced around the spark plug.[38]

The slow manner in which the flame propagates after ignition is clearly shown on photographs in the works of Rassweiler and Withrow[10], Rasswiler et al[11], Withrow and

Cornelius[12], Clarke[26] and Wentworth and Daniel[39].

The main period of combustion follows the "delay period." This is the phase of the combustion process during which the flame speeds and heat release rates are greatest since the temperature, pressure and density of the unburnt gas is being continuously increased owing to its compression by both the expanding burnt gases and the movement of the piston when this is on the upstroke. To ensure a reasonably efficient combustion, it is important to arrange for the flame propagation at this time to be occurring, and nearing completion, when the piston is within the close vicinity of top dead centre. For a given compression ratio, this criterion is primarily determined by the crankangle at which ignition occurs and by the duration of the "delay period."

A detailed discussion of the action of the turbulence existent in the combustion chamber during this combustion phase is given in Chapter 4. It should be noted that the piston is continuously in motion which not only modifies the degree of turbulence but also changes the volume and shape of the combustion chamber with consequent effects upon the flame pattern development (see Chapter 5). Because the temperatures and pressures are highest during this main period of combustion, the heat transfer rates from the engine are also at a maximum.

In normal combustion, the final period of the flame travel is characterized by the slowing down of the flame speeds and by a reduction in the heat release rates. The reasons for this are:

i) the piston is usually on its downstroke when this phase of the combustion process is reached. This has the effect of expanding the final unburnt charge

volume with consequent reductions in its temperature, pressure and density.

ii) the generally low degrees of turbulence near the combustion chamber wall at the end of the flame travel.

The expansion of the newly burnt increments of charge at this time takes place mainly in the direction of the burnt portion (see Fig. 2-2). Thus, the main component of the flame speed is the turbulent burning velocity.

During the propagation of the flame throughout the combustion chamber, the unburnt gas is subject to a further source of heat supply in addition to those from compression by the burnt gases and the piston motion. This additional source is caused by some chemical energy release in the unburnt gas itself, an effect which has been found to exist by Harrow[40], Salooja[41] and Johnson[42]. Johnson, in fact, attempted to derive a technique for calculating its magnitude under various conditions. Such a phenomenon should strictly be incorporated in the analytical model in this work. It is not because of the difficulties involved in relating the time dependent kinetic quantities to the time independent thermodynamic considerations.

It should be noted that an abnormal combustion situation could be attained in the final stages of flame propagation under certain conditions. This occurs when the remaining unburnt gases (the end gases) reach a condition at which drastically high heat release rates are evolved, which result in the phenomenon known as 'knock.' Whether in fact such a condition is reached depends on whether the normal flame, spreading from the spark plug, engulfs the remaining unburnt

volume with consequent reductions in its temperature, pressure and density.

ii) the generally low degrees of turbulence near the combustion chamber wall at the end of the flame travel.

The expansion of the newly burnt increments of charge at this time takes place mainly in the direction of the burnt portion (see Fig. 2-2). Thus, the main component of the flame speed is the turbulent burning velocity.

During the propagation of the flame throughout the combustion chamber, the unburnt gas is subject to a further source of heat supply in addition to those from compression by the burnt gases and the piston motion. This additional source is caused by some chemical energy release in the unburnt gas itself, an effect which has been found to exist by Harrow[40], Salooja[41] and Johnson[42]. Johnson, in fact, attempted to derive a technique for calculating its magnitude under various conditions. Such a phenomenon should strictly be incorporated in the analytical model in this work. It is not because of the difficulties involved in relating the time dependent kinetic quantities to the time independent thermodynamic considerations.

It should be noted that an abnormal combustion situation could be attained in the final stages of flame propagation under certain conditions. This occurs when the remaining unburnt gases (the end gases) reach a condition at which drastically high heat release rates are evolved, which result in the phenomenon known as 'knock.' Whether in fact such a condition is reached depends on whether the normal flame, spreading from the spark plug, engulfs the remaining unburnt

charge before it reaches its explosive state. If it does, normal combustion will result. If it does not, knocking combustion ensues.

The reason for the end gases attaining such explosive proportions has been attributed to many causes. It seems clear, however, that certain preflame reactions are taking place in these gases, the rates of which increase with increases in:

i) the rates of change of temperature and pressure.
ii) the levels of temperature and pressure.
iii) the time lag before the arrival of the normal flame front.

Although the actual mechanism of knocking combustion is still the subject of great debate and conflicting views, it appears that there are at least three possibilities for its occurrence:

i) spontaneous ignition in the end gases at either a point or at a number of points in advance of the normal flame front.
ii) spontaneous combustion of the entire unburnt charge.
iii) an acceleration of the flame front to many times its normal speed owing to the increased temperatures in the unburnt charge and the increasing concentrations of active particles and radicals from the preflame reactions. This mechanism has been suggested by Curry [36,43].

The ability to set a criterion to differentiate between knocking and normal combustion in such an analytical model as is being derived in this work is most difficult and is beyond the scope of this work.

charge before it reaches its explosive state. If it does, normal combustion will result. If it does not, knocking combustion ensues.

The reason for the end gases attaining such explosive proportions has been attributed to many causes. It seems clear, however, that certain preflame reactions are taking place in these gases, the rates of which increase with increases in:

i) the rates of change of temperature and pressure.
ii) the levels of temperature and pressure.
iii) the time lag before the arrival of the normal flame front.

Although the actual mechanism of knocking combustion is still the subject of great debate and conflicting views, it appears that there are at least three possibilities for its occurrence:

i) spontaneous ignition in the end gases at either a point or at a number of points in advance of the normal flame front.
ii) spontaneous combustion of the entire unburnt charge.
iii) an acceleration of the flame front to many times its normal speed owing to the increased temperatures in the unburnt charge and the increasing concentrations of active particles and radicals from the preflame reactions. This mechanism has been suggested by Curry [36,43].

The ability to set a criterion to differentiate between knocking and normal combustion in such an analytical model as is being derived in this work is most difficult and is beyond the scope of this work.

Flame progression in spark ignition engines has been the subject of much study and observation for a period of about 40 years. Numerous techniques have been used to gain what information we now have on it. These include:

i) gas sampling at various points throughout the combustion process[44]. In this, the disappearance of the oxygen indicates the presence of the flame.

ii) the fitting of quartz windows into cylinder heads[10,26]. This method provides a useful means for easy observation and photography of flame progress, the accuracy of which is beyond reproach.

iii) the use of ionization gaps in the wall surfaces of the combustion chamber[45,46,34]. The presence of the flame front is indicated by the ionization of the gap and the generation of an electrical discharge across it.

These techniques have indicated that any factor which tends to increase the temperatures of the burnt or unburnt fractions of the charge or the turbulence levels also increases the burning velocities in the combustion chamber. Also, any effect which reduces the temperatures or turbulence levels (e.g. heat losses, the presence of diluents etc.) reduces the propagation rates.

Other phenomena which are know to be associated with spark ignition engine combustion are:

i) variations in the temperature of the burnt fraction.

ii) cyclic dispersion.

Flame progression in spark ignition engines has been the subject of much study and observation for a period of about 40 years. Numerous techniques have been used to gain what information we now have on it. These include:

i) gas sampling at various points throughout the combustion process[44]. In this, the disappearance of the oxygen indicates the presence of the flame.

ii) the fitting of quartz windows into cylinder heads[10,26]. This method provides a useful means for easy observation and photography of flame progress, the accuracy of which is beyond reproach.

iii) the use of ionization gaps in the wall surfaces of the combustion chamber[45,46,34]. The presence of the flame front is indicated by the ionization of the gap and the generation of an electrical discharge across it.

These techniques have indicated that any factor which tends to increase the temperatures of the burnt or unburnt fractions of the charge or the turbulence levels also increases the burning velocities in the combustion chamber. Also, any effect which reduces the temperatures or turbulence levels (e.g. heat losses, the presence of diluents etc.) reduces the propagation rates.

Other phenomena which are know to be associated with spark ignition engine combustion are:

i) variations in the temperature of the burnt fraction.

ii) cyclic dispersion.

Hopkinson[47] was the first to notice variations in the temperature of the burnt fraction during flame propagation. Its cause is attributed to the compression of the previously burnt fractions of charge by the expansion of the newly burnt small increments (see Fig. 2-2). For an enlarged discussion on this, see Lichty[30]. The process leads to a condition where the temperature of the products at the point of ignition is much higher than at the flame front. This occurrence has been recognised by both Newhall[48] and Starkman et al[49] in relation to predictions of obnoxious emissions (see Section 22). In this work, such an effect is not catered for since the temperature of the combustion products is assumed uniform throughout.

Cyclic dispersion is the name given to the variation in the combustion development from one cycle to another. Numerous investigators have studied these irregularities including Vichnievsky[50], Soltau[33], Patterson[51], Karim[52], Curry[34] and Harrow et al[31]. In this connection, there is general agreement that the faster the mixture burns, the less is the extent of the dispersion. Many hypotheses have been made regarding its underlying causes including:

i) fluctuations from cycle-to-cycle in the time occupied by the "delay period." Patterson[51] in fact made some hot wire anemometer measurements of the gas velocities around the spark plug and proposed that cyclic dispersion is primarily a function of the mixture velocity variation near the spark plug at ignition.

ii) variations in the gas flow pattern in the mass of the turbulent charge from cycle-to-cycle. Harrow et al[31] support this view since they found that a large

part of the cyclic dispersion originates from variations in the speed of the fully developed flame.

It is more than likely, however, that both of these mechanisms are involved. The need for a more uniform flow pattern from cycle-to-cycle in the engine combustion chamber is thus apparent. It has been suggested[50] that, if the flame propagation rate under a given set of engine operating conditions could be maintained at a uniform constant maximum level, power increases of from 2 to 10% could be achieved with subsequent savings in fuel economy and obnoxious emissions.

2.3. EXHAUST EMISSION FUNDAMENTALS.

2.3.1. GENERAL.

In view of the current legislation in the U.S.A. and the proposed legilation in many other parts of the world against the encroachment of motor vehicle emissions on man and his environment, the study and control of these have assumed enormous importance in recent years. Such emissions are introduced into the atmosphere from the engine exhaust, the crankcase vent, the carburettor and the fuel tank. However, it is only these products which are produced as a consequence of the combustion process which are of direct interest here. These are by far the more complex, the more plentiful, the more easily measured, the potentially more harmful and the less easy to control. They contribute about 85% of the total unburnt hydrocarbon emissions from 'untreated' motor vehicles[53], most of which reach the atmosphere through the exhaust pipe. The remainder are emitted from the crankcase vent as a result of leakage from the combustion chamber past the piston and piston rings into the crankcase.

Exhaust gases have been found to contain all of the following:

i) unburnt hydrocarbons.
ii) carbon monoxide.
iii) oxides of nitrogen.
iv) carcinogens.
v) particulate matter.
vi) lead.
vii) odour.
viii) oxides of sulphur.

Thus far, the solution of the exhaust emission problem has been confined almost exclusively to the attempted elimination of these pollutants which are considered to be present in the greatest quantities viz. the unburnt hydrocarbons, carbon monoxide and the oxides of nitrogen. Such partially oxidized constituents represent a loss in the efficiency of the combustion process. It will be appreciated that the mode of engine operation exerts a controlling influence on the concentrations of these pollutants. This is shown in Table 2-A[54] from which it is clear that:

i) the idle and deceleration modes are the most productive of unburnt hydrocarbons.
ii) the idle, acceleration and deceleration produce the highest concentrations of carbon monoxide.
iii) the cruise and acceleration yield the most oxides of nitrogen.

Information such as is given in Table 2-A must be related to a time base in order to be meaningful in terms of air pollution control. These time bases are conceived to represent arbitrary typical driving schedules of motor

TABLE 2-A.

TYPICAL VARIATIONS IN EXHAUST GAS COMPOSITION WITH THE MODE OF ENGINE OPERATION.

Mode of Operation.	Unburnt Hydrocarbons p.p.m.	Carbon Monoxide %	Oxides of Nitrogen p.p.m.
Idle	750	5.2	30
Cruise	300	0.8	1500
Acceleration	400	5.2	3000
Deceleration	4000	4.2	60

From Starkman [54]

vehicles e.g. the U.S. Federal and European test cycles (Fig. 2-3). These cycles show the approximate contributions of each driving mode to the total amount of emissions. As yet (1969), there are no limits on the pollutant amounts relating to the European cycle. However, the intense smog problem in the Los Angeles basin has accelerated the onset of legislation in California and the U.S.A. This is becoming progressively more severe with the passage of time.

2.3.2. THE UNBURNT HYDROCARBONS, HC.

Haagen-Smith[55] in 1952 established that unburnt hydrocarbons and the oxides of nitrogen in the presence of ultraviolet radiation were the factors mainly responsible for the irritating and damaging consequences of "smog" in Los Angeles. He further postulated that a photosynthetic chemical reaction was involved.

In spark ignition engines, the mechanism of formation of the hydrocarbons in the combustion chamber varies with the mode of the engine operation. At low intake manifold depressions (i.e. at quite large throttle openings), the following are considered to be involved:

i) when the combustion chamber wall temperatures are high, the predominant mechanism of HC formation is thought to be the quenching of the propagating flame at the walls. Daniel[56] found that the flame failed to propagate through the mixture located within about 0.005 to 0.038 cm. of the combustion chamber wall. This region of the charge he termed the "quench layer."

ii) at low wall temperatures, the HC formation by wall quenching is augmented by fuel condensation[57,66].

iii) very small concentrations of hydrocarbons can be formed as equilibrium products of the combustion reaction [56].

iv) the highly turbulent condition of the gases in the combustion chamber can allow small pockets of unburnt mixture to pass through the reaction zone without being ignited. Again, the concentrations from this source are bound to be small.

v) inhomogeneity in the unburnt gas can result in regions of very rich and very weak mixtures in which the flame might fail to propagate. Under such conditions, quite large concentrations of hydrocarbons would be exhausted.

During idling (i.e. at quite high manifold vacua), the sources of HC generation listed above are swamped by the effects of incomplete burning of the charge. At such times, the throttle is only open enough to provide a small flow necessary for the engine to run slowly and this condition engenders a comparatively high depression in the inlet manifold. When the inlet valve opens towards the end of the exhaust stroke, this depression draws some of the exhaust gases from the cylinder and the exhaust manifold back into the inlet manifold so that the imcoming fresh charge is considerably diluted before the subsequent compression and combustion phases of the engine cycle. During combustion, owing to the presence of comparatively large amounts of inert exhaust gases, the fuel molecules have great difficulty in finding oxygen molecules with which to combine and burn. Thus, in order to use up all the limited supply of oxygen, it is usually necessary to supply proportionately more fuel than would be required for cruise conditions with the result

that the mixture for best idle is always richer than stoichiometric and generates high CO and quite high HC concentrations. The actual amount of exhaust dilution present and the amount of enrichment required will depend on a number of factors, one of which is the degree of valve overlap.

During deceleration, the engine is rotating faster than at idle and the manifold vacuum is increased beyond that at idle. This results in a much increased exhaust dilution and a grave deterioration in combustion which is often so bad as virtually to amount to a complete misfire. Unburnt fuel is thus exhausted in large proportions and appears as excessive HC emission.

Wentworth and Daniel[39] have observed and photographed combustion under such a light load conditions in an engine having a quartz window in its cylinder head. They found that the flame usually failed to propagate throughout the entire mixture and that the two main reasons for this were:

i) either it was quenched at some point before the completion of its travel.

ii) or it travelled so slowly that the exhaust valve opened before flame propagation was completed.

Both these effects can be attributed to the presence of excess exhaust residual gases. It should be noted that the transient act of closing the throttle produces an abrupt rise in the inlet manifold depression which, in turn, produces a sudden evaporation of any liquid fuel present on the inlet manifold walls. The first stage of deceleration or idling is, therefore, accompanied by a much greater enrichment of the mixture strength. Consequently, the CO and HC emissions are much greater at this time. Several methods have been used to overcome this problem including:

i) heating the intake manifolds.

ii) reduction of the internal surface area of the manifolds and ports.

iii) preventing the rapid closure of the throttle.

iv) intake valve throttling[58].

The concentrations and chemical character of the unburnt hydrocarbons resulting from engine combustion are extremely variable; almost every possible design factor and operating condition is involved.

Air/Fuel Ratio.

A typical variation in hydrocarbon concentration with this parameter is shown in Fig. 2-4.[59] A possible discrepancy from the general indicated trend occurs at very lean mixtures when the flame might fail to propagate completely, a condition which would result in very high hydrocarbon quantities in the exhaust. Good mixture formation and distribution is thus required.

Surface/Volume Ratio.

The combustion chamber surface/volume ratio exerts considerable influence on hydrocarbon formation as might be expected when these pollutants have been shown to be formed primarily in the "quench layer." Thus, increases in this ratio also lead to corresponding gains in hydrocarbon concentrations. The ratio does, in fact, increase with increases in the number of cylinders, the bore/stroke ratio and the compression ratio. Other factors which can influence it are:

i) piston movement.

ii) poor piston ring design[60].

iii) combustion chamber shape[61,67,68].

Turbulence and Swirl.

One of the effects of increasing the turbulence and swirl in the combustion chamber is to reduce the "quench layer" next to the walls[68]. As a consequence, the tendency for hydrocarbons to form is lowered. This effect can be achieved by increasing engine speed and/or by careful design of the induction manifold[62,63,64,69]. Care must be used in its application, however, since, beyond a certain level of turbulence, the burnable range of air/fuel ratios decreases.

Spark Timing.

Variations in this parameter have a great influence on hydrocarbon emissions. For example, a retarded spark increases the concentrations at the exhaust valve because of inefficient combustion and the increasing surface area of the cylinder walls across which the flame has to propagate towards the end of its travel. However, because the exhaust temperature is higher with a retarded spark, further oxidation reactions can take place in the exhaust pipe (if sufficient oxygen is present) and this reduces the quantity of hydrocarbons leaving it. This method of HC reduction must be weighed against the penalties of losses in fuel economy and power. Increasing the spark advance, on the other hand, has exactly the opposite effects.

Deposits.

Deposits in the combustion chamber have been found to increase HC emissions[65]. The mechanisms for this have been postulated as being:

i) because of slight increases in the compression ratio and the surface/volume ratio.

ii) by the charge being squeezed into the rather porous structure of the deposits during the compression stroke and escaping being burnt.

Compression Ratio.

Compression ratio increases tend to give higher HC concentrations for three main reasons:

i) the surface/volume ratio influence already alluded to.

ii) the observed fact[70] that the exhaust gas temperatures decrease. The effect of this is a retardation of the oxidation reactions in the exhaust manifold.

iii) the more efficient scavenging of residual exhaust gases from the combustion chamber. Daniel and Wentworth[39] have found that, because of the viscous property of the gases adjacent to the combustion chamber walls, these are the last to exit the chamber during the exhaust process. Their importance in this context is that they are much cooler and they contain approximately eleven times the HC concentration of the remaining exhaust gases. Consequently, for high compression ratios, the residual gas volume is smaller and more high HC concentration gases are expelled into the exhaust manifold tending to raise the average concentration level.

Combustion Chamber Wall and Coolant Temperatures.

High values of these parameters reduce the amounts of fuel condensation and HC emissions and vice versa.

Fuels.

Fuels having a low temperature of vapourization (e.g. propane, methane etc.) do not condense on the combustion

chamber walls and provide more homogeneous charges. Both of these effects reduce HC emissions. In comparing fuels, note should be taken of variations in air/fuel ratio and burning velocity.

Valve Overlap.

Under deceleration and idling conditions, it would be ideal to have zero valve overlap in order to prevent dilution of the fresh charge by the residual exhaust gases. This would, however, considerably reduce the power output at higher engine loads. The possibility of variable valve timing is thus significant.

Knock.

In fuel-lean mixtures, Davis et al[70] found that there was no significant influence of knock on HC concentrations. For mixtures richer than stoichiometric; however, it was found that knock tended to decrease these concentrations in the exhaust and that the extent of the decrease increased with the intensity of knock. Two mechanisms have been proposed for these reductions:

i) the pressure differences and oscillations in the combustion chamber under knocking conditions cause the gas to vibrate and scrub the chamber walls. This action removes the quench zone gases into the bulk of the charge where they have higher probability of being burnt.

ii) the quench zone stays intact but is subject to the high pressure oscillations caused by knock. The high pressure in the quench zone causes its temperature to rise and the unburnt hydrocarbons in the zone to react with the oxygen in the zone itself.

Although photo chemical smog is formed by reactions between oxides of nitrogen and hydrocarbons in the presence of sunlight, individual hydrocarbons differ in their tendency to enter this reaction. This reactivity is very much a function of chemical structure and the degree of saturation. Olefinic hydrocarbons, aldehydes, long chain paraffinic hydrocarbons and aromatics (with the exception of benzene) are recognized as the more reactive components of the organic materials which are emitted from engines. On the other hand, the saturated lower paraffins (methane, ethane, propane, butane and pentane), benzene and acetylene are found to be practically non-reactive in the photo chemical process and are now considered to be virtually harmless. In this connection, it has additionally been reported that:

i) no significant change in reactivity occurs because of engine conditions[71].

ii) the reactivity increases with spark retard and decreases with leaning of the mixture air/fuel ratio[72].

iii) the reactivity of the exhaust gases may increase with increasing engine displacement[71].

Three methods have been contemplated in attempts to reduce the HC emissions from the exhausts of motor vehicles:

i) oxidation of the unburnt hydrocarbons in the exhaust system by low pressure air injection into the exhaust ports[73,74].

ii) engine modification to reduce the volume of these pollutants being emitted from the cylinders[75,76].

Since this generally involves lean mixture operation, good carburetion and mixture preparation is vital.

iii) the use of a petrol injection, stratified charge engine. This ensures a uniform distribution between cylinders at all times. In such an engine, the area of the quench zone next to the combustion chamber wall is automatically reduced at reduced load. However, a new quench zone at the interface between the combustible mixture and the air is introduced where considerable mixing and quenching can occur.

2.3.3. CARBON MONOXIDE, CO.

Although the nature of carbon monoxide as a poisonous gas and a health hazard is well known, it is only recently that concern has developed over the harmfullness of long term exposure of urban populations to the gas[77]. Thus, legislation in recent years has attempted to ensure that the quantities of CO in exhaust gases are being minimized.

Unlike the hydrocarbons, CO is primarily formed in the bulk of the charge. Of all the engine design variables and operating conditions which can influence its formation, the air/fuel ratio effect is by far the greatest (Fig. 2-4). At rich mixtures, when the supply of oxygen is limited, large quantities of CO are formed. The converse is true at weak mixtures.

Basic requirements for low CO emissions are therefore:

i) operation at weak mixtures.

ii) good mixture distribution between individual cylinders to avoid some cylinders running richer or weaker than others.

iii) good mixture homogeneity within individual cylinders thereby ensuring that a uniform air/fuel ratio exists at all points in the charge.

These criteria can effectively be achieved by good design of the induction system and carburettor.

Carbon monoxide formation is not greatly affected by the temperature and pressure levels attained in reciprocating engine combustion processes. This is especially so at the richer fuel/air ratios (see Figs. 6-4, 6-19 and 6-34 in Chapter 6). Thus, discounting air/fuel ratio, the influences of the many other remaining engine design and operating conditions are not very well defined.

Spark Advance.

Although, theoretically, a very slight increase in CO emissions leaving the engine cylinder with an advancing spark is expected due to the higher levels of temperature and pressure attained, in practice, any possible trend is completely confused by volumetric efficiency differences.

Compression Ratio.

Increases in compression ratio result in better scavenging of the exhaust residual gases from the engine combustion chamber and higher combustion temperatures and pressures. Very slight gains in CO emissions might thus be expected.

Air Inlet Temperature.

Rises in this parameter can either reduce CO concentrations because of the improved mixture distribution and preparation or increase them very slightly due to the higher temperatures involved.

Deposits.

No significant effect has been observed on CO emissions with deposit accumulation. Theoretically, one might expect them to increase a very small amount because of the reduced heat transfer and the slight rise in compression ratio.

Fuel.

The amount of air available for combustion is the most significant factor affecting the CO concentrations produced. It dwarfs any differences between fuels[78]. The physical characteristics of the fuel (e.g. viscosity, volatility etc) can, however, have great influences on the mixture distribution between cylinders. This is why CO concentrations have been found to be lower with liquefied petroleum gases than with petrols[79,80]. The effect of fuel temperatures on air/fuel ratios can also not be discounted[81].

Ambient Temperature and Pressure.

Changes in these quantities under operating conditions can radically affect CO formation because of fluctuations in the air/fuel mixture ratios being supplied to the engine[82].

As already shown in Table 2-A, the engine operating mode has an important bearing on the CO quantities produced in engine exhausts mainly because of the influence of air/fuel ratio. Generally speaking, the same considerations are involved in reducing these emissions as are found to hold for HC concentration reductions. An additional approach to obtain slight reductions is to add an inert gas to the inducted fresh mixture, the effect of which is to reduce the temperatures. Close watch must be kept on the air/fuel

ratios if this technique is used.

Exhaust gas analyses and direct spectroscopic observations through windows in combustion chambers[83,84] have both revealed that CO once formed during combustion, does not change concentration very much during the ensuing expansion and cooling. Thus, it is present in greater quantities in the exhaust gases than it would have been if equilibrium conditions had persisted through the expansion. The concentrations in fact have been found to more nearly reflect a frozen composition at combustion temperature and pressure equilibrium values than the equilibrium composition at exhaust temperature values (see Fig. 2-5[85]). This is observed to be especially so at the leaner mixtures.

Starkman and Newhall[85] sought an explanation for this behaviour in the water/gas reaction

$$H_2 + CO_2 \rightleftharpoons H_2O + CO \quad \text{--------- 2-2}$$

after observing that there were non-equilibrium amounts of all these four constituents in engine exhausts[54]. This reaction was viewed as a combination of the two dissociation reactions

$$CO_2 \rightleftharpoons CO + \tfrac{1}{2} O_2 \quad \text{------- 2-3}$$

and

$$H_2O \rightleftharpoons H_2 + \tfrac{1}{2} O_2 \quad \text{------- 2-4}$$

which were combined linearly to give

$$CO_2 + H_2 \rightleftharpoons CO + H_2O \quad \text{----- 2-5}$$

and

$$CO_2 + H_2O \rightleftharpoons CO + H_2 + O_2 \quad \text{-- 2-6}$$

Starkman and Newhall noted that the oxygen concentration effectively vanishes for fuel rich mixtures and that the system of major species could be represented by Equation 2-5. The equilibrium corresponding to this reaction was

found to be influenced only slightly by temperature so that the equilibrium species distribution of combustion products reflected only minor variations throughout expansion (see Fig. 2-5).

For lean and stoichiometric mixtures however, significant quantities of oxygen were noted to be present in addition to the other species. As a result, EQuation 2-6 was thought to be the operative reaction for inclusion in the equilibrium system. This was found to exhibit a strong temperature dependence with the result that the cooling process, associated with the expansion stroke, resulted in a rapid shifting of the equilibrium species distribution (Fig. 2-5).

Thus, for rich mixtures, the exhaust concentrations of CO tended to correspond to those predicted by equilibrium theory. For weak and stoichiometric mixtures, on the other hand, the maximum rate of CO oxidation to CO_2 appears to be exceeded when equilibrium conditions are assumed to exist with the result that the CO concentrations in engine exhausts under such conditions correspond more nearly to those predicted for the peak temperature state than to those predicted for the exhaust temperature state.

In a further attempt to explain why CO concentrations at the end of expansion correspond more closely to combustion temperature equilibrium values than to exhaust temperature equilibrium values, Newhall[86] analysed the kinetics involved. Rate expressions for 32 elementary chemical reactions were combined to yield 13 coupled, non-linear differential equations representing the following 13 chemical species:

N_2, O_2, H_2, H_2O, CO_2, OH, N, O, H, NO, CO, N_2O and NO_2.

These equations were integrated numerically in a stepwise

manner using the Runge-Kutta technique. The procedure was started at the initial point of expansion where conditions were considered to be adequately represented by a chemical equilibrium distribution of the species corresponding to average conditions of real engine combustion processes. The temperature variation during expansion was approximated by a simple polynomial relationship with the cylinder volume. Results were obtained as concentration - time histories throughout expansion for each of the 13 species.

For carbon monoxide, it was found that, during the initial stages of expansion, this pollutant was destroyed at a rate corresponding to a shifting chemical equilibrium condition. As the process continued, however, an increasing deviation from equilibrium occurred until, at the end of expansion, the CO concentration was as much as ten times the equilibrium value. An explanation for this behaviour was found in the concentration-time histories of the atomic species O and H and the hydroxyl radical OH the behaviour patterns of which were noted to be very similar to that of CO. On this evidence, Newhall formed the opinion that the inhibition of CO oxidation during expansion is due to the failure of these atomic species and radicals to recombine at a rate sufficient to maintain a continuous chemical equilibrium. Thus, in addition to CO, O, H and OH persist in excess quantities throughout expansion.

The mechanism for this state of affairs was thought to be contained in the bimolecular reaction:

$$CO + OH \rightleftharpoons CO_2 + H \cdots\cdots 2\text{-}7$$

This atom exchange reaction was found to be relatively fast in both forward and reverse directions and was also

continuously equilibrated throughout expansion, an observation which was most surprising in view of the noted non-equilibrium behaviour of CO. If, however, it is at all times in equilibrium, the relative levels of CO and CO_2 will be controlled solely by the existing levels of the OH and H species according to the relationship:

$$\frac{(CO)}{(CO_2)} = \frac{1}{k_c} \cdot \frac{(H)}{(OH)} \qquad \text{--------- 2-8}$$

where k_c is the equilibrium constant.

When the temperature falls during expansion, therefore, the partial equilibrium, which controls the concentrations of H and OH, favours a disproportionately large number of H atoms relative to OH radicals. It was in fact found that, at a certain point in the expansion, the OH concentration was approximately four times its equilibrium value whereas the H concentration was over twenty times its equilibrium value. Thus, during expansion, the ratio of H atoms to OH radicals, as dictated by partial equilibrium, is much greater than would be the case for total equilibrium. From this, it is deduced that the ratio of CO to CO_2 is correspondingly greater than for total equilibrium and, as a result, there exists an excess of CO. The CO concentrations calculated in this way over a range of air/fuel ratios were in substantial agreement with some measured exhaust concentration levels.

2.3.4. THE OXIDES OF NITROGEN, NO_x.

As has already been stated, the oxides of nitrogen are major participants in photochemical smog reactions. Under strong sunlight, they evolve the poisonous gases ozone and

nitrogen dioxide, NO_2, which react with the hydrocarbons to significantly reduce atmospheric visibility and to cause respiratory diseases and eye irritation[77]. Much controversy persists over their importance to the photosynthetic reactions since at least one author[87] has suggested that the levels being currently produced by engines are greater than the quantities required for the maximum reactivity rate and that to reduce these levels might only produce a more severe situation than presently exists. However, in spite of these arguments, legislation is being enacted to reduce their concentrations in engine exhausts.

Because of the thermodynamics involved, the oxides of nitrogen produced at the engine exhaust port consist almost entirely of nitric oxide, NO. In the presence of oxygen, this constituent rapidly becomes nitrogen dioxide, NO_2. This oxidation usually takes place in the atmosphere but it can also commence in the exhaust system particularly if air has been added to the gases at the exhaust valve in efforts to oxidize the unburnt hydrocarbons and carbon monoxide. Besides being a toxic gas and contributing to the photocatalytic synthesis of smog, NO_2 produces a characteristic red colour when present in the atmosphere and is acidic in its reaction to other materials. From the foregoing, two points are clear thus far:

i) the engine produces NO in amounts which completely swamp its production of NO_2 and N_2O.

ii) the reactive material in the smog photocatalysis is NO_2.

Attempts to control the emission of these oxides to

the atmosphere are extremely difficult because the air/fuel ratios required to suppress their formation are the very opposite of those required to minimize CO and the unburnt hydrocarbons (see Fig. 2-4). In addition, the modes of engine operation at which the NO_x are low in concentration conflict entirely with those at which the unburnt hydrocarbons and carbon monoxide are low. (see Table 2-A).

Like carbon monoxide, however, the oxides of nitrogen are products of the more or less homogeneous combustion region of the charge in the combustion chamber. They are primarily functions of air/fuel ratio and combustion temperature. Thus, the importance of good mixture distribution between individual cylinders and of uniform charge homogeneity needs hardly be stressed.

NO_x concentrations in combustion processes can be decreased by:

a) decreasing the combustion temperature.

b) decreasing the oxygen availability (Fig. 2-4).

Means of achieving combustion temperature reductions are:

i) by decreasing the compression ratio.

ii) by retarding the spark.

iii) by avoiding knock.

iv) by decreasing the inlet charge temperature.

v) by decreasing the coolant and combustion chamber wall temperatures.

vi) by reducing deposit accumulations.

vii) by increasing the surface/volume ratio of the combustion chamber.

viii) by decreasing the mixture pressure. This causes a greater percentage heat loss which might be countered in part by increased NO formation at low combustion temperatures. (see Figs. 6-9, 6-24 and 6-39 in Chapter 6).

ix) by adding an inert substance to the inducted charge. This is discussed in greater detail later.

x) by operating at very weak mixtures.

Methods of decreasing the oxygen availability for combustion reactions include:

i) operation at very rich mixtures.

ii) decreases in the homogeneity of the charge.

Other factors affecting NO formation in spark ignition engines are:

a) engine speed - it has been reported[49,88] that increases in engine speed reduce the formation of NO_x in engine cylinders. Two factors may be involved in the explanation for this. The first of these is concerned with the peak combustion temperatures attained at various engine speeds. It is well-known that the flame takes a longer time (in terms of crankangle degrees) to traverse the combustion chamber when the engine speed is increased. This is because the flame speeds do not increase in direct proportion to engine speeds[89]. Thus the peak temperatures become progressively lower as the engine speeds increase. The second factor is concerned with the kinetics of the reactions responsible for the formation of NO. At

the lower engine speeds, where the peak combustion temperatures are higher, there is more time available for the NO formation, and this leads directly to increased quantities of these pollutants. Contravening this general trend, however, is the greater heat transfer from the gases in the combustion chamber at the lower engine speeds owing to there being more time available for it to occur.

b) temperature gradients in both time and space in the combustion chamber - the reason why the temperature of the burnt gas charge is higher at the spark plug than at the flame front has already been described in Section 2.2. Newhall[48] found, from a theoretical analysis, that such effects do not significantly influence NO concentrations if the mean bulk temperature of the charge is used. On the other hand, however, Starkman et al[49] obtained evidence, by direct experimental means using sampling valves, to show that large gradients in composition are created across the combustion chamber as a result of the temperature gradients which persist through expansion.

Several techniques have been suggested to obtain reductions in the oxides of nitrogen concentrations in the exhaust gases leaving the engine. These include:

i) the burning of a mixture which is either very rich or very lean. (see Fig. 2-4). Although quite effective, the use of rich mixtures is undesirable because of increases in the CO and HC emissions and the disastrous effect on fuel economy. On the lean side, it

is difficult to burn a mixture which is weak enough to decrease the NO_x to the desired amount. There appear, therefore, to be limits to both the richness and the leanness that can be used.

ii) the addition of an inert substance to the fresh inducted mixtures. Useful substances to adopt in this technique are nitrogen, carbon dioxide, water and exhaust gases. From considerations of practicality, it is clear that water and exhaust gases possess considerable advantages over carbon dioxide and nitrogen. It should be noted that the reductions in the oxides of nitrogen caused by operation at very weak mixtures result, in fact, from the presence of excess air which acts as an inert diluent. The mechanism of the NO_x reduction by this technique is the lowering of the combustion temperatures since the inert diluent in effect absorbs a portion of the chemical energy released. Even a moderate decrease in the combustion temperature results in a significant drop in the NO_x production because the amount produced from nitrogen and oxygen is an exponential function of this temperature [48]. It should be realised that the addition of an inert diluent to the ingoing charge is only really required during the acceleration and cruising modes of engine operation (see Table 2-A) when the concentrations of NO_x are excessive.

Exhaust Gas Recirulation.

Because of the ready availability of exhaust gases, the feasibility of using them as the inert or non-combustible

substance to be added to the fresh charge is evident. Great success has been achieved in reducing NO_x emissions whenever the technique has been attempted [90,91] but usually at the expense of a decreased power output, an increased fuel consumption and poor driveability.

Newhall [48] carried out a theoretical digital computer analysis of NO_x formation in spark ignition engines with exhaust gas recirculation. Although his results are somewhat limited in application as the influences of heat transfer and finite flame propagation rates were not considered, they are instructive in supplying the mechanisms and the trends involved. For example, it was found that:

i) the percentage reduction of NO is greatest at rich mixtures. This was explained by the fact that the change in equilibrium NO concentration resulting from a given temperature change is much greater for fuel/rich than for fuel/lean mixtures.

ii) the greater the quantity of the recycled exhaust, the greater obviously is the drop in NO concentrations.

iii) the temperature of the recycled gas has virtually no effect.

iv) the compression ratio had relatively little influence on the effectiveness of the recycle.

v) any oxgen in the recirculated exhaust adversely affects the NO reduction.

Water Injection.

Water injection either into the inlet manifold or directly into the combustion chamber is a further technique which has been used in attempts to reduce combustion temperatures and

NO_x emissions[92]. Various properties of water render it thermodynamically suitable as an inlet charge diluent. For example:

i) it has a relatively low vapour pressure at normal induction system temperatures.

ii) it possesses a high latent heat of vapourization.

iii) it has a low boiling point relative to the maximum engine cycle temperatures.

A theoretical analysis[92] based on chemical equilibrium calculations has indicated that the reduction of the oxides of nitrogen from water injection at rates comparable to the fuel consumption rate is quite significant. The analysis also revealed that the mechanism primarily responsible for this effect was the combustion temperature reduction which far outweighed the effects of any evaporative cooling. These theoretical results were confirmed by experimental measurements which further indicated that there was no change in the volumetric efficiency and that the b.m.e.p. and b.s.f.c. were slightly improved.

As with carbon monoxide, the oxides of nitrogen in engine exhaust gases were much greater than would be expected if equilibrium conditions had been maintained throughout the expansion process. Fig. 2-6 (taken from Ref. 54) compares actual exhaust gas measurements with some concentrations which were calculated when equilibrium was assumed at the maximum bulk cylinder temperature and at the exhaust temperature. It is evident that the actual amounts of NO in the exhaust are greater by far than the amounts calculated for equilibrium and that the disparity is evident over

greater ranges of mixture ratios than with CO. Even the assumption of a frozen composition at the peak combustion temperature is a poor prediction. This is supported by spectrometer observations[83] which have shown that:

i) NO freezes in concentration at least as early as the point of overall peak cycle temperature.

ii) the overall or peak cycle temperature will not account for the NO concentrations.

Several workers have attempted to find explanations for these occurrences. Starkman[93] considered the reaction

$$N_2 + O_2 \rightleftharpoons 2NO \quad \text{-------} \quad 2\text{-}9$$

as the most important one controlling the rate of NO formation and destruction. From Ref. 94, he obtained the reverse rate for this reaction to be

$$k_r = 2.6 \times 10^{12} \cdot \exp(-63800/RT) \text{ cc/mole-sec.}$$

Calculations using this showed that NO, once formed in the combustion chamber, does not appreciably decrease in quantity throughout expansion.

Newhall's basic approach[86] in considering the kinetics of species behaviour in engine cylinders has already been described in the section on carbon monoxide. The reactions influencing NO decomposition were thought to be:

$$NO + O \rightleftharpoons O_2 + N \quad \text{-----} \quad 2\text{-}10$$

$$NO + N \rightleftharpoons N_2 + O \quad \text{-----} \quad 2\text{-}11$$

$$NO + NO \rightleftharpoons N_2O + O \quad \text{-----} \quad 2\text{-}12$$

Each of these was found not to be equilibrated during expansion so that not one was sufficiently rapid to achieve appreciable decomposition. In fact, reactions 2-10 and 2-11 were noted to be about 500 times more effective in this respect than reaction 2-12. Thus, Newhall's results

agreed with previously noted trends indicating that NO is essentially fixed in concentration throughout expansion.

A similar, but much more simplified, approach in attempts to elucidate the generation and behaviour of NO during combustion was used by Eyzat and Guibet[95]. These authors consider that there is a temperature-time effect (due to the varying flame propagation rates) on NO formation. After estimating the temperatures, pressures and per cent masses of charge burnt at various points in the combustion process from pressure-time diagrams, they utilised the reaction in Equation 2-9 to obtain the rates of NO formation according to the relationship:

$$\frac{d(NO)}{dt} = \frac{k_{r_1}\left((N2)_o - \frac{NO}{2} \right)\left((O_2)_o - \frac{(NO)}{2} \right)}{V} - \frac{k_{r_2}(NO)^2}{V}$$

where

NO is the instantaneous number of moles of NO.

kr_1 and kr_2 are the forward and reverse reaction rate constants respectively (cc/mole sec)

$(N2)_o$ and $(O_2)_o$ are the number of moles of nitrogen and oxygen at ignition.

and V is the combustion chamber volume (cc).

The Runge-Kutta technique was used to solve this equation and the resulting NO concentrations throughout combustion were in very close agreement with continuous experimental observations. Despite this, however, the underlying theory to this work is very flimsy and does not account for the many reactions which are known to be involved in the formation of NO during combustion[94,96].

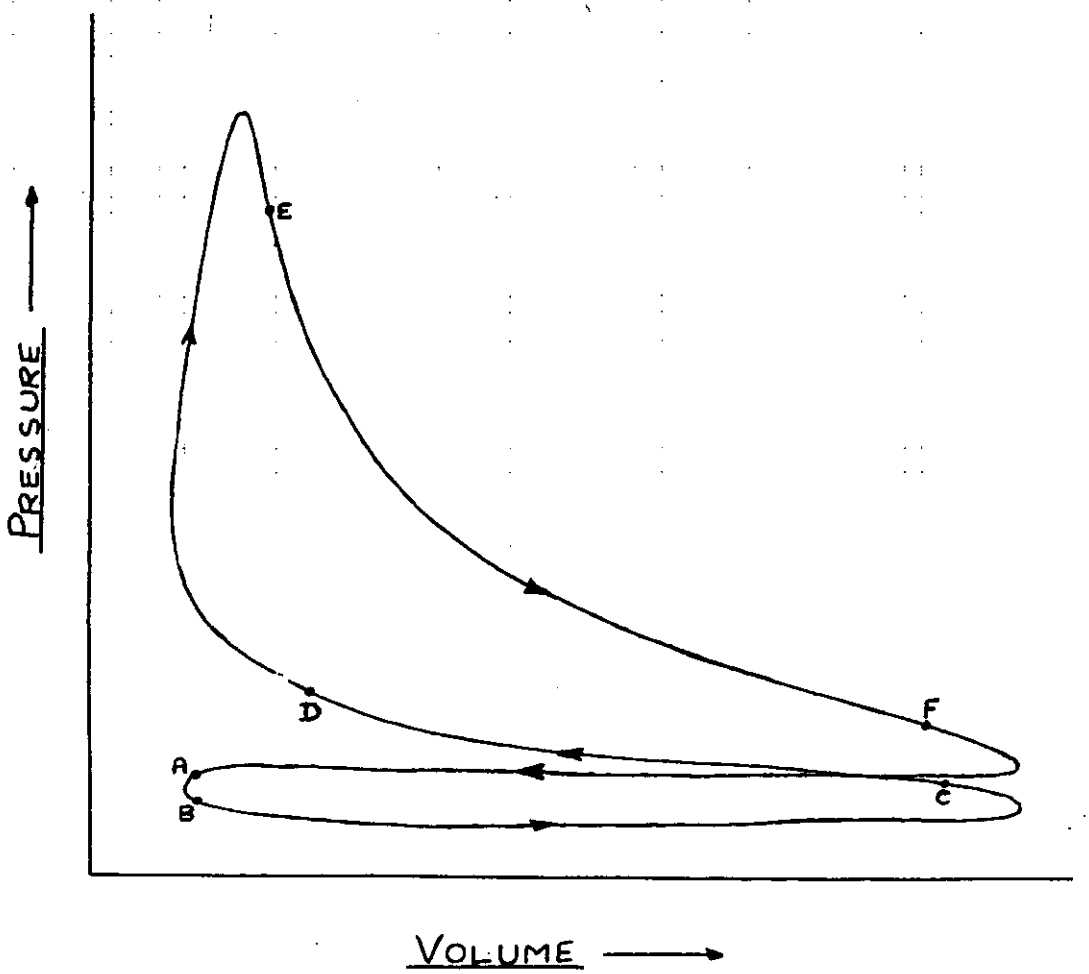

FIG. 2-1 — A TYPICAL SPARK IGNITION ENGINE CYCLE

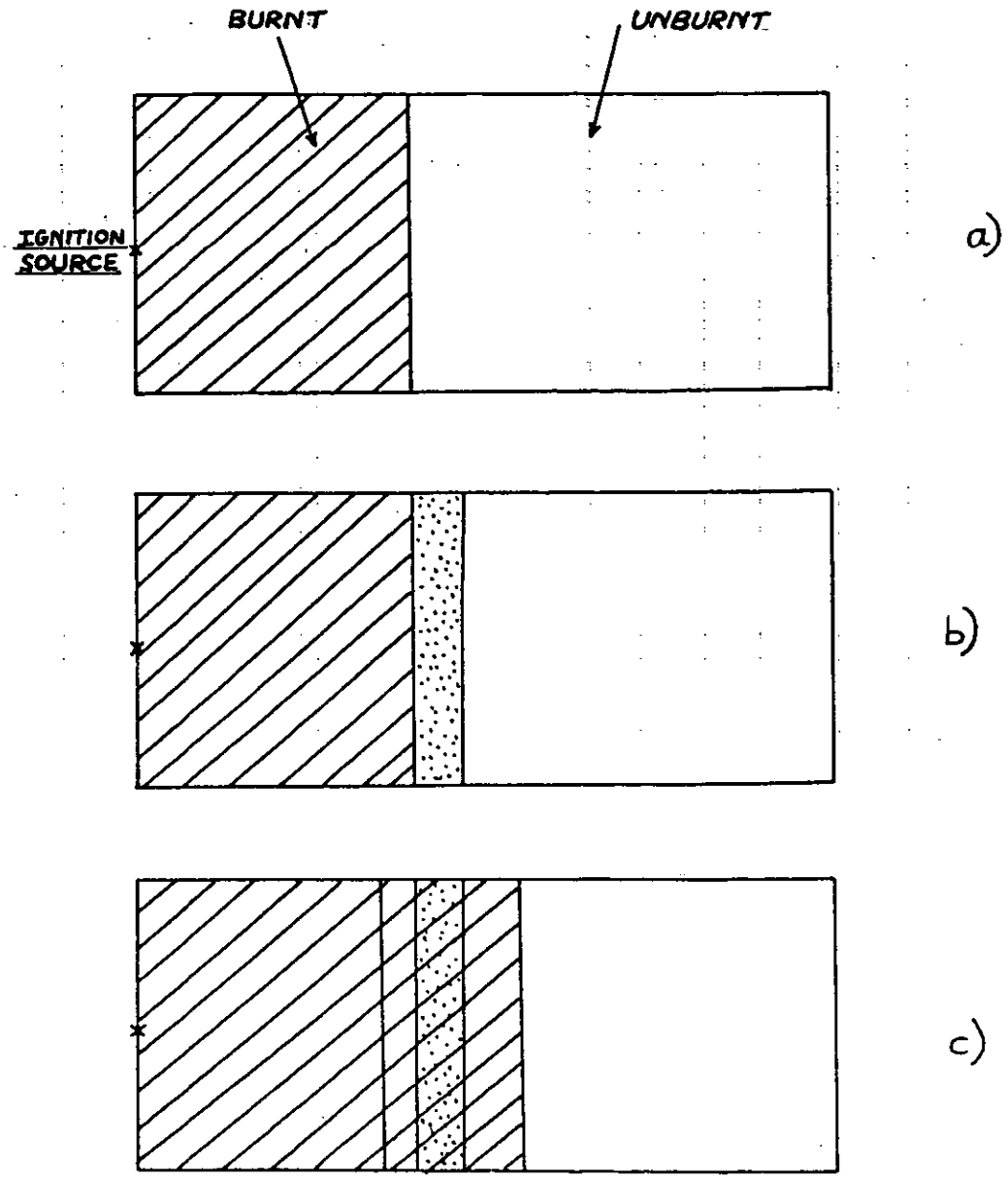

FIG. 2-2 — THE ASSUMED MECHANISM OF COMBUSTION.

a) THE CONDITION AT AN INSTANT OF TIME.

b) THE BURNING OF A SMALL INCREMENTAL VOLUME.

c) THE EXPANSION OF THIS VOLUME INTO THE UNBURNT AND THE ALREADY BURNT PORTIONS OF CHARGE.

FIG. 2-3 — U.S. FEDERAL AND EUROPEAN DRIVING CYCLES

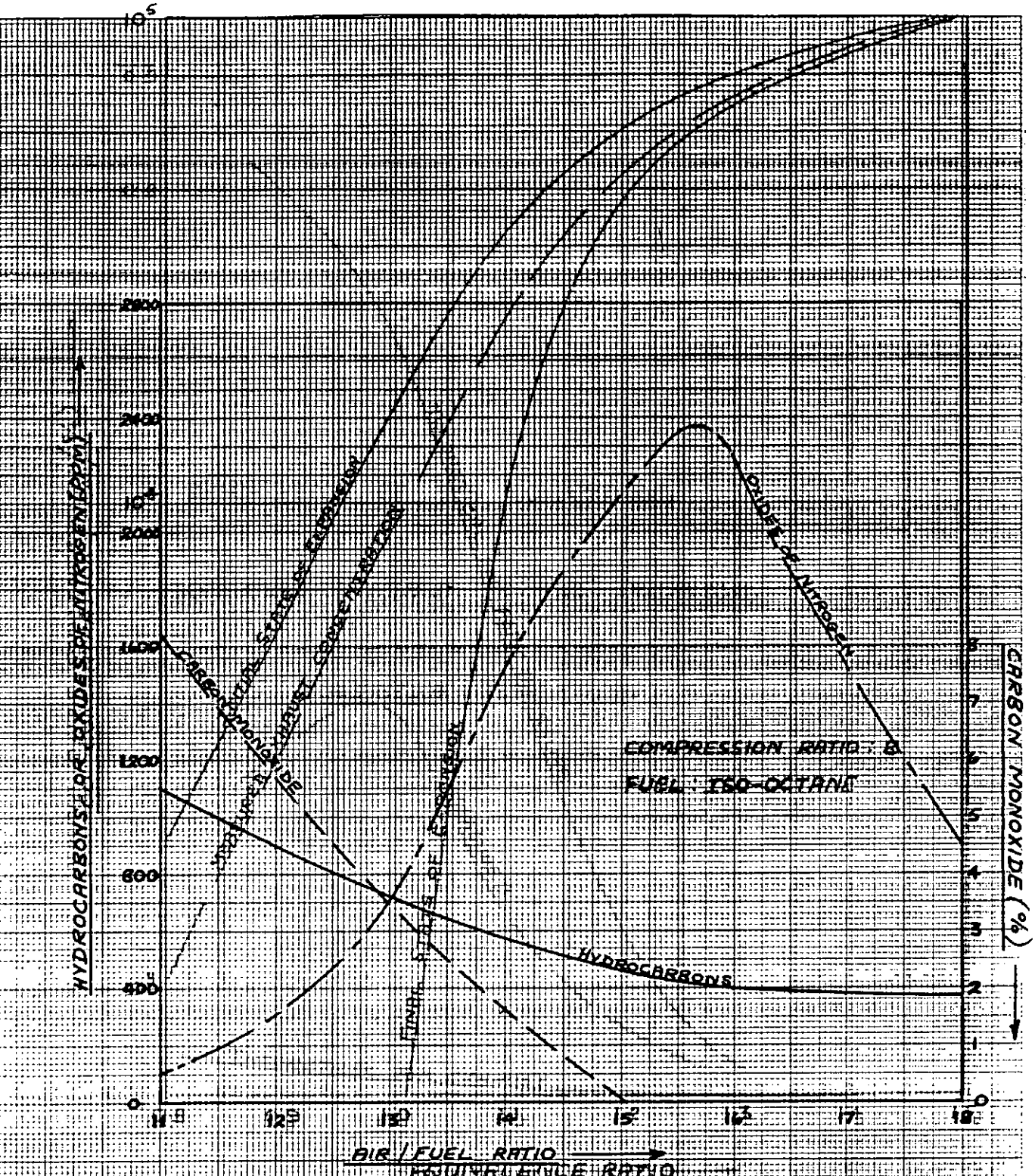

FIG. 2-4 — TYPICAL VARIATION WITH MIXTURE STRENGTH OF THE THREE PRINCIPAL POLLUTANT CONSTITUENTS PRODUCED BY A SINGLE CYLINDER ENGINE (FROM TOSEN[59]) AND EXPERIMENTAL ENGINE (FROM STARKMAN AND NEWHALL[60])

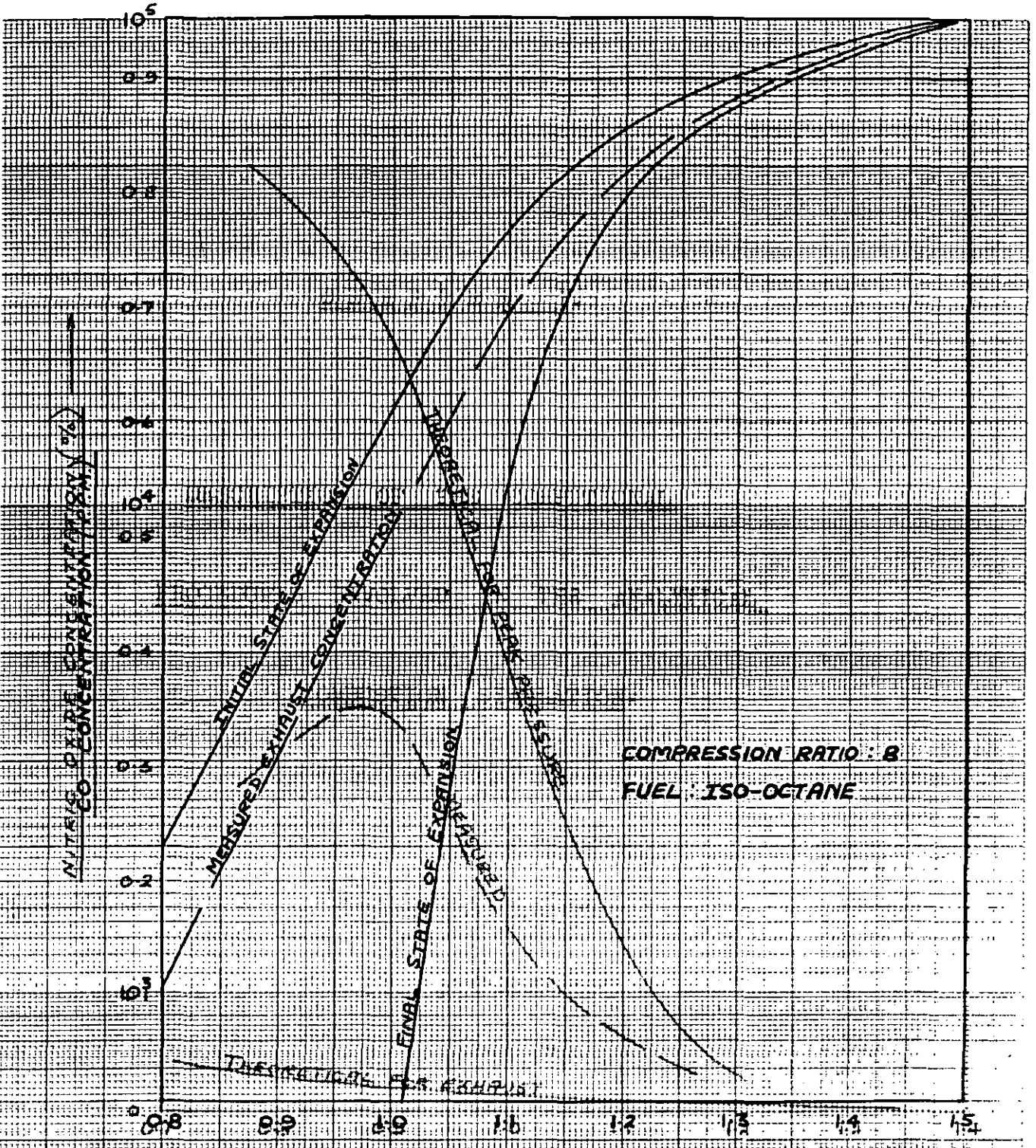

FIG. 2-5 — INFLUENCE OF EQUIVALENCE RATIO ON THEORETICAL AND EXPERIMENTAL CARBON MONOXIDE CONCENTRATIONS (FROM STARKMAN AND NEWHALL[85])

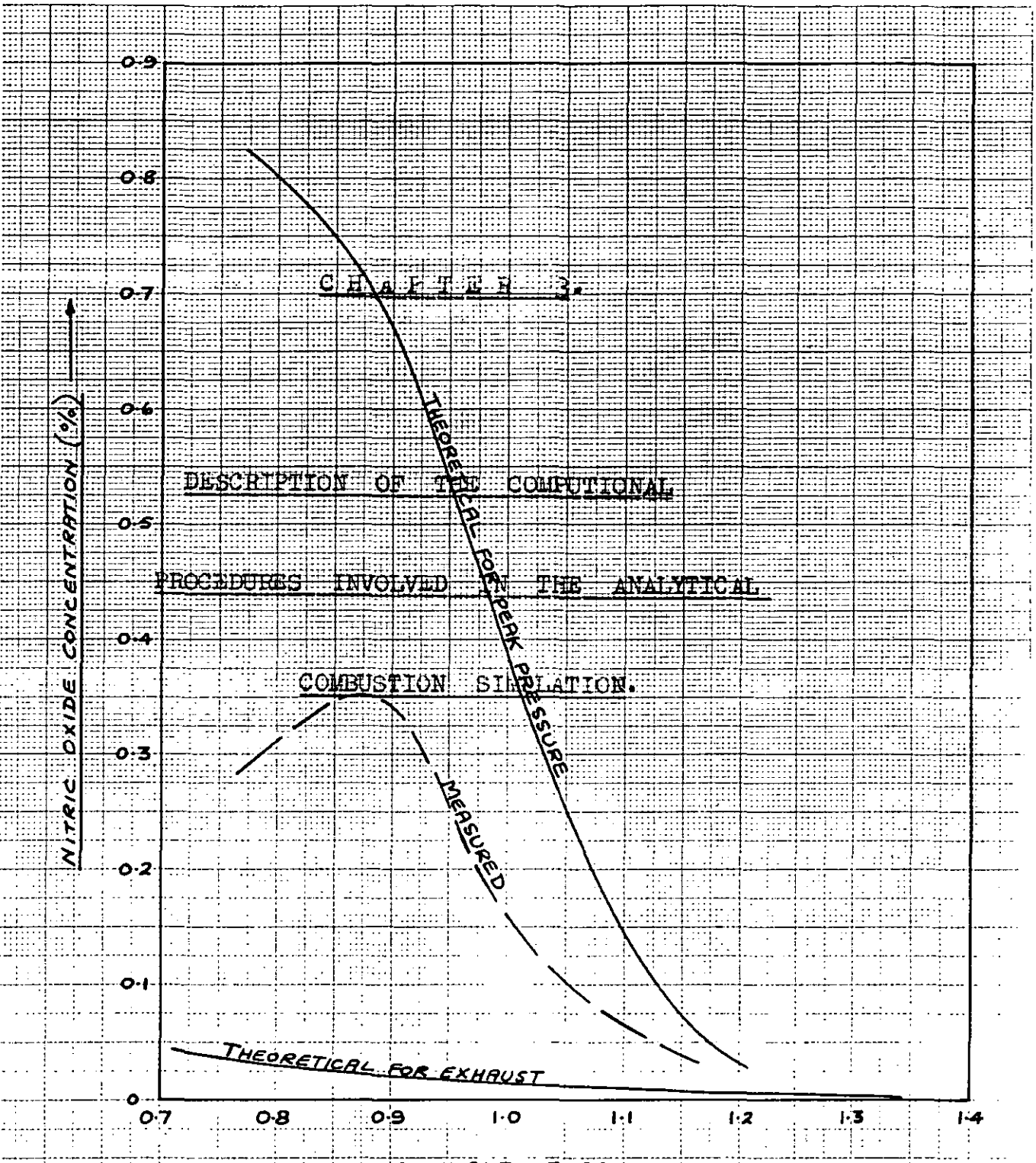

FIG. 2-6 — INFLUENCE OF EQUIVALENCE RATIO ON THEORETICAL AND EXPERIMENTAL NITRIC OXIDE CONCENTRATIONS (FROM STARKMAN[93])

CHAPTER 3.

DESCRIPTION OF THE COMPUTATIONAL PROCEDURES INVOLVED IN THE ANALYTICAL COMBUSTION SIMULATION.

C H A P T E R 3.

DESCRIPTION OF THE COMPUTIONAL PROCEDURES INVOLVED IN THE ANALYTICAL COMBUSTION SIMULATION.

CHAPTER 3.

DESCRIPTION OF THE COMPUTIONAL PROCEDURES INVOLVED IN THE ANALYTICAL COMBUSTION SIMULATION.

3.1. GENERAL.

The synthesis of internal combustion engine cycles by digital computers is now an established aid in the design and development of reciprocating engines[97,98]. Such syntheses involve stepwise calculations of the state of the charge in the engine cylinder from point to point around the cycle. The basic problem is to determine the state of the charge at crankangle $(\theta + \Delta\theta)$ knowing the state at crankangle θ. Here, $\Delta\theta$ is the step length being considered.

The problem can be approached in either of two ways:

i) by numerical integration of an appropriate set of non-linear differential equations.

ii) by estimating the values of the state properties at $(\theta + \Delta\theta)$, whence it is possible to evaluate the corresponding energy changes and exchanges during the step. The property values are finally adjusted by an iterative procedure until the energy balance required by the First Law of Thermodynamics is satisfied to some stipulated precision.

Non-linearities in the relationships between properties affect these two approaches in different ways. If the Euler method is adopted for the numerical integration, although the rates of change of contained energy, heat transfer and work transfer may be correctly related at θ, the overall energy balance need not be correct at $(\theta + \Delta\theta)$ because of non-linearities. Even with more elaborate in-

tegration procedures (e.g. Runge-Kutta), this balance may drift during a series of steps. Of course, a suitable choice of step length can reduce the imprecisions involved.

In the iterative technique, the evaluation of heat, work and mass exchanges during a step requires the choice of an interpolation procedure. Thus, although the changes may be inaccurately estimated, the overall energy balance between them is held.

Annand[99] attempted to establish a rational basis of selection between these two techniques from direct comparisons of computer programs developed to carry out identical operations. His conclusions were that:

i) iteration is always the faster method.

ii) iteration does not show the instabilities common with integration techniques.

iii) the integration method cannot be used for a charge exchange process involving two separate systems when heat transfer is incorporated. Without heat transfer, the method can be used. Such a process presents no difficulty with an iterative technique.

Thus, the iteration method is clearly to be preferred and is, in fact, used in this work.

As stated in Chapter 2, the period of the engine cycle under examination is that from inlet valve closure on the compression stroke to exhaust valve opening on the expansion stroke. Three distinct phases are, therefore, under consideration:

i) the compression of the charge from its physical and thermodynamic conditions at inlet valve closure to the predetermined crankangle at which the combustion commences.

ii) the combustion process itself lasting until all the charge has been completely burnt.

iii) the expansion of the products of combustion to the crankangle at which the exhaust valve opens.

The procedure in cycle synthesis work, as previously noted, is to divide the period under examination into a series of stages, each of which occupies a specified angle of crankshaft rotation. Each stage is associated with a change in the cylinder volume, with heat transfer from the charge to the cylinder walls or vice versa and, during combustion, with the conversion of the chemical energy of a part of the unburnt charge. A quantitative analysis of these processes allows the conditions in the cylinder at the end of any stage to be calculated from the known conditions at the start of that stage. These final values then provide the initial conditions for the succeeding stage. In this way, the calculation works round the cycle evaluating the properties of the working fluid at the end of every stage.

3.2. THE COMPRESSION PROCESS.

3.2.1. DESCRIPTION OF THE ANALYSIS DURING COMPRESSION.

The gas trapped in the cylinder when the inlet valve closes is regarded as a homogeneous mixture of air, gaseous fuel and residual exhaust gases left over from the previous cycle. This mixture is called the "unburnt charge." All chemical reactions in it are neglected and its composition

is calculated only once at the start of the cycle from the chemical composition of the fuel, the equivalence ratio of the charge and the mass fraction of residual exhaust gases present. Details of this calculation are given in Appendix 1.

The cycle calculation can start at any convenient point in the compression stroke when the unburnt charge fills the cylinder at known temperature and pressure. Inlet valve closure has been chosen as the starting point in this work. The revised temperature and pressure at the end of the first stage of step length $\Delta\theta$ must now be established. The volume of the cylinder is easily calculated from the dimensional configuration of the engine and the entropy at this point is estimated from the known initial value and from the quantity of heat transferred between the charge and the cylinder walls during the stage. Corresponding values of temperature and pressure cannot be found directly and an iterative procedure is used. An estimate is made of these values and corresponding values of entropy and volume are calculated. If these do not agree with the known final values of entropy and volume, corrections are calculated for the originally estimated values. In practice, the final value of the entropy is corrected in each iteration because the heat transfer depends on the temperature and pressure at the end of the stage.

The corrections to the temperature and pressure diminish rapidly as the iteration proceeds until they become small enough to satisfy the desired degree of accuracy. These last estimates then provide the initial values for the next stage. In this way, the calculation works through the compression process until the specified crankangle is reached

at which combustion begins. A step length of 10^0 of crankshaft rotation is used in this work.

3.2.2. THE COMPUTATIONAL PROCEDURES FOR STAGE CALCULATIONS DURING THE COMPRESSION PROCESS.

The contents of the engine cylinder consist entirely of unburnt charge during the compression process and its mass, m_u is assumed constant throughout.

The initial and final crankangles at the beginning and end of a stage are represented by the symbols θ_0 and θ_2. Likewise, all the remaining properties of the charge at the beginning and end of a stage are denoted by the subscripts (0) and (2) respectively.

The total cylinder volume at the end of a stage is calculated from the expression:

$$V_2 = \frac{\pi b^2}{4}\left[\frac{2r}{(CR-1)} + r + l - r\cos\theta_2 - \sqrt{l^2 - r^2\sin^2\theta_2}\right] \quad \ldots\ldots 3\text{-}1$$

It is also given by:

$$V_2 = m_u \cdot v_{u2} \quad \ldots\ldots 3\text{-}2$$

where v_{u2} is the specific volume (cc/gm) of the unburnt mixture at the end of a stage.

Heat transfer to or from the charge is assumed to take place reversibly. The reversible transfer of a small quantity of heat, ΔQ_u to a system, accompanied by a small finite change in temperature, results in a change in the specific entropy of the system given closely by:

$$\Delta s = \Delta Q_u / m_u T_m \quad \ldots\ldots 3\text{-}3$$

where Tm is the mean system temperature during the stage. Thus,

$$s_{u2} = s_{u0} + \frac{2\Delta Q_{uj}}{m_u(T_{u0} + T_{u2j})} \quad \ldots\ldots 3\text{-}4$$

where

S_{uz} is the specific entropy of the unburnt charge at the end of a stage.

S_{uo} is the specific entropy of the unburnt charge at the beginning of a stage.

T_{uo} is the unburnt charge temperature at the beginning of a stage.

T_{uzj} is the j'th estimate of the value of the unburnt charge temperature at the end of a stage. When the required degree of accuracy has been achieved in the iterative procedure, T_{uzj} adopts the final value T_{uz}.

Equations 3-2 and 3-4 are solved simultaneously for the pressure, P_z and unburnt charge temperature, T_{uz} at the end of a stage. As previously stated, this is accomplished by an iterative procedure in which successive estimates of these values are improved until the required accuracy is achieved. Thus, approximating these properties of the charge by the first few terms of a Taylor series expansion, we have

$$v_{uz} = v_{uzj} + (T_{uz} - T_{uzj}) \cdot \frac{\partial v_{uzj}}{\partial T} + (P_z - P_{zj}) \cdot \frac{\partial v_{uzj}}{\partial P} + \cdots\cdots \qquad 3\text{-}5$$

$$s_{uz} = s_{uzj} + (T_{uz} - T_{uzj}) \cdot \frac{\partial s_{uzj}}{\partial T} + (P_z - P_{zj}) \cdot \frac{\partial s_{uzj}}{\partial P} + \cdots\cdots \qquad 3\text{-}6$$

where v_{uzj}, s_{uzj} and P_{zj} are the j'th estimates of the required values.

On substitution of these expressions for v_{uz} and s_{uz} into Equations 3-2 and 3-4, two simultaneous equations are

obtained which can conveniently be expressed in the matrix form:

$$\begin{bmatrix} \frac{\partial s_{uzj}}{\partial T} & \frac{\partial s_{uzj}}{\partial P} \\ \frac{\partial v_{uzj}}{\partial T} & \frac{\partial v_{uzj}}{\partial P} \end{bmatrix} \begin{bmatrix} \Delta T_j \\ \Delta P_j \end{bmatrix} = \begin{bmatrix} s_{uo} + \frac{2.\Delta Q_{uj}}{m_u(T_{uo}+T_{uzj})} - s_{uzj} \\ V_2 - m_u.v_{uzj} \end{bmatrix} \quad \text{——— 3-7}$$

where $\Delta T_j = (T_{uz} - T_{uzj})$

and $\Delta P_j = (P_2 - P_{zj})$

Values of s_{uo} and V_2 are calculated from the known conditions at the beginning of the step and the known value of θ_2. Initial estimates are made of the final temperature and pressure and these are used to calculate the coefficients of the matrix. The equations are solved and improved estimates of the temperature and pressure are obtained thus:

$$T_{uz(j+1)} = T_{uzj} + \Delta T_j \quad \text{..... 3-8}$$

$$P_{z(j+1)} = P_{zj} + \Delta P_j \quad \text{..... 3-9}$$

These are then used to recalculate the coefficients of the matrix. This procedure is repeated until the calculated corrections to the temperature and pressure become acceptably small.

The values of ΔQ_{uj} are written with the subscript j because they are functions of both the initial and final states, and must, therefore, be evaluated within the iterative cycle. The techniques involved in the calculations of $\frac{\partial s_{uzj}}{\partial T}$, $\frac{\partial s_{uzj}}{\partial P}$ and $\frac{\partial v_{uzj}}{\partial T, \partial P}$ are described in Appendix 7.

3.3. THE COMBUSTION PROCESS.

3.3.1. DESCRIPTION OF THE ANALYSIS DURING COMBUSTION.

At ignition, a small quantity of charge is converted from an unburnt condition to a burnt condition, which process releases the chemical energy stored in the fuel in this

small portion of charge. Thus, the cylinder contents can no longer be regarded as a single homogeneous system but must now be treated as two separate sub-systems having equal pressures. One sub-system is called the 'unburnt fraction' and the other the 'burnt fraction.'

The burnt fraction is assumed to consist of a homogeneous mixture of the products of combustion which are regarded as a mixture of fifteen chemical species whose concentrations are governed by chemical equilibrium considerations. The method used to calculate these equilibrium concentrations is given in Chapter 6 of this report.

Each separate stage during the combustion phase occupies 2^{o} of crankshaft rotation and is subdivided into two successive steps:

i) the combustion step - this takes place adiabatically and at constant total volume. The new temperatures and pressure of the sub-systems resulting from the transfer of a small mass of charge from the unburnt to the burnt fraction are calculated. An iterative procedure is again used to obtain these from the known values of total volume, total energy and entropy.

ii) the piston movement and heat transfer step - this calculates the new temperatures and pressure resulting from the piston movement corresponding to the 2^{o} of crankshaft rotation and from the heat losses to the surroundings. An iterative procedure similar to that described for the compression process is used.

3.3.2. THE COMPUTATIONAL PROCEDURES FOR STAGE CALCULATIONS DURING THE COMBUSTION PROCESS.

The states of the two sub-systems at the start of a

given stage are defined by the common pressure P_o and the temperatures T_{uo} and T_{bo}. The initial masses of the sub-systems are given the symbols m_{uo} and m_{bo} whilst the initial crankangle is represented by θ_o. The mass of charge is assumed to remain constant throughout and complete combustion is considered. As just described, the processes undergone by the sub-systems during a complete combustion stage are treated in two steps.

During the combustion step, a known incremental mass, Δm, is transferred from the unburnt to the burnt fraction. The final states at the end of this step are denoted by the subscript (1).

In the piston movement and heat transfer step, the crankshaft is rotated through a known increment $\Delta\theta$ so that the total system volume undergoes a corresponding change. Certain quantities of heat ΔQ_u and ΔQ_b are transferred from the sub-systems during this period. The final states are denoted by the subscript (2).

The object is thus to determine P_1, T_{u1} and T_{b1} and, hence, P_2, T_{u2} and T_{b2}. These last values then define the states of the sub-systems at the end of the stage i.e. at the start of the succeeding stage.

The Combustion Step.

The total system mass is assumed to remain constant. Therefore,

$$m_{u1} = m_{uo} - \Delta m \quad \ldots\ldots 3\text{-}10$$

and $$m_{b1} = m_{bo} + \Delta m \quad \ldots\ldots 3\text{-}11$$

The reaction takes place at constant total volume.

$$\therefore V_1 = V_o \quad \ldots\ldots 3\text{-}12$$

The expression enabling the calculation of the total cylinder volume is given by Equation 3-1. This volume is

also given by

$$V_o = m_{ui} \cdot v_{ui} + m_{bi} \cdot v_{bi} \quad \text{3-13}$$

where v_{ui} and v_{bi} are the specific volumes of the unburnt and burnt fractions respectively.

In addition, the process is adiabatic and, consequently, the total internal energy, E, remains constant. Thus

$$E_i = E_o \quad \text{3-14}$$

and

$$E_o = m_{ui} \cdot e_{ui} + m_{bi} \cdot e_{bi} \quad \text{3-15}$$

where e_{ui} and e_{bi} are the specific internal energies of the unburnt and burnt fractions respectively.

One further equation is required to define the final states which relates to the interaction between the sub-systems. Here, one can assume either that:

i) any process in the burnt fraction is isentropic:

i.e. $s_{bi} = s_{bo}$

or that

ii) any process in the unburnt fraction is isentropic,

i.e. $s_{ui} = s_{uo}$

However, because at ignition the initial value of the specific burnt entropy is not known, the condition

$$s_{ui} = s_{uo} \quad \text{3-16}$$

must be used since s_{uo} is known at this time.

The equations 3-13, 3-15 and 3-16 must be solved simultaneously for P_i, T_{ui} and T_{bi}. As before, this is done by an iterative procedure in which successive estimates of these values are improved until the required accuracy is achieved. Thus, approximating these properties of the sub-systems by the first few terms of a Taylor series expansion, we have

$$v_{ui} = v_{uij} + (T_{ui} - T_{uij}) \cdot \frac{\partial v_{uij}}{\partial T} + (P_i - P_{ij}) \cdot \frac{\partial v_{uij}}{\partial P} + \ldots\ldots \qquad 3\text{-}17$$

$$v_{bi} = v_{bij} + (T_{bi} - T_{bij}) \cdot \frac{\partial v_{bij}}{\partial T} + (P_i - P_{ij}) \cdot \frac{\partial v_{bij}}{\partial P} + \ldots\ldots \qquad 3\text{-}18$$

$$e_{ui} = e_{uij} + (T_{ui} - T_{uij}) \cdot \frac{\partial e_{uij}}{\partial T} + \ldots\ldots \qquad 3\text{-}19$$

$$e_{bi} = e_{bij} + (T_{bi} - T_{bij}) \cdot \frac{\partial e_{bij}}{\partial T} + (P_i - P_{ij}) \cdot \frac{\partial e_{bij}}{\partial P} + \ldots\ldots \qquad 3\text{-}20$$

$$s_{ui} = s_{uij} + (T_{ui} - T_{uij}) \cdot \frac{\partial s_{uij}}{\partial T} + (P_i - P_{ij}) \cdot \frac{\partial s_{uij}}{\partial P} + \ldots\ldots \qquad 3\text{-}21$$

On substitution of these expressions for v_{ui}, v_{bi}, e_{ui}, e_{bi} and s_{ui} into Equations 3-13, 3-15 and 3-16, three simultaneous equations are obtained which can be conveniently expressed in the matrix form:

$$\begin{bmatrix} \frac{\partial s_{uij}}{\partial T} & 0 & \frac{\partial s_{uij}}{\partial P} \\ m_{ui}\frac{\partial e_{uij}}{\partial T} & m_{bi}\frac{\partial e_{bij}}{\partial T} & m_{bi}\frac{\partial e_{bij}}{\partial P} \\ m_{ui}\frac{\partial v_{uij}}{\partial T} & m_{bi}\frac{\partial v_{bij}}{\partial T} & \sum_{u,b} m_i \frac{\partial v_{ij}}{\partial P} \end{bmatrix} \begin{bmatrix} T_{ui} - T_{uij} \\ T_{bi} - T_{bij} \\ P_i - P_{ij} \end{bmatrix} = \begin{bmatrix} s_{uo} - s_{uij} \\ E_o - \sum_{u,b} m_i e_{ij} \\ V_o - \sum_{u,b} m_i v_{ij} \end{bmatrix} \qquad 3\text{-}22$$

The quantities v_{uij}, v_{bij}, T_{uij}, T_{bij}, e_{uij}, e_{bij} and s_{uij} are the j'th estimates of the required values v_{ui}, v_{bi}, T_{ui}, T_{bi}, e_{ui}, e_{bi} and s_{ui} respectively.

The procedure consists of evaluating s_{uo}, E_o and V_o at the known conditions at the start of the stage. First estimates are then made of the final temperatures and pressure. These are used to calculate the burnt fraction composition as described in Chapter 6. The coefficients of

the matrix can then be evaluated using the methods outlined in Appendix 7. The three simultaneous equations are then solved and the resulting values of $(T_{u1} - T_{uij})$, $(T_{b1} - T_{bij})$ and $(P_1 - P_{ij})$ used to obtain improved estimates as follows:

$$T_{u1(j+1)} = T_{uij} + (T_{u1} - T_{uij}) \quad \text{3-23}$$

$$T_{b1(j+1)} = T_{bij} + (T_{b1} - T_{bij}) \quad \text{3-24}$$

$$P_{1(j+1)} = P_{ij} + (P_1 - P_{ij}) \quad \text{3-25}$$

These improved estimates are used to recalculate the burnt fraction composition and, hence, the coefficients of the matrix. This iteration is repeated until the calculated values of $(T_{u1} - T_{uij})$, $(T_{b1} - T_{bij})$ and $(P_1 - P_{ij})$ become acceptably small.

The Piston movement and Heat Transfer Step.

The masses of the sub-systems are assumed constant throughout this step. Thus,

$$m_{u2} = m_{u1} \quad \text{3-26}$$

$$m_{b2} = m_{b1} \quad \text{3-27}$$

The final crankangle is given by

$$\theta_2 = \theta_1 + \Delta\theta \quad \text{3-28}$$

and the corresponding final total volume by the expression in Equation 3-1. It is also given by

$$V_2 = m_{u2} \cdot v_{u2} + m_{b2} \cdot v_{b2} \quad \text{3-29}$$

As for the compression process, heat transfer is assumed to take place reversibly to both sub-systems. Thus, for the processes in the burnt and the unburnt fractions:

$$s_{b2} = s_{b1} + \frac{2 \cdot \Delta Q_{bj}}{m_{b2} \cdot (T_{b1} + T_{b2j})} \quad \text{3-30}$$

$$s_{u2} = s_{u1} + \frac{2 \cdot \Delta Q_{uj}}{m_{u2} (T_{u1} + T_{u2j})} \quad \text{3-31}$$

The equations 3-29, 3-30 and 3-31 must be solved simultaneously for P_2, T_{u2} and T_{b2}. This is achieved by first of

all expressing the quantities v_{uz}, v_{bz}, s_{uz} and s_{bz} as Taylor series expansions as follows:

$$v_{uz} = v_{uzj} + (T_{uz} - T_{uzj}) \cdot \frac{\partial v_{uzj}}{\partial T} + (P_z - P_{zj}) \cdot \frac{\partial v_{uzj}}{\partial P} + \ldots\ldots \qquad 3\text{-}32$$

$$v_{bz} = v_{bzj} + (T_{bz} - T_{bzj}) \cdot \frac{\partial v_{bzj}}{\partial T} + (P_z - P_{zj}) \cdot \frac{\partial v_{bzj}}{\partial P} + \ldots\ldots \qquad 3\text{-}33$$

$$s_{uz} = s_{uzj} + (T_{uz} - T_{uzj}) \cdot \frac{\partial s_{uzj}}{\partial T} + (P_z - P_{zj}) \cdot \frac{\partial s_{uzj}}{\partial P} + \ldots\ldots \qquad 3\text{-}34$$

$$s_{bz} = s_{bzj} + (T_{bz} - T_{bzj}) \cdot \frac{\partial s_{bzj}}{\partial T} + (P_z - P_{zj}) \cdot \frac{\partial s_{bzj}}{\partial P} + \ldots\ldots \qquad 3\text{-}35$$

The values v_{uzj}, v_{bzj}, T_{uzj}, T_{bzj}, P_{zj}, s_{uzj} and s_{bzj} are the j'th estimates of v_{uz}, v_{bz}, T_{uz}, T_{bz}, P_z, s_{uz} and s_{bz} respectively. The expressions 3-32 to 3-35 are substituted into Equations 3-29, 3-30 and 3-31 to provide the following three simultaneous equations expressed in matrix form:

$$\begin{bmatrix} \frac{\partial s_{uzj}}{\partial T} & 0 & \frac{\partial s_{uzj}}{\partial P} \\ 0 & \frac{\partial s_{bzj}}{\partial T} & \frac{\partial s_{bzj}}{\partial P} \\ m_{uz} \cdot \frac{\partial v_{uzj}}{\partial T} & m_{bz} \cdot \frac{\partial v_{bzj}}{\partial T} & \sum_{u,b} m_z \frac{\partial v_{zj}}{\partial P} \end{bmatrix} \begin{bmatrix} T_{uz} - T_{uzj} \\ T_{bz} - T_{bzj} \\ P_z - P_{zj} \end{bmatrix} =$$

$$\begin{bmatrix} s_{u1} + \frac{2 \cdot \Delta Q_{uj}}{m_{uz}(T_{u1} + T_{uzj})} - s_{uzj} \\ s_{b1} + \frac{2 \cdot \Delta Q_{bj}}{m_{bz}(T_{b1} + T_{bzj})} - s_{bzj} \\ V_z - \sum_{u,b} m_z \cdot v_{zj} \end{bmatrix} \qquad 3\text{-}36$$

Values of S_{u1}, S_{b1} and V_2 are calculated from the known conditions at the beginning of the step and the known value of θ_2. Initial estimates are made of the final temperatures and pressure, and these are used to calculate the burnt fraction composition and, hence, the coefficients of the matrix utilising the techniques in Chapter 6 and Appendix 7. The equations are solved and improved estimates of the temperatures and pressure are obtained from

$$T_{u2(j+1)} = T_{u2j} + (T_{u2} - T_{u2j}) \qquad 3\text{-}37$$

$$T_{b2(j+1)} = T_{b2j} + (T_{b2} - T_{b2j}) \qquad 3\text{-}38$$

$$P_{2(j+1)} = P_{2j} + (P_2 - P_{2j}) \qquad 3\text{-}39$$

These are then used to recalculate the burnt fraction composition and the coefficients of matrix 3-36. This iteration is repeated until the calculated corrections to the temperatures and pressure become acceptably small when the final estimations become the initial values for the next combustion step.

The values of ΔQ_{uj} and ΔQ_{bj} are written with the subscript (j) because they are functions of both the initial and final states and, thus, must be evaluated within the iterative cycle.

3.4. THE EXPANSION PROCESS.

3.4.1. DESCRIPTION OF THE ANALYSIS DURING EXPANSION.

When all the unburnt charge has been completely burnt, the expansion phase of the engine cycle begins. This process is conducted in successive steps of 10^{o} of crankshaft rotation in this work and each step is now associated only with piston movement and heat transfer. The calculations

are very similar to those already described for the compression process except that the unburnt charge considerations are replaced by those of the burnt charge. Thus, dissociation effects are included. The evaluations continue until the exhaust valve opens.

3.4.2. THE COMPUTATIONAL PROCEDURES FOR STAGE CALCULATIONS DURING THE EXPANSION PROCESS.

The cylinder contents now contain exclusively burnt combustion products and the mass of charge, m_b is assumed constant throughout the process. The crankangles at the beginning and end of a stage are denoted by θ_0 and θ_2 where

$$\theta_2 = \theta_0 + \Delta\theta$$

The initial states at the beginning of a stage are again defined by the subscript (o) and the final states by the subscript (2).

The total cylinder volume at the end of a stage, V_2, can be calculated from the expression in Equation 3-1 and also from

$$V_2 = m_b v_{b2} \qquad \text{3-40}$$

Heat Transfer is assumed again to take place reversibly so that

$$s_{b2} = s_{bo} + \frac{2.\Delta Q_{bj}}{m_b(T_{bo}+T_{b2j})} \qquad \text{3-41}$$

in which T_{b2j} is the j'th estimate of the value of the temperature at the end of a stage.

Equations 3-40 and 3-41 have to be solved simultaneously for P_2 and T_{b2}. As before, an iterative procedure is used in which successive estimates of these values are improved until the required accuracy is achieved. The properties of the

charge v_{bz} and s_{bz} are approximated by the first few terms of a Taylor series expansion to give:

$$v_{bz} = v_{bzj} + (T_{bz} - T_{bzj}) \cdot \frac{\partial v_{bzj}}{\partial T} + (P_z - P_{zj}) \cdot \frac{\partial v_{bzj}}{\partial P} + \ldots \quad 3\text{-}42$$

$$s_{bz} = s_{bzj} + (T_{bz} - T_{bzj}) \cdot \frac{\partial s_{bzj}}{\partial T} + (P_z - P_{zj}) \cdot \frac{\partial s_{bzj}}{\partial P} + \ldots \quad 3\text{-}43$$

On substitution of these two expressions into Equations. 3-40 and 3-41, two simultaneous equations are obtained. In matrix form, these are:

$$\begin{bmatrix} \frac{\partial s_{bzj}}{\partial T} & \frac{\partial s_{bzj}}{\partial P} \\ \frac{\partial v_{bzj}}{\partial T} & \frac{\partial v_{bzj}}{\partial P} \end{bmatrix} \begin{bmatrix} T_{bz} - T_{bzj} \\ P_z - P_{zj} \end{bmatrix} = \begin{bmatrix} s_{b_o} + \frac{2.\Delta Q_{bj}}{m_b(T_{b_o} + T_{bzj})} - s_{bzj} \\ V_z - m_b . v_{bzj} \end{bmatrix} \quad 3\text{-}44$$

Values of s_{bo} and V_z are calculated from the known conditions at the start of a stage and from the known value of Θ_z. Initial estimates are made of the final temperature and pressure and these are used to calculate the burnt fraction composition and, hence, the coefficients of the matrix by utilising the techniques in Chapter 6 and Appendix 7. The equations are solved and improved estimates of the temperature and pressure obtained from

$$T_{bz(j+1)} = T_{bzj} + (T_{bz} - T_{bzj}) \quad 3\text{-}45$$

$$P_{z(j+1)} = P_{zj} + (P_z - P_{zj}) \quad 3\text{-}46$$

This process is repeated until the calculated corrections to the temperature and pressure become acceptably small. The value of ΔQ_{bj} is written with the subscript (j) because it is a function of both the initial and final states and must, therefore, be evaluated within the iterative cycle.

3.5. COMPUTER PROGRAMMING OF THE ANALYTICAL PROCEDURES.

The above analytical procedures have been programmed for use on a digital computer as is shown in the main part of the complete program listing in Appendix 8. This Appendix also contains a Flow Diagram showing the manner in which the computer program has been built up and some of the main considerations and techniques used.

C H A P T E R 4.

THE RATE OF FLAME PROPAGATION.

CHAPTER 4.

THE RATE OF FLAME PROPAGATION.

4.1. INTRODUCTION.

Since the analytical model postulated in Chapter 3 assumes a finite period of time for the combustion of the charge to be completed in, it is necessary to be able to calculate the mass of charge burnt at any particular point of the flame travel in the combustion chamber. This is achieved from a knowledge of the rate of flame propagation, the volume of charge consumed by the flame during a particular interval of time and the density of the unburnt charge.

The apparent rate of flame propagation in an engine is very high. As stated in Chapter 2, this is due to both the rate of the reaction and the expansion of the burnt gases. The fundamental quantity to be investigated is, therefore, the flame front motion due to the reaction only i.e. the flame propagation relative to the unburnt gas, U_T. The remainder of this Chapter is devoted to obtaining a general expression for this quantity in order that calculations can be made of its magnitude under the many varying conditions of the charge e.g. equilence ratio, temperature etc.

The derivation of such an expression of necessity involves a number of simplifying assumptions, the most serious of which are those of steady state and one dimensionality. Thus, it must be recognized from the outset that any equation used to represent the rate of flame travel in an engine can only be approximate. Its validity may only be determined by a direct comparison of calculated

and experimental burning rates. Alternatively, this could be achieved indirectly through a comparison of calculated and experimental pressure-time diagrams. Both these approaches are used in this work as a means of comparison (see Results).

It is well known from observed and calculated rates of flame propagation in spark ignition engines that combustion is of the turbulent type. Thus, the starting off point must be to consider in some detail the fundamentals of turbulence and turbulent flame propagation in engine cylinders.

4.2. TURBULENCE AND TURBULENT FLAME PROPAGATION IN SPARK IGNITION ENGINE COMBUSTION CHAMBERS.

4.2.1. TURBULENCE GENERATION.

It has been known for many years that the complex, unsteady flow existing in engine cylinders during combustion results from the following sources:

i) the flow of the charge through the carburettor, the inlet manifold and the inlet valve during the induction stroke.

ii) the mixing of streams of differing velocities in the cylinder during induction.

iii) localised flow disturbances originating during compression and combustion. These are due mainly to the contour of the combustion chamber.

iv) the mass movement of the unburnt charge immediately ahead of the flame front during combustion. This is the so-called "flame turbulence" and it can be visualized as follows. During the thermal expansion of the hot gases in the combustion zone, every element of the

combustion wave introduces into the unburnt gas a velocity component normal to it. In turbulent flames, these small elements fluctuate at random and, in so doing, they impart a supplementary turbulent effect to the unburnt gas. It is this which constitues flame generated turbulence.

4.2.2. THE NATURE OF THE TURBULENT FLOW.

The nature of the turbulent flow can generally be subdivided into three distinct effects, each of which has a varying degree of influence on the overall turbulent flame speed. These are:

a) swirl.

b) large-scale turbulence.

c) small-scale turbulence.

Swirl.

This is a large-scale mass motion of the charge. It takes place in an orderly fashion and it usually has some eddying or turbulence associated with it (see Fig. 4-1).

There are several ways in which a swirl can be generated in an engine cylinder. The most common is by the use of shrouded, or masked, intake valves and/or the use of inlet ports that direct the air flow in a tangential direction to the cylinder walls (see Figs. 4-5 to 4-8). Another method is to force the air through a tangential passage into a separate swirl chamber during the compression stroke (Fig. 4-2). A well-defined swirl can also be generated by a "squish" action. Normally, the combustion space is incorporated in the piston here (Fig. 4-3). Sometimes, squish is used in combination with an inlet vortex in order to

either reinforce the rotation or to produce a toroidal flow pattern (Fig. 4-4).

The general effects of swirl in an engine have been known for some time, particularly to those designing direct injection combustion chambers.[101] The early work of Ricardo showed that, if the air in the cylinder of a direct injection engine was motionless, only a small proportion of the fuel would find sufficient oxygen for combustion. This is because it is impossible to distribute the fuel droplets uniformly throughout the combustion space. An orderly and controlled air movement is required in order to bring a continuous supply of fresh air to each burning droplet and to sweep away the products of combustion which otherwise would tend to suffocate it.

Some recent fundamental studies on the mapping of airflow patterns in engines with induction swirl have been carried out by Willis et al[102]. A water analogue model was constructed and neutral density beads used to define the swirl pattern. This work revealed that swirl is characterized by solid body rotation near the centre and potential flow in the outer portions of the cylinder. During induction, the vortex generated by the swirl was unstable and non-symmetrical with its centre of rotation offset from the cylinder axis and forming a helix extending the length of the cylinder. Figs. 4-5, 4-6, 4-7 and 4-8 (taken from this work[102]) give a clear indication of how the flow into the cylinder generates different kinds of swirl when different mask angles are used.

In carburetted, spark-ignition engines, such large-scale swirl is not really very desirable for four main

reasons:

i) in order for a flame to propagate through an externally prepared, pre mixed charge, a condition of general and indiscriminate turbulence is required to act on the flame front. An orderly, large scale flow merely tends to displace the flame bodily without much distortion of the flame surface being apparent.

ii) it can greatly increase the heat losses from the engine.

iii) its generation may adversely affect the volumetric efficiency of the engine.

iv) under some conditions, it can lead to rough and irregular combustion due to the rates of pressure rise being considerably increased. A possible mechanism for this effect has been suggested by Patterson[51] who proposes that the swirl shears the flame kernel just after ignition and, in so doing, increases its flame front area (see Fig. 4-9). This increases the surface over which combustion reactions occur and thus accelerates the burning of the charge.

Most spark ignition engines, however, have a certain amount of a general charge rotation or a mean flow movement in a particular direction but it is considerably less than would be induced by such large, directed air flows as discussed above. The amount depends on the inlet valve location and design and on the porting configuration.

The effects of a large swirl on flame propagation in a spark ignition engine have been analysed by Johnson[103]. He used ionization gaps and a radiation detector to determine flame travel data in a multi-hole CFR engine. With swirl

induced by a masked valve, he found that the centre of rotation of the charge did not coincide with the geometric centre, which observation substantiates the results of Willis et al[102] already referred to. There also appeared to be a force acting on the flame tending to move it in a curved path towards the centre, in much the same way as a centrifuge moves less dense particles towards the centre and more dense particles to the outside. Johnson concluded that this centrifugal force resulted from the flame being approximately one-third the density of the unburnt gas. The swirling burnt gas was found to follow the same path irrespective of how fast the swirl was.

Small and large scale turbulence.

In this context, turbulence is defined as a confustion of whirls and eddies having no general direction of flow (Fig. 4-10). It may or may not be superimposed on a swirl or a mean motion. As previously mentioned, turbulence of the charge in the combustion chamber arises mainly from its flow into the cylinder during induction. It is a consequence of eddy formation on obstacles (e.g. inlet valves and ports) and the shear flows set up due to the retarding effect of the cylinder walls and the mixing of streams of different velocities.

The chief characteristics of turbulent motion are its 3-dimensionality and randomness. Due to these, it exhibits a certain similarity to molecular motion and has similar transport properties. However, it is vastly more complex in its nature because the turbulent quantities corresponding to the molecular mass and the mean free path are not constants of the medium. In particular, the variable eddies and

vortices, which constitute the turbulent motion, are not all of the same size and velocity (see Fig. 4-10) but are distributed over wide ranges.

Because the masses of the fluid elements and the average distances they move are much larger than the molecular mass and the mean molecular free path, turbulent transport of mass and momentum is several magnitudes larger than molecular transport. It is this property of turbulence which is important in its utilization in flow phenomena, heat transfer, mixing and flame propagation.

A typical oscillogram, taken with a hot wire anemometer placed in such a turbulent field as exists in Fig. 4-10, might indicate the fluctuations, as a function of time in the x-direction, shown in Fig. 4-11. It should be noted that such fluctuations also occur in the y and z directions. The instantaneous velocity, u_i is seen to fluctuate abouts its mean value $\bar{u}$ with respect to both time and spatial direction. Theoretically, it is convenient to split the instantaneous velocities u_i, v_i and w_i into their time average components $\bar{u}$, $\bar{v}$ and $\bar{w}$ and their momentary fluctuation components u', v' and w'. Thus,

$$u_i = \bar{u} + u'$$

$$v_i = \bar{v} + v'$$

and $$w_i = \bar{w} + w'$$

These relationships were developed by Osborne Reynolds in connection with his investigation of turbulent flow.

In a theoretical analysis of fluid turbulence, the instantaneous velocity components must be expressed mathematically in terms of both spatial coordinates and time. These functions have been found to be so extremely compli-

cated however as to defy accurate description. It thus appears that the theoretical solution requires the application of statistics. On this basis, since the root mean square (r.m.s.) value of the turbulent velocity fluctuations is a definite quantity in a given turbulent field and represents a suitable statistical measure of the magnitude of the fluctuations, it is termed the <u>intensity</u> or <u>level</u> of the turbulence. Thus,

the intensity of turbulence = $\sqrt{u'^2}$ for isotropic flow.

Sometimes, the ratio of this value to a mean flow velocity (i.e. the relative intensity) is termed the intensity. That is,

intensity or relative intensity = $\frac{\sqrt{u'^2}}{U}$ for isotropic flow.

When the turbulence is not isotropic, the mean value of the three fluctuating components may be used so that

the intensity or relative intensity = $\frac{1}{U}\left(\frac{u'^2 + v'^2 + w'^2}{3}\right)^{\frac{1}{2}}$

The <u>scale</u> of turbulence is considered to be the dimension of a typical eddy or vortex making up the turbulent field. Even though these eddies vary in size over a considerable range, it is possible to conceive of some typical or average size. In practice, two specific scales are defined, one representing the size of the larger eddies and the other the size of the smaller eddies (Fig. 4-10). These are known as:

a) the macroscopic scale (large-scale turbulence).

b) the microscopic scale (small-scale turbulence).

When considering a turbulent field, it is important to compare the scale of the turbulence to the size of the body in which the field is contained. Both scales are present in

the turbulent flow in a reciprocating engine combustion chamber since states of macroscopic and microscopic turbulence cannot be produced separately without great difficulty.

In this context also, the mixing length in turbulent flow is defined as the average distance over which a fluid element moves before it loses its identity by mixing with the surrounding fluid.

Several classifications of turbulent flows exist[104]. The more important of these are:

a) homogeneous turbulence - in which the scale and intensity of the turbulent field are independent of the co-ordinate position.

b) isotropic turbulence - where the scale and intensity are independent of direction. Here, the intensity of the turbulent fluctuations is the same in all directions.

In the cylinders of internal combustion engines, isotropic and homogeneous turbulence are ideal cases since usually the fluctuations are completely random in magnitude, direction and position.

A turbulent field can be further defined in terms of the velocities of motion of the individual eddies. This criterion is termed the spectrum of turbulence and it represents the average fraction of the kinetic energy of the turbulent motion, $F(f)$, between, for example, the fluctuating frequencies f and $(f + df)$ — see Fig. 4-12. The availability of spectrum presentations of turbulence information permit one to consider the manner in which the energy of turbulence is distributed among the various eddy sizes.

Thus, since the lower frequencies indicate the larger eddies or scales, and vice versa, inspection of Fig. 4-12 indicates that much of the energy is associated with the large eddies. Above some frequency, or below some size, the energy is seen to drop off very rapidly with increase in frequency and decrease in size or scale. The indication is, therefore, that the kinetic energy is communicated to the turbulent motion from the mean flow (if present) by the large scale eddies. From these, it is transferred down the scales from the larger to the smaller eddies where it is finally dissipated into heat by the action of viscous friction. This transference of energy has been found to occur rather rapidly so that the size of the turbulent eddies decays quite quickly with time.

4.2.3. ACTUAL TURBULENCE MEASUREMENTS IN ENGINE CYLINDERS.

From the foregoing, it is clear that the basic problem in determining the effects of the confused flow pattern in the engine cylinder on the combustion of fuel-air mixtures is primarily one of characterizing the mixture motion. This entails the separation of the total effect into its various sub-effects and the determination of the influence of each of these on the overall flame speed. In this way, it may then be possible to find the degree of influence of:

a) the mean mixture motion (or swirl) if present.

b) the large scale turbulence.

c) the small scale turbulence.

This ideal involves the direct measurement of air currents in the cylinders of piston engines. Very little fundamental work has been carried out on such investigations,

however, in spite of their great influence on the velocity and efficiency of the combustion process and on the design of suitable combustion chambers. The dearth of such investigations is largely explained by the great difficulties encountered in the measurement of unsteady flow. The results of the few workers who have attempted such measurements will thus be quoted in some detail in this report.

Several techniques are available including hot wire anemometry, the use of electrical discharges[105,106] and laser doppler methods[107]. However, to date, only hot wire or hot film anemometry has been used to measure the small and large scale turbulence in engine cylinders. These instruments have the advantage of a very low inertia so that the turbulent pulsations are not disrupted and the flow itself is not disturbed to any marked degree.

The principle of operation of this instrument in its application to gas velocity measurements depends upon the relationship between the forced transfer of heat from a heated, cylindrical filament and the velocity of the flow in which it is placed. A discussion of the construction, development and operation of a typical hot-wire anemometer for use in piston engines is given in Ref. 108.

It should be realized that the results of the few people who have carried out turbulence measurements in engine cylinders refer only to the particular engine and combustion chamber configuration used by them in their work. The results are not transferrable to other engine designs although one can hypothesize that many of the trends noted are common to all engine-combustion chamber relationships.

The Turbulence Measurements of Molchanov.

In 1953, Molchanov completed some work on determinations of the dynamic state of the charge in an engine cylinder during the induction stroke, the compression stroke and the period of the engine cycle during which flame propagation occurs viz. up to approximately 30° after top dead centre. He used an instrument having only a single hot wire which meant that direct measurements of turbulence in three coordinates could not be made. It did, however, enable measurements to be made of flow velocities and fluctuations of these flow velocities (with frequencies up to 2000 cycles/second) under the prevailing conditions of varying temperatures and pressures. A variable compression ratio engine was used with a cylindrical combustion chamber. The engine was motored in the 'cold' condition and no combustible mixture was supplied.

During Induction.

This period was considered to extend from the opening to the closing of the inlet valve. The noted variation in gas velocities with crankangle rotation at certain points in the combustion space are shown in Fig. 4-13. There is seen to be a sharp increase in flow velocity when the inlet valve is first opened which is followed by quite a sharp decrease to a periodic oscillation recorded simultaneously at all the measured points in the combustion chamber. It is feasible to attribute these oscillations to inlet pipe tuning effects. The maximum flow velocities appear to occur when the piston speed is greatest. Conversely, they tend to decrease as the piston slows down on approaching bottom dead centre.

During compression.

During this stage of the cycle, Molchanov hypothesized that the high velocity streams during induction were destroyed and converted into a swirl motion. This, however, was not substantiated by measurements he made of flow velocities at neighbouring points in the combustion space when the hot wire was rotated through 360°. These indicated:

a) the absence of any large scale, directed flow.

b) evidence of local swirl currents or vortices as in Fig. 4-10. This conclusion was drawn from the regularly repeated transition of local flow velocities from maximum to minimum for two adjacent positions of the filament. This indicated the presence of locally directed streams of different magnitudes at neighbouring points in the combustion chamber.

On this evidence, therefore, it was postulated that the flow during compression consisted entirely of uniform eddies of varying scales with no constant direction of flow. The conception of a relative intensity of turbulence, $\frac{\sqrt{u'^2}}{U}$, under these conditions no longer makes sense: only the absolute intensity, $\sqrt{u'^2}$, can be contemplated.

Treating the measurements of the large scale turbulent eddies as the mean velocity of the flow, the results shown in Fig. 4-14 were obtained for variation of this quantity with change in compression ratio at the point 2 in Fig. 4-13. The following conclusions can be drawn:

i) on closure of the inlet valve, the gas flow velocities fall sharply and become approximately equal to the mean piston speed for all compression ratios.

ii) the flow velocities vary in different ways as a function of compression ratio up to about 20° before top dead centre. After this point, during the period corresponding to flame propagation, it appears that they decrease slightly as the compression ratio is increased.

iii) the maximum gas velocities are attained at the same point in the cycle for all compression ratios viz. at 20° B.T.D.C. A systematic decrease is observed from this point onwards throughout the flame propagation period however.

Molchanov, perhaps erroneously, concluded that the "variation of compression ratio within wide limits had practically no effect on the velocities of ordered gas streams in the combustion chamber." This is certainly true up to 20° B.T.D.C. However, if one considers the velocities at T.D.C. in Fig. 4-14, it will be noted that the difference in flow velocities between compression ratios of 6 and 12 is approximately 0.7 metres/second. Compared with the mean flow velocity at this point of 2.5 metres/second, this variation achieves quite large proportions of some 28%. The effect of this on the burning velocities in a firing engine can clearly not be ignored.

By filtering out the low frequency flow velocities so as just to record the high frequency fluctuations, the measurements in Fig. 4-15 were obtained. It can be seen that there is an increase in the magnitudes of the fluctuation velocities during the flame propagation period. At some points, these are considerably greater than the maximum velocities of the large scale motion. The reasons for this

are given later.

The Turbulence Measurements of Semenov[110].

Molchanov's work was followed in 1958 by Semenov's findings on the same problem. Again the measuring instrument was a hot-wire anemometer with a single wire which means that the results are subject to the same criticisms as Molchanov's regarding the inability to measure flow in the co-ordinates. A single cylinder, variable compression ratio C.F.R. engine having a cylindrical combustion chamber was used and this was motored 'cold' with no combustible mixture supplied.

The arrangement of the measuring hot-wire filament and the correction element (which compensates for the varying gas temperatures) in the combustion chamber is shown in Fig. 4-16. The measuring element was free to move along the bore diameter between the valves at a distance of 10 mm from the top of the chamber. It could also be rotated about its axis.

Semenov defined three velocities to describe the aerodynamic conditions in the cylinder:

i) a directional velocity, u, - this is the flow velocity averaged over a measured interval (about 24^{o} of crank-angle) for one cycle. It involves eddies with frequencies below 300 cycles/second.

ii) an average velocity, $\bar{u}$, - this is the flow velocity, measured over the same cycle interval as for the directional velocity but averaged for several cycles. It was necessary to define an average velocity because the unsteady flow in engine cylinders gives rise to

continual variations in the magnitude and direction of the directional velocity at a given point in the cycle over successive cycles. Fig. 4-17[108] shows this phenomenon to good effect.

iii) a fluctuating velocity, u', - this is the deviation of the instantaneous velocity from the directional velocity at a given point in a cycle. The root mean square value of the fluctuating velocity, $\sqrt{\bar{u}'^2}$, calculated over a great many cycles was considered a measure of the intensity of turbulence. The lower limit of the frequency range for $\sqrt{\bar{u}'^2}$ recordings was chosen rather arbitrarily to be 300 c/s and the upper limit to be 6200 c/s. It was considered that only the average values $\bar{u}$ and $\sqrt{\bar{u}'^2}$ could serve as objective criteria of the gas flow in engine cylinders.

During Induction.

The variation in $\bar{u}$ with crankangle rotation at various points in the combustion space is shown in Fig. 4-18. These results give the same kind of indicative effects as those of Molchanov (Fig. 4-13). The periodic oscillations are again present because of the accoustical oscillations of the gas column in the intake pipe.

The marked velocity differences between neighbouring points in the combustion chamber provide evidence of the jet nature of the gas flow during intake. These differences ensure the formation of considerable velocity gradients during this phase of the cycle, the magnitudes of which reach thousands per second at the limits of the jet.

Second maxima of $\bar{u}$ are observed at points M in Fig. 4-18.

Since these are larger than would be caused by periodic oscillations alone, one must look elsewhere for an explanation of their origin. It appears feasible to suggest that their generation is due to certain points in the combustion chamber being located within the core of the jet at the end of intake which, during the rest of the stroke, remain outside of the jet (e.g. at r = 23 mm and 28 mm). Such displacements of the jet at varying inlet valve lifts have been discussed by Annand[111] and Tanaka[112].

Fig. 4-19 shows the variation in the values of $\bar{u}$ grad $\bar{u}$ and $\sqrt{\overline{u'^2}}$ during intake with changes in a) engine speed and b) volumetric efficiency. It is clear that these three parameters vary linearly with engine speed and decrease with increase in throttling, the decrease being linear for grad $\bar{u}$ and $\sqrt{\overline{u'^2}}$. These results indicate that, whenever there is a linear change in grad $\bar{u}$, a corresponding linear change in $\sqrt{\overline{u'^2}}$ is also apparent. One might hypothesize from this that the velocity gradients in the flow during induction are largely responsible for the turbulent fluctuations.

The decrease in the three velocity parameters with throttling demonstrates the need for a device in the inlet pipe downstream of the throttle to "churn up" the flow during idle and part load operations. This would give more efficient combustion and better economy in addition to improving the exhaust emissions. Such devices have been used by Volvo[64] and Zenith-Solex[62] to achieve just these effects. A most interesting suggestion on this problem is that of Stivender[58] who proposes the use of a variable lift intake valve, instead of a carburettor butterfly, for throttling the charge intake. It is claimed that turbulence of a

smaller scale and of a greater intensity is achieved.

Other observations from Semenov's work during the induction period include:

i) the presence of sharp variations in the velocity fluctuations over the combustion chamber cross-section.

ii) the throttling had hardly any effect on the initial jet velocity during intake but tended to reduce it considerably throughout the remainder of the stroke.

During_compression.

It was assumed that there was no continuous, directed stream present in this particular combustion chamber during this stage of the cycle. Thus, the values of $\bar{u}$ refer to a large scale, eddying gas motion originating from the jet flow during intake.

The manner in which $\bar{u}$ and $\sqrt{\overline{u'^2}}$ varied from B.D.C. to about 60° A.T.D.C. is shown in Fig. 4-20. These results are in substantial agreement with Molchanov's with the exception of the point during compression at which $\bar{u}$ peaks. Molchanov finds it to be at 20° B.T.D.C. whilst Semenov's results show it to be at 40° B.T.D.C. A possible reason for this discrepancy could be that the low frequency motion was considered over different frequency ranges in the two works.

Figs. 4-21 and 4-22 summarize Semenov's results for changes in $\bar{u}$ and $\sqrt{\overline{u'^2}}$ with variation in the hot wire anemometer measuring point, the compression ratio, the volumetric efficiency and the engine speed. Briefly, the main indications from these graphs are:

i) the tendency for $\bar{u}$ to decrease with increasing distance from the combustion chamber centre.

ii) the fluctuating velocities ($\sqrt{\overline{u'^2}}$) achieve a shallow minimum at about three-quarters of the distance from the combustion chamber centre to the cylinder wall.

iii) $\bar{u}$ decreases by about 20 % with increase in compression ratio from 4 to 9.5. This observation agrees with the indications from Molchanov's work.

iv) $\sqrt{\overline{u'^2}}$ is virtually independent of compression ratio, only decreasing by 8% over the compression ratio range examined.

v) both $\bar{u}$ and $\sqrt{\overline{u'^2}}$ decrease linearly with throttling.

vi) $\bar{u}$ increases with engine speed according to the relationship

$$\bar{u} \propto n^{2.1}$$

whilst $\sqrt{\overline{u'^2}}$ increases almost linearly with this parameter.

vii) a correlation can be drawn between the velocity gradients originating during intake and the fluctuations, $\sqrt{\overline{u'^2}}$, during this stage of the cycle.

During the period when flame propagation takes place therefore, it is clear that the following aerodynamic conditions prevail in this cylindrical disc combustion chamber:-

a) a field of turbulence composed for the most part of relatively low frequency fluctuations.

b) variations in the turbulent fluctuations, $\sqrt{\overline{u'^2}}$, and the average velocity, $\bar{u}$, of the flow with crankshaft rotation (Fig. 4-20%.

c) variations in $\sqrt{\overline{u'^2}}$ and $\bar{u}$ at different points in the combustion space (Fig. 4-21).

Semenov maintains that these conditions represent

practically constant turbulence for combustion to develop in. This is certainly true if one compares the state of the flow with the aerodynamic conditions during the remainder of the cycle. However, the effects of such varying flow conditions on flame propagation cannot be ignored in an accurate attempt at depicting combustion development.

The change in turbulent energy during compression.

Measurements of the variation in the energies of the turbulent fluctuations as the cycle approached and passed through the combustion stage are summarized in Fig. 4-23. This shows:

i) the variation in the sum of the energies of the high frequency fluctuations (>300 c/s) and the low frequency eddies (<300 c/s) per unit mass. i.e. $\frac{1}{2}(\bar{u}'^2 + \bar{u}^2)$.

ii) the variation in the energy per unit mass of the high frequency fluctuations (>300 c/s) only i.e. $\frac{1}{2}\bar{u}'^2$.

iii) the variation in the sum of the energies per unit volume of the high frequency fluctuations and the low frequency eddies. i.e. $\frac{1}{2}\rho(\bar{u}'^2 + \bar{u}^2)$.

The three curves indicate:

a) a pronounced minimum energy at 90° B.T.D.C. caused by the jet flow of gas during intake suddenly being cut off.

b) the energy of the large scale eddies $(\frac{1}{2}\bar{u}^2)$ being redistributed among the high frequency fluctuations as the chamber volume decreases.

This latter phenomenon can be seen more clearly in Fig. 4-20 from Semenov's results and Fig. 4-15 from Molchanov's

results. It is noted from these two graphs that $\bar{u}$ decreases linearly from 40° and 20° B.T.D.C. respectively onwards through T.D.C. At the same time, $\sqrt{\bar{u}'^2}$ increases up to T.D.C. and decreases thereafter. This is due to the redistribution of the energy of the large scale eddies among the small scale eddies being great enough to maintain an increase in $\sqrt{\bar{u}'^2}$ before T.D.C. whilst, after this point, the energy redistribution decreases, possibly because most of the kinetic energy in the large scale eddies has already been given up. As a result of this energy dissipation during compression, the turbulence 'intensity' is at a maximum near T.D.C.

As an aside to his work, Semenov substantiated Clerk's claim[113] that combustion is slowed down considerably when the induction process is eliminated (see Fig. 4-24). This confirms that the turbulent gas motion during the combustion period originates from the flow into the cylinder during the intake stroke. Without induction, the energy sum, $\frac{1}{2}(u'^2 + \bar{u}^2)$, at T.D.C. on the compression stroke constitutes only about 10% of the energy of a normal cycle. This is the fraction of the energy produced by the piston motion alone.

The Spectral composition of the turbulent fluctuations.

Using bandpass filters over the range 0 to 6200 c/s, Semenov made the following observations:

i) during compression, a considerable fraction of the turbulent energy was in the range below 500 c/s.

ii) the increase in turbulence 'intensity' with opening of the throttle and with increasing engine speed was attended by an increase in the overall energy balance

of the high frequency part of the flow.

iii) there was an increase in the fraction of high frequency energy with an increase in compression ratio. This denotes an increased dissipation of the large scale, low frequency eddies.

Turbulence Measurements in Constant Volume Bombs.

Attempts are made from time to time at simulating the aerodynamic conditions and the combustion in piston engine cylinders by experiments in constant volume bombs. In these devices, turbulence and swirl are commonly generated by rotating mechanical stirrers, the number of which control the flow pattern generated. The advantages of this type of approach are:

i) the mixture swirl velocities can be easily varied.

ii) turbulence measurements, involving the use of hot-wire anemometers, are considerably simplified because the anemometer can be calibrated for any desired initial pressure and temperature. Calibration is a most difficult task in an engine.

iii) the separate quantitative effects of mixture pressure, temperature and swirl velocity can be easily obtained.

Bolt and Harrington[114] used this approach in a study on the effect of mixture motion on some important combustion parameters for various lean mixture ratios and initial pressures. Their results refer to experiments made with a single stirrer. It was found that a mean mixture velocity and a turbulent velocity were associated with each stirrer speed (see Fig. 4-25) and that whilst the mean mixture

velocity increased almost linearly with the stirrer speed, the fluctuating velocity component remained essentially constant above 750 rev/min.

Further studies on these same lines were carried out by Sokolik, Karpov and Semenov[115]. These authors were mainly concerned with the mechanism of turbulent combustion however. A two-element, hot-wire anemometer was used in the central part of their bomb and turbulence was produced by four stirrers spaced symmetrically around its circumference. It was found that isotropic turbulence was created up to a radius of half the distance from the bomb centre to the bomb wall without directed streams and without circulating flows of gas. These conditions were considered analogous to those in engine cylinders without any large-scale swirl at the end of the compression stroke.

The big drawback to bomb simulation of course is that the effect of piston motion on the flow pattern cannot be allowed for.

4.2.4. TURBULENT FLAME PROPAGATION - THEORIES AND MECHANISMS.

Although a great amount of research has been done on the nature and laws of turbulent combustion, no single theory has yet been established which adequately describes turbulent burning processes. It might be more correct at present, therefore, to speak of a model of turbulent combustion rather than a theory. Nevertheless, theories of turbulent burning velocity abound and the more important of these are summarized in the following pages.

First of all, however, it is important to define how a turbulent flame is characterized in comparison with a laminar

flame. The main differences are:

i) the absence of a uniform and infinitely thin combustion zone which is instead much thicker and more complex. In connection with this, there can be included the observations of various investigators [116] that there is a large increase in the distances between the emission maxima of the species OH, CH and H_2O in turbulent hydrocarbon reaction zones and that the ionization currents are much greater.

ii) a considerable increase in the speed of flame propagation.

iii) a turbulent flame is usually accompanied to some degree by noise and rapid fluctuations of the flame envelope.

iv) a contraction in the limits of inflammability when the intensity of turbulence is increased.

Above all, it is the effect of turbulence on the speed of flame propagation which is of interest in this work. In this connection, there is general agreement that macroscopic turbulence has the greatest effect whilst the influence of the microscopic fraction is considered to be much less important. Nevertheless, since states of purely microscopic and macroscopic turbulence do not exist in engine combustion chambers, an adequate theory of turbulent combustion for this application must consider both influences.

The increased rate of burn of a turbulent flame over a laminar flame is normallly accepted as being due to either one or a combination of the three following processes:

i) the turbulent field may distort and wrinkle the flame

front thereby markedly increasing its surface area. At the same time, the normal component of the burning velocity is the laminar burning velocity.

ii) the turbulence may increase the rate of transport of heat and active particles, thus increasing the actual burning velocity normal to the flame surface.

iii) the turbulence may rapidly mix the burnt and the unburnt gas in such a way that the flame becomes a homogeneous reaction, the rate of which depends on the ratio of burnt to unburnt gas produced in the mixing process.

In all these three processes, the large scale turbulent effect is considered to predominate. There is more or less complete agreement on the influence of the microscopic turbulence on the burning velocity. It is thought to increase the speed of propagation slightly because of increases in the transport of heat and active particles and because of micro-recycles of burnt, unburnt and partially burnt gas in the combustion front[117]. An expression for these processes has been derived and is of the form:

$$U_{T_{micro}} = U_L \cdot \left(\frac{D_{T_{micro}}}{D_m} \right)^{1/2} \quad \ldots\ldots\ldots\ldots 4\text{-}1$$

where

U_T micro = the burning velocity due to microscopic turbulence.

U_L = the laminar burning velocity.

D_T micro = the coefficient of microscopic turbulent diffusion.

D_M = the coefficient of molecular diffusion.

Turbulent burning theories, which are based on the assumption of increased surface areas (Process i) above) are given the name Surface or Wrinkled Flame Front Theories.

The remaining theories, which have their foundation in Processes ii) and iii) above, are defined as Three-dimensional or Volume turbulent combustion theories.

The Surface or Wrinkled Flame Front Theories.

These theories take as the starting point the front of a laminar flame and consider its behaviour in large scale turbulence. Under the influence of this, the laminar front is thought to undergo fluctuating deformations, thus becoming wrinkled. The surface area of the turbulent flame, A_T, is, therefore, considered to be greater than that of the laminar flame, A_L, to an extent which satisfies the greater part of the increase of turbulent flame speed over laminar flame speed. This is expressed by the relationship:

$$\frac{U_T}{U_L} = \frac{A_T}{A_L}$$

The Damköhler Theory.

Damköhler[118] pioneered the theoretical work on turbulent combustion. He considered separately the presence of both large-scale, low intensity turbulence and small-scale, high intensity turbulence but chose the former as the predominant effect. In comparison with laminar flow, he suggested that the flame surface area was much increased by the large-scale fluctuations but that the laminar transport processes remained unaffected (see Fig. 4-26).

Because of the complex nature of the wrinkling, Damköhler confined his expression for the turbulent burning velocity to a proportional relationship with the Reynolds Number of the flow as follows:

$$U_T \propto Re \qquad \text{----------} \qquad 4\text{-}2$$

By experiment, he derived the plot shown in Fig. 4-27 for propane-air flames. This is of the form

$$U_T = a_1.Re + a_2$$

for the linear part of the graph where 'a_2' is assumed to be the influence of small-scale turbulence and 'a_1' is the slope.

To explain the influence of this microscopic turbulence on the burning velocity Damköhler investigated the changes in diffusion and heat transfer with the Reynolds Number of the flow since the small-scale turbulence was assumed to produce no roughening of the flame surface. Using this approach, he derived the expression

$$\frac{U_{T\ micro}}{U_L} = \sqrt{\frac{\epsilon}{\nu}} \quad \text{--------} \quad 4\text{-}3$$

where ϵ is the eddy diffusivity.

and ν is the kinematic viscosity.

This is of the form of equation 4-1. For further details of Damköhler's theory, see Refs. 118 and 25.

The Theory of Shchelkin.

Shchelkin[119] expanded Damköhler's model but eventually came to similar conclusions. He suggested that the breaking up of the laminar flame front under large scale turbulence results in the formation of a series of regular flame cones (see Fig. 4-28). The following relationship was thought to apply in this case:

$$\frac{U_T}{U_L} = \frac{\text{Average cone surface area}}{\text{average cone base area}} \quad \text{--------} \quad 4\text{-}4$$

The base area, b_A, was taken to be proportional to the square of the scale of turbulence, L.

$$\text{i.e.} \quad b_A = \frac{\pi L^2}{4}$$

and the height of the cone, h, was assumed proportional to both the average fluctuating velocity, $\sqrt{\bar{u}'^2}$, and the time, t, during which an element of the combustion wave was associated with an eddy moving in a direction normal to the wave. Thus,

$$t = \frac{L}{U_L}$$

and

$$h = \frac{L\sqrt{\bar{u}'^2}}{U_L} = t.\sqrt{\bar{u}'^2}$$

From geometrical considerations of a cone, the following relationship exists:

$$\text{Cone Surface Area} = \frac{\pi L^2}{4}\left(1 + \left(\frac{2\sqrt{\bar{u}'^2}}{U_L}\right)^2\right)^{1/2}$$

When this was substituted into Equation 4-4, Shchelkin obtained the expression

$$U_T = U_L.\sqrt{1 + \left(\frac{2\sqrt{\bar{u}'^2}}{U_L}\right)^2} \quad \ldots\ldots\ldots\ldots 4\text{-}5$$

for the large scale turbulent burning velocity. From this, it is clear that U_T becomes practically independent of U_L for very large values of

For small scale turbulence, Shchelkin utilised the following relationship from the early thermal theories of laminar burning velocity (see Section 4. 3):

$$U_L = \left(\frac{\lambda_L}{t_{re}}\right)^{1/2} \quad \ldots\ldots\ldots\ldots\ldots\ldots 4\text{-}6$$

where t_{re} is the reaction time.

and λ_L is the laminar component of the thermal conductivity. Applying this to turbulent flow, he combined the laminar and turbulent heat transfer quantities (which are proportional to the thermal conductivities) and, in so doing, obtained the expression:

$$U_{T_{micro}} = \left(\frac{\lambda_L + \lambda_T}{t_{re}}\right)^{1/2} \quad \ldots\ldots\ldots 4\text{-}7$$

which, on rearrangement, gives

$$U_{T_{micro}} = U_L \left(1 + \frac{\lambda_T}{\lambda_L}\right)^{1/2} \quad \ldots\ldots\ldots\ldots\ldots 4-8$$

For further details on Shchelkin's work, see Refs. 119 and 25.

The Theory of Karlovitz.

A model of turbulent flame propagation proposed by Karlovitz[120] is based on instantaneous schlieren photographs of turbulent flames. The irregularities in the flame front were seen as acute angles pointing towards the products of combustion and rounded surfaces towards the unburnt gas. Karlovitz assumed that the combustion wave was propagated only by those elements which were projected forward by the turbulent fluctuations into the unburnt gas. The elements left behind or sent in the opposite direction were not considered.

The time of contact between an eddy of scale, L, and the laminar flame front was taken to be

$$t = \frac{L}{U_L}$$

Assuming that the average displacement of an element in the flame front under the influence of the turbulent fluctuations was $\sqrt{\overline{x^2}}$, Karlovitz defined a turbulent movement velocity as

$$U_T' = \frac{\sqrt{\overline{x^2}}}{t} \quad \ldots\ldots\ldots\ldots\ldots\ldots 4-9$$

Because this velocity was just considered to fluctuate backwards and forwards with no net movement of the reaction zone apparent, it was supplemented by the laminar burning velocity to allow for the propagation.

i.e. $$U_T = U_T' + U_L \quad \ldots\ldots\ldots\ldots 4-10$$

$$U_T = U_T^1 + U_L \quad \text{---------- 4-10}$$

This expression was transformed (by considerations of the theory of turbulent diffusion) into

$$U_T = \left\{ 2.\sqrt{\bar{u}'^2}.U_L \left[1 - \frac{U_L}{\sqrt{\bar{u}'^2}} \left(1 - \exp\left(-\sqrt{\bar{u}'^2}/U_L \right) \right) \right] \right\}^{\frac{1}{2}} + U_L \quad \text{.....4-11}$$

For values of large in relation to U_L, the expression becomes

$$U_T = \sqrt{2U_L(\bar{u}'^2)^{\frac{1}{2}}} + U_L \quad \text{.....4-12}$$

and for $U_L \gg \sqrt{\bar{u}'^2}$,

$$U_T = \sqrt{\bar{u}'^2} + U_L \quad \text{.....4-13}$$

Karlovitz finally added a term to allow for the effects of flame generated turbulence (see Section 4.2.1). This was estimated[25] to be given by the equation

$$\frac{1}{\sqrt{3}} \cdot U_L \cdot \left(\frac{\rho_b}{\rho_u} - 1 \right)$$

for isotropic flow.

The Theory of Leason.[121]

Leason also considered the effect produced when an eddy passed through a laminar flame. The physical picture he imagined is based on an eddy containing a sinusoidal velocity profile. This is illustrated in Fig. 4-29.

From geometric considerations, the following relationship was obtained:

$$\frac{U_T}{U_L} = \left[1 + \left(\frac{2\sqrt{\bar{u}'^2}}{U} \right)^2 \right]^{\frac{1}{2}} \quad \text{.....4-14}$$

However, Leason found by experiment that the area extension alone did not account for all of the burning velocity increase and he, therefore, added a diffusivity factor based on the intensity of the turbulent field.

The Theory of Scurlock and Grover.

Scurlock and Grover[122] developed in detail the processes that can produce wrinkling of the flame surface in turbulent flow. Like Shchelkin and Leason, they assumed that the passage of an eddy through the undisturbed flame front produced the wrinkling. The manner of this wrinkling was envisaged as is represented in Fig. 4-30.

It was assumed that the average height of the wrinkles was proportional to the root mean square displacement $\sqrt{\bar{Y}^2}$ of a flame element from the mean flame front position and that the average base width was proportional to the Eulerian scale of turbulence, L_{EU}.

An expression of the form

$$\frac{U_T}{U_L} = \frac{A_T}{A_L} = \left[1 + k_3 \left(\frac{\bar{Y}^2}{L_{EU}^2}\right)\right]^{1/2} \quad \ldots\ldots\ldots 4\text{-}15$$

was developed in which k_3 is a constant.

Three effects were believed to be important in determining $\bar{Y}^2$:-

i) eddy diffusion associated with turbulence in the unburnt gases - this tends to increase $\bar{Y}^2$.

ii) the propagation of the flame into the unburnt gases which tends to reduce $\bar{Y}^2$.

iii) flame generated turbulence which is associated with the density decrease across a flame and which tends to increase $\bar{Y}^2$.

For further details on this theory, see Ref. 122.

The Volume or Three-Dimensional Theories.

These theories and models were developed for the following reasons:

i) there was great suspicion that the surface models might not truly represent the actual conditions in turbulent flames.

ii) it was noted that the concept of the surface model did not result from empirical data and was not substantiated experimentally by subsequent investigations.

iii) the virtual impossibility that the surface area of a turbulent flame could increase to such an extent as to satisfy the greater part of the increase in flame velocity.

iv) differences in the very nature of turbulent and laminar flames. e.g. the surface models (which are fundamentally based on the concept of laminar burning velocities) do not represent the characteristic feature of turbulent motion viz. the continuous mixing through eddy diffusion.

v) the fact that ionization currents are greater in turbulent than in laminar flames.

The eddy diffusion in turbulent flow is thought to increase the transport properties of the two basic mechanisms of flame propagation viz. the thermal and diffusional mechanisms. An enlarged discussion of the influences of these is given in Section 4.3 in connection with laminar flame propagation. Thus both the heat transfer and the mass transfer of active particles and radicals from the burnt to the unburnt gas, and vice versa, across the flame front are increased. The heat transfer increase is a direct result of the thermal conductivity of the fluid being increased, which quantity is proportional to the density and the velocity of the fluid motion and the scale of its

where

D_T is the coefficient of turbulent diffusion.

e_L is the laminar flame front thickness.

e_T is the turbulent flame front thickness.

The turbulent flame front is thus considered to be a unified and continuous wave, just as in the laminar case, but made thicker by the action of the increased heat and active particle transportation due to the turbulent diffusion.

The Theory of Sokolik. [123,115]

Sokolik envisages the turbulent flame front as a number of microvolumes, the composition, temperature and reaction rate of which depend on the influence and the degree of turbulent diffusion. The individual microvolumes are assumed to consist of mixtures of partial and total combustion products and fresh gases. When these small mixtures are more or less completely burnt, there is considered to be a local extinction of the flame in the heart of the microvolumes.

Sokolik proposes the following expression for the speed of propagation under these conditions:

$$U_T = \frac{\sqrt{\bar{u}'^2}\, t_L}{t_i} = \frac{L_L}{t_i} \qquad \text{4-17}$$

in which

$\sqrt{\bar{u}'^2}$ is the turbulence intensity.

t_i is the autoignition delay period.

and t_L is the characteristic time of defining the Lagrange scale, L_L, of turbulence.

It is clear that Sokolik's approach results in the speed of turbulent flame propagation being independent of

the laminar burning velocity.

The Model of Shchetinkov.[124]

Shchetinkov proposed that an analysis of the processes occurring in a turbulent flame must consider both the increase in the surface area of the flame front and the volume combustion of the unburnt mixture by combination with combustion products within individual eddies.

On this basis, he formulated the hypothesis that turbulent fluctuations carry out burnt and partially burnt eddies from the interior of the combustion zone. These then ignite adjacent eddies containing fresh gas which begin to burn at their surfaces or at parts of their surfaces. It is considered that surface combustion predominates at the beginning of the combustion zone whilst volume combustion is most in evidence at the end of the zone. Because of the general lack of detailed knowledge on turbulent combustion however, Shchetinkov simplified this basic comprehensive model by ignoring the surface mechanism.

He then proposed that the burning eddies, which are projected ahead of the flame front by fluctuations, fail to ignite the neighbouring fresh gas eddies but, instead, mix with them and increase their temperature. The rate of the volume reaction which ensues depends on the initial temperatures within the eddies and on the concentrations of active particles and radicals present. Eddies are thus thought to exist close to each other in the unburnt, the burnt and the still burning states.

Shchetinkov's final simplified model is seen to closely resemble that of Sokolik described previously.

Summary.

In summary of the foregoing review of turbulent combustion models and theories, it can be clearly concluded that, at the present time, no theoretical expression exists which satisfies all the requirements. Shchetinkov's comprehensive model (in which both the surface and the volume mechanisms are considered to be important) is probably the most accurate hypothesis of the processes involved in turbulent flame propagation but the degrees of influence of these two mechanisms need much greater clarification. Also required is a knowledge of:

i) the relationship between the size and velocities of the eddies present in a given turbulent field.

ii) the individual effects of these on flame propagation.

4.2.5. EXPERIMENTATION ON COMBUSTION IN TURBULENT FLOW.

Attention is now directed to some detailed experimentation on combustion in turbulent flow in order to provide a firmer basis in deciding which of the two mechanisms (i.e. the Surface or the Volume combustion mechanisms) is predominant in turbulent combustion and which should be utilised in deriving an expression to calculate the burning velocities of the charge in the Renault combustion chamber. In connection with this, the work of Sokolik, Karpov and Semenov[115] deserves particular attention.

These workers proved conclusively that turbulent combustion must not be associated with laminar combustion as is, in fact, assumed in the Surface models. The initial

aims of their work were, however, to determine:

i) the relationship between the velocities of turbulent and laminar flames.

ii) the justification in assuming the mechanism of flame propagation to be similar in the two types of flames.

Their instrumentation and apparatus has already been described in Section 4.2.3 and results from their work indicate that:

a) within similar volumes, combustion in a turbulent flame gives a considerably lower increase in pressure than does combustion in a laminar flame. This is attributed to combustion extending over quite large reaction zones in turbulent flames whereas, in laminar flames, it is completed in a very narrow zone (see Fig.4-31[115]).

b) the turbulent combustion velocity is determined by the combustion temperature and the chemical reaction rate in the flame, and not by the laminar burning velocity. This conclusion was drawn from experiments performed with stoichiometric burning mixtures of oxygen with propane, methane and hydrogen, when these were diluted with identical quantities of argon and helium. The resulting mixtures yielded flames with identical combustion temperatures but with different laminar burning velocities (see Table 4-A). On the other hand, the velocities of turbulent combustion for these mixtures were in good agreement over a wide range of turbulence intensities. (see Fig. 4-32). This figure also shows a reduction in the velocity of turbulent combustion when a certain value of the intensity was exceeded. A partial extinction of the turbulent flame in certain

TABLE 4 - A.

MIXTURE	COMBUSTION TEMPERATURE (OK.)	LAMINAR BURNING VELOCITY (metres/sec)	SYMBOLS IN FIG. 4-32
$C_3H_8 + 5O_2 + 18A$	2500	0.8	1
$C_3H_8 + 5O_2 + 18He$	2500	1.4	2
$CH_4 + 2O_2 + 4.9A$	2500	0.7	3
$C_3H_8 + 5O_2 + 28.5A$	2150	0.45	4
$C_3H_8 + 5O_2 + 28.5He$	2150	0.74	5
$2H_2 + O_2 + 17A$	1650	0.29	6
$2H_2 + O_2 + 17He$	1650	0.7	7

eddies could be the reason for this.

The independence of the turbulent burning velocity of the laminar velocity was confirmed by experiments with hydrogen-air flames (see Fig. 4-33). At rich mixtures with these flames, the laminar velocity, U_L, increased when the combustion temperature was reduced. The reason for this was thought to be that the thermal conductivity of the mixture increased. At the same time, however, the turbulent combustion velocity diminished. These observations reflect the fact that turbulent diffusion, with which turbulent combustion is linked, is not connected with molecular diffusion on which laminar combustion depends.

Such discrepancies between the equivalence ratios at which the maximum laminar and turbulent burning velocities occur (see Fig. 4-33) have also been noted by Wöhl et al[125]. In butane-air mixtures, these workers report a slight shift of the maximum burning velocity towards the richer mixtures with increasing turbulence.

Sokolik, Karpov and Semenov also considered possible differences between laminar and turbulent combustion from the viewpoint of the different relationships existing between the velocities of combustion and the rates of reaction, in the two types of flame. These were known to be of the form

$$U_L \propto \sqrt{\omega} \quad \ldots\ldots\ldots\ldots\ldots\ldots 4\text{-}18$$

and

$$U_T \propto \omega \quad \ldots\ldots\ldots\ldots\ldots\ldots 4\text{-}19$$

Thus, for the Surface models of turbulent flame propagation,

$$U_T \propto \sqrt{\omega} \quad \ldots\ldots\ldots\ldots\ldots\ldots 4\text{-}20$$

and, for the volume combustion theories,

$$U_T \propto \omega \quad \text{.....} \quad 4\text{-}21$$

Verification of which of these two alternative mechanisms in Equations 4-20 and 4-21 is valid was made by the method of macrokinetic characteristics. This approach became quite involved and the reader is referred to the actual work[115] for greater detail. A brief summary is only given here.

A proportional relationship for the turbulent burning velocity was derived which involved the assumption that the reaction time, t_{re}, depends on the pressure and the temperature of combustion in the microvolume as

$$t_{re} \propto P^{(1.4-q)} \exp(E/RT) \quad \text{-----} \quad 4\text{-}22$$

where q is the reaction order.

Thus,

$$U_T = \frac{L_L}{t_{re}} \propto \frac{1}{t_{re}}$$

so that

$$U_T \propto P^{(q-1.4)} \cdot \exp(-E/RT) \quad \text{---} \quad 4\text{-}23$$

For laminar combustion, similarly, a square-root proportional relationship of the form derived by Zeldovich and Frank-Kamenetsky[126] was used.

i.e.

$$U_L \propto B \cdot P^{\left(\frac{q}{2} - 1\right)} \cdot \exp(-E/2RT) \quad \text{--} \quad 4\text{-}24$$

where B is a multiplier which takes account of all the non-Arrhenius functions of temperature.

The macrokinetic characteristics of such reactions were taken to be the energy of activation, E, and the reaction order, q. However, because q is considerably affected by the scale of the turbulence, which is itself rather indefinite, only E was considered a reliable kinetic character-

istic. Two methods of determining these macrokinetic characteristics were used:

i) from changes in the laminar and turbulent burning velocities with combustion temperature and pressure variations. For hydrazine flames, with this method, E was 34000 cal/mole and q was 2.4 in turbulent combustion and 37,000 to 40,000 cal/mole and 2.0 in laminar combustion.

ii) by calculating values of the reaction time, tre, from measurements of the time between the instants of initiation and decay of ionization currents in propane-air flames. This technique was used for both laminar and turbulent flames under two sets of conditions:

a) at constant combustion temperature and varying pressure.

b) at constant pressure and varying combustion temperature.

For turbulent combustion, E was calculated to be 17000 cal/mole and q was 2.0 and, for laminar combustion, E was 21000-25000 cal/mole and q 1.4 to 1.6.

Thus, the macrokinetic characteristics for both methods were found to be in close agreement. Even for great differences in the propagation distinguishing features of laminar and turbulent flames therefore, results indicated virtually identical mechanisms of reaction in flames of the two types and equality of the overall reaction rates. Semenov and co-workers thus considered it proved that

$$U_L \propto \sqrt{\omega}$$

and

$$U_T \propto \omega$$

and also that the Surface models of turbulent combustion are groundless.

The technique of ionization current measurements in this reviewed work[115] yielded some most interesting observations on the structure of a turbulent combustion zone. Two types of fluctuation of the ionization current were recorded (see Fig. 4-34):

i) one, of period θ_1, corresponded in frequency to the microturbulent fluctuations and, therefore, to the intensity of turbulent diffusion.

ii) the other, of period θ_2, corresponded to the macroscale of turbulence and defined the instants of the beginning and decay of the ionization current (and, consequently, the beginning and disappearance of the ignition reactions themselves).

In these oscillograms of turbulent ionization currents, θ_2 can be hypothesized as being the time intervals in the passage of microvolumes of gas, surrounded by ignition reactions, passed a stationary ionization detector. (Fig. 4-35). On this basis, it can be visualized that the contours of the reacting volumes are changing continuously with time under the effect of the continuously acting turbulent diffusion.

In contrast, a typical laminar reaction zone ionization current oscillogram is shown in Fig. 4-36. This is taken from the work of Sokolik[123]. It is seen that there is a sudden increase in the ionization current which then drops slowly to an equilibrium value. The duration of the reaction within the flame is represented only by the current rise-

time, t_1. The fall-off time, t_2, is mainly determined by the rate of recombination of the active particles formed in the reaction zone. The laminar reaction zone thickness, e_L, can be calculated from such an oscillogram by the equation

$$e_L = t_1 . U \quad \text{--------} \quad 4\text{-}25$$

where U is the average flow velocity in the flame zone.

4.2.6. SUMMARY.

From the foregoing analysis of turbulence and turbulent flame propagation, it is clear that it is virtually impossible at present to conceive of an accurate theory and expression for the rate of turbulent flame propagation which takes account of all the variables. It appears also that the Surface or Wrinkled flame front theories of turbulent combustion are fundamentally unsound since experimentation has revealed that the Volume combustion theories contain more of the noted mechanisms involved in the propagation of such flames.

In this work, the desirability of using a turbulent Volume combustion theory (to express the rate of flame propagation in the engine under consideration) is frustrated as no direct measurements of air currents in the combustion space were made. In addition, certain time constant values are required, (see Equation 4-17), the attainment of which are beyond the scope of this work. Resort has, thus, to be made to a Surface theory of turbulent combustion. In this, it is necessary to use a laminar burning velocity expression which must then be multiplied by a term to allow for the varying effects of turbulence and swirl in the engine.

4.3. THE DEVELOPMENT OF AN EXPRESSION FOR THE RATE OF TURBULENT FLAME PROPAGATION IN THE RENAULT ENGINE COMBUSTION CHAMBER BASED ON A SURFACE MODEL OF COMBUSTION.

As just stated in Section 4.2.6. the rate at which the flame propagates in the combustion chamber has to be based on a Surface model of turbulent combustion. This means that the turbulent burning velocity is the product of a laminar burning velocity (calculated from a laminar flame theory) and a correction factor, K_T. Thus,

$$U_T = K_T \times U_L \qquad \text{---------- 4-26}$$

The correction factor allows for the many parameters affecting the rate of burn in the combustion chamber which are not directly catered for in the laminar flame velocity expression. This predominantly means the level of turbulence and swirl in the chamber. Section 4.3.2 contains a more detailed account of this in addition to a description of the manner in which the value of K_T is calculated, bearing in mind that no actual measurements of turbulence were made.

First of all, however, a review of the more important aspects and theories of laminar flame propagation is given and this includes a detailed account of the derivation of the theory used in this work.

4.3.1. THEORIES OF LAMINAR FLAME PROPAGATION.

Although many of the physical and chemical processes involved in steady state, laminar flame propagation have been recognized in recent years, major difficulties still

remain in the problem of describing such flames. These are generally of two kinds:

i) ignorance of the details of the chemical processes actually occurring.

ii) the inability to handle satisfactorily the complex mathematical equations which must be used to adequately define the system. This difficulty has been eased in recent years by the advent of digital computers.

Evans[127] gives a review of the fundamental laws which should form the basis of laminar flame propagation theory. From this, it is clear that contributions from the fields of fluid dynamics, chemistry and mathematics are required for an effective solution. Certain difficulties are encountered, however, in attempting to satisfy all the requirements of these fundamental laws. These arise through attempting to comprehensively describe a laminar burning process when the reaction rate is a function of both the temperature and the concentrations of the components taking part in the reaction. The expression for the dependence of the reaction rate, ω, on temperature and pressure has been found to vary according to the individual reaction but, in general, it is of the form:

$$\omega = B_1 \exp\left(-E/RT\right) g_1^{\alpha_1} g_2^{\alpha_2} \ldots\ldots\ldots \qquad 4-27$$

where

B_1 is a constant

α_i represents the number of molecules of species i involved in the reaction.

and gi are the concentrations of the i'th components present.

The majority of combustion processes consist of a set of reactions proceeding simultaneously, and include not only the

molecules of the original components but also intermediate active particles and radicals. Ideally, it is necessary to have a knowledge of all these reactions occurring in the flame and of the dependence of their rates on the temperature and on the concentration of the reacting species. Studies of chemical kinetics have supplied such complete data in only a few instances however.

In view of these difficulties, various assumptions and approximations are made in order to simplify the problem. The nature of these distinguish the theories i.e. the type of simplifications used tend to emphasize one aspect of the mechanism of flame propagation to the relative exclusion of the other.

Based on this, two limiting mechanisms for laminar flame propagation are conceived:

a) the thermal mechanism.

b) the diffusional mechanism.

The Thermal mechanism is based on the assumption that heat conduction is the most important physical process involved in the transfer of the reaction zone from one layer of gas to the next. Diffusion processes are not considered and the concentration of a given component at a point is assumed to be governed only by flow and reaction processes.

The Diffusional mechanism maintains that the flame velocity is determined principally by diffusional processes. It is postulated that active particles and radicals (e.g. H, O and OH), produced by dissociation in the hot burnt gases and by chain branching, diffuse into the fresh gas and cause it to react explosively.

Thermal Theories of Laminar Flame Propagation.

As just stated, flame propagation is here assumed to be caused by heat conduction from the burnt to the unburnt gas. The temperature of the unburnt gas is considered to be raised to a point at which it ignites and releases the chemical energy stored in the fuel. The products of combustion then cool as they transfer heat to the yet unburnt mixture ahead of the flame front. (see Fig. 4-37).

Very often, thermal theories use the concept of an "ignition temperature," T_i, as the point at which the unburnt gas instantaneously ignites. With these theories, the zone preceding this point is called the preheating zone and the zone following it is called the reaction zone (Fig. 4-37). The early thermal theories [128,129,130,20] regarded the ignition temperature as a characteristic physical constant of the mixture. Nowadays, however, it is known to depend upon the experimental conditions under which the heat is liberated. The reaction rate was also assumed to be discontinuous at the ignition point jumping from zero in the preheating zone to a finite value in the reaction zone. Moreover, it was often assumed to maintain a constant value in the reaction zone as the temperature increased from T_i to T_B (see Fig. 4-37) where T_B is the flame temperature. In view of the present conception of the dependence of the reaction rate on temperature (see Equation 4-27), these ideas are at best approximations to actual conditions.

The demarcation of the flame zone into two separate zones is often used, however, as an approximation in some

of the more modern thermal theories[131,132,133]. In these, the combustion process is considered to have an induction period during which the mixture is prepared for ignition by an increase to the required temperature. With such theories, the ignition temperature is no longer regarded as a characteristic physical constant of the mixture and an explicit statement of the expression for the reaction rate is often avoided by the substitution of an experimentally determined value for the thickness of the reaction zone.

Among the laminar burning velocity theories based on the thermal mechanism are those of:

i) Mallard and Le Chatelier[20].
ii) Nusselt[134].
iii) Jouget and Crussard[129,130].
iv) Daniell[128].
v) Damköhler[135].
vi) Bechert[136].
vii) Barthólomé[131,132].
viii) Emmons, Harr and Strong[137].

The Mallard and Le Chatelier equation is the original and most frequently quoted of these. Its derivation and application to burning velocity predictions is described in Appendix 2. This is the theory used by Phillipps and Orman[19] in their computer simulation of combustion in the Ricardo E6 engine. It is not used in this work for the following reasons:

a) the concept of the ignition temperature is used, the value of which is difficult to determine accurately since the experimental conditions under which such determinations are made have a great influence on its value.

b) a reaction zone thickness is involved. Besides the difficulties associated with obtaining this quantity, it is in itself a poor way of accounting for the reaction rate.

c) the variation in the burning velocity with unburnt gas temperature for propane-air flames as predicted by this theory with that observed experimentally by Dugger and Heimel[25,138] is not all that good (see Fig. 4-40).

A review of the derivations of the remaining thermal theories mentioned above is given by Evans[127].

Diffusion Theories of Laminar Flame Propagation.

Several approximate equations for laminar burning velocity have been derived in which the diffusion of atoms and free radicals has been considered of major importance. These equations are based to some degree on speculation but they do follow from considerations of flame structure and the possible influence of a small concentration of reaction-chain initiators on the rate of the chemical reaction and, subsequently, on the process of flame propagation.

The reasoning for a diffusional mechanism begins with the assumption that potential oxidation chain carriers (e.g. H, O and OH) are present in the flame front in thermodynamic equilibrium concentrations for the flame temperature or the mean reaction zone temperature[139]. It is known that hydrogen atoms are by far the lightest and, thus, the fastest of all active particles being nearly four times as fast as any other[38,142]. Because such particles as these diffuse

rapidly, it is assumed that their concentrations in the colder unburnt gas ahead of the flame front is increased by diffusion to a value far greater than the equilibrium concentration for that region. A concentration profile similar to that shown in Fig. 4-38 for H atoms is therefore assumed to exist.

These active particles react rapidly even in the unburnt gas. This is because chemical reactions involving atoms and free radicals generally have low energies of activation, i.e. the reaction rate is not very dependent on the temperature. Thus, these particles are considered to serve as initiators of the oxidation reactions. Since the concentrations of active particles and radicals reaching the unburnt gas by diffusion must be related to the maximum concentration in the flame front, the conclusion is that the flame velocity should be related to the equilibrium concentrations at the flame temperature.

The demarcation of the flame zone into two zones, which is often used in thermal flame theory considerations, is still applicable in these diffusion theories. The induction period for the reaction is now characterized, however, by the accumulation, through diffusion, of active particles. At the point of ignition, the concentrations of these and the reaction velocities of the intermediate reactions have become so large that the combustion reaction suddenly begins.

The following theories are based on the diffusional mechanism of flame propagation:

i) The Theory of Tanford and Pease[139,140,141]

ii) The Theory of Manson[143]

iii) The Theory of Van Tiggelen[144]

iv) The Theory of Gaydon and Wolfhard[145]

v) The Theory of Bartholome[146]

By far the most well-known of these are the Theories of Tanford and Pease, and Manson. Their derivations are described in Appendices 3 and 4 respectively. Neither was used in this work however. For the Tanford and Pease theory, this was because:

a) there was a general prediction in the literature that the Semenov bi-molecular theory is more accurate. This theory is described later.

b) its accuracy of prediction is quite poor over the entire equivalence ratio range[147,148].

c) it requires detailed knowledge on the rate constants for the reactions which are occurring. These can only be obtained from observations on burning velocities and no information could be found on the laminar burning velocities at the temperatures and pressures which occur during the combustion processes in petrol engines.

The Manson theory was not used to predict laminar burning velocities in this work because:

a) the postulated analytical model of the combustion process (see Chapter 3) assumes that no pressure gradients exist in the combustion chamber. The Manson theory, however, is based on there being a small pressure drop across the flame front.

b) when the total range of equivalence ratio data is considered, the accuracy of prediction is quite poor[147,148].

Comprehensive Theories of Laminar Flame Propagation.

These theories attempt to account for both the thermal and the diffusional mechanisms since it is a reasonable hypothesis that, in reality, both are involved. Strictly speaking, with these theories it is necessary to identify each chemical specie occurring during the combustion reaction and to know all its physical and thermodynamic properties. This information is generally completely lacking for hydrocarbon-air flames. As a result, comprehensive equations have only been derived for a few flames e.g. azo-methane [149], nitric oxide [150] and ozone [27].

The most well-known of the comprehensive theories are those of:

i) Lewis and Von Elbe [27].

ii) Boys and Corner [151].

iii) Hirschfelder and Curtiss [152].

iv) Zeldovich, Frank-Kamenetsky and Semenov [126].

A detailed survey of Theories i), ii) and iii) is given in Ref. 127 together with references to the original works.

Theory iv) will, however, be discussed at some length as it is the one used in the computer analytical model in this work. Semenov [16] has presented the derivation of this equation in detail and, consequently, it is now widely known as the Semenov theory.

The Theory of Semenov.

Zeldovich and Frank-Kamenetsky derived an equation

for flame velocity predictions, the initial basic equations of which were quite comprehensive. In its final, simplified form, however, it includes the diffusion of fuel molecules but not free atoms and radicals. As a result, it tends to emphasize the thermal mechanism. The original full derivation of this theory is given in Ref. 16 whilst Refs. 25, 15 and 127 review this derivation.

A second-order, bi-molecular reaction is considered. This is in accord with some other reported work on flame propagation in which the reaction between a hydrocarbon fuel and air is treated as such. Clarke[26] reports experimental work confirming the reaction to be bi-molecular up to 25 atmospheres pressure.

A one-dimensional, steady state combustion model is assumed (see Fig. 4-39). The reaction is propagated solely by the heating of the unburnt gas in the preheat zone, initially at temperature T_u, to a temperature T_i, at which point the reaction begins. This is taken to occur completely in the reaction zone wherein the temperature is raised to T_B. The width of this zone is 'd' and beyond it no further reaction occurs.

The general equation for a bi-molecular, second-order reaction is

$$\omega = Cf_u \cdot Co2_u \cdot W.Z. \exp(-E/RT) \quad \text{--- 4-28}$$

in which

Cf_u is the concentration of fuel in the unburnt mixture (molecules/cm3).

$Co2_u$ is the concentration of oxygen in the unburnt mixture (molecules/cm3).

W is a steric or probability factor which allows for the geometry of collision between two reacting species.

Z is an impact coefficient (no. of collisions/cm^3sec).

In the Semenov theory, an ignition temperature is used only as a mathematical device for approximate computations. Semenov assumes that this ignition temperature is near the flame temperature. By approximations, the ignition temperature is entirely eliminated from the final equation thus making the equation more useful than the previous ones.

The following assumptions are made in addition to that regarding the ignition temperature:

i) the pressure is constant.

ii) the total number of molecules is constant.

iii) the specific heat at constant pressure, Cp, and the thermal conductivity, λ, are constant in the reaction zone.

iv) Thermal diffusivity $\frac{\lambda}{C_p \rho}$ is equal to molecular diffusivity, D.

v) Below T_i, the reaction rate, ω, is zero.

vi) In the reaction zone, the convection term in the energy balance equation is small with respect to the conduction and heat generation terms.

vii) Diffusion is important only as it affects energy balance.

The basic equations which apply to the reaction zone are:

The Continuity Equation for the fuel.

$$D\rho \frac{d^2\gamma}{dx^2} - M \frac{d\gamma}{dx} + \omega = 0 \qquad \text{4-29}$$

where

$$\gamma = \frac{C_{fu}}{\rho_u} - \frac{C_f}{\rho}$$

and M is the mass rate of flow ($gm/cm^2 sec$).

The Energy Equation.

$$\frac{\lambda}{C_p} \cdot \frac{d^2\psi}{dx^2} - M \cdot \frac{d\psi}{dx} + \omega = 0 \qquad \text{4-30}$$

where

$$\psi = C_p \cdot (T_B - T_u) / Q_v$$

and Q_v is the Heat of the Reaction (cal/mole of reactant).

The Equation of State.

$$\frac{\rho}{\rho_u} = \frac{T_u}{T} \qquad \text{4-31}$$

The Conservation of Mass.

$$M = \rho U = \rho_u U_u = \rho_B U_B \qquad \text{4-32}$$

The boundary conditions for these equations are (see Fig. 4-39):

$$\text{At } x = -\infty, \gamma = 0, \psi = 0 \qquad \text{4-33}$$

$$\text{At } x = \infty, \gamma = \frac{C_{fu}}{\rho}, \psi = C_p (T_B - T_u)/Q_v \qquad \text{4-34}$$

If $\gamma = \psi$ over the entire reaction zone, Equations 4-29 and 4-30 are identical in form and have identical solutions (see assumption iv) above). That is,

$$C_p \cdot T + \frac{C_f \cdot Q_v}{\rho} = C_p \cdot T_u + \frac{C_{fu} \cdot Q_v}{\rho_u} = C_p \cdot T_B \qquad \text{4-35}$$

This means that the sum of the thermal and chemical energies per unit mass of mixture is constant in the reaction zone. Thus, the differential equation 4-29 can be replaced by the algebraic equation 4-35. Only the differential equation 4-30 must now be solved.

In light of assumption vi), this equation can now be written

$$\frac{d^2T}{dx^2} + \frac{\omega \cdot Q_v}{\lambda} = 0 \qquad \text{4-36}$$

where,

at $x = 0$, $T = T_i$

and

at $x = d$, $T = T_B$

In the preheat zone, $\omega = 0$ according to assumption v) and the energy equation becomes

$$\frac{\lambda}{C_p} \cdot \frac{d^2T}{dx^2} - M \cdot \frac{dT}{dx} = 0 \qquad \text{--------} \qquad 4\text{-}37$$

where

at $x = -\infty$, $T = T_u$

and

at $x = 0$, $T = T_i$

The condition which determines the value of 'M' is that the heat transferred from the reaction zone to the preheat zone is equal to that received by this latter zone. That is,

at $x = 0$,

$$\left(\frac{dT}{dx}\right)_{U_{Preheat}} = \left(\frac{dT}{dx}\right)_{U_{Reaction}} \qquad \text{----} \qquad 4\text{-}38$$

Solving Equations 4-36 and 4-37 and equating their derivatives according to Equation 4-38, the following expression is obtained:

$$U_L = \frac{M}{\rho_u} = \sqrt{\frac{2\lambda J}{C_p \rho_u (T_B - T_u)}} \qquad \cdots\cdots\cdots\cdots\cdots 4\text{-}39$$

where

$$J = \frac{1}{C_{fu}} \int_{T_u}^{T_B} \omega . dT \simeq \frac{1}{C_{fu}} \int_{0}^{T_B} \omega . dT$$

Since T_i is assumed to be near T_B, the reaction rate equation 4-28 can be approximated in order to facilitate the integration of Equation 4-39. The approximate equation

is:

$$\omega = C_f\, C_{O_2}\, WZ \exp(-E/RT_B) \exp(-\sigma E/RT_B^2) \quad \text{---- 4-40}$$

where

$$\sigma = T_B - T$$

From Equation 4-35,

$$\frac{C_f}{C_{f_u}} = \frac{T_u\, \sigma}{T(T_B - T_u)} \quad \text{---- 4-41}$$

Semenov suggests that, for lean mixtures, the concentration of O_2 in the reaction zone can be approximated by its value in the combustion products. This quantity is:

$$\frac{C_{O_2}}{C_{O_{2u}}} = \frac{T_u}{T}\left(1 - \phi\left(1 - \frac{C_f}{C_{f_u}\frac{T_u}{T}}\right)\right) \quad \text{---- 4-42}$$

where ϕ is the equivalence ratio.

Dugger and Simon[25] have performed the integration of Equation 4-39 in an approximate manner. Their results are:

$$\int_0^{T_B} \omega\, dT \simeq C_{f,eff} \cdot C_{O_2,eff} \cdot WZ \cdot \frac{RT_B^2}{E} \cdot \exp\left(-E/RT_B\right) \quad \text{---- 4-43}$$

where

$C_{f_{eff}}$ and $C_{O_{2eff}}$ are the effective mean concentrations of fuel and oxygen in the reaction zone (molecules/cm^3)

For rich mixtures ($\phi > 1$),

$$C_{f_{eff}} = C_{f_u} \cdot \frac{T_u}{T_B}\left(1 - \frac{1-\beta}{\phi}\right)$$

$$C_{O_{2eff}} = C_{O_{2u}} \cdot \frac{T_u}{T_B} \cdot \beta \quad \text{---- 4-44}$$

and, for lean mixtures ($\phi < 1$),

$$C_{f_{eff}} = C_{f_u} \cdot \frac{T_u}{T_B} \cdot \beta$$

$$C_{O_{2eff}} = C_{O_{2u}} \cdot \frac{T_u}{T_B}\left(1 - \phi(1 - \beta)\right) \quad \text{---- 4-45}$$

In these equations,

$$\beta = \frac{RT_B^2}{E(T_B - T_u)} \qquad \text{----------} \qquad 4\text{-}46$$

The quantity, Z, is proportional to the square root of temperature and is given by Dugger and Simon[25] as:

$$Z = \left(\frac{d_{col_f} + d_{col_{O_2}}}{2}\right) \cdot \sqrt{\frac{8\pi RT}{A} \cdot \left(\frac{M_f + M_{O_2}}{M_f \; M_{O_2}}\right)}$$

in which

d_{col} is the effective collision diameter. (cm)

M is the Molecular weight.

A is Avogadro's Number (6.025×10^{23} molecules/gm-mole)

It does, in fact, represent the total number of collisions per unit time and volume between the fuel and oxygen molecules.

Semenov later relaxes some of the restrictions in assumptions ii), iii) and iv) so that

a) the number of moles of products, n_g, to reactants, n_u, can be given by the ratio n_u/n_g in the stoichiometric equation.

b) $\frac{\lambda}{C_P}$ is allowed to have the value $\frac{\lambda_g}{C_{P_B}}$ in the reaction zone.

c) $\frac{\lambda}{C_P}\Big/D\rho$ is allowed to assume any constant value - not necessarily unity.

With the above considerations included, the final equation for the laminar flame propagation velocity of a second-order, bi-molecular reaction according to Semenov's method is:

$$U_L = \left(\frac{n_u}{n_g}\right) \cdot \frac{\beta}{C_{P_g} D_g} \sqrt{\frac{2 \cdot \lambda_g^3 \, WZ \, C_{f_u} \left(1 - \frac{1-\beta}{\phi}\right) \exp\left(-E/RT_g\right)}{\rho_u^3 \, C_{P_g} \, \phi \left(\frac{C_{f_u}}{C_{O_2 u}}\right)_{st}}}$$

4-47

where

$\left(\frac{C_{f_u}}{CO_{2_u}}\right)_{st}$ is the stoichiometric fuel-oxygen ratio.

For lean mixtures, the term $\left(1 - \frac{1-\beta}{\phi}\right)$ is replaced by $(1 - \phi(1-\beta))$.

For stoichiometric mixtures ($\phi = 1$), it becomes simply β.

In using Equation 4-47, Dugger and Simon[25] suggest that

$$\lambda = \left(C_p + \frac{5}{4_R}\right) \cdot \frac{\mu}{M}$$

and $D = 1.336 \cdot \frac{\mu}{\rho}$

where μ is the viscosity (gm/cm sec)

and M is the molecular weight.

The remaining properties are calculated by interpolation from thermodynamic tables. Because of the assumptions involved in the integration, Semenov concluded that, for a bi-molecular reaction, Equation 4-47 is only valid for values of $\frac{RT_B}{E} \leq 0.1$. However, recent investigations have demonstrated its reliability for values of RT_B/E up to 0.15.

This theory was used in the analytical combustion model of the present study because it appears to give the most accurate results for a wide variety of hydrocarbon fuels and because it is possibly the most comprehensive of all the theories available. A slight drawback to its use is that it dictates that pressure has no effect on the burning velocity whereas it has been reported[153,154], in some instances[155,156] to have a very slight effect.

In Fig. 4-40, a comparison is shown between the laminar burning velocities of propane as predicted by our Semenov equation and some experimental measurements taken from Ref. 25 over a range of unburnt gas temperatures. A constant equivalence ratio of 1.135 was used. On the same graph is plotted burning velocities calculated from the Mallard and Le Chatelier Thermal theory (see Appendix 2). The agreement with experimental results is seen to be much better with Semenov.

Data on experimental burning velocities of benzene and iso-octane over a range of equivalence ratios and unburnt gas temperatures is remarkably scant. However, the following values are reported in Ref. 157 which pertain to the laminar combustion of iso-octane. Also shown are the burning velocities predicted by the Semenov equation. The agreement is seen to be quite good.

UNBURNT GAS TEMP. (^{o}K)	BURNT GAS TEMP. (^{o}K)	EQUIVALENCE RATIO (ϕ)	EXPERIMENTAL BURNING VELOCITY (cm/sec)	SEMENOV BURNING VELOCITY (cm/sec)
311	2285	1.05	34.9	34.6
422	2337	1.05	61.6	56.8

In Ref. 157 also, the following results appear for some benzene experimental measurements. Again, these are compared with the Semenov predicted values and the agreement is seen to be quite good to an average accuracy of 6%.

UNBURNT GAS TEMP. (^{o}K)	BURNT GAS TEMP. (^{o}K)	EQUIVALENCE RATIO (ϕ)	EXPERIMENTAL BURNING VELOCITY (cm/sec)	SEMENOV BURNING VELOCITY (cm/sec)
311	2362	1.08	48.2	45.6
395	2400	1.08	73.8	70.5

In the application of the basic Semenov expression (Equation 4-47) to burning velocity calculations, it is assumed that the physical properties of the unburnt mixture do not differ appreciably from those of air. In addition, the activation energies of propane iso-octane, and benzene mixtures are taken to be 40000 calories/mole[158].

4.3.2. THE DERIVATION OF AN EXPRESSION TO ALLOW FOR THE EFFECTS OF TURBULENCE AND SWIRL ON THE BURNING VELOCITY.

The correction factor, K_T, in Equation 4-26 must, ideally, allow for the many parameters affecting the rate of burn in the combustion chamber which are not directly catered for in Semenov's laminar burning velocity expression (Equation 4-47). These involve primarily the aerodynamic conditions (viz. the turbulence and swirl) existing in the chamber. It is also necessary to know the manner in which these conditions vary with:

i) engine speed
ii) piston movement
iii) throttling
iv) compression ratio
v) inlet pipe tuning effects

Patterson and Van Wylen[159] suggest that the values of K_T be estimated from experimental pressure-time diagrams for the particular engine under consideration when running under known conditions. Although such an approach caters in an indirect manner for the varying effects on the laminar burning velocity of most of the factors listed in i) to v) above, it was not used in this work since it was not con-

sidered to be very realistic owing to its inherent trial and error nature.

A method suggested by Spalding[160] is based on the Reynolds Number of the flow in the combustion chamber which he defined as

$$Re = \frac{\rho b^2}{t_{str.} \mu} \qquad \text{----------} \qquad 4\text{-}48$$

in which

b is the engine bore (cm)

and

t_{str} is the time (seconds) for the piston to travel from B.D.C. to T.D.C.

Using this expression, the following values were calculated for the Renault engine:

Engine Speed rev/min	Reynolds Number
1000	30000
3000	98000
4500	147500

It was proposed that such Reynolds Number calculations be incorporated either into the results of Damköhler[118] (see Section 4.2.4) or into those of Bollinger and Williams[161]. Damköhler found that, for propane-oxygen flames, at Reynolds Numbers between 5000 and 18000, the following relationship held (see Fig. 4-27):

$$\frac{U_T}{U_L} = 1.75 + 0.0001.\ Re \qquad \text{--------} \qquad 4\text{-}49$$

Bollinger and Williams, on the other hand, proposed a relationship of the form:

$$\frac{U_T}{U_L} = 1 + 0.0002\ Re \qquad \text{--------} \qquad 4\text{-}50$$

for propane-air mixtures at Reynolds Numbers between 2000 and 35000. The different responses to turbulence in the two expressions are thought to be due to the two different reagents used to oxidize the fuel.

It should be noted that the flow becomes laminar at Reynolds Numbers below about 2000 (see Fig. 4-27). As a result, there is a discontinuity in the relationship between $\frac{U_T}{U_L}$ and Re at this point. This Reynolds Number value corresponds to the Renault engine running at 60 rev/min, however, which is far removed from its usual operating range. The discontinuity can, thus, be safely discounted if this method is used. It was, in fact, not used for the following reasons:

a) the very arbitrary nature of the Reynolds Number definition in Equation 4-48.

b) because the relationships in Equations 4-49 and 4-50 only apply within the Reynolds Number ranges stated. The maximum Reynolds Number value was 35000 which, according to Spalding's definition, corresponds to the Renault engine running at about 1200 rev/min. This speed is untypical of the engine's usual operating range which extends up to 4500 rev/min.

The method actually adopted is based on the work of Harrow and Orman[31] and used in the cycle simulation of Phillipps and Orman[19]. It involves measurements of flame speed in the combustion chamber between two ionization probes (see Fig. 4-41).

The principle of this technique stems from the fact that active particle concentrations in the flame front are greater than both those in the already burnt combustion

products and, obviously, those in the unburnt part of the charge. When a flame passes an ionization gap, therefore, a pulsed electrical potential is generated and a pulsed current starts to flow. Consequently, flame arrival times at a probe or probes can be recorded on any suitably available equipment e.g. an oscilloscope.

The usefulness of flame speed measurements over the engine's speed range lies in the fact that they give an indication of the gas velocities which are present in the combustion chamber during normal operation. Such indications are only reliable, however, when the other parameters which affect flame speeds (e.g. air/fuel ratio, compression ratio, spark timing etc.) are kept constant. Thus, by observing the flame travel times between two ionization probes (one (ionization probe 1) close (5 mm) to the centre electrode of the sparking plug and the other (ionization probe 2) diagonally remote (73.5 mm) from it - see Fig. 4-41) over the Renault engine's speed range at constant values of air/fuel ratio, compression ratio, spark timing and at full throttle, it was possible to evaluate the manner in which the gas velocities in the combustion chamber vary with engine speed.

If measurements were to be confined to the total time taken for the flame to propagate right across the combustion chamber from the sparking plug to the point at which it is finally quenched, then the events occurring immediately after the spark, when the flame is travelling very slowly, are grouped with those occurring later in the process when it is travelling much faster. Thus, in attempting to determine the variation in the gas velocities with engine speed

by these techniques, it is desirable to eliminate from the overall flame travel times the varying effects of the 'delay periods' just after ignition and the periods at the end of the combustion process when the flame is slowing down. These are the reasons for ionization probes 1 and 2 being in the positions they are (see Fig. 4-41).

Knowing the distance between the two probes (68.5 mm) and the flame travel times between them over a range of engine speeds, it is possible to calculate both 'apparent flame speed' and 'apparent delay period' values. True estimates of these quantities cannot be made because the actual path and length of the flame travel between the probes is not known. A method of calculating these apparent values has been suggested by Harrow and Orman[31]. It ignores any flame accelerations between the probes and thereby assumes a steady velocity over the whole flame path. The following expressions are proposed:

$$V_{FS}^{1} = \frac{x_2 - x_1}{t_{b2} - t_{b1}} \qquad \text{-------- 4-51}$$

and

$$T_o^{1} = \frac{x_2\, t_{b1} - x_1 t_{b2}}{x_2 - x_1} \qquad \text{--------- 4-52}$$

where

V_{FS}^{1} = apparent flame speed (cm/sec)

T_o^{1} = apparent delay period (seconds)

$x_1 x_2$ = distances from the spark plug to the ionization probes 1 and 2 (see Fig. 4-41).

t_{b1}, t_{b2} = mean flame travel times to the ionization probes 1 and 2.

Details of the instrumentation used in measurements of the mean flame travel times in this work are given in Appendix 5. A general view of the engine layout and instrumentation set up appears in Fig. 4-42. Figs. 4-43 and 4-44 show typical oscillograms obtained. A polaroid camera was used for these. The reference signal at the top in these photographs is the one coming from the sparking plug whilst the signals on the middle and bottom lines correspond respectively to those from ionization probes 2 and 1. The horizontal scale is callibrated in milliseconds.

As will be appreciated from these oscillograms, considerable difficulty was experienced in determining average values of the flame travel times to the two probes due to the phenomenon known as cyclic dispersion (see Chapter 2). In spite of this, however, it was possible to conceive of an average value at each of the probes under all running conditions either by mere observation or by a sampling technique. The latter method was considerably simplified by the availability of a Storage Oscilloscope. Average values at the probes could be obtained much more easily and accurately by the use of more sophisticated electronic equipment. Such facilities would enable instantaneous statistical analyses to be made of a large number of ionization signals at a probe. In this connection, the equipment used in the works of Harrow[40], Higashino[162] and Curry[34] is instructive.

Results of the experiments performed to try and achieve a relationship between flame speed ($\propto$ mixture motion) and engine speed, under running conditions of constant air/fuel ratio, spark timing, compression ratio and at full throttle,

are listed in Table 4-B. Table 4-C contains the calculated apparent flame speed and delay period values. Plots of these listed quantities in Tables 4-B and 4-C are given in Figs. 4-45, 4-46, 4-47 and 4-48.

It is seen from Fig. 4.45 that the flame speed between the two ionization probes in the Renault combustion chamber increases linearly with engine speed up to 3250 rev/min. A slight "tailing off" is apparent above this speed however. Similar trends to these were observed by Harrow and Orman[31] and Harrow[40]. Possible explanations for these effects are given later.

Figs. 4-46 and 4-47 show alternative ways of representing the results. These graphs indicate:

i) that the flame travel time between the two ionization gaps approximates a linear function of the time taken by the engine crankshaft to perform one revolution.

ii) that the flame travel time to the two probes decreases with increasing engine speed.

Fig. 4-48 shows the way in which the apparent delay period, T_o^1, decreases with increasing engine speed over the speed range examined. It is clearly evident that turbulence and swirl ($\propto$ engine speed) accelerates the initial stages of combustion.

To derive an expression relating the resulting values of flame speed (Table 4-C) to values of K_T for use in equation 4-26, use is made of the linear relationship between the flame speeds and the engine speeds over the greater part of the speed range (see Fig. 4-45).

TABLE 4-B

Engine Operating Conditions.

Spark Advance	=	25° B.T.D.C.
Air/Fuel Ratio	=	12.0
Compression Ratio	=	8
Ambient Temperature	=	18° C.
Ambient Pressure	=	29.85" Hg.
Fuel	=	Iso-octane.

ENGINE SPEED REV/MIN	FLAME TRAVEL TIME FROM SPARK PLUG TO (millisecs)		FLAME TRAVEL TIME BETWEEN PROBES
	PROBE 1 t_{b_1}	PROBE 2 t_{b_2}	1 and 2 (millisecs) $(t_{b2} - t_{b1})$
1150	2.0	7.5	5.5
1350	1.6	6.5	4.9
1810	1.3	5.4	4.1
2000	1.3	4.9	3.6
2500	1.0	4.0	3.0
2720	1.0	3.8	2.8
3400	0.8	3.2	2.4
4100	0.7	2.9	2.2

TABLE 4-C

ENGINE SPEED (REV/MIN)	APPARENT FLAME SPEED (cm/sec)	APPARENT DELAY PERIOD (millisecs)
1150	1245	1.6
1350	1400	1.25
1810	1670	1.0
2000	1900	1.04
2500	2285	0.78
2720	2450	0.79
3400	2850	0.63
4100	3120	0.54

This is of the form:

$$V_{FS}^{1} = 0.75\ n + 380 \qquad \text{------ 4-53}$$

It is clear that the flame speed values obtained refer to the rate of burn relative to the combustion chamber walls. They are vector sums of the turbulent burning velocities relative to the unburnt gas, U_T, and the unburnt gas velocities, Ug, themselves (see Section 2.1). Referring to Fig. 4-45, if the flame speed values are extrapolated back to zero engine speed, the resulting value, V_L, will be that due to laminar combustion only since the flow in the chamber at zero and low engine speeds (< 60 rev/min) is essentially laminar. Although such an extrapolation is most dangerous, it does nevertheless give a value of laminar flame speed (380 cm/sec in this case) which can be compared for accuracy with known burning velocity values of iso-octane-air mixtures. These latter values are normally determined in a rig at atmospheric pressure and over a range of unburnt mixture temperatures. However, no data could be found, in a literature search, relating to the combustion of iso-octane-air mixtures under conditions approximating those at which these engine tests were conducted viz. at an unburnt gas temperature of about 600°K and an equivalence ratio of 1.25. It was noticed, however, that the laminar burning velocities of iso-octane-air and propane-air mixtures were in reasonable agreement and so a propane-air value was used for the comparison instead. This was found to be about 125 cm/sec[25] under the above conditions.

There is general agreement that flame speeds are approximately $2\frac{1}{2}$ to 3 times the burning velocities over the greater part of the flame travel in an engine. The laminar flame speed of 380 cm/sec at zero engine speed thus corresponds to a laminar burning velocity of about 130-150 cm/sec. Such a value compares reasonably with the already stated laminar burning velocity of propane as determined in a rig.viz. 125 cm/sec.

Equation 4-53 can now be rearranged into the form:-

$$\frac{V_{FS}^{1}}{V_L} = 1 + .00197\,n \qquad \text{------ 4.54}$$

where V_L is 380 cm/sec. Since $V_{FS}^{1} \simeq 2\frac{1}{2}$ to 3 times U_T over a wide range of engine conditions, it is reasonable to assume also that $V_L \simeq 2.5$ to 3 times U_L. On this basis,

$$\frac{U_T}{U_L} = \frac{V_{FS}^{1}}{V_L} = 1 + 0.00197n \qquad \text{------ 4.55}$$

Equation 4-55 shows a similar dependence on engine speed as expressions derived by other workers in this field. For example, Phillipps and Orman[19] obtained the relationship

$$\frac{U_T}{U_L} = 1 + .002n \qquad \text{------ 4.56}$$

for a Ricardo E6 engine and Hodgetts'[163] results for a Ford Zodiac Mark III engine can be rearranged into the form:

$$\frac{U_T}{U_L} = 1 + .0017n \qquad \text{------ 4-57}$$

Comparing the flame speed values calculated in Table 4-C with those from Hodgetts' work however, it was apparent that they were quite appreciably lower. For example, at 3500 rev/min, the flame speed in Hodgetts' results was 6000 cm/sec whereas it was only 2900 cm/sec in this work. This was most surprising as comparable running conditions were maintained with regard to compression ratio and air/fuel ratio. An explanation of such large discrepancies in the two sets of results was sought and attributed mainly to a combination of the four following effects:-

a) greater turbulence in the Ford combustion chamber.

b) larger quantities of exhaust residuals in the Renault engine over the speed range examined in the tests the effects of which are to slow down combustion. The Ford engine results were all taken with a centrifugal mechanism on the distributor which advanced the spark timing with increasing engine speed. This is desirable because, for a given engine speed increase, there is not a corresponding proportional increase in turbulence and, thus, also in flame speed. Such advances ensure that combustion is completed reasonably efficiently and is not prolonged down the expansion stroke with the consequent effects of poor volumetric efficiency and increased concentrations of exhaust residuals in the fresh charges. In the Renault results, the spark timing was fixed at 25° B.T.D.C. so that it seems feasible to suggest that, at

the higher speeds, the spark advance was not great enough to prevent these effects occurring. At the low engine speeds, the advance was probably adequate. It is, thus, apparent that such tests should have been performed not at constant spark timing but under conditions which attempt to maintain a constant exhaust residual fraction in the combustion chamber over the entire engine speed range. Such an ideal can only be reasonably approached by the inclusion of a speed sensitive, spark advance device as was done in the Ford tests.

In this connection also, it appears that Harrow and Orman's results[31], which were utilized in the Phillipps and Orman combustion simulation work[19], are subject to the same criticism as those obtained in the Renault. In Fig. 4-49, some of these results are reproduced. Close scrutiny reveals the same trend of a falling off in the flame speed values with increasing engine speed at a constant spark timing. This is especially noticeable when the ignition timing is at 15° B.T.D.C. and at engine speeds above 2000 rev/min. These observations are explainable by the above discussions. At 25° B.T.D.C. spark timing on the other hand (see Fig. 4-49), such effects are not really too apparent since the spark advance is probably great enough over the speed range of up to 2500 rev/min.

Some authors have attributed such "fallings off" in flame speed at high engine speeds and constant ignition timings to lack of turbulence and swirl in the engine. It is apparent from the foregoing discussion, however, that such a conclusion can only be drawn if the tests show a similar response when repeated with variable spark timing.

c) the positioning of the ionization probe 1 too close to the sparking plug (see Fig. 4-41). This, however, was unavoidable for the reasons stated in Appendix 5. The effect of this on the flame speed is that the period when the flame is moving very slowly (i.e. the 'delay period') was not entirely eliminated from the overall time to ionization probe 2. Thus, the mean flame travel time between the probes was greater than it would have been if the engine speed sensitive 'delay period' had been completely removed by positioning the ionization probe 1 at about 10 to 15 mm. from the sparking plug. In Harrow and Orman's work[31], it was 16.5 mm away.

d) the positioning of the ionization probe 2 too near to the combustion chamber wall (see Fig. 4-41). The consequence of this is the disproportionate effect on the mean flame travel time to ionization probe 2 of the slowing down of the flame speed as the cylinder wall is approached at the end of the flame travel.

It is difficult to predict the exact influence of these factors on the results obtained during the tests and on the relationship derived in equation 4-55. However, since this expression is of the same order as those derived by Harrow and Orman[31] and Hodgetts[163], and bearing in mind the approximations used in its derivation anyway, it was taken to represent the manner in which the aerodynamic conditions in the combustion chamber vary with engine speed. The linear nature of the relationship compares favourably with the virtual linear rises in the mean flow velocity and in the root mean square values of the fluctuating flow velocities with engine speed as observed by Semenov (see Fig. 4-22).

Such an expression, however, only takes account of the manner in which the mixture motion in the Renault combustion chamber is influenced by engine speed. It does not allow for the variation in the aerodynamic conditions with piston movement, throttling, compression ratio and inlet pipe tuning effects. The correction factor, K_T, in Equation 4-26 ideally requires a knowledge of this. Since this ideal can only be realistically achieved by direct measurements of the flow in engine cylinders, it is necessary to estimate what sort of errors will be involved if these effects are ignored and Equation 4-55 alone is used to represent K_T.

The indications of the effects of piston movement on flow velocities during the flame propagation period can be determined from Molchanov's and Semenov's results (Figs. 4-14, 4-15 and 4-20).

These show that the variations in the mixture motion can be quite significant if complete accuracy is desired.

The influence of throttling on the mixture motion and combustion development is virtually impossible to define using the flame speed measurement technique described above. This is because the quantities of residual exhaust gases increase with increased throttling and tend to reduce flame speeds so that the mixture motion variation cannot be accurately estimated. Reference to Semonov's work, however, (see Fig. 4-22) shows that both the average velocities of the large scale eddies and the turbulent fluctuations decrease with increased throttling. Quite large errors might be expected in the value of Equation 4-55, therefore, if this is used to represent turbulence and swirl under throttled conditions.

The effect on the gas flows in the engine cylinder of compression ratio variations is again most difficult to determine by flame speed techniques. This is once more attributable to the varying quantities of residual exhaust gases present in the combustion chamber at different compression ratios. It should be noted that increases in compression ratio reduce the exhaust residual fractions because of the improved scavenging of the engine. Semenov[110] found that the mean velocities of the large scale eddies in the combustion chamber decreased whilst the turbulent fluctuations remained essentially constant as the compression ratio was increased (see Fig. 4-21). He formed the opinion that such variations in the gas flows had almost no effect on the turbulent burning velocity within the compression ratio range 6 to 10 : 1,

whilst for a drop in compression ratio from 6 to 4 : 1, there was quite a large decrease in the burning velocity.

The effects of compression ratio variation on the flame travel times throughout combustion have however been studied by Harrow, Ellison and Hayward[164]. These workers found that the flame travel times decreased at all stages of combustion development with increasing compression ratio. The interpretation of their results, however, is dependent, as already stated, on the ability to differentiate between increases in flame speed due to reduction in exhaust residuals and increases in flame speed due to the aerodynamic conditions and the higher temperatures existent in the combustion chamber. Despite this, substantially the same conclusions were drawn from these results as were obtained by Semenov. On this basis, therefore, it is concluded that decreases in compression ratio from quite high values down to about 6 : 1 produce no significant changes on the effects of mixture motion on burning velocity. Since, also, modern engines usually have compression ratios greater than 6 : 1, it is reasonable to ignore any such changes to a first approximation.

It was shown by Semenov[110] and Molchanov[109] (see Figs. 4-13 and 4-18) that accoustical oscillations of the gas column in the intake pipe influenced the gas velocities only during induction. These oscillations were found to have largely disappeared by the time the flame propagation period was reached. Such observations were only appropriate, however, up to an engine speed of 1200 rev/min. Kumag ai and Kudo[46], on the other hand, showed that in high speed (up to

manifold temperatures and pressures[165], humidity,[165] combustion chamber deposits[31] and exhaust residuals or other diluents[165].

The derived correction factor, K_T, in Equation 4-55 resulted from experiments with iso-octane only. It appears perfectly reasonable, however, to assume that this relationship also applies to the other two fuels used in this work. viz. propane and benzene. This is because the degree of mixture motion is independent of fuel type.

Thus, in this work, the turbulent burning velocity is given by the expression

$$U_T = U_L \times (1 + 0.00197.n) \qquad \text{---- 4-58}$$

where U_L is the laminar burning velocity given by the Semenov relationship in Equation 4-47.

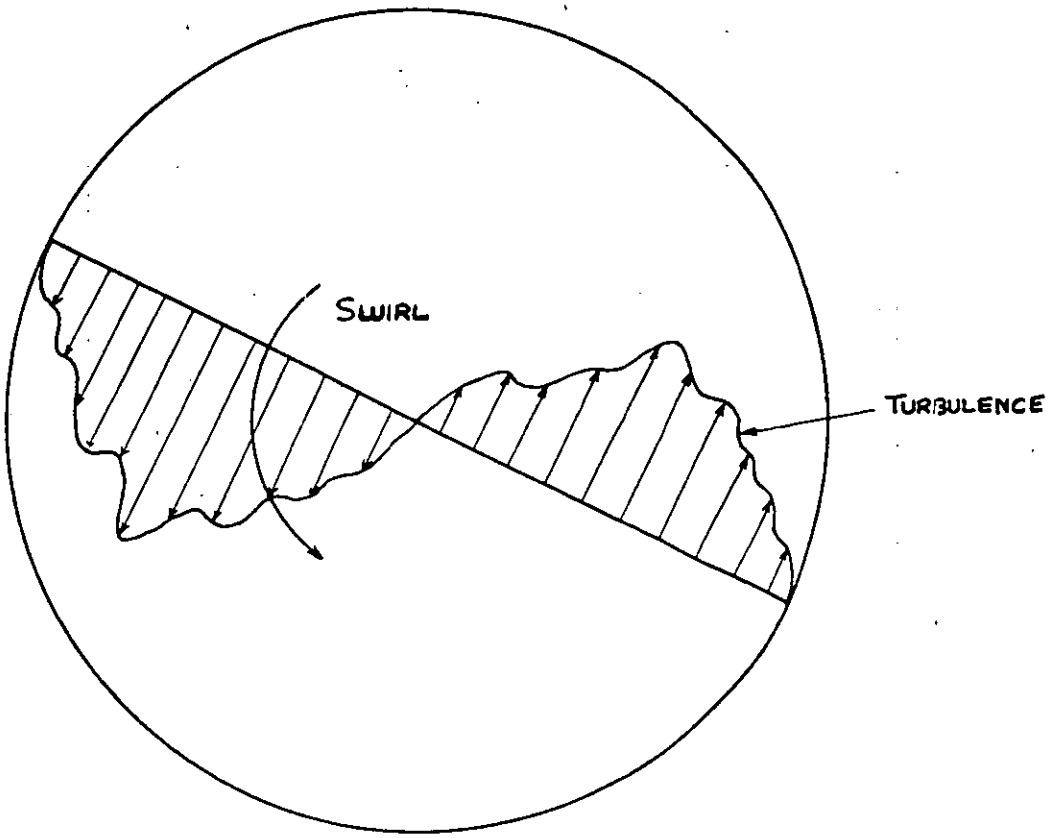

FIG. 4-1 —— A HYPOTHETICAL ILLUSTRATION OF SWIRL IN AN ENGINE CYLINDER AT AN INSTANT OF TIME.

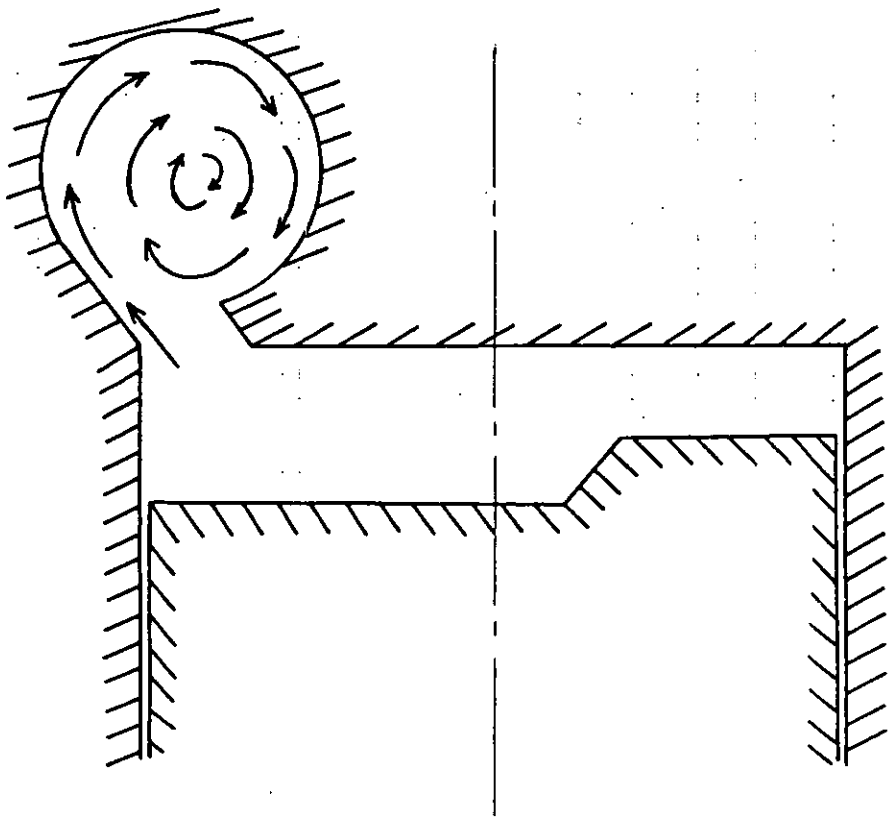

FIG. 4-2 — A SWIRL CHAMBER ENGINE (RICARDO COMET).

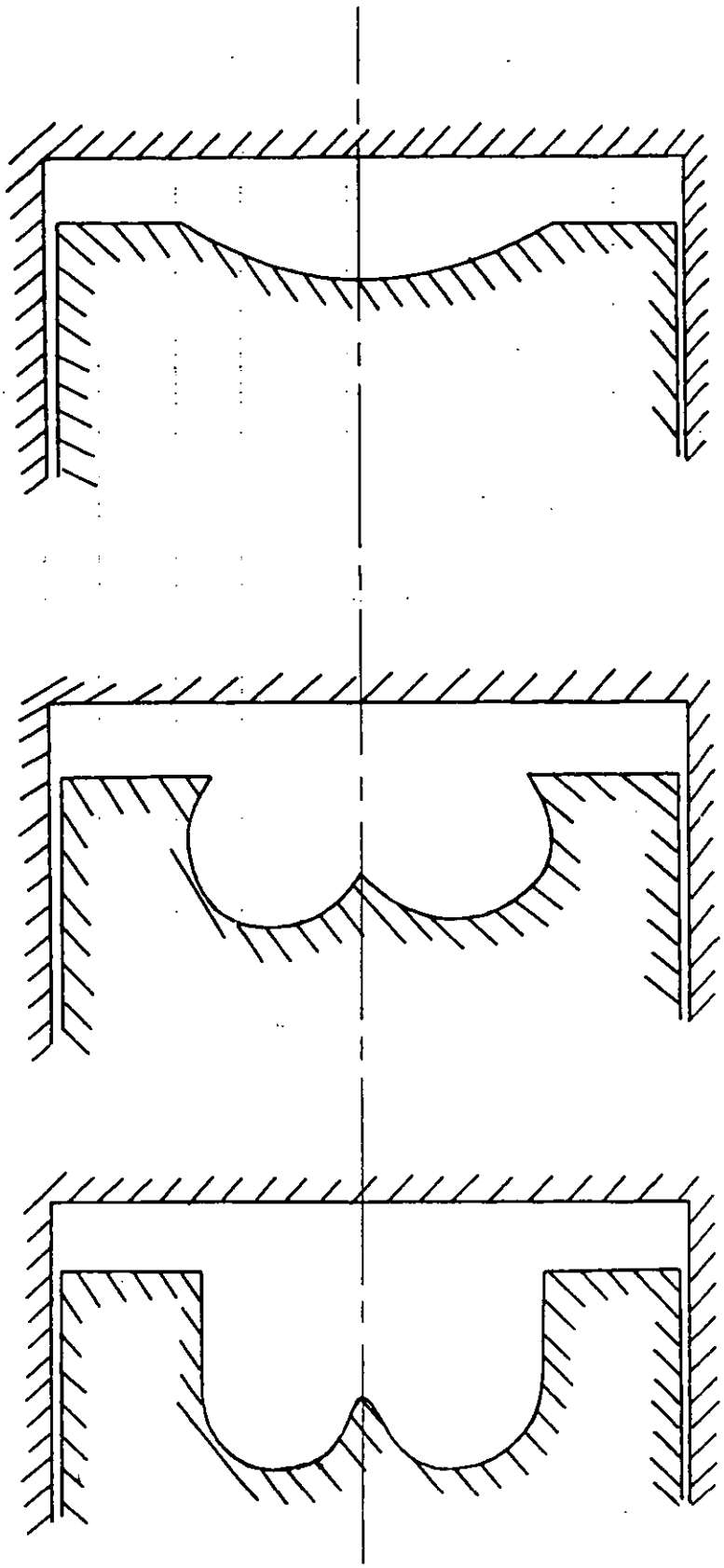

FIG. 4-3 — PISTON SHAPES USED TO GENERATE A SWIRL BY MEANS OF A 'SQUISH' EFFECT.

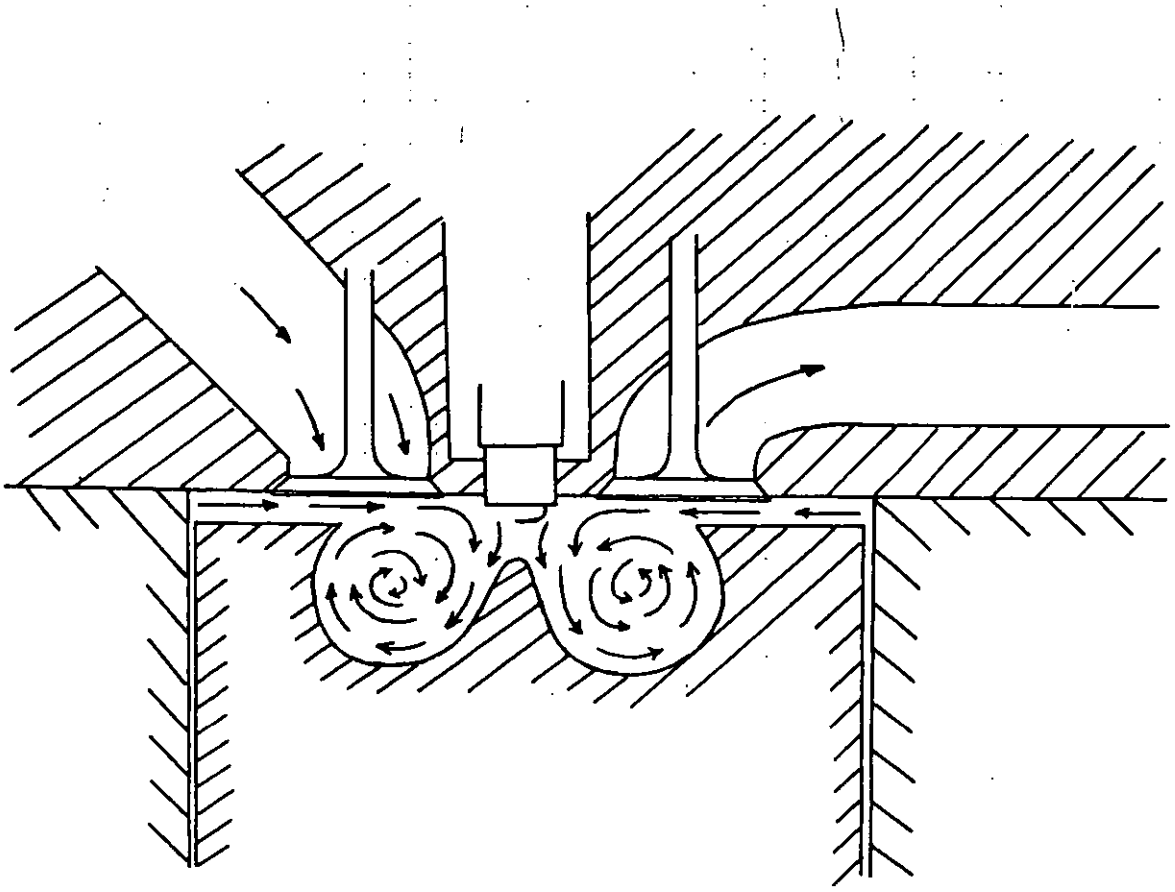

FIG. 4-4 — TOROIDAL OR SMOKE RING MOTION PRODUCED BY 'SQUISH' (FROM CLARKE[26])

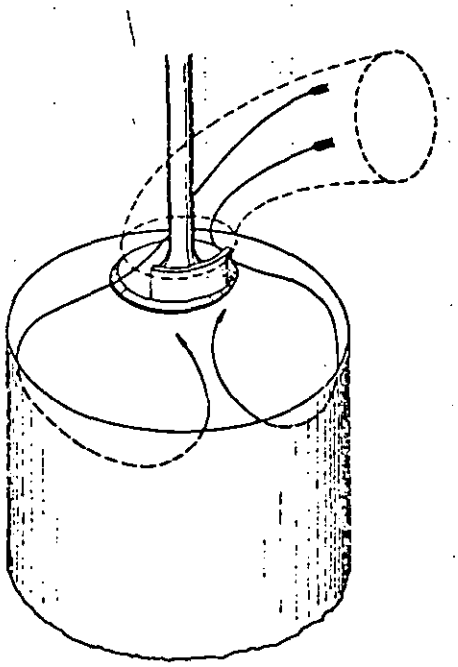

FIG. 4-5 — AIR FLOW THROUGH VALVE WITH MASK AT POSITION $\alpha = 90°$ (FROM WILLIS ET AL[102])

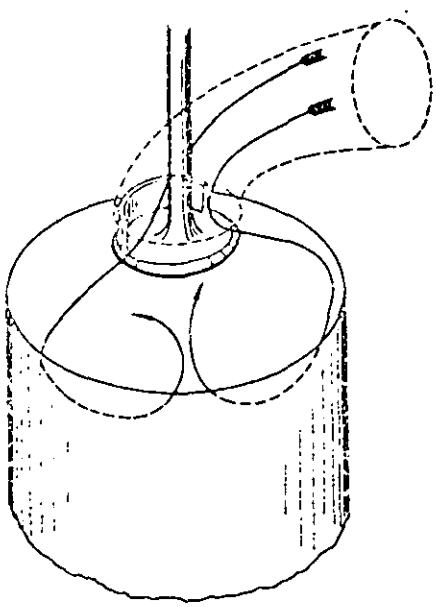

FIG. 4-6 — AIR FLOW THROUGH VALVE WITH MASK AT POSITION $\alpha = 270°$ (FROM WILLIS ET AL[102])

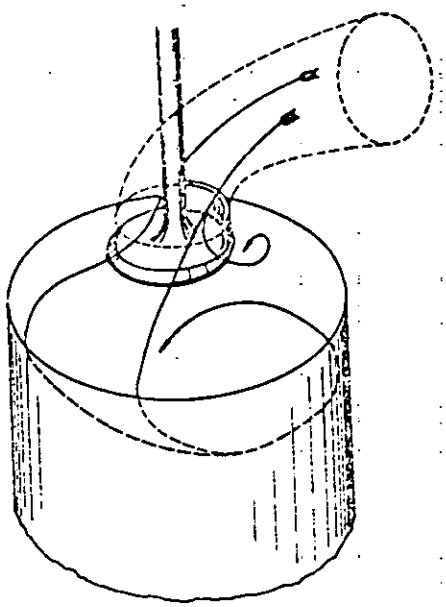

FIG. 4-7 — AIR FLOW THROUGH VALVE WITH MASK AT POSITION $\alpha = 0°$ (FROM WILLIS ET AL[102])

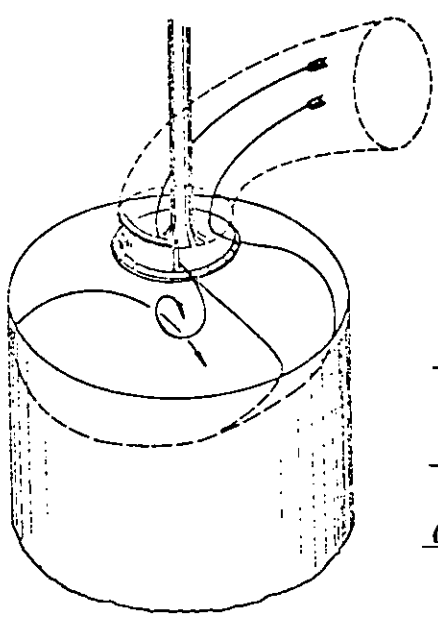

FIG. 4-8 — AIR FLOW THROUGH VALVE WITH MASK AT POSITION $\alpha = 180°$ (FROM WILLIS ET AL[102]).

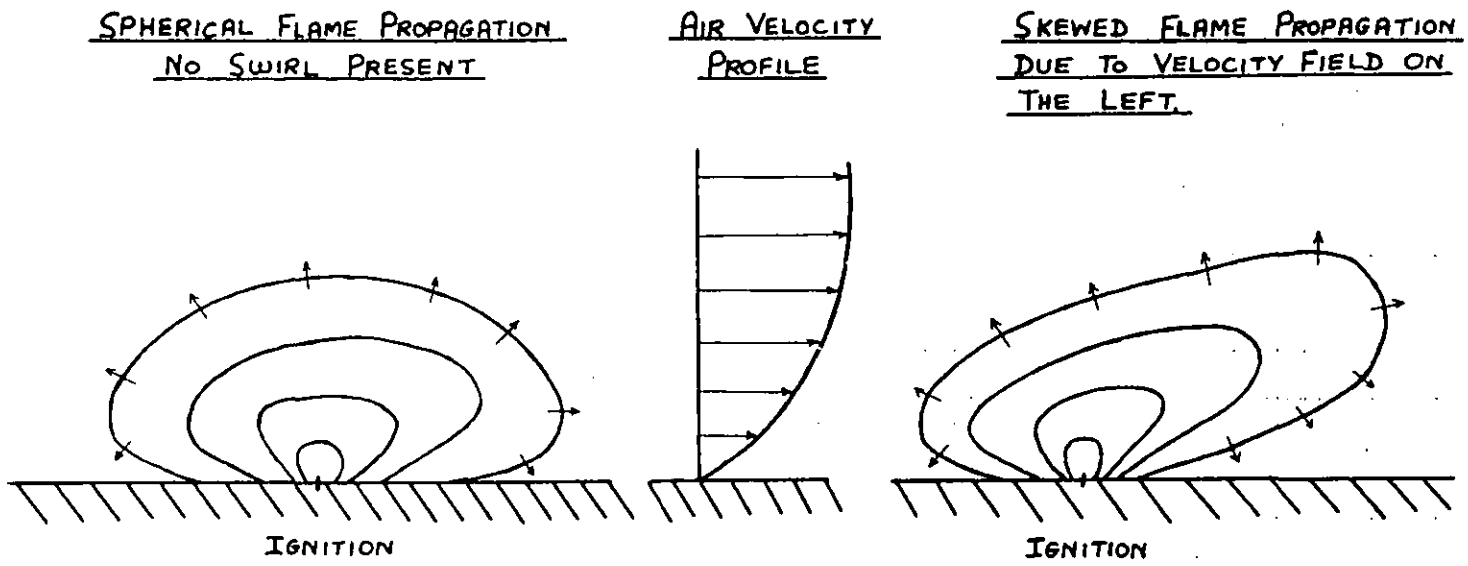

FIG. 4-9 —— A HYPOTHETICAL ILLUSTRATION OF THE MANNER IN WHICH THE VELOCITY GRADIENTS SMEAR THE FLAME KERNEL JUST AFTER IGNITION AND INCREASES ITS FLAME FRONT AREA (FROM PATTERSON[51])

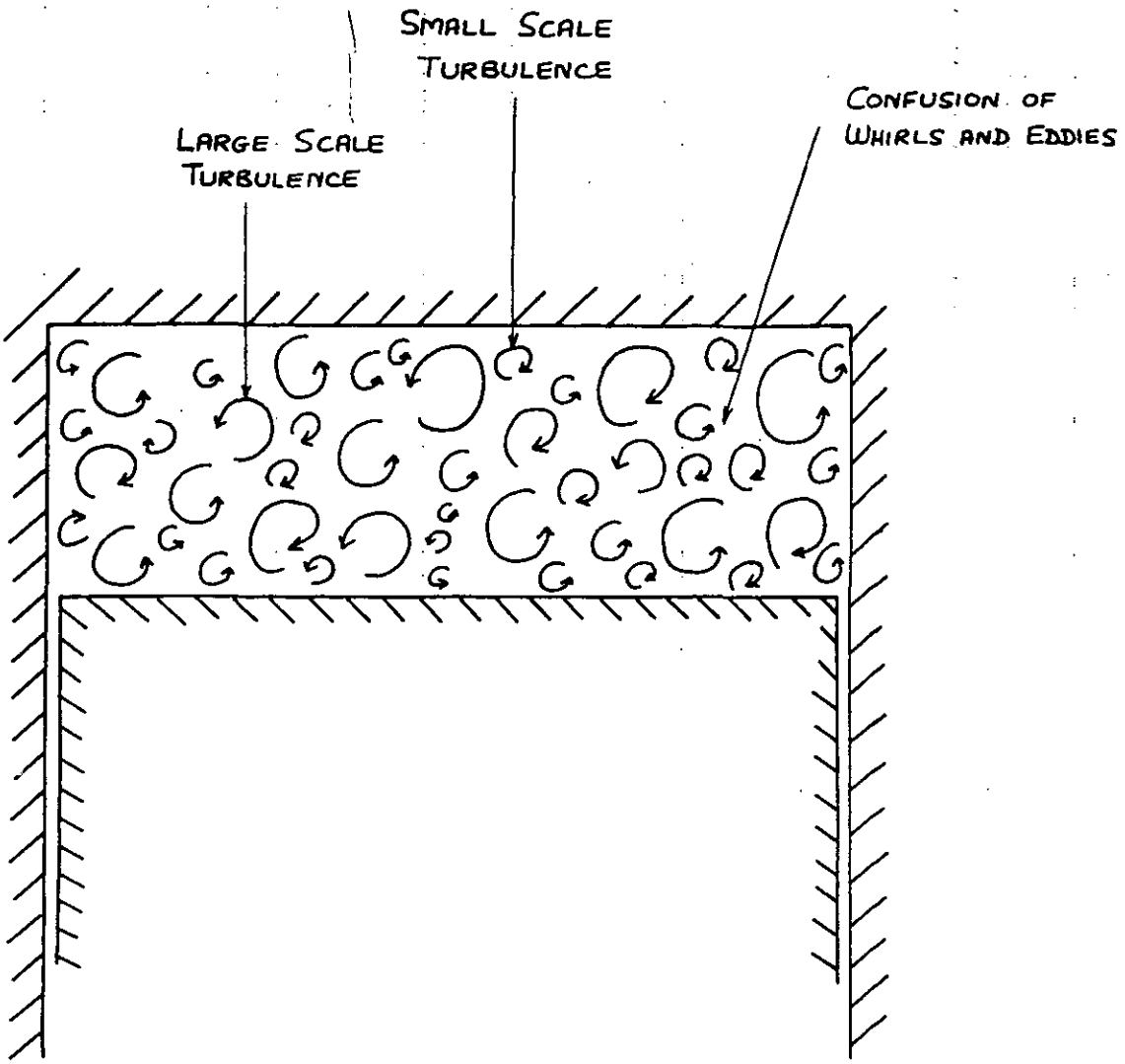

FIG. 4-10 — HYPOTHETICAL ILLUSTRATION AT AN INSTANT OF TIME OF A POSSIBLE AERODYNAMIC CONDITION IN A COMBUSTION CHAMBER WITH NO SWIRL.

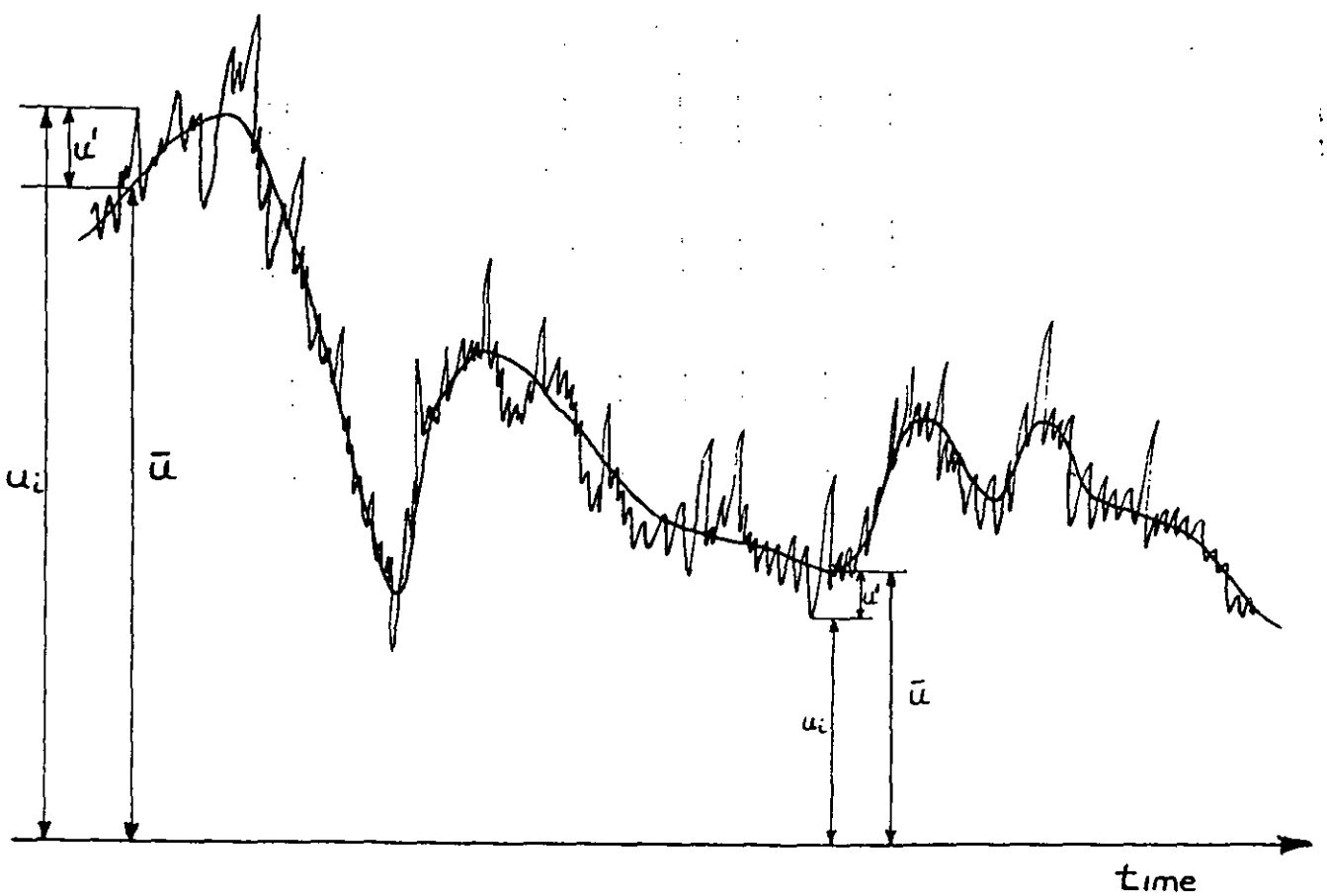

FIG. 4-11 — FLUCTUATIONS OF THE INSTANTANEOUS FLOW VELOCITY WITH RESPECT TO TIME IN THE X-DIRECTION WHEN NO LARGE-SCALE, MASS MOVEMENT EXISTS.

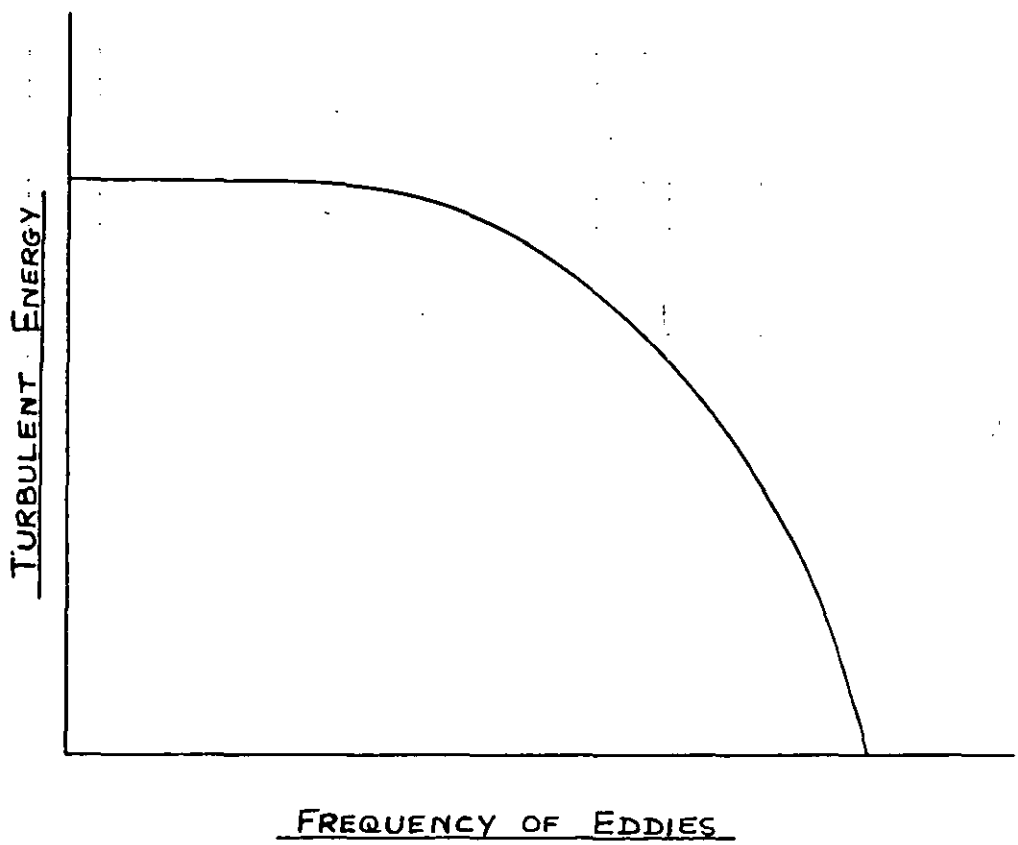

FIG. 4-12 — A TYPICAL TURBULENCE SPECTRAL DISTRIBUTION.

IVO – INLET VALVE OPENING
IVC – INLET VALVE CLOSING

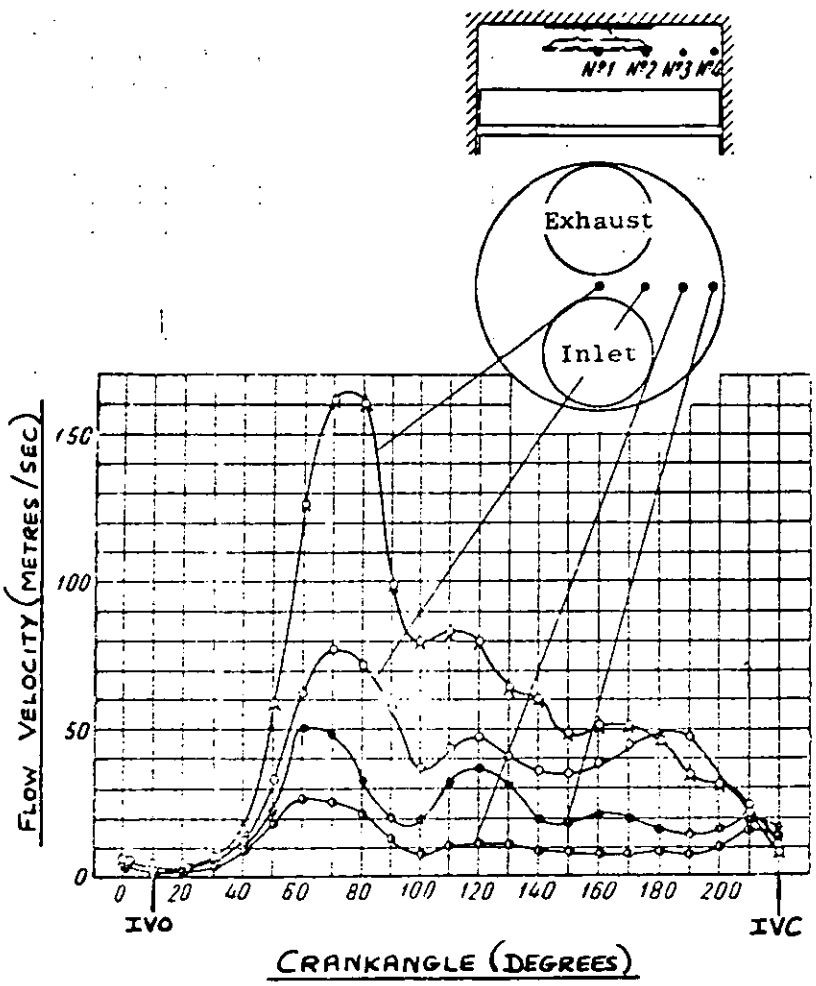

FIG. 4-13 — VARIATION OF GAS FLOW VELOCITIES AT VARIOUS POINTS DURING THE CHARGING PERIOD (FROM MOLCHANOV[109])

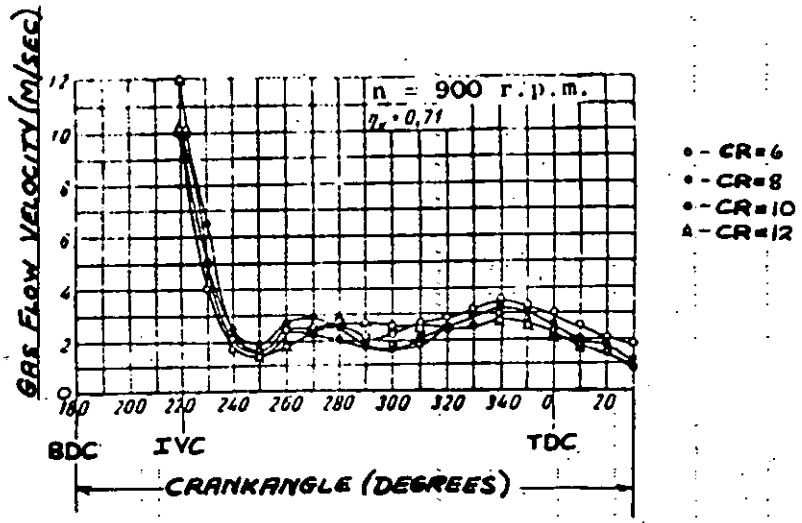

FIG. 4-14 — GAS FLOW VELOCITIES IN THE COMBUSTION CHAMBER DURING COMPRESSION AT VARIOUS COMPRESSION RATIOS (FROM MOLCHANOV[109])

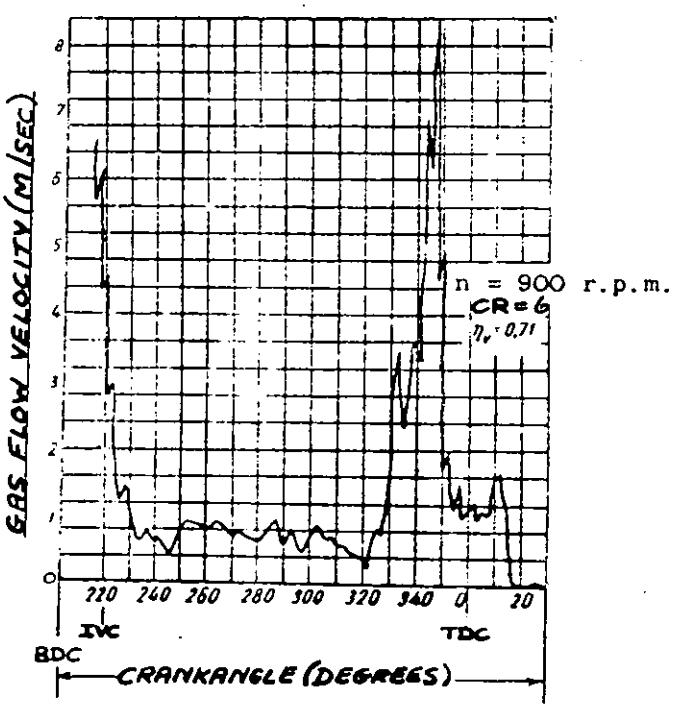

FIG. 4-15 — VARIATIONS IN THE GAS FLOW VELOCITY FLUCTUATIONS IN THE COMBUSTION CHAMBER DURING COMPRESSION (FROM MOLCHANOV[109])

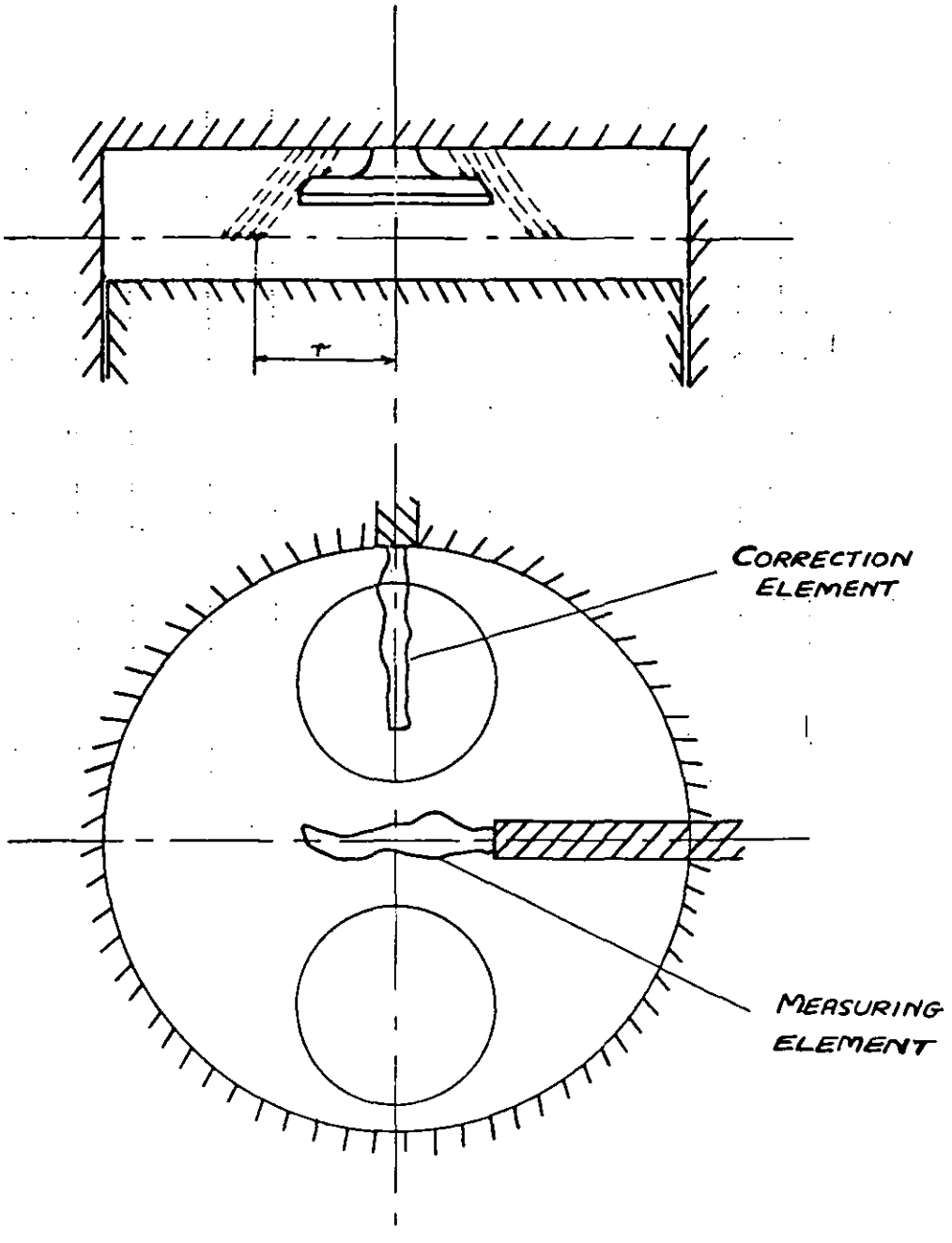

FIG. 4-16 —— ARRANGEMENT OF MEASURING ELEMENTS IN THE COMBUSTION CHAMBER USED BY SEMENOV[110]

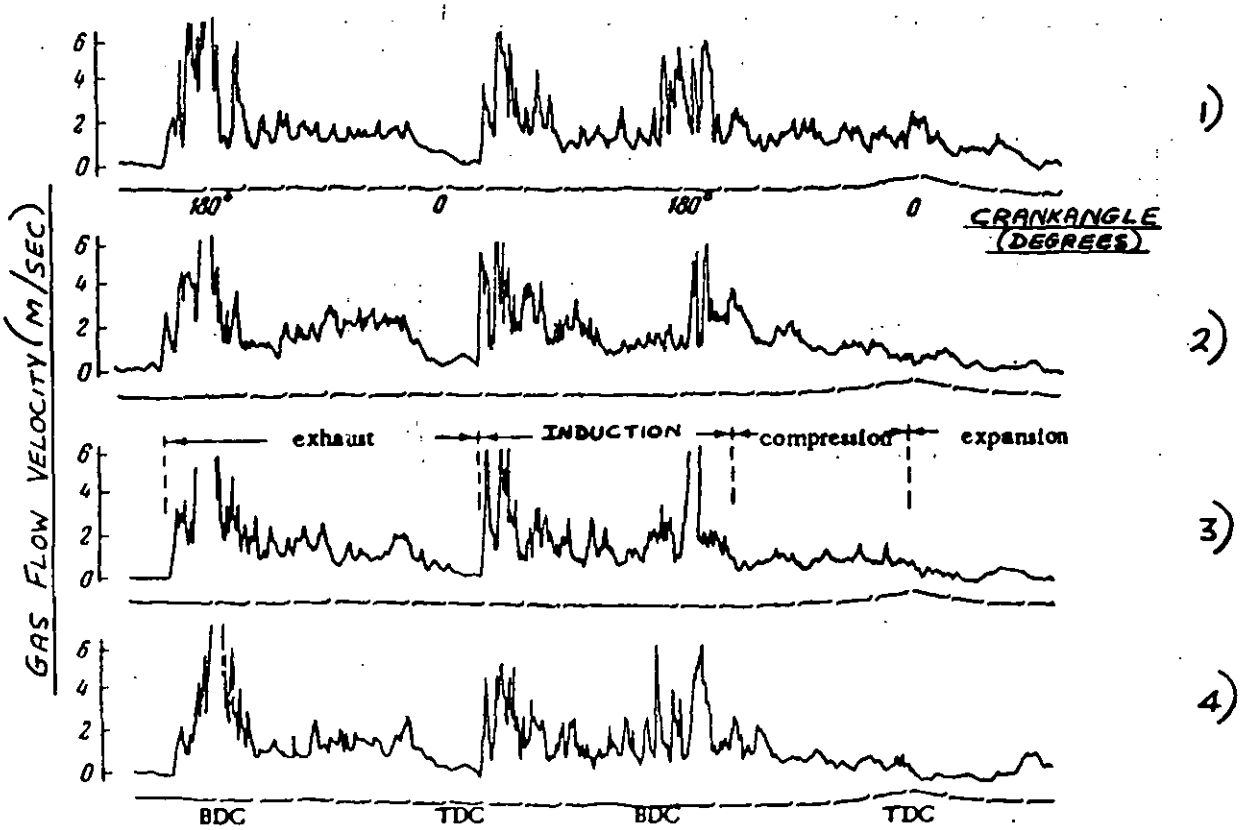

FIG. 4-17 — OSCILLOGRAMS OF THE INSTANTANEOUS FLOW VELOCITY AT A POINT IN A CYLINDER FOR FOUR SUCCESSIVE CYCLES (FROM SEMENOV[108])

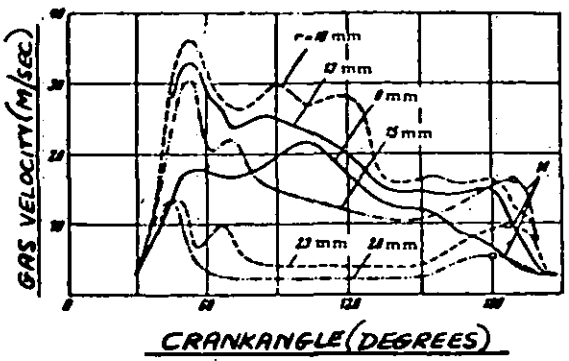

FIG. 4-18 — VARIATION OF GAS VELOCITY DURING INTAKE AT VARIOUS POINTS IN THE COMBUSTION CHAMBER (FROM SEMENOV[110])

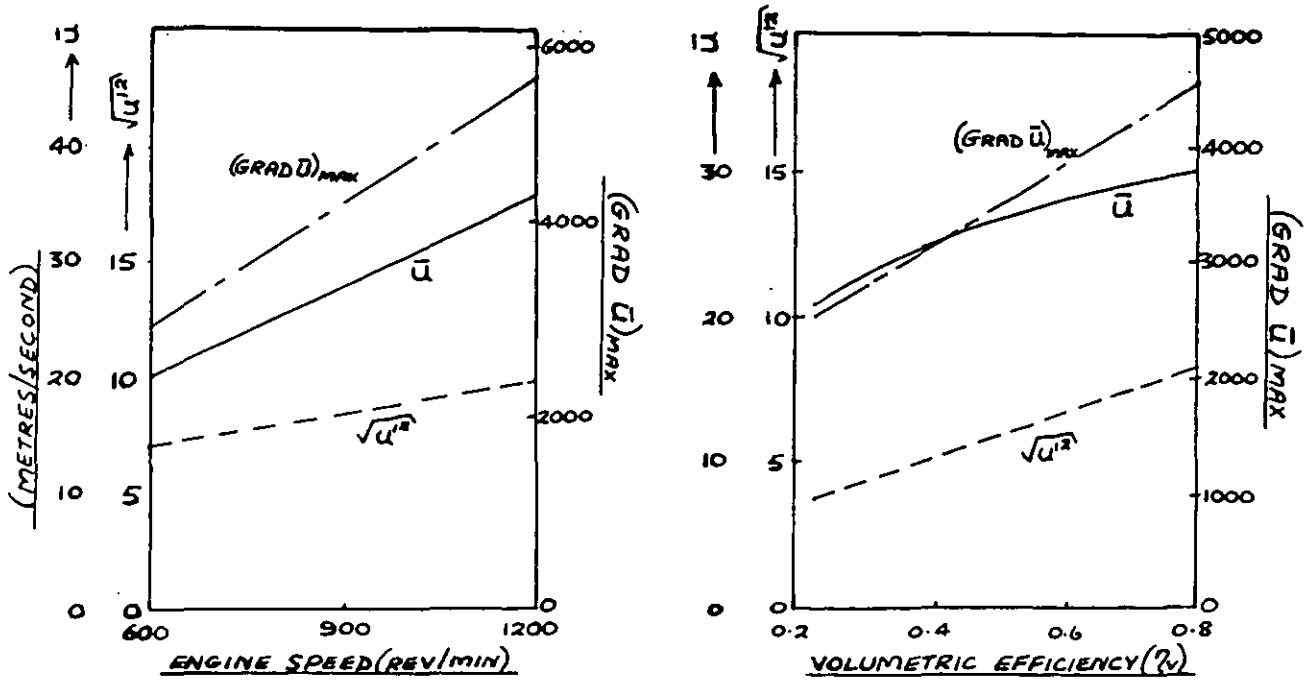

FIG. 4-19 — VARIATION OF THE AVERAGE VELOCITIES, THE FLUCTUATING VELOCITIES AND THE VELOCITY GRADIENTS OF THE GAS FLOW DURING INTAKE WITH ENGINE SPEED AND VOLUMETRIC EFFICIENCY (FROM SEMENOV[110])

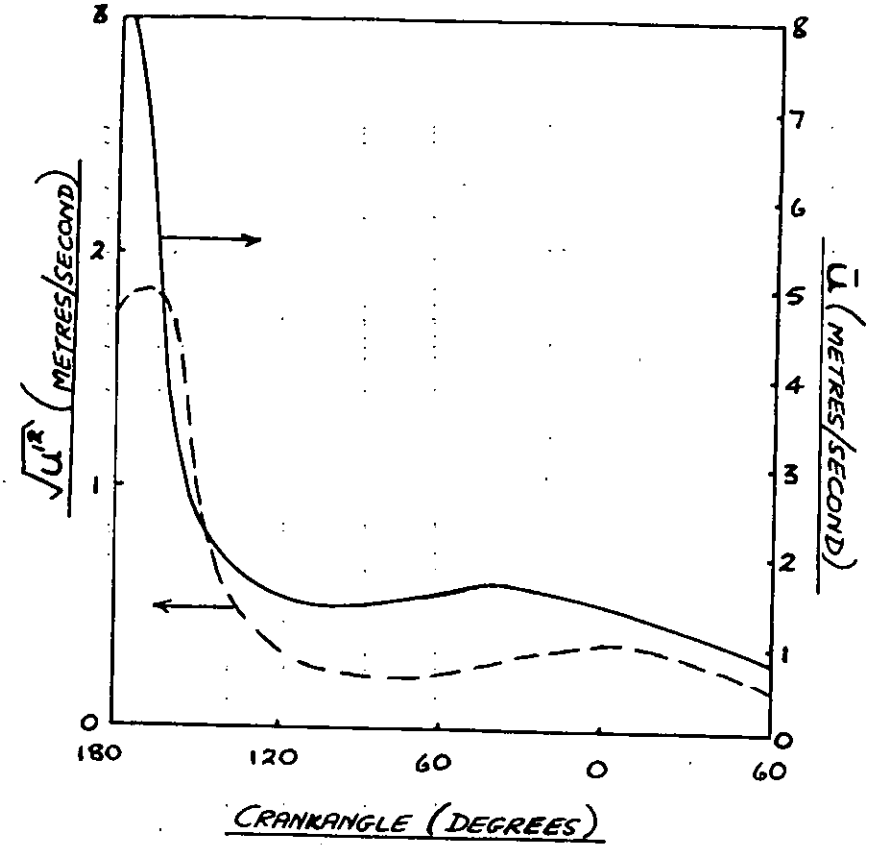

FIG. 4–20 — AVERAGE AND FLUCTUATING FLOW VELOCITIES DURING COMPRESSION (FROM SEMENOV[110])

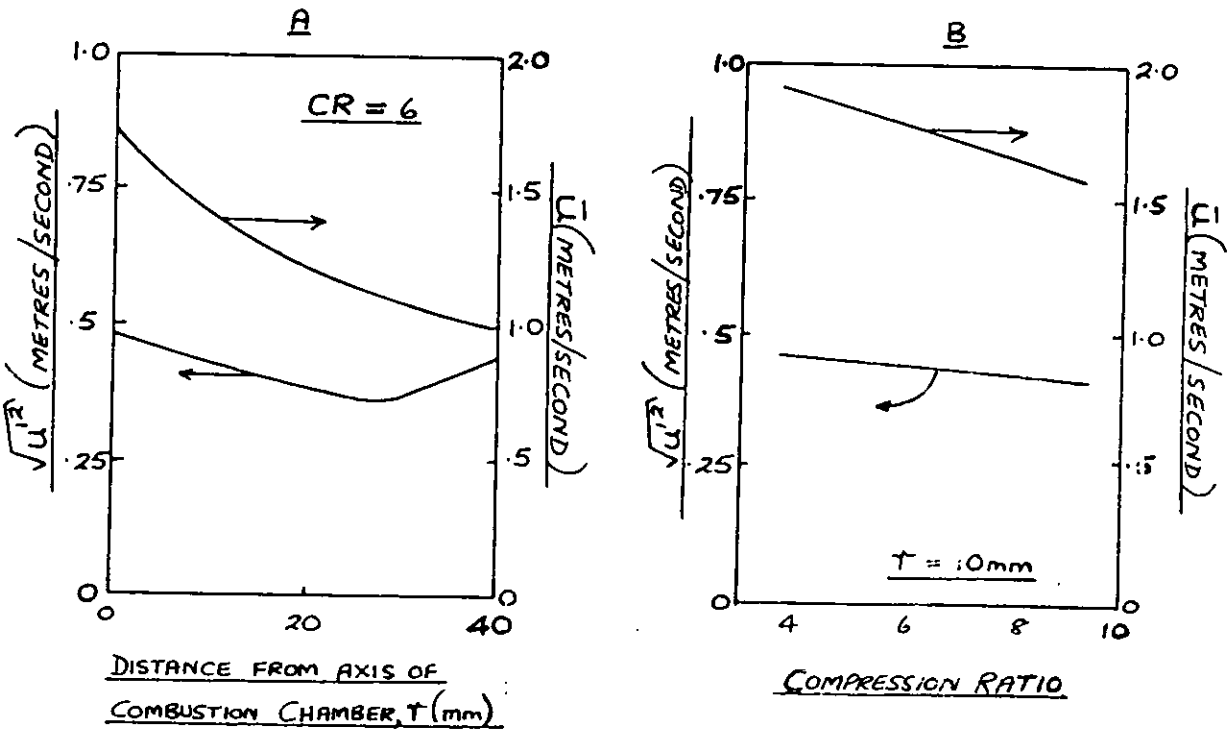

FIG. 4–21 — AVERAGE AND FLUCTUATING VELOCITIES AT T.D.C. ON THE COMPRESSION STROKE AT AN ENGINE SPEED OF 900 REV/MIN. A) AT VARIOUS POINTS IN COMBUSTION CHAMBER B) WITH VARYING COMPRESSION RATIO (FROM SEMENOV[110])

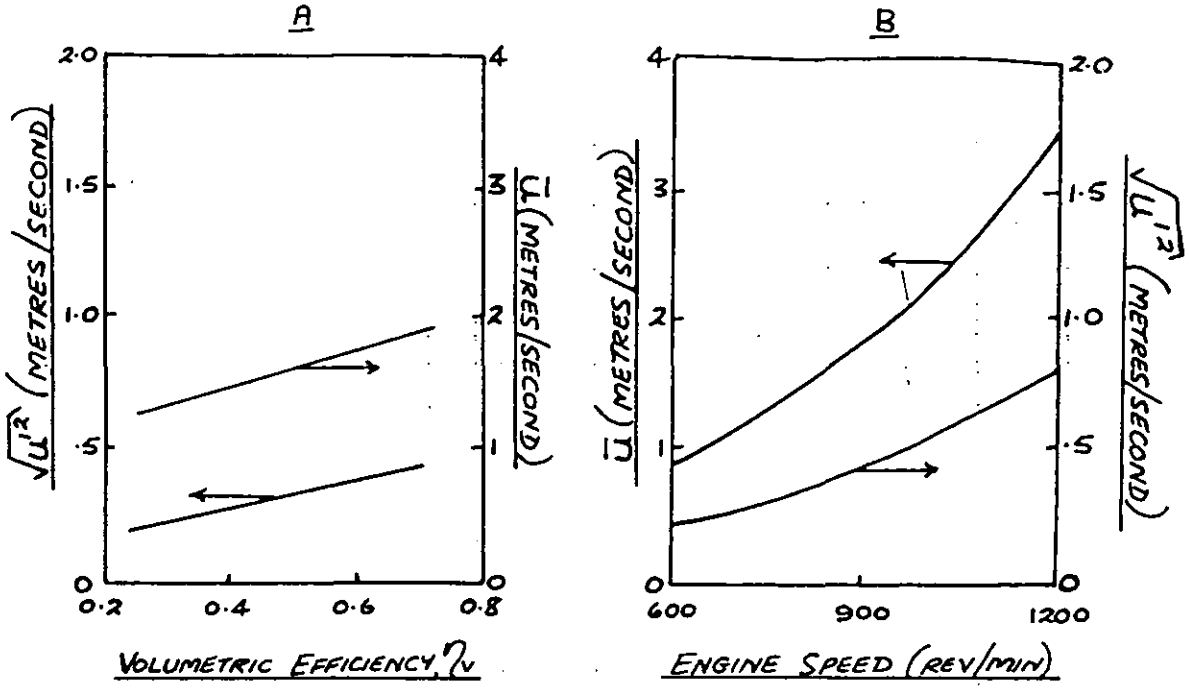

FIG. 4-22 — AVERAGE AND FLUCTUATING FLOW VELOCITIES AT T.D.C. ON THE COMPRESSION STROKE FOR CR = 6 AND t = 10mm. A) WITH VARYING η_v AND AT 900 REV/MIN. B) WITH VARYING ENGINE SPEED.[110]

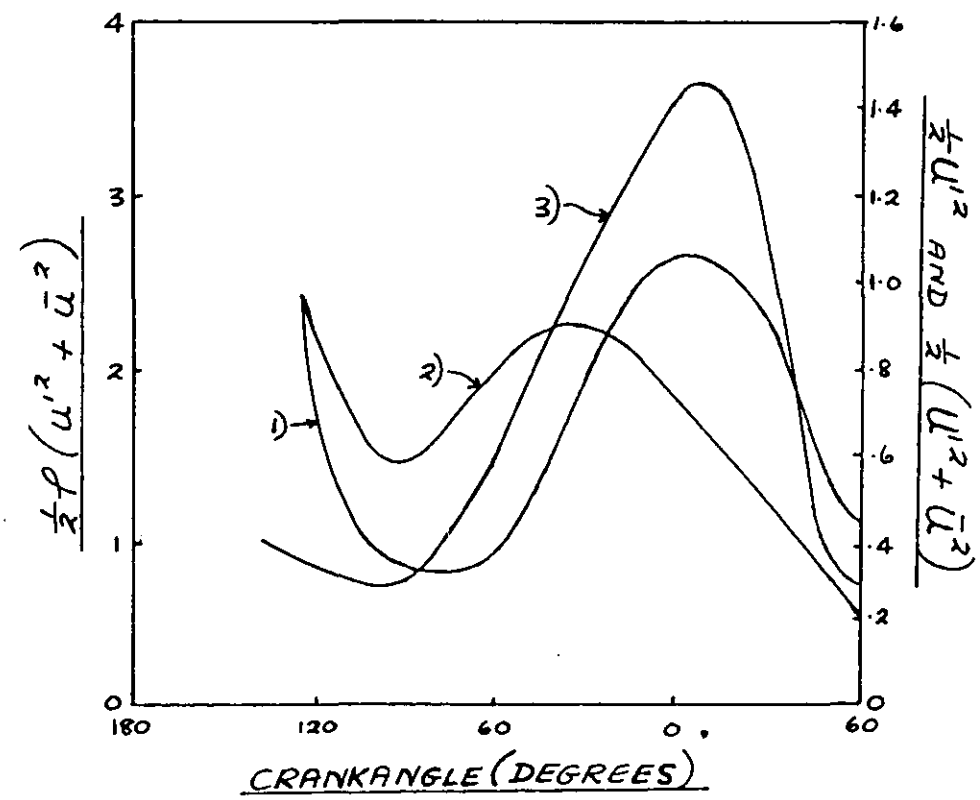

FIG. 4-23 — VARIATION OF THE FLUCTUATION ENERGY DURING THE COMPRESSION STROKE (CR = 6, t = 23mm AND n = 900 REV/MIN).
1) $\frac{1}{2}u'^2$: 2) $\frac{1}{2}(u'^2+\bar{u}^2)$: 3) $\frac{1}{2}\rho(u'^2+\bar{u}^2)$ — (FROM SEMENOV[110])

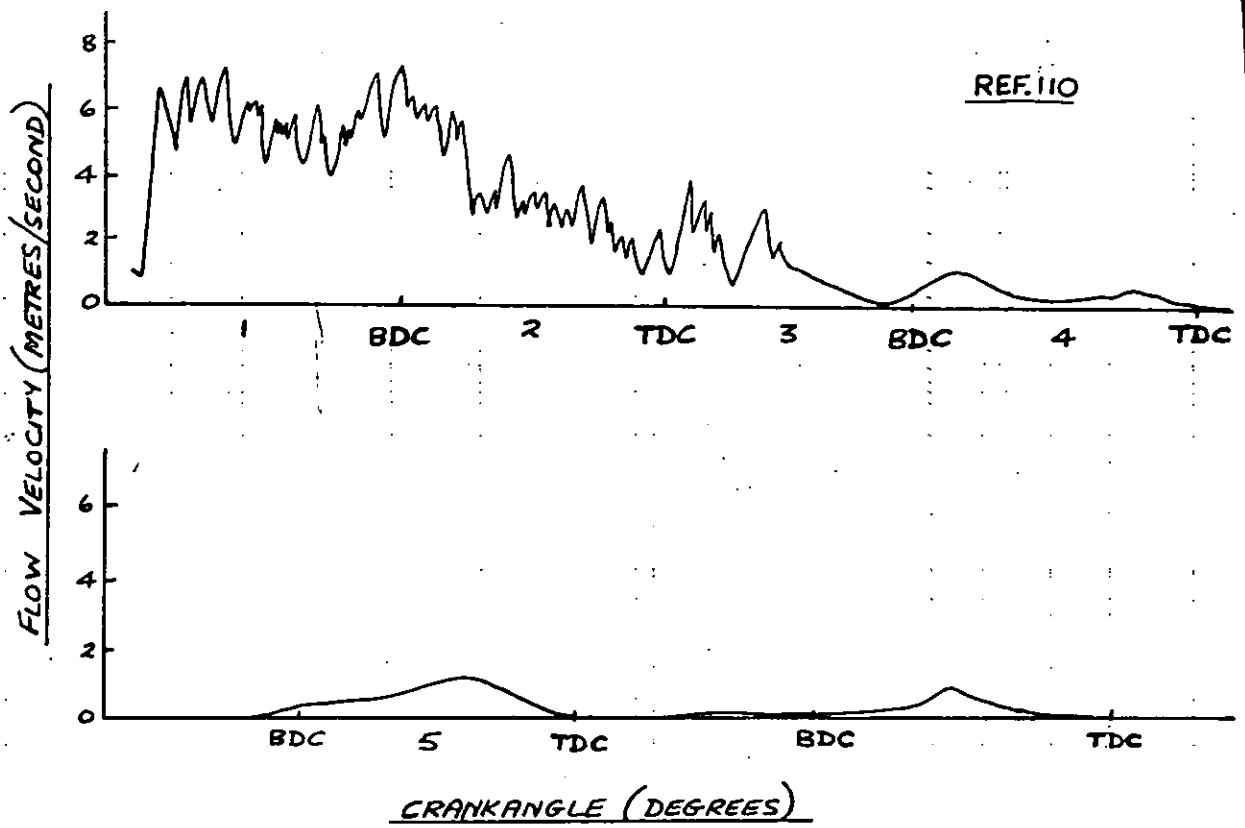

FIG. 4-24 — OSCILLOGRAM OF VELOCITY VARIATION DURING TRANSITION FROM A NORMAL CYCLE TO A CYCLE IN WHICH INTAKE AND EXHAUST ARE ABSENT. 1) INTAKE : 2) COMPRESSION : 3) EXPANSION : 4) SECOND COMPRESSION : 5) THIRD COMPRESSION

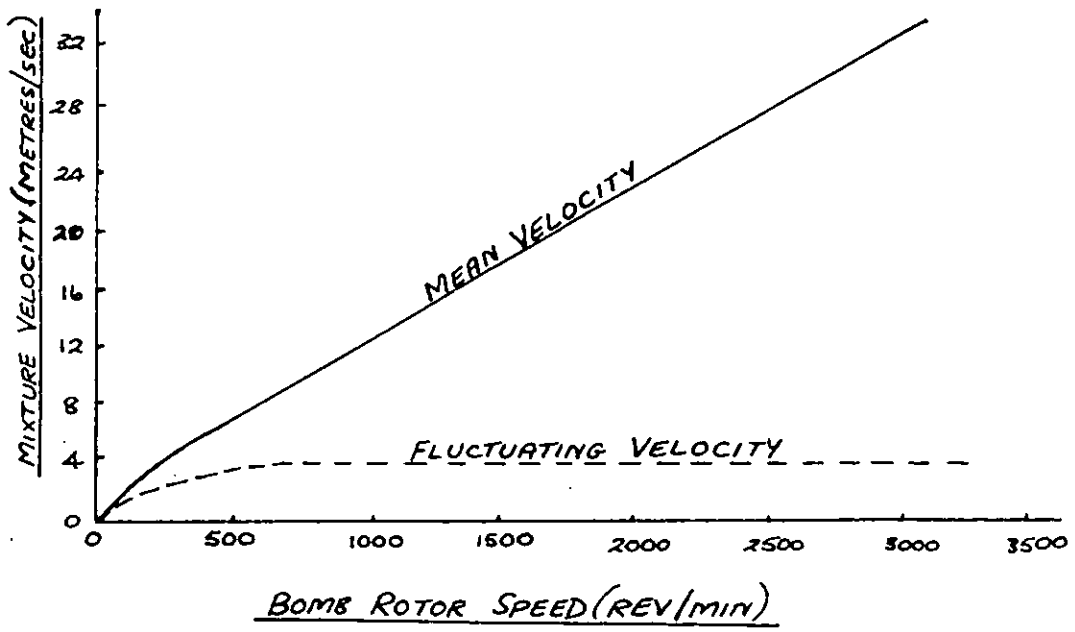

FIG. 4-25 — VARIATION OF MIXTURE VELOCITY CHARACTERISTICS WITH ROTOR SHAFT SPEED IN A CONSTANT VOLUME BOMB (FROM BOLT AND HARRINGTON[114])

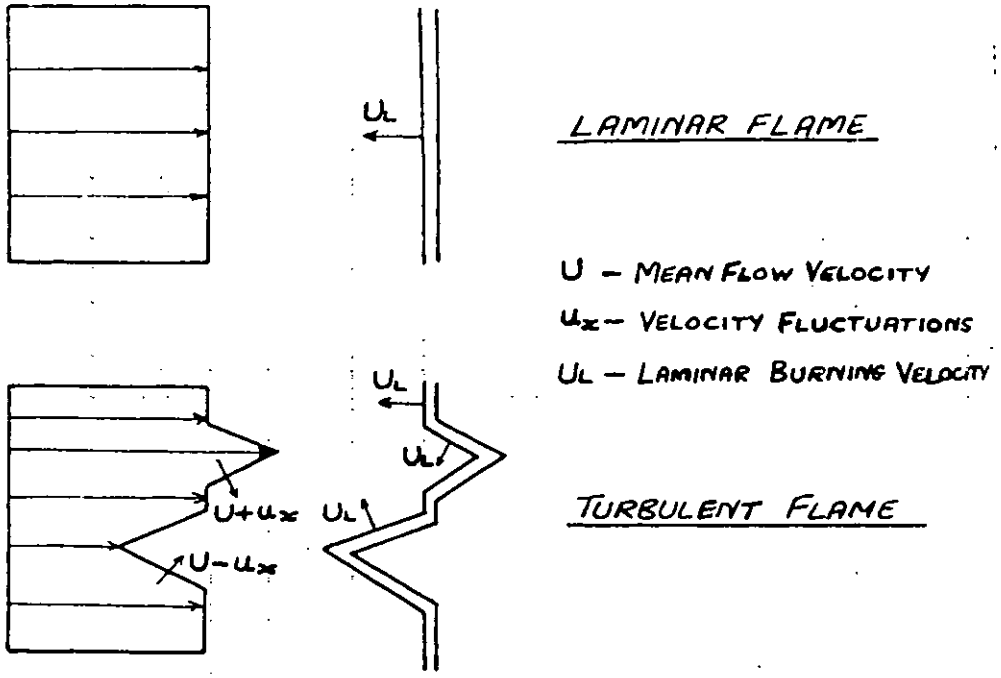

FIG. 4-26 — DAMKÖHLER'S EXPLANATION OF THE MANNER IN WHICH VELOCITY FLUCTUATIONS AFFECT A LAMINAR FLAME

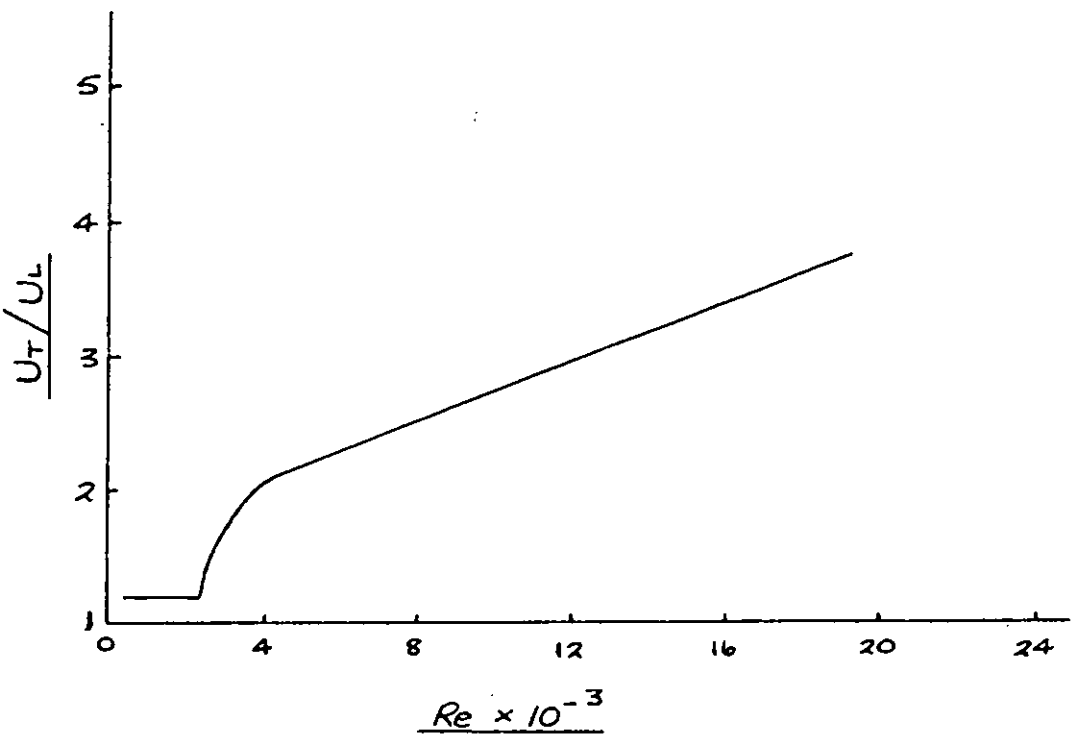

FIG. 4-27 — TURBULENT BURNING VELOCITY AS A FUNCTION OF THE REYNOLDS NUMBER OF THE APPROACH FLOW, ACCORDING TO DAMKÖHLER.

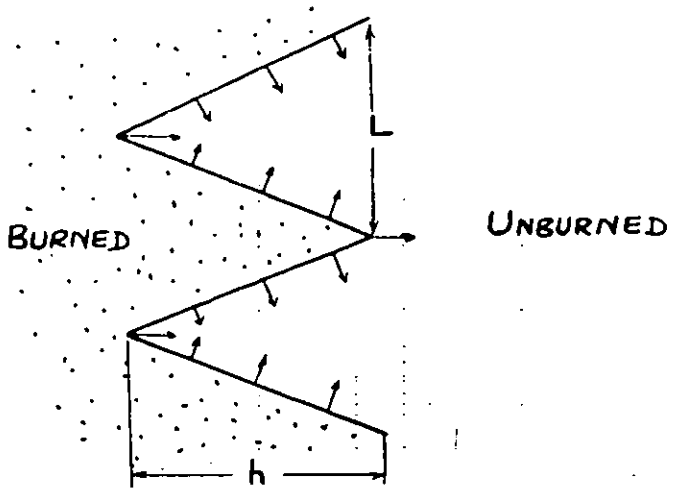

FIG. 4-28 — TURBULENT FLAME FRONT STRUCTURE ACCORDING TO SHCHELKIN.

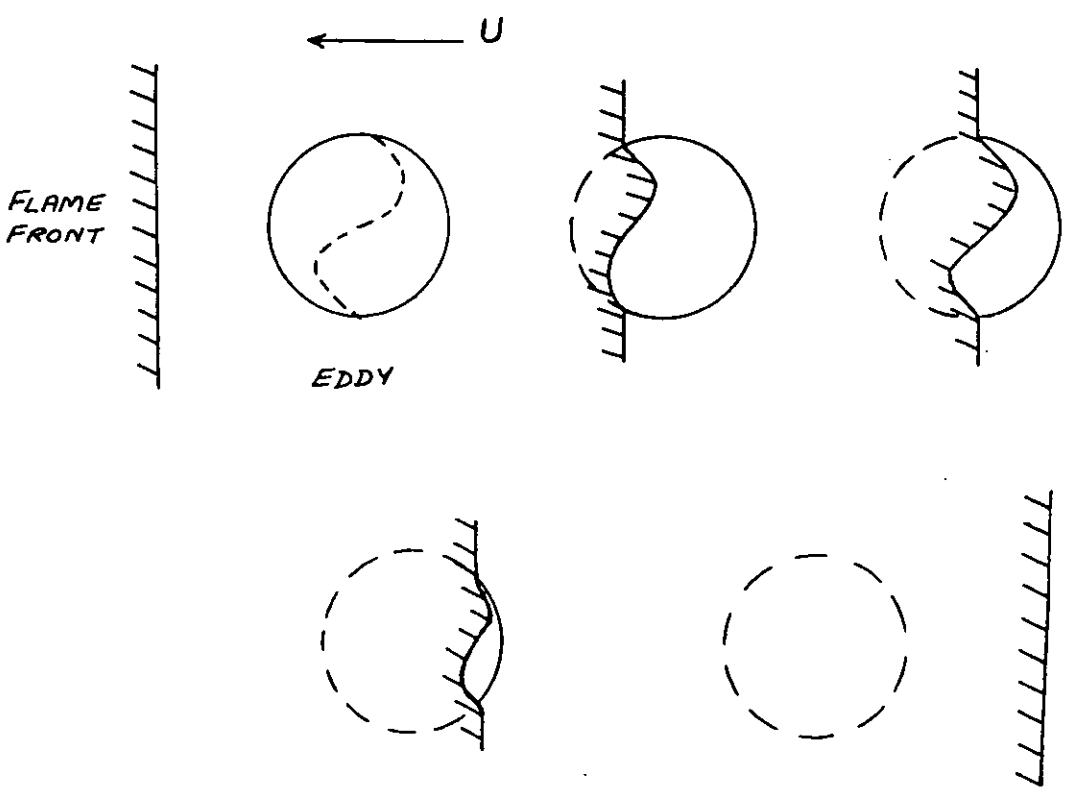

FIG. 4-29 — LEASON'S ANALYSIS OF THE PASSAGE OF AN EDDY THROUGH A FLAME

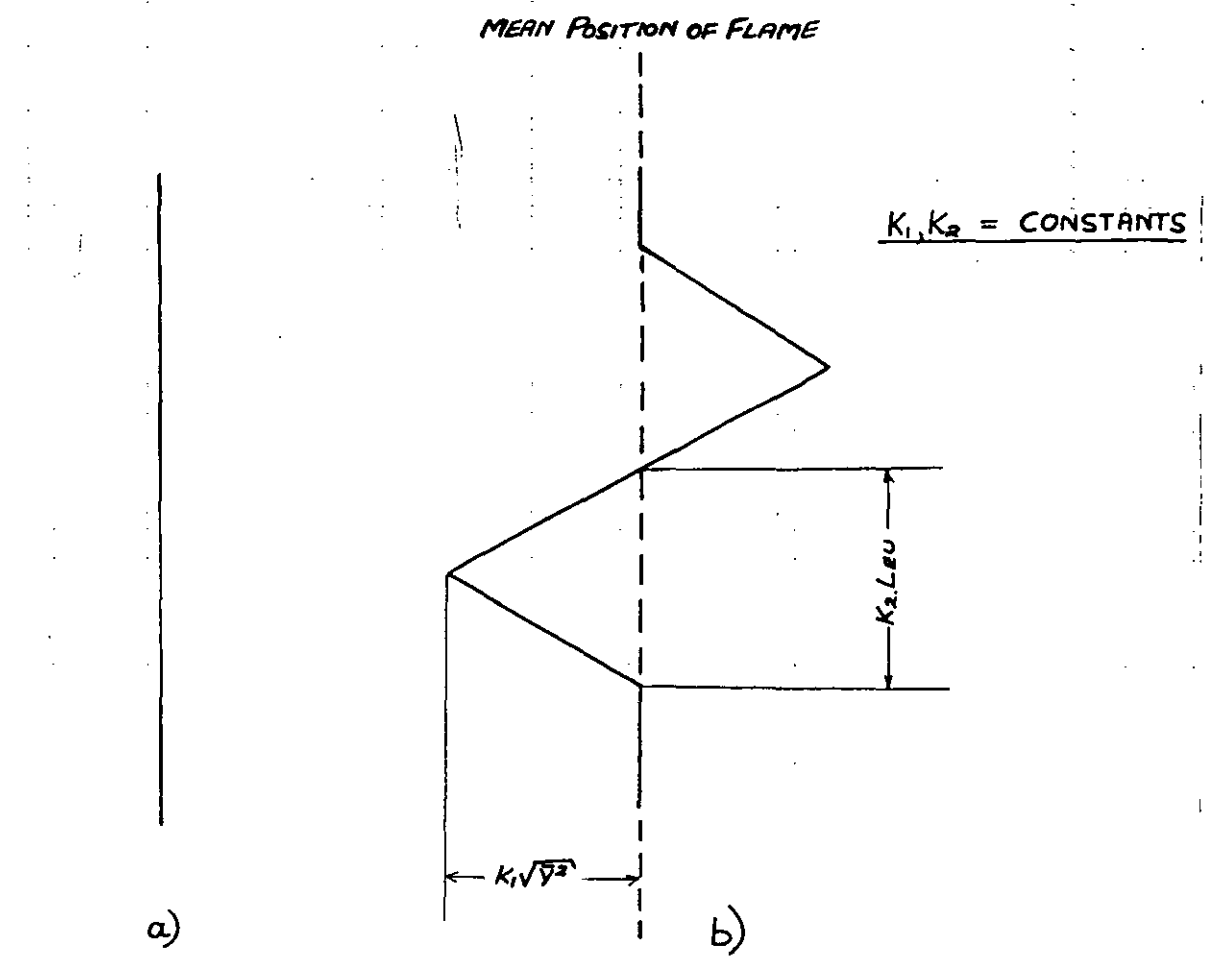

FIG. 4 – 30 — THE TURBULENT FLAME FRONT SURFACE ENVISAGED BY SCURLOCK AND GROVER

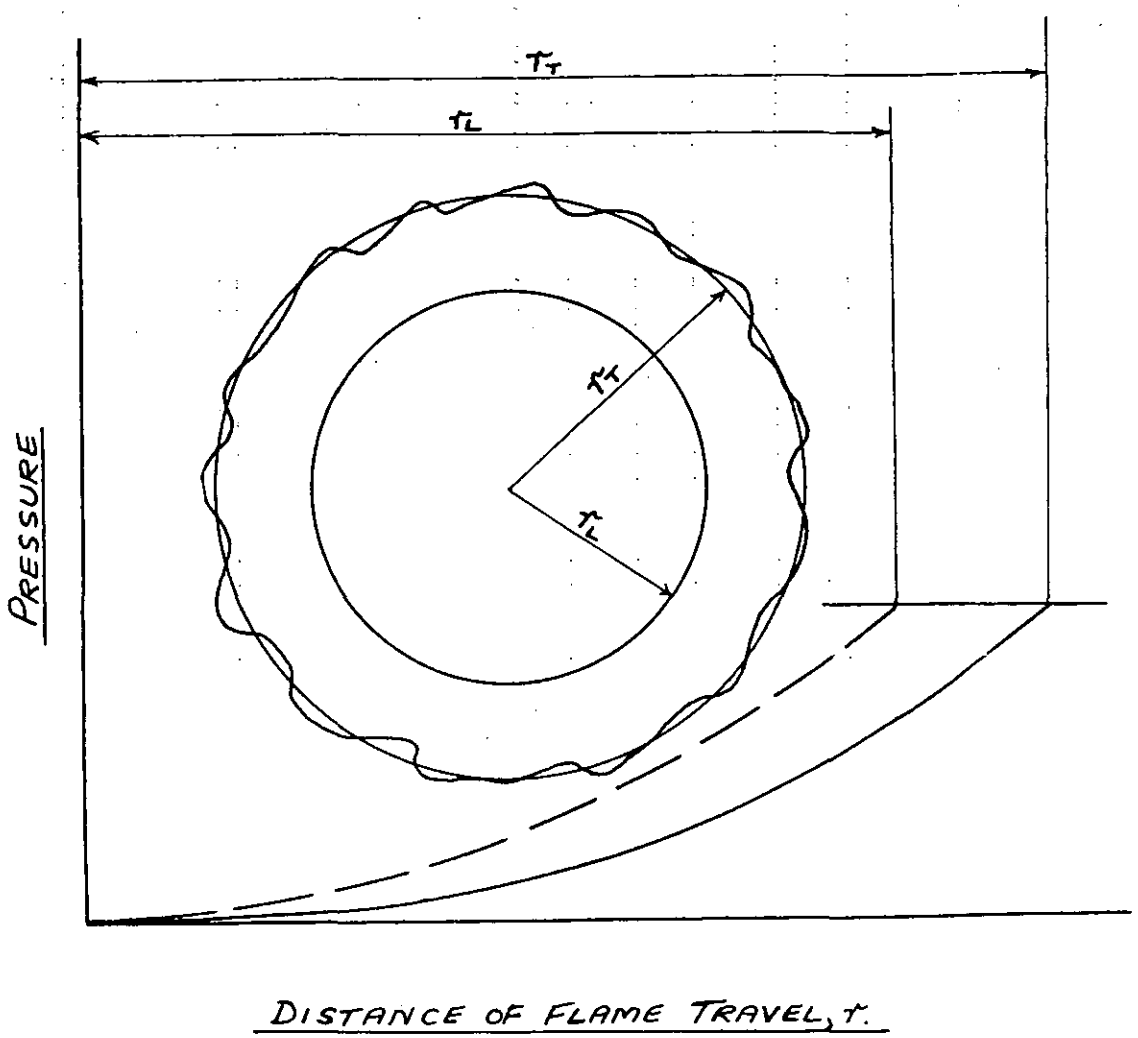

FIG. 4-31 — COMPARISON OF THE INCREASES IN PRESSURE WITH FLAME TRAVEL IN LAMINAR AND TURBULENT FLAMES (FROM SOKOLIK ET AL[115])

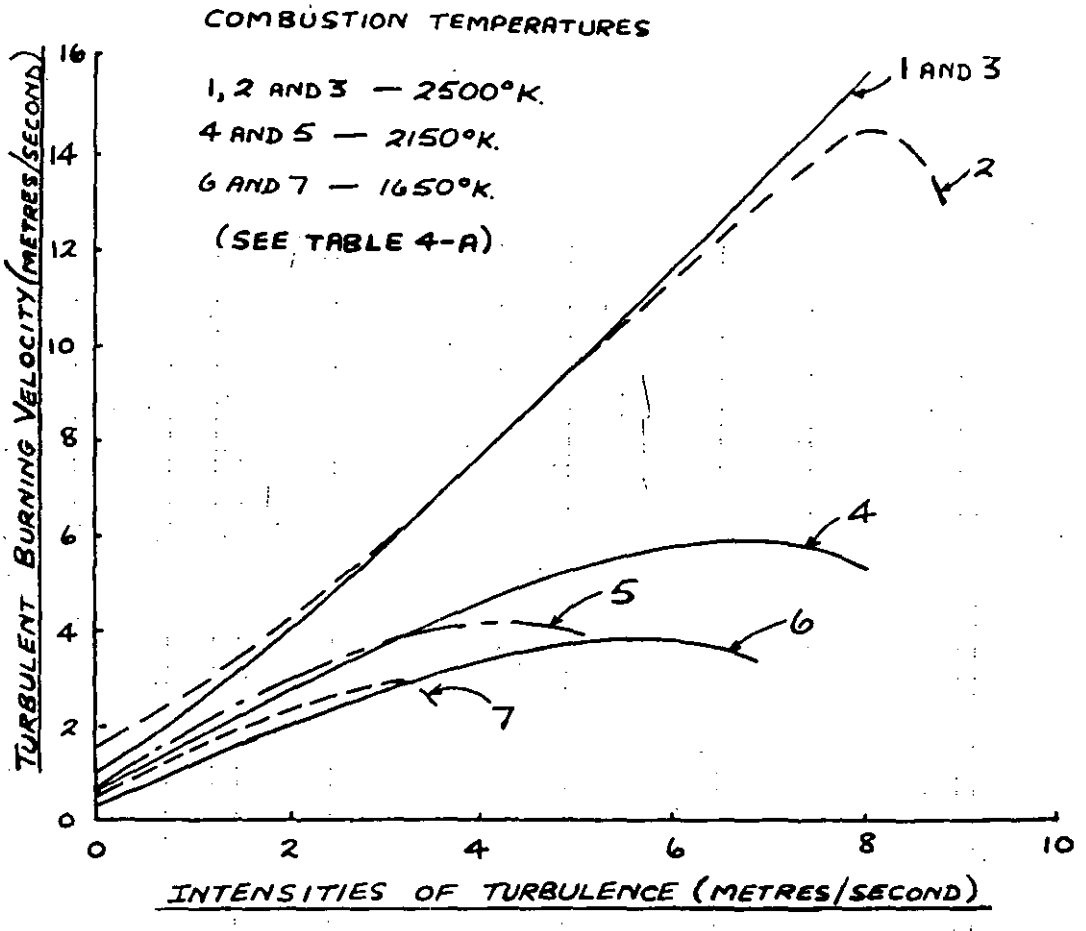

FIG. 4-32 — VELOCITIES OF TURBULENT COMBUSTION WITH VARYING TURBULENCE INTENSITIES (FROM SOKOLIK[115])

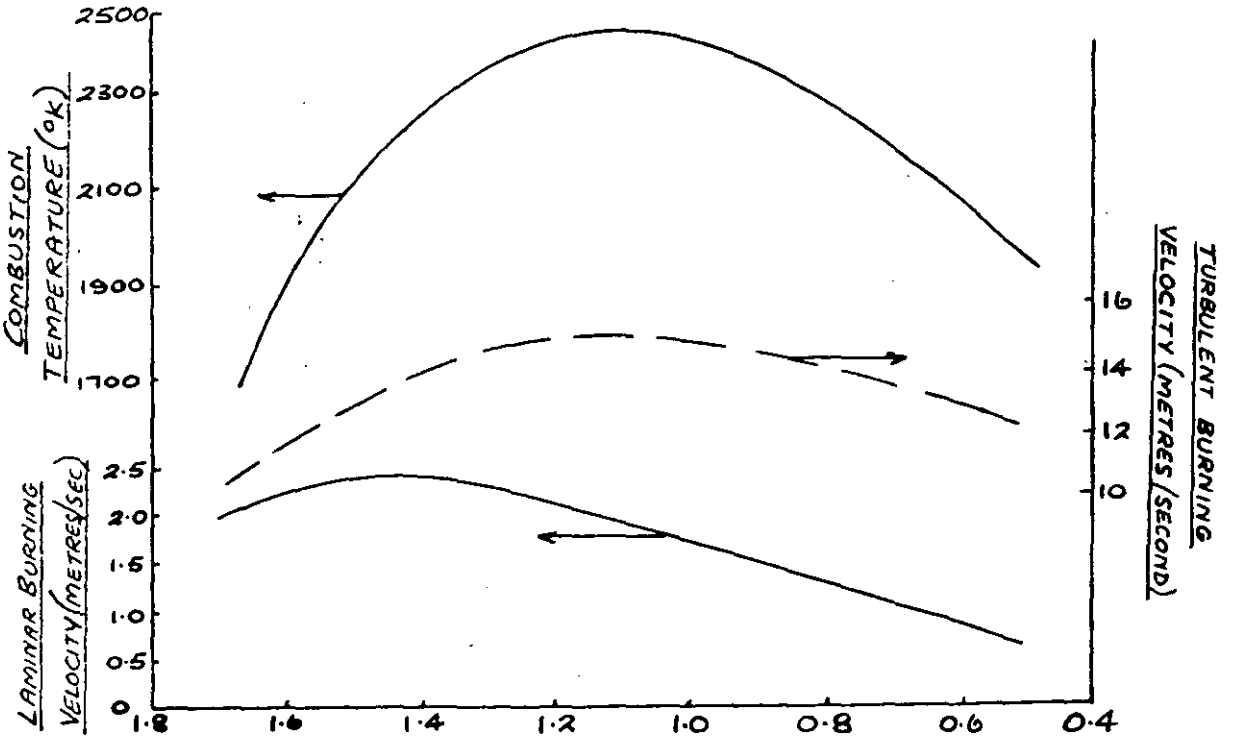

FIG. 4-33 — VARIATION IN THE TEMPERATURES AND BURNING VELOCITIES OF HYDROGEN FLAMES WITH MIXTURE

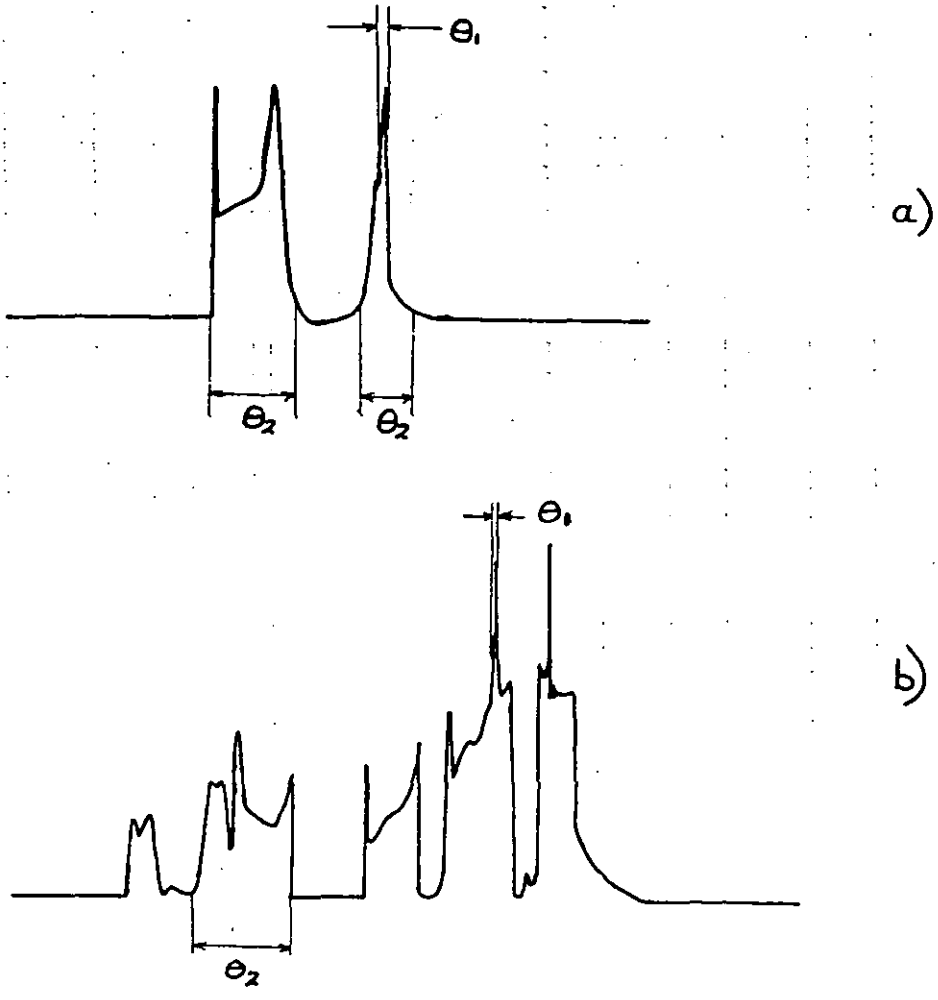

EQUIVALENCE RATIO = 1·1 PRESSURE = 1 ATM.

a) TURBULENCE INTENSITY = 2·2 METRES/SECOND

b) TURBULENCE INTENSITY = 3·0 METRES/SECOND.

FIG. 4–34 — OSCILLOGRAMS OF THE IONIZATION CURRENTS IN THE TURBULENT FLAMES OF PROPANE–AIR MIXTURES. (FROM SOKOLIK ET AL[115])

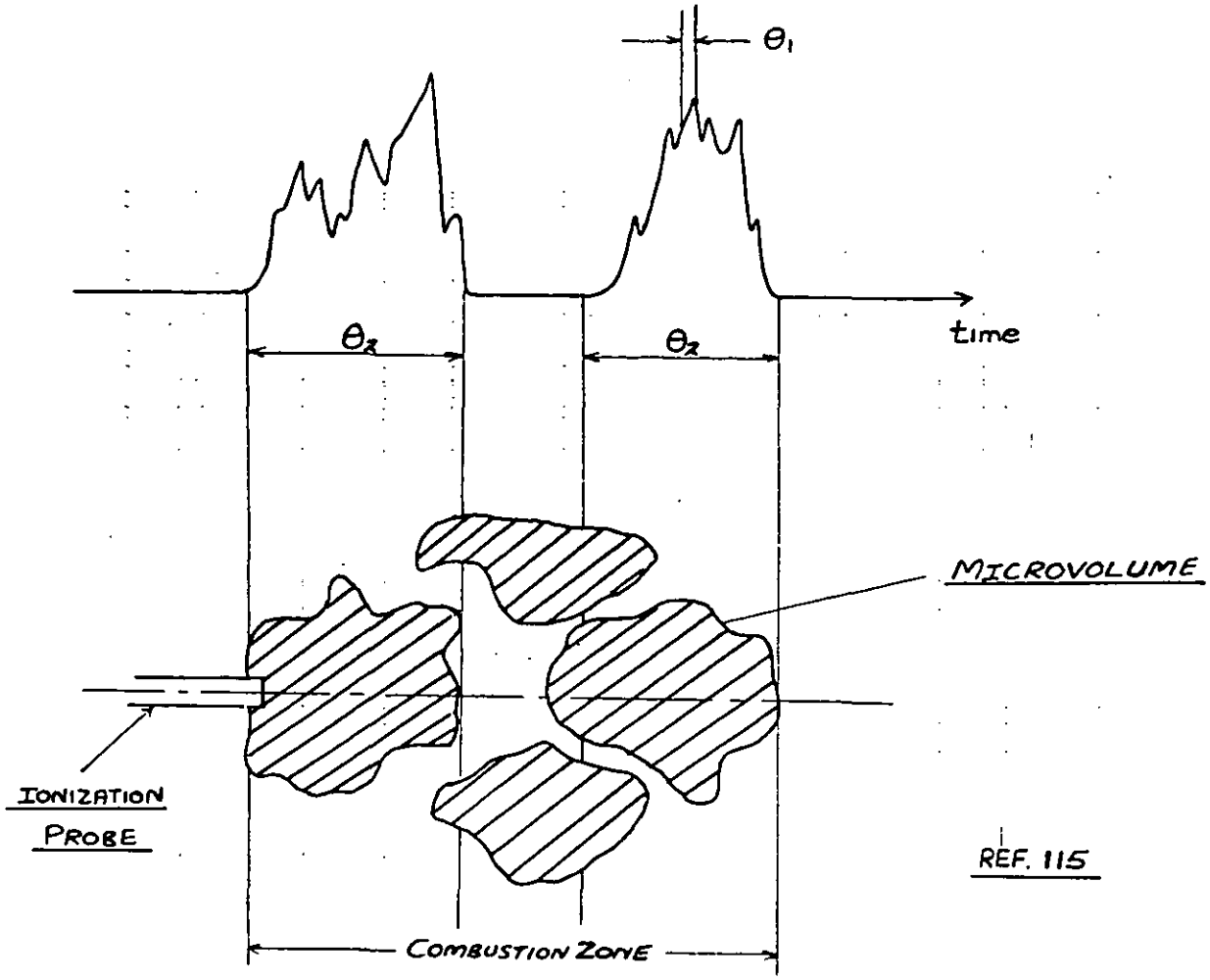

FIG. 4-35 — DIAGRAM OF THE PASSAGE OF REACTING MICROVOLUMES OF GAS PASSED AN IONIZATION PROBE AND OF THE GENERATED IONIZATION CURRENTS RESULTING THEREFROM.

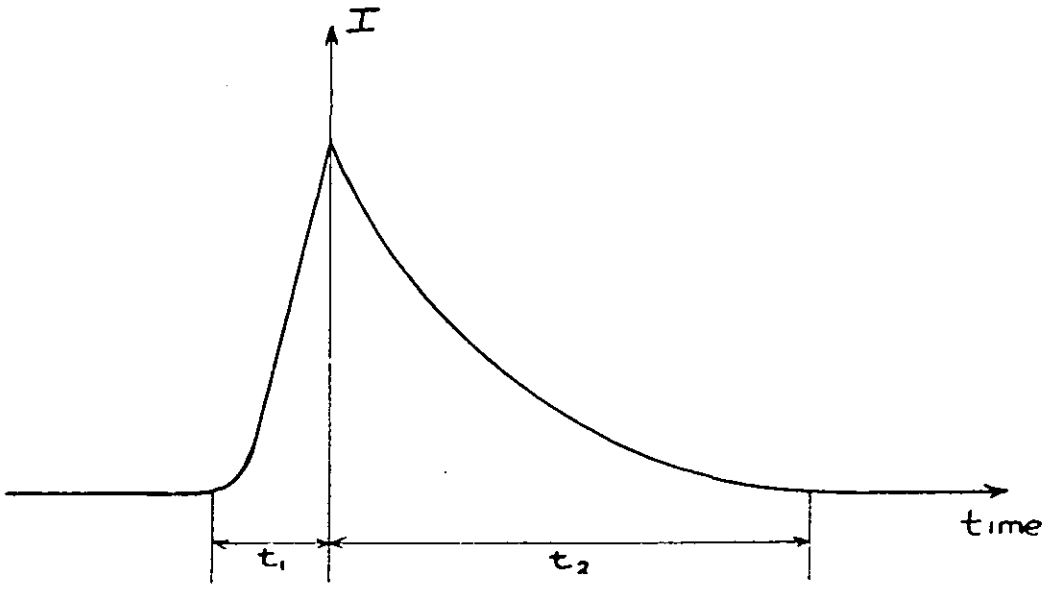

FIG. 4-36 — TYPICAL IONIZATION CURRENT OSCILLOGRAM FOR A LAMINAR FLAME (FROM SOKOLIK[123])

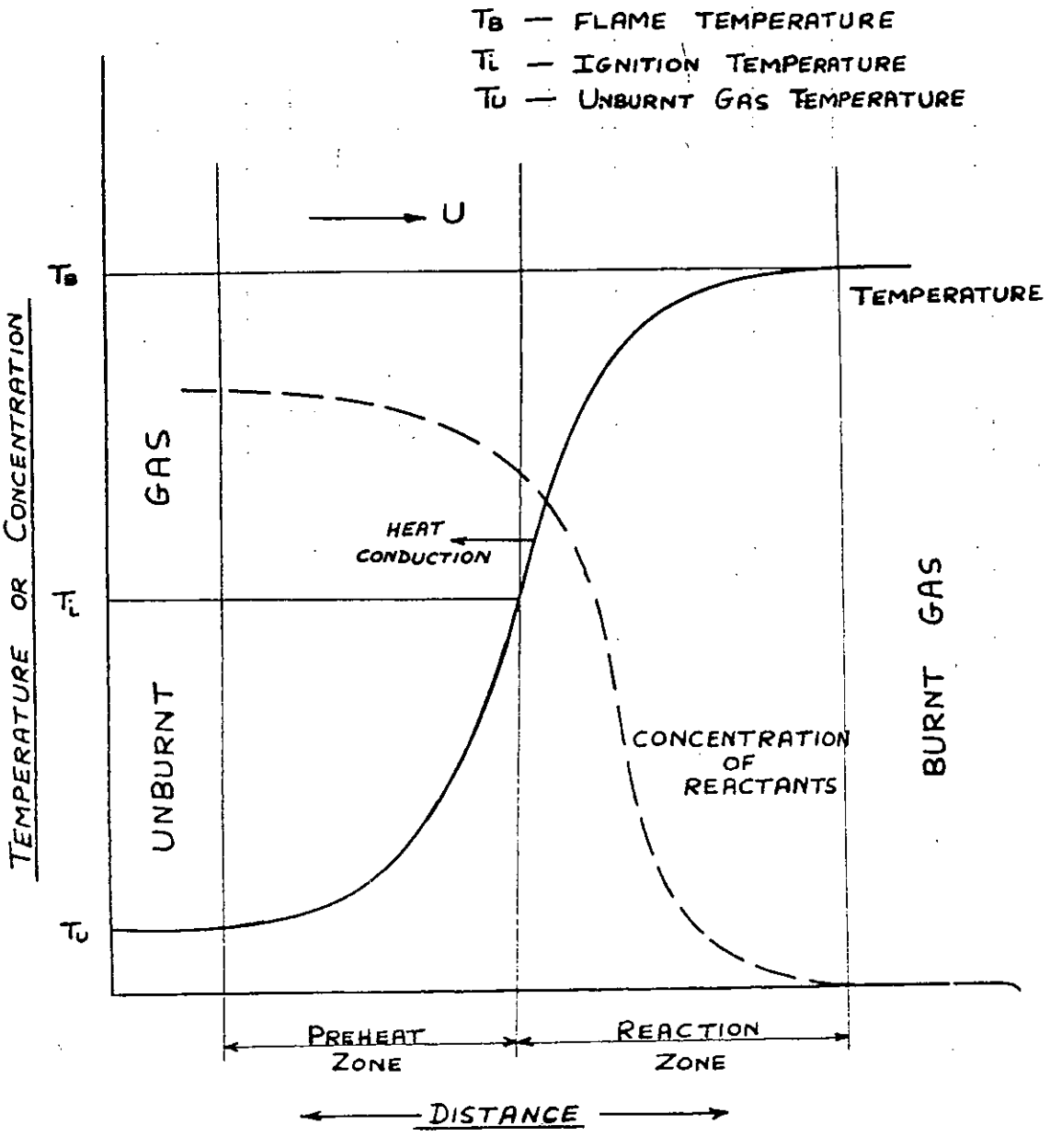

FIG. 4-37 — SCHEMATIC DIAGRAM OF A LAMINAR FLAME FRONT (THERMAL MECHANISM)

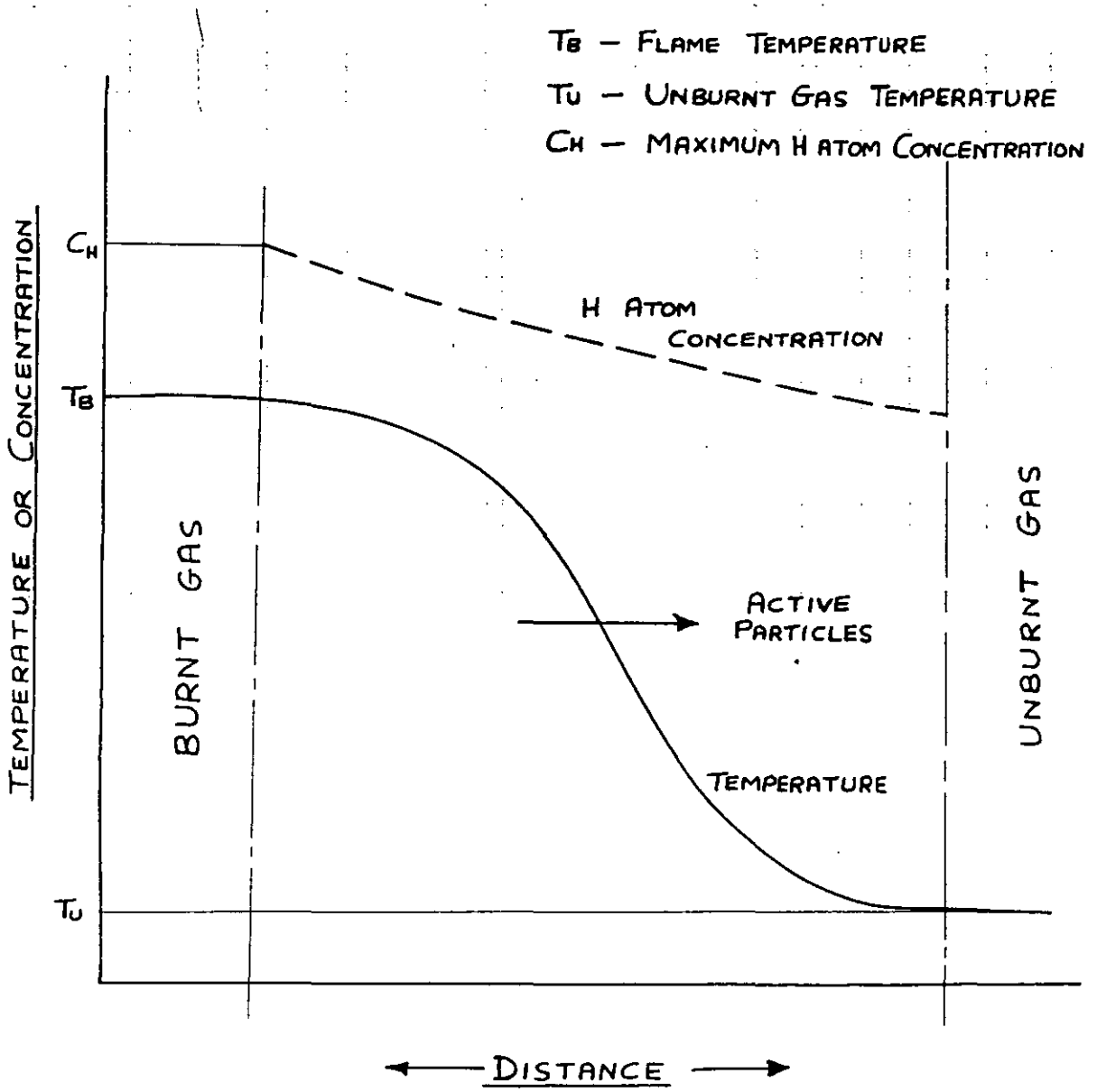

FIG. 4-38 — SCHEMATIC DIAGRAM OF A LAMINAR FLAME FRONT (DIFFUSIONAL MECHANISM)

T_B – FLAME TEMPERATURE

T_i – IGNITION TEMPERATURE

T_u – UNBURNT GAS TEMPERATURE

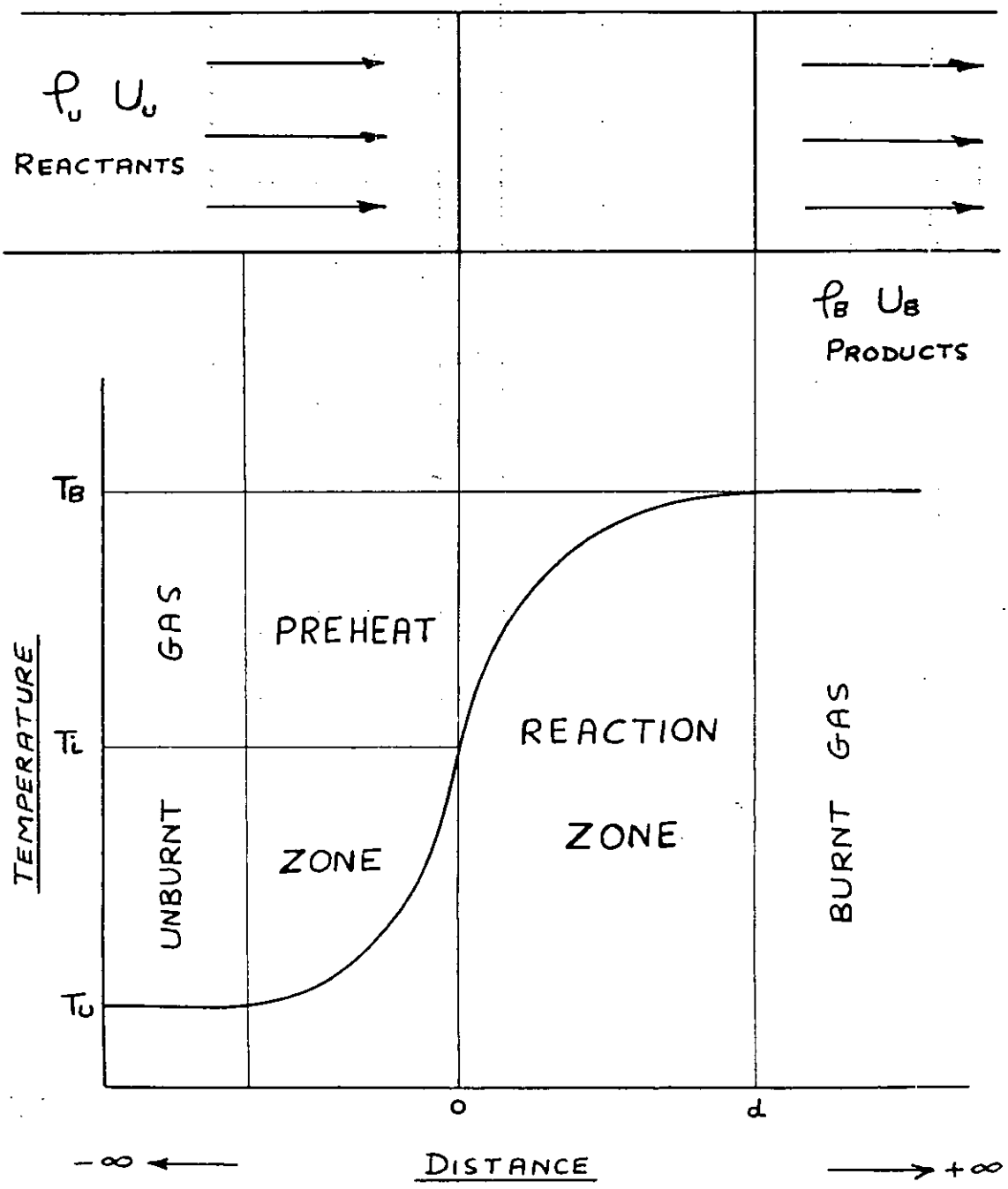

FIG. 4-39 — SCHEMATIC DIAGRAM AND TEMPERATURE PROFILE IN THE REGION OF THE REACTION ZONE

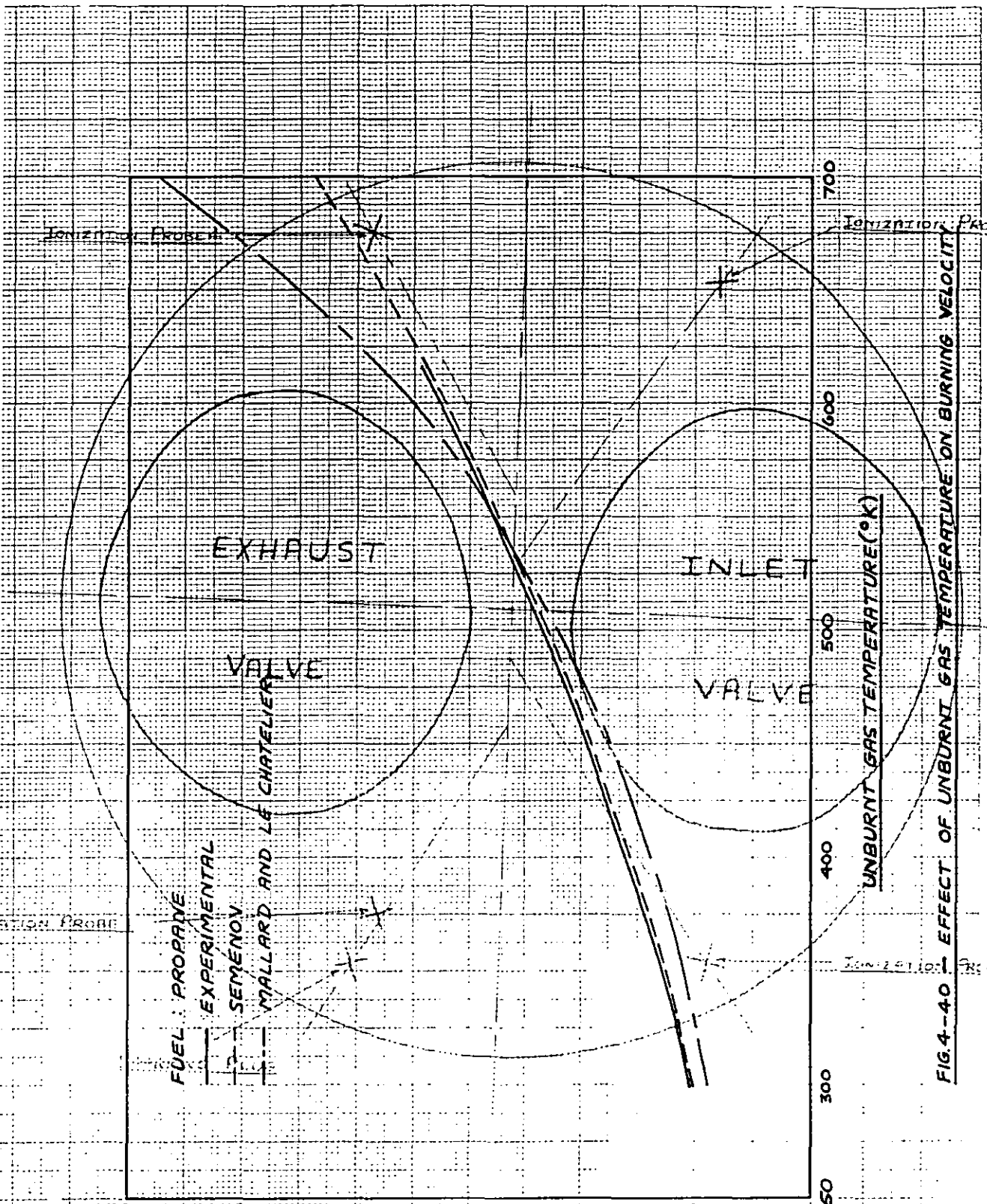

FIG. 4-40 : EFFECT OF UNBURNT GAS TEMPERATURE ON BURNING VELOCITY

FIG. 4-41 : SCHEMATIC SKETCH OF THE LAYOUT OF THE IONIZATION PROBES IN THE RENAULT COMBUSTION CHAMBER.

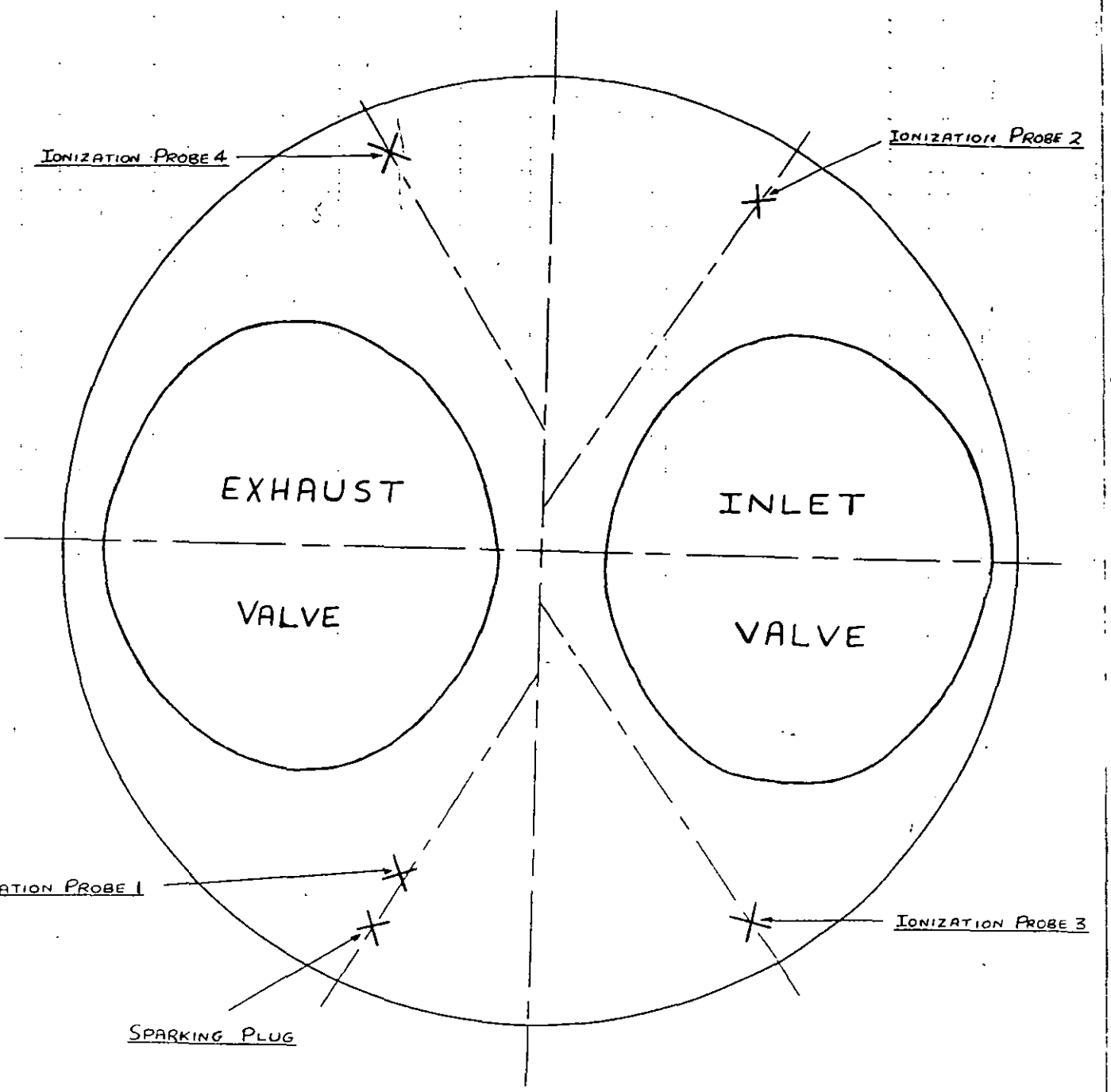

FIG. 4-41 — DIAGRAMMATIC SKETCH OF THE LAYOUT OF THE IONIZATION PROBES IN THE RENAULT COMBUSTION CHAMBER.

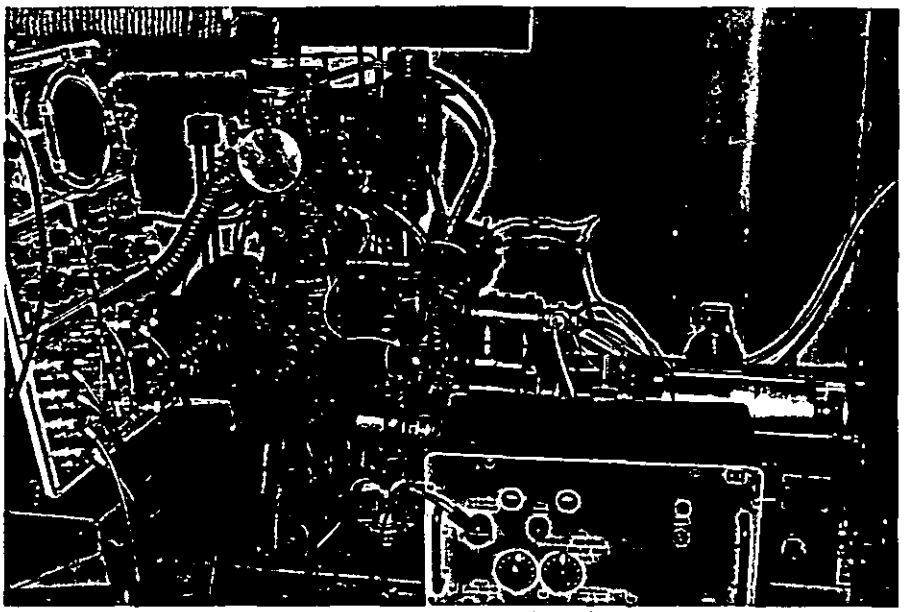

FIG. 4-42 — GENERAL VIEW OF ENGINE LAYOUT AND INSTRUMENTATION SET UP.

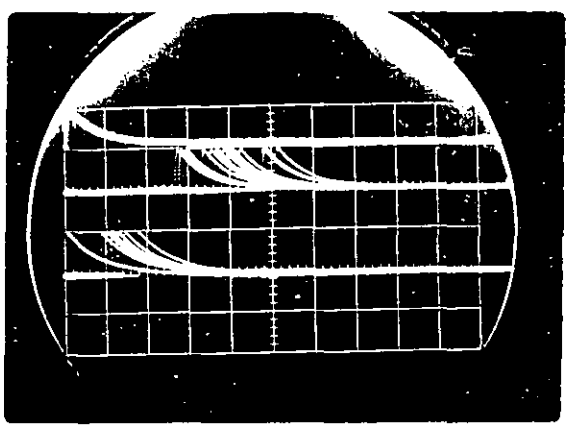

FIG. 4-43 — TYPICAL OSCILLOGRAM OBTAINED.

FULL THROTTLE : 3300 REV/MIN

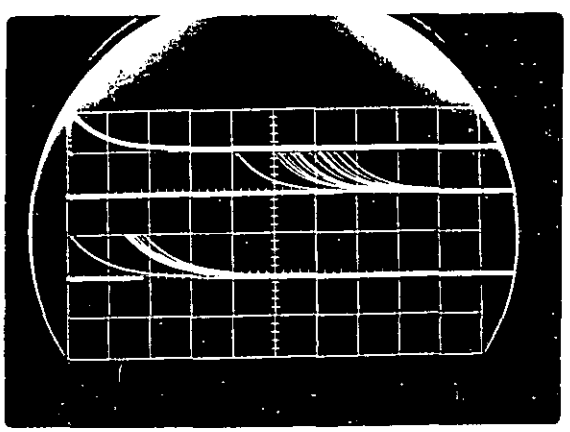

FIG. 4-44 — TYPICAL OSCILLOGRAM OBTAINED.

PART THROTTLE : 1200 REV/MIN

FIG. 4-45 — PLOT OF FLAME SPEED AGAINST ENGINE SPEED FOR THE RENAULT ENGINE

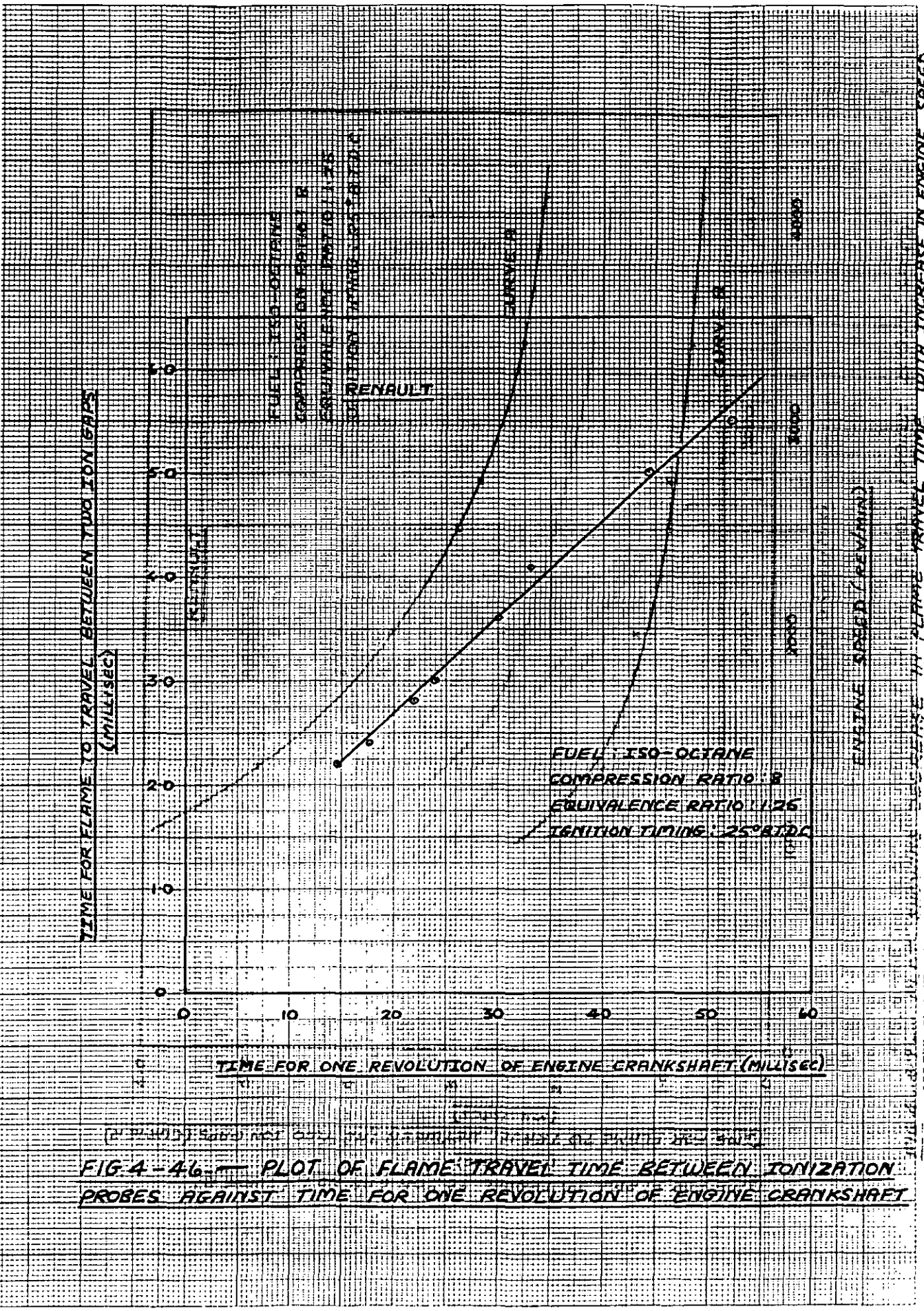

FIG 4-46 — PLOT OF FLAME TRAVEL TIME BETWEEN IONIZATION PROBES AGAINST TIME FOR ONE REVOLUTION OF ENGINE CRANKSHAFT

FIG. 4-47 — PLOT SHOWING DECREASE IN FLAME TRAVEL TIME WITH INCREASE IN ENGINE SPEED.

FIG. 4-48 — PLOT OF APPARENT DELAY PERIOD AGAINST ENGINE SPEED

FIG. 4-49 — PLOT OF THE RECIPROCAL OF MEAN FLAME TRAVEL TIME AGAINST ENGINE SPEED (RENAULT HAIRPIN INLET CONFIGURATION)

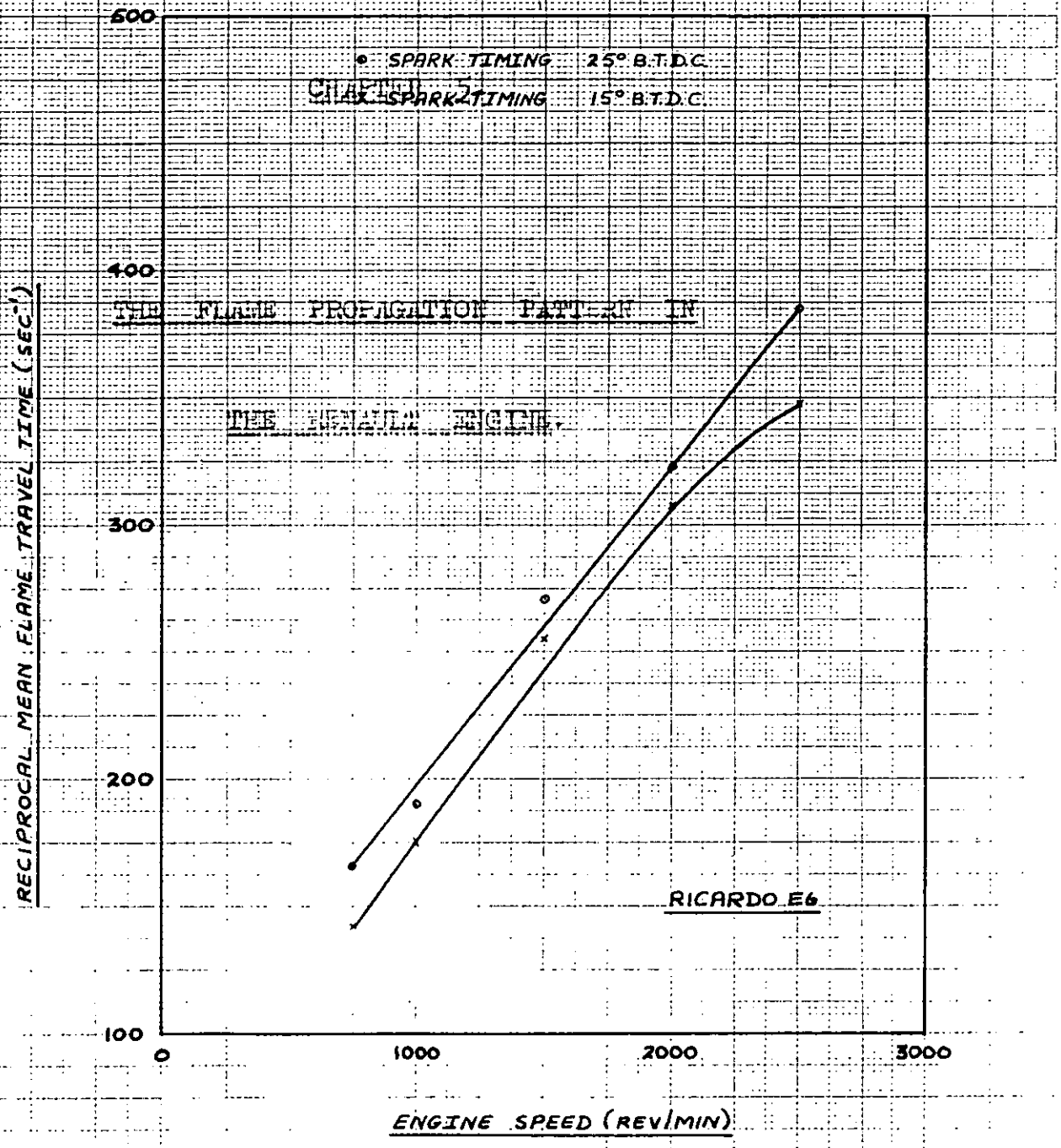

FIG. 4-49 — PLOT OF THE RECIPROCAL OF MEAN FLAME TRAVEL TIME AGAINST ENGINE SPEED (FROM HARROW AND ORMAN[31])

CHAPTER 5.

THE FLAME PROPAGATION PATTERN IN THE RENAULT ENGINE.

CHAPTER 5.

5. THE FLAME PROPAGATION PATTERN IN THE RENAULT ENGINE.

It has been assumed in previous computer simulations of combustion in spark ignition engines[19,159] that the flame which propagates outwards from the sparking plug is spherical in shape with the centre of the sphere at the sparking plug. Fig. 5-1 typifies this assumption. From the works of Withrow and Cornelius[12], Rassweiler et all[11], Rassweiler and Withrow[10], Rabezzana et al[13], Curry 34,36, Clarke[26], Wentworth and Daniel[39] and many others however, it is clear that the flame does not propagate spherically in any type of combustion chamber used on piston engines. Such a situation is only approached when a quiescent combustible mixture in a spherical constant volume bomb is ignited at the centre.

In this work on the simulation of combustion in the hemispherical combustion chamber of the Renault engine, an attempt is made to incorporate into the model a realistic flame pattern depicting the incremental position of the flame front as a function of time. In this connection, the observations of many workers have been drawn upon.

Numerous factors are known to exert some influence on the manner in which a flame propagates through a combustible mixture in a combustion chamber. These include:

i) combustion chamber design.

ii) swirl.

iii) piston movement.

iv) charge homogeneity.

v) locally generated turbulence.

vi) combustion chamber surface temperature variations.

vii) compression ratio.

viii) the flame speeds in the chamber.

Combustion Chamber Design.

It is obvious that the combustion chamber design is one of the main influences in determining the flame propagation pattern appropriate to a particular engine. There is no flame pattern applicable to all types of combustion chamber - each must be analysed individually. Rabezzana et al [13,89] proposed that the flame pattern development from the sparking plug is distorted in relation to the combustion chamber wall contour and the volumes ahead and behind the flame front.

Swirl.

The influence of swirl on combustion in spark ignition engines has already been dealt with in Chapter 4. It is noted that the main effect of a swirl is to deviate the flame pattern from a symmetrical path about the sparking plug and, in so doing, to increase the flame front area (see Fig. 4-9).

Piston Movement.

Piston movement affects the flame propagation pattern because the combustion chamber shape is continuously chang-ing. In addition, due to mass movements of the charge, it can change the position and contour of a burnt volume of charge especially when this is small just after ignition. Such effects were observed and noted by Marvin et al [32].

Charge Homogeneity.

In-homogeneity of the charge during combustion necessarily leads to a condition where the air/fuel ratio at different points in the combustion chamber varies from very rich to very weak. When a flame is propagating through such a mixture, there is going to be an acceleration of the flame front in the rich areas of the charge and a 'deceleration' in the weaker areas. Thus, the flame pattern can be grossly distorted at the flame front. In all combustion chambers, there is bound to be a certain amount of charge inhomogeneity unless special precautions have been taken in the preparation of the charge. It is most difficult to define an accurate flame pattern under such conditions.

Locally Generated Turbulence.

Experimental evidence indicates that, whenever a flame front approaches a sudden change in the combustion chamber contour, there is an increase in the burning velocity. This is manifested as an increase in the rate of pressure rise. Such effects can be attributed to the generation of local turbulence[89]. Its influence on the flame pattern is similar to the rich areas in an inhomogeneous charge.

Combustion Chamber Surface Temperature Variations.

In all combustion chambers, considerable differences in the temperatures of the surfaces comprising the chamber are apparent. For example, Johnson et al[42] suggest that typical values of the cylinder wall, cylinder head, piston and exhaust valve in a spark ignition engine are 395°K, 422°K, 520°K and 610°K respectively. Experiments[34] indicate

that the flame moves faster over the hotter surfaces (e.g. the piston and exhaust valve) and more slowly over the relatively cooler surfaces (e.g. the inlet valve). At certain times under certain conditions in engine combustion, hot spots are formed in the chamber. These influence the flame pattern in the same manner as just described. In an accurate analysis of flame propagation patterns in various combustion chambers, all such effects must be taken into account.

Compression Ratio.

The influence of compression ratio on the flame pattern is largely confined to its influence on the degree of flame curvature between the cylinder head and the piston. A more detailed discussion of this is given later. It must be appreciated that the combustion zone moves more rapidly through the middle portions of the combustion chamber than along the surface walls. This is probably due to the cooling effects of these walls. Thus, the portion of the charge midway between the head and the piston burns more quickly than those portions near the walls.

The Flame Speeds.

Flame speeds assume their greatest importance on the flame pattern development whenever a large scale swirl is present in the combustion chamber. Engine operation under conditions which tend to increase the flame speeds result in a minimization of the effects of the swirl on the flame pattern.

Before embarking on considerations of the manner in which the flame progresses in the Renault combustion chamber,

it is necessary to determine whether a two-dimensional flame map is an accurate enough criterion in depicting flame propagation or whether the influences of flame curvature must be considered also. In this context, the term flame curvature is used to describe the deviation of the flame front from a surface which is perpendicular to the plane from which the flame progession is being viewed or detected.

Curry[34] investigated this problem in a C.F.R. engine in which good charge homogeneity was ensured and in which the incremental position of the flame front as a function of time was detected and depicted by the use of 48 ionization gaps in the combustion chamber - 26 in the cylinder head and 22 in the piston. He first of all considered separately a diagrammatic spherical flame propagation (see Fig. 5-1) and realised that, as the radius of the spherical flame front increases, the arc segment of the flame front between the cylinder head and the piston approaches a straight line. This is the reason why it has been generally assumed that, if the distance between the two surfaces is sufficiently small, a negligible error is introduced by assuming that the flame front is a surface perpendicular to the cylinder head. Thus, two-dimensional flame maps, determined by measurements with ionization gaps on one surface of the combustion chamber only or by optical techniques, have been presumed to represent adequately the positions of three-dimensional flame surfaces.

Curry's three-dimensional studies, however, have shown that this general concept is not necessarily valid. Such factors as swirl and uneven surface temperatures were found

to generate a quite different picture of flame propagation from that derived by two-dimensional measurements only. Fig. 5-2 is a three-dimensional flame map taken from Curry's work - it clearly illustrates the extent of the flame curvature in an engine without swirl. The magnitude of the curvature is most pronounced in the earlier stages of the flame travel. This is as expected since the flame approximates a sphere rather than a plane surface shortly after ignition. The influences of the surface temperatures of the valves on the propagation are also evident. In the region of the cool intake valve, the rate of the flame propagation across the relatively hot piston is greater than across the cylinder head. The reverse effect is noted in the region of the hot exhaust valve.

Flame curvature effects similar to those shown in Fig. 5-2 were observed over a wide range of engine speeds, compression ratios and other operating conditions. It was found, however, that the magnitude of the flame curvature decreased with increasing compression ratio. This observation is explainable by the previous discussion on the manner in which a spherical burning pattern in the vertical plane approaches a straight line when the piston is near the cylinder head surface.

When a large degree of swirl was induced in the C.F.R. combustion chamber, however, marked flame curvatures were still apparent even at very high compression ratios (see Fig. 5-3). Unexpectedly, combustion was completed first across the piston in these cases and the last fraction of charge to burn was that across the exhaust valve. It must be assumed, therefore, that the induced swirl velocity is

different across the piston surface from that along the cylinder head surface.

From the foregoing, it can be concluded that the flame pattern development in an engine combustion chamber is much more complex than is generally assumed, so much so that a detailed two-dimensional flame map is unacceptable when accuracy is required.

In this work, the flame pattern development in the Renault combustion chamber is the result of attempts to incorporate as many as possible of the foregoing influences on the flame propagation. First of all, therefore, some flame travel time measurements were made to the ionization probes 2, 3 and 4 (see Fig. 4-41) in order to see if there was any marked degree of swirl present. The techniques of such measurements have been described in Chapter 4. Results of these tests, over a range of air/fuel ratios, appear in Table 5-A. From this, it is noted that the flame travel times to the probes predict that the flame propagates in an almost symmetrical manner from the sparking plug with the end gas region being finally located in a position almost directly across the combustion chamber from it. It, thus, appears that there is not much, if in fact any, swirl present.

The assumption of complete charge homogeneity in this work precludes the idea of the effects of charge inhomogeneity on the flame pattern development. Likewise, the influence of piston movement, locally generated turbulence and surface temperature variations are most difficult to account for in a realistic assessment of the incremental

TABLE 5 - A.

ENGINE OPERATING CONDITIONS:

FUEL	:	ISO-OCTANE
ENGINE SPEED	:	2000 REV/MIN.
COMPRESSION RATIO	:	8
IGNITION TIMING	:	40° B.T.D.C.
AMBIENT TEMPERATURE	:	18° C.
AMBIENT PRESSURE	:	29.938" Hg.

AIR/FUEL RATIO	FLAME TRAVEL TIMES (MILLISECS) TO IONIZATION PROBES		
	2	3	4
9.38	4.4	3.2	4.25
11.5	4.5	3.0	4.3
12.7	4.7	3.1	4.3
14.9	4.7	3.4	4.6
17.6	5.2	3.6	5.0

flame front position since these effects tend to vary with the mode of engine operation. All that can be done, therefore, is to generalize as accurately as possible on the flame pattern and to include the influences on this pattern of those parameters which it is possible to allow for.

The result of these considerations in the Renault hemispherical combustion chamber is the flame development shown in Fig. 5-4. It will be noted that the flame is spherical in form in its initial stages of travel from the sparking plug but, thereafter, it propagates outwards into the greatest volume of unburnt charge where the constraint to its motion by the combustion chamber walls is least. As the distance of the flame front from the sparking plug increases, the 'resistance' to its motion tends to equalize over its entire surface and the corresponding rate of travel across the flame front becomes uniform. A spherical flame propagation thus ensues towards the end of its travel.

The manner in which flame curvature is accounted for in the vertical plane is also shown in Fig. 5-4. A spherical propagation is assumed to exist in this plane throughout the entire flame travel with the centre being at the spark plug. Justification for this is obtained from Curry's work[34] in which he showed that little accuracy is lost when this technique is used. It also approximates closely the observance of less flame curvature with increasing compression ratio and distance of the flame front from the sparking plug.

Having developed this flame front progression, it was required to be able to calculate the volume (and hence mass) of charge burnt in the combustion chamber at any particular piston position and at any desired flame front distance from

the sparking plug. This was achieved by constructing plaster casts of the combustion chamber and cylinder bore. These were shaped to correspond to the flame pattern development and flame curvature (see Figs. 5-5 and 5-6). The procedure was to weigh the 'burnt' volumes of the plaster casts at all the ten flame front positions and at all the eleven piston positions shown in Fig. 5-4. Knowing the densities of these casts, plots were constructed of their 'burnt' volumes against the distances of the "flame fronts" from the sparking plug at all eleven piston positions. Polynomials were fitted to each of these plots thereby allowing estimates to be made by interpolation of the 'burnt' volumes at intermediate piston positions between those for which actual measurements were made.

Several sources of inaccuracy were apparent in this technique including very slight non-uniform densities in the plaster casts and errors in getting the flame curvatures in the vertical plane to coincide exactly with those shown in Fig. 5-4. These are not too important, however, because the burnt volumes are, at best, approximations to actuality. The technique, itself, became quite tedious but it was recognised as being the only way of attempting to accurately simulate the flame propagation.

Results from this section of work thus enable the burnt volumes of the charge in the combustion chamber to be estimated at any particular flame front or piston position. The pertinent polynomial equations which apply in this case are listed in SUBROUTINE BURNTVOL of the complete program listing in Appendix 8. In addition, it is possible to calculate the flame front positions when the burnt volumes

and piston positions are known. The polynomials for these calculations are given in SUBROUTINE FLAMDIST in Appendix 8.

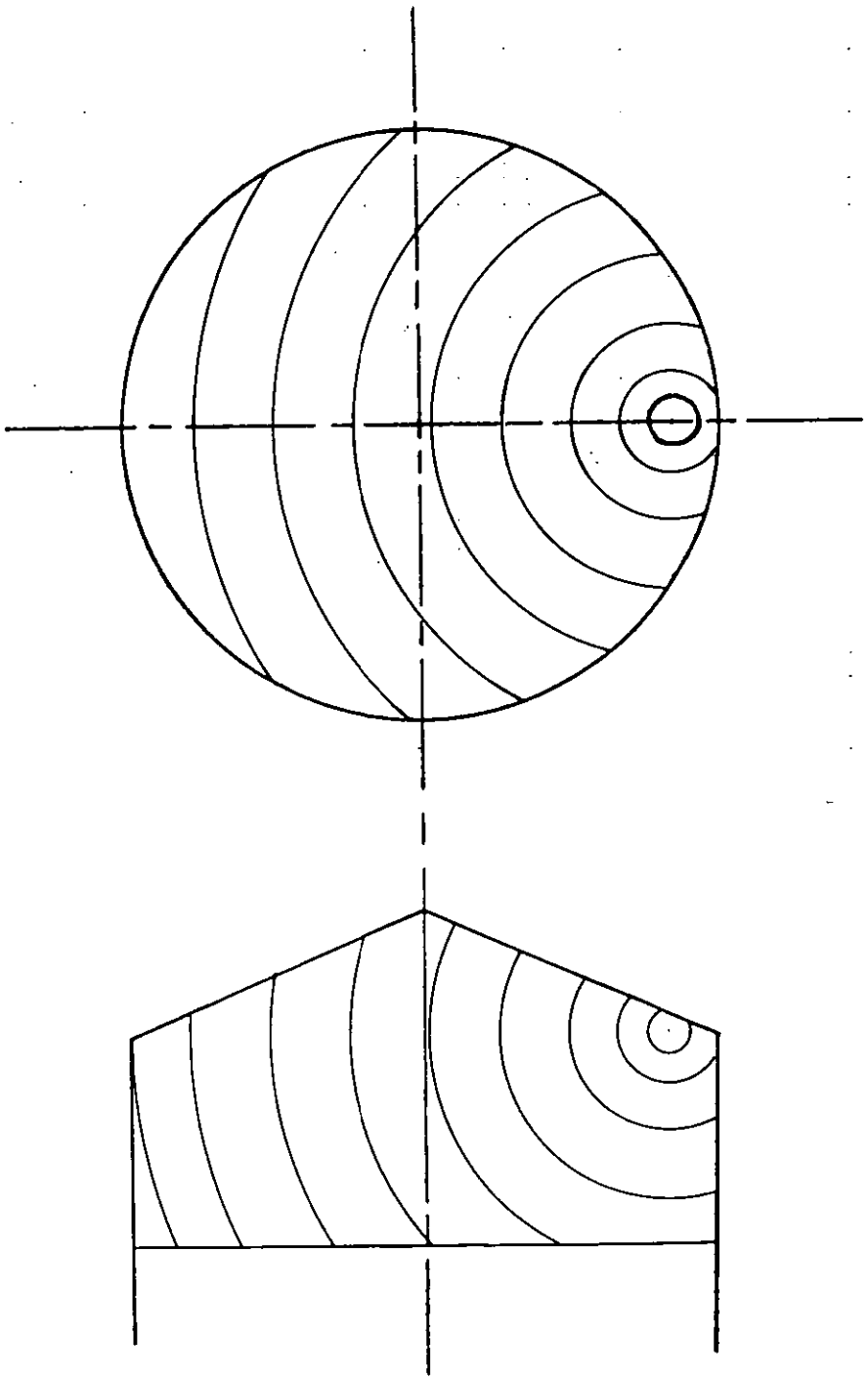

FIG. 5-1 — A TYPICAL SPHERICAL FLAME PROPAGATION.

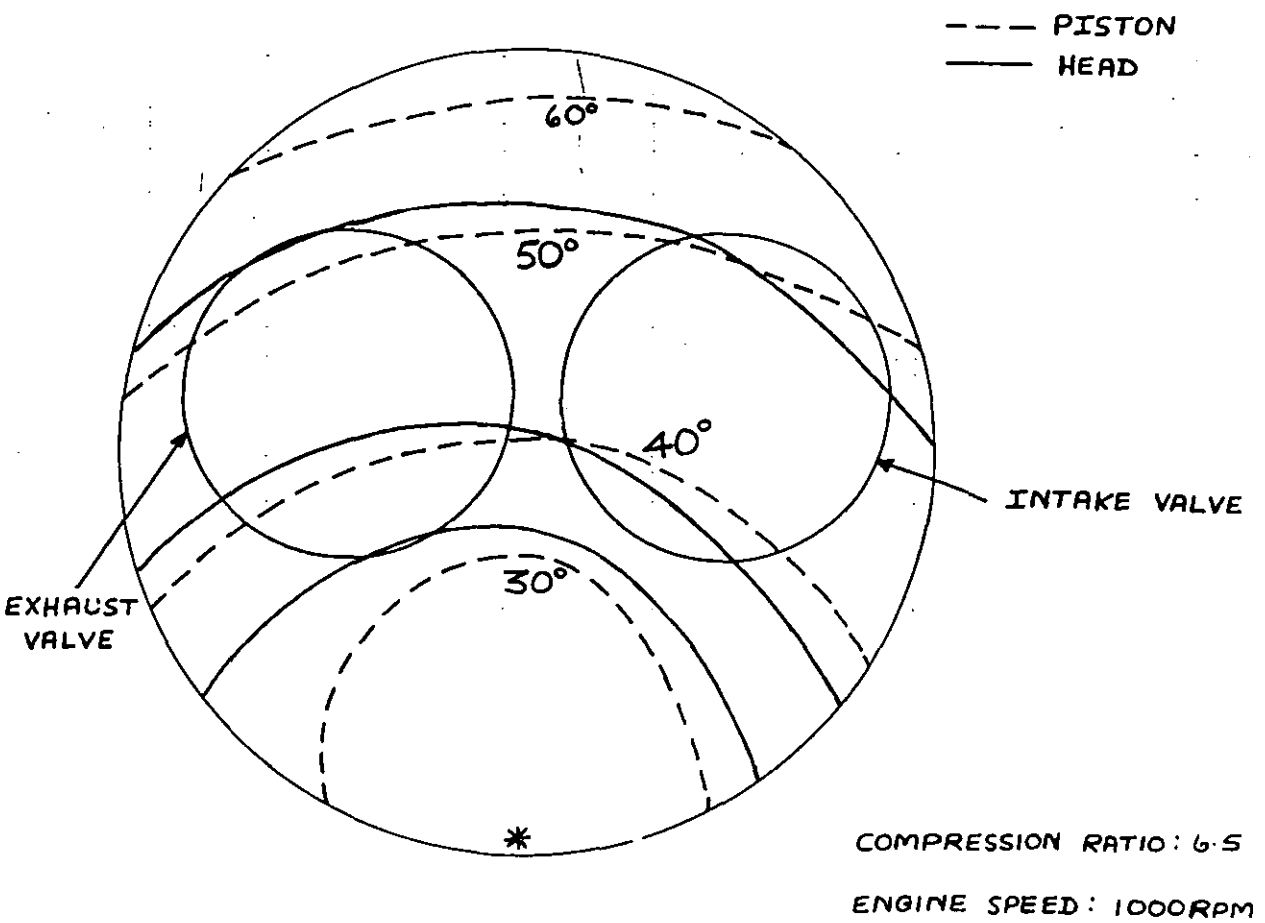

FIG. 5-2 — COMPLEX PICTURE OF THREE-DIMENSIONAL FLAME PROPAGATION SHOWING FLAME CURVATURE EFFECTS. (FROM CURRY[34]).

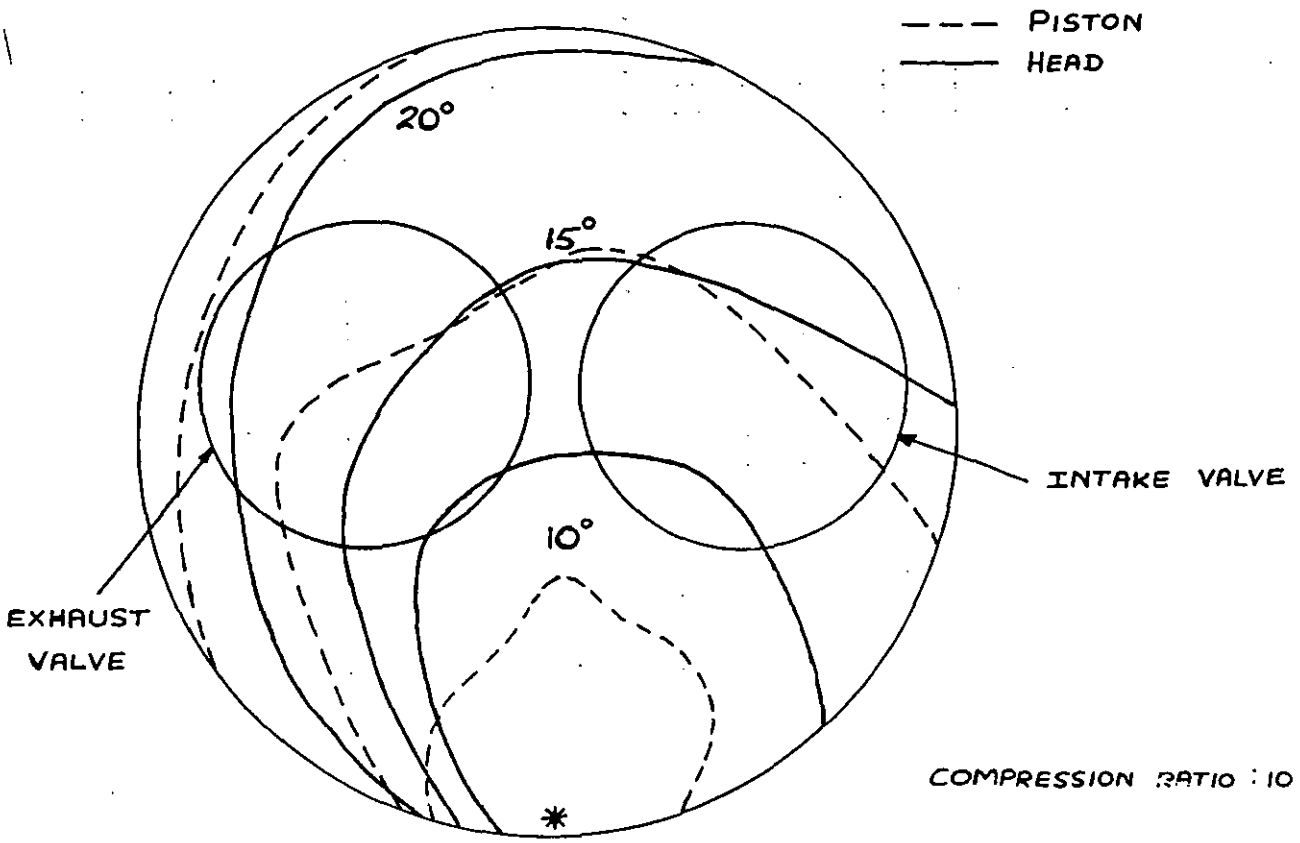

FIG. 5-3 — COMPLEX PICTURE OF THREE-DIMENSIONAL FLAME PROPAGATION SHOWING FLAME CURVATURE EFFECTS WHEN A LARGE DEGREE OF SWIRL IS PRESENT (FROM CURRY[34]).

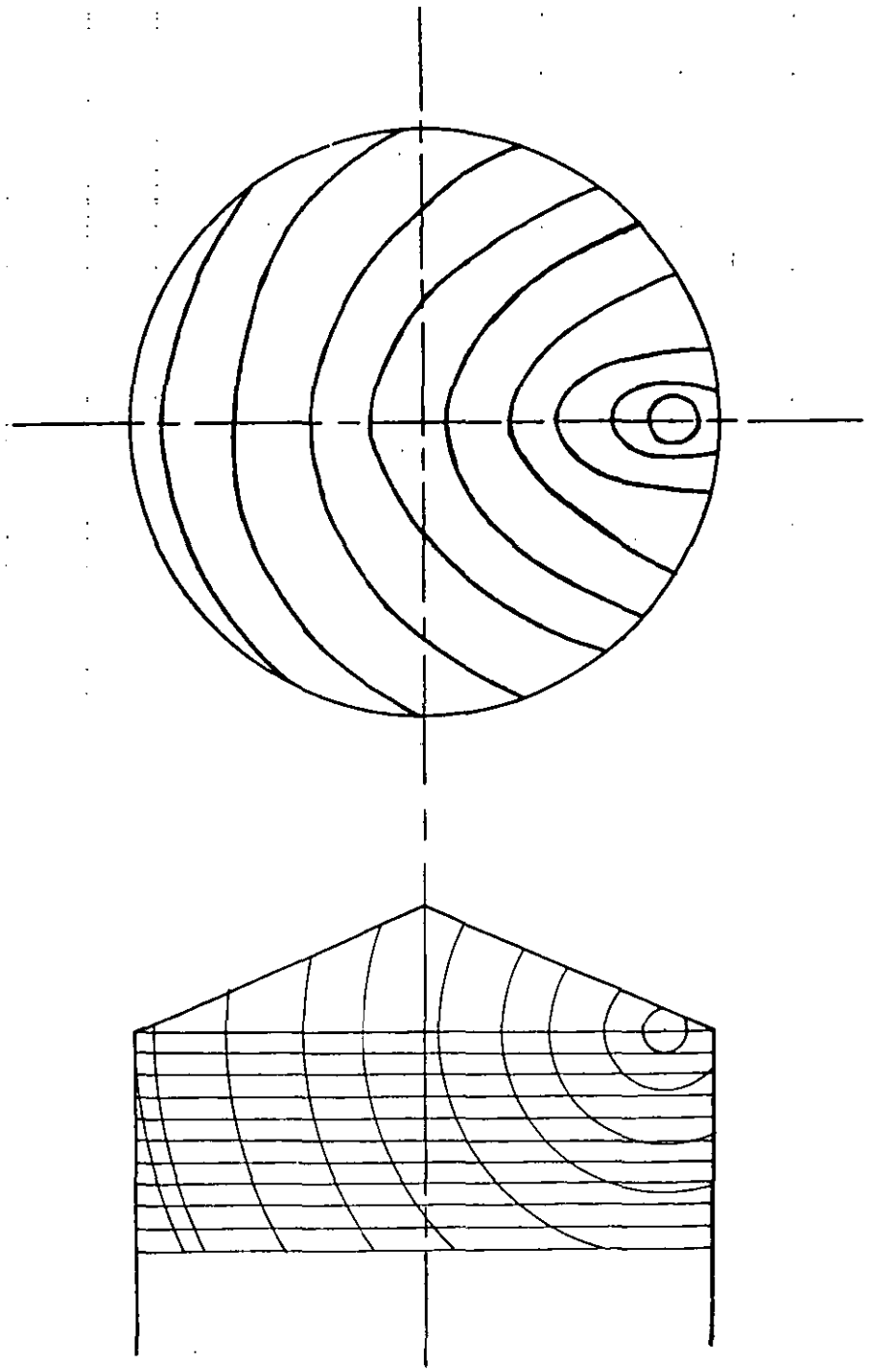

FIG. 5-4 — THE ASSUMED FLAME PATTERN DEVELOPMENT IN THE RENAULT COMBUSTION CHAMBER.

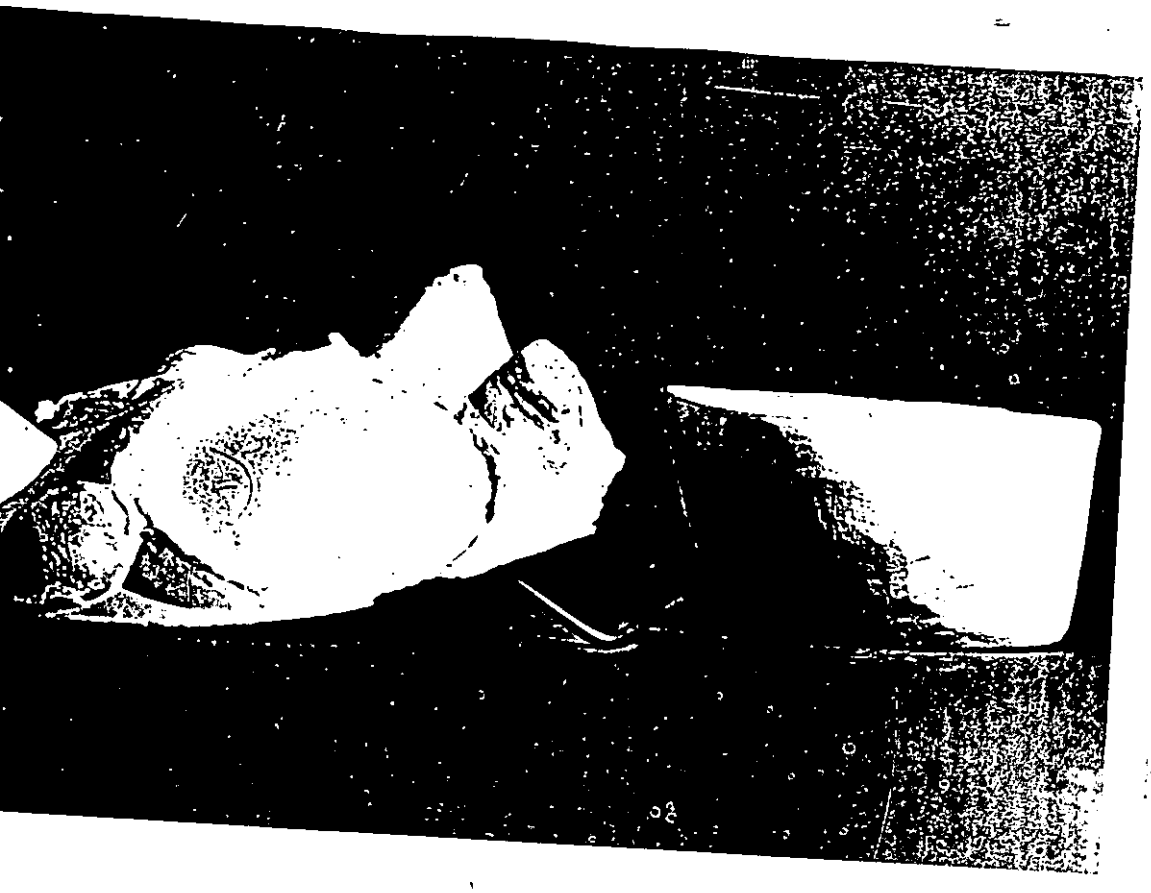

— PLASTER CASTS OF THE COMBUSTION CHAMBER ON THE LEFT

E FLAME PATTERN DEVELOPMENT AT A POINT IN CYLINDER BORE ON THE RIGHT.

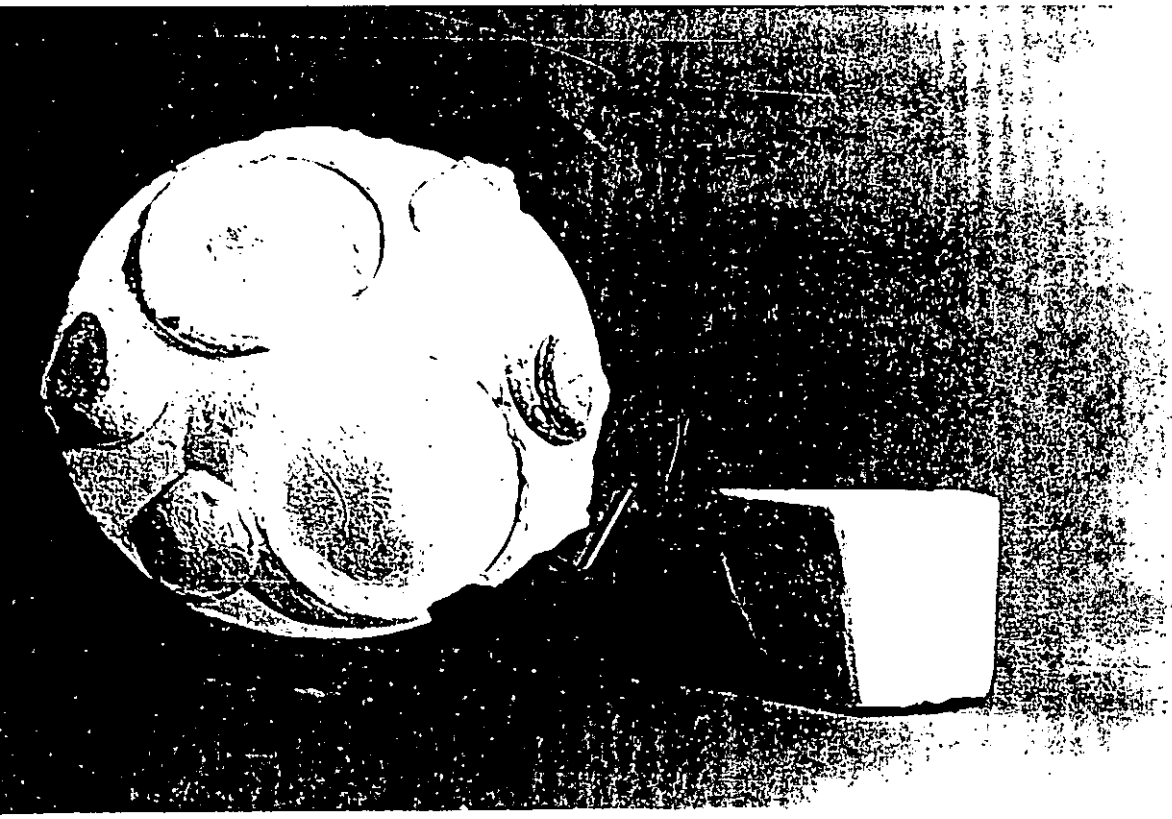

— DIFFERENT VIEWS OF THE PLASTER CASTS SHOWN

CHAPTER 6.

DISSOCIATION.

6. DISSOCIATION.

6.1. INTRODUCTION.

In a spark ignition engine operating over the normal range of air/fuel ratios, it is observed that the maximum temperatures attained during combustion are less than those calculated when it is assumed that the combustion reaction proceeds directly from the initial reactants to the final products. One of the reasons for this is the phenomenon of dissociation of the combustion products. An appreciable amount of this can occur at high temperatures and it is accompanied by an absorption of internal energy which is transformed into chemical energy. This implies that the temperature rise will be less with dissociation than with no dissociation for an adiabatic combustion process.

Experiments show that, in a reaction between two or more elements or compounds, the rate of conversion of the initial reactants to the final products is retarded by the dissociation of some of the final products to the initial reactants. Equilibrium is established when, for the dissociating elements or compounds, the speed of the forward reaction equals the speed of the backward reaction (this is called the Law of Mass Action). For given initial reactants, the degree of dissociation has been found to increase with increases in temperature. Alternatively, for a given temperature, the degree of dissociation depends on the composition of the initial reactants.

In this work, the dissociation of the products of combustion of hydrocarbon fuels are of direct interest.

These consist of various combinations of carbon, hydrogen, oxygen and nitrogen. The way in which these four elements are combined after combustion and the proportion of the various species in the burnt mixture depends on:

a) the proportions of these elements present in the original mixture (i.e. the air/fuel ratio).

b) the temperature.

c) the pressure.

d) the extent to which chemical equilibrium has been approached. A discussion of this is given later.

In a high temperature, combustion reaction between a hydrocarbon fuel and oxygen and nitrogen, the following general equation can be written when the burnt combustion products consist of the fifteen species on the right hand side of the equation:

$$C_m H_n + x\left(m + \frac{n}{4}\right) O_2 + xg\left(m + \frac{n}{4}\right) N_2 = n_1.\ CO_2 + n_2.\ CO + n_3.\ N_2 + n_4.\ H_2O + n_5.\ O_2 + n_6.\ H_2 + n_7.\ NO + n_8.\ OH + n_9.\ H + n_{10}.\ O + n_{11}.\ NO_2 + n_{12}.\ N_2O + n_{13}.\ NH_3 + n_{14}.\ HNO + n_{15}.\ N \qquad \text{----------} \quad 6\text{-}1$$

In this Equation, m and n are the number of carbon and hydrogen atoms in a molecule of the fuel and 'g' is the mole ratio of nitrogen to oxygen in air. This latter quantity has been estimated as being 79.01/20.99 (= 3.764) in Appendix 1. Additionally, n_k ($k = 1,15$) are the number of moles of CO_2, CO, N_2, H_2O, O_2, H_2, NO, OH, H, O, NO_2, N_2O, NH_3, HNO and N respectively in the burnt mixture.

In practice, many other dissociated species are also present in this mixture after combustion e.g. H_2O_2, HO_2, C solid, CH_4 etc. However, besides these species being so

low in concentration as to have virtually negligible influence on the reaction, they are in themselves of no direct interest in this work. It should be noted that such combustion reactions as in Equation 6-1 are less complete at high temperatures than at low temperatures when the concentrations of many of the dissociated species are very small.

The remainder of this chapter describes the method and assumptions used in this work for calculating the composition of the burnt combustion products for given values of temperature, pressure and air/fuel ratio.

6.2. THE COMPOSITION OF THE PRODUCTS OF COMBUSTION.

6.2.1. ASSUMPTION OF CHEMICAL EQUILIBRIUM.

In this work, the conditions under which combustion occurs are necessarily idealized for the purpose of calculating the concentrations of the chemical species in the burnt mixture. Such idealization includes assumptions of steady state conditions, charge homogeneity and the absence of any flame quenching at the combustion chamber walls.

It is apparent, however, that, in practice, combustion in spark ignition engines occurs under conditions which are usually far from ideal. Consequently, results based on the idealized assumptions above generally tend to over-estimate the performance of the engine. As a preliminary to methods of calculating the concentrations of chemical species in a burnt mixture therefore, it is necessary to investigate what effects deviations from these idealizations might have upon the chemical composition of the working fluid and the performance of the engine.

Steady state conditions.

The assumption of steady state is tantamount to the assumption of chemical equilibrium. The implication is that the system, comprising the products of combustion, has been allowed to remain in a given state of temperature, pressure and volume long enough to attain an equilibrium condition. This can best be explained by consideration of the reaction:

$$n_A . A + n_B . B \rightleftharpoons n_C . C + n_D . D \qquad \text{-------- 6-2}$$

where A and B are the reactants, C and D are the products, and n_A, n_B, n_C and n_D are the moles of A, B, C and D respectively.

At the equilibrium state, all the chemical reactions have proceeded to such an extent that the rate of the forward reaction is just equalled by the rate of the reverse reaction. The reaction rate for the forward reaction AB is usually written as:

$$\omega_{AB} = -\frac{1}{n_A}\cdot\frac{dC_A}{dt} = k_{AB} . C_A^{n_A} . C_B^{n_B} \qquad \text{..... 6-3}$$

where n_A and n_B correspond to the values from the stoichiometric equation 6-2 and C_A and C_B are the concentrations of the reactants A nd B. k_{AB} is the specific rate constant.

Similarly, for the reverse reaction,

$$\omega_{CD} = -\frac{1}{n_C}\cdot\frac{dC_C}{dt} = k_{CD} . C_C^{n_C} . C_D^{n_D} \qquad \text{..... 6-4}$$

The symbols have the same significance in this equation as in Equation 6-3.

Thus, at equilibrium

$$\omega_{AB} = k_{AB} . C_A^{n_A} . C_B^{n_B} = \omega_{CD} = k_{CD} . C_C^{n_C} . C_D^{n_D}$$

and the ratio of the specific rate constants is

$$\frac{k_{AB}}{k_{CD}} = \frac{C_C^{n_C} \cdot C_D^{n_D}}{C_A^{n_A} \cdot C_B^{n_B}} \quad \ldots\ldots\ldots\ldots\ldots\ldots\ldots\ldots 6\text{-}5$$

The significance of this expression is explained in Appendix 6. At this point, the free energy of the system is at a minimum and no spontaneous change can occur within an isolated system. Thus, because this is an equilibrium state, the composition can be completely determined by the methods of classical thermodynamics.

The problem, however, is that the time available for combustion may be so short that true equilibrium is not attained. A finite time is required for equilibrium to be established in all dissociation processes. This time is called the 'relaxation time.' If a system passes through a rapid change in pressure or temperature, then it is possible that there will be insufficient time for equilibrium to be established. Calculations of the composition of the gases in these circumstances require a knowledge of reaction kinetics.

Strictly speaking, the relaxation time is zero in an internal combustion engine because the system volume, temperature and pressure are constantly changing. Fortunately, this change is usually relatively slow in comparison with the time required to achieve equilibrium. This is especially true during combustion because:

i) the temperatures, pressures and reaction rates are at a maximum during this stage of the engine cycle.

ii) piston velocity and volume changes are quite small owing to the kinematics of the engine mechanism.

Patterson[15] has attempted to compare the orders of magnitude of the relaxation times in i.c. engines during

combustion with the time required for one degree of crank rotation during which period changes in temperature and pressure are not large. For an engine operating at 2000 rev/min, this latter time is about 10^{-4} seconds. Although accurate quantitative estimates of the time intervals necessary to reach near equilibrium conditions in a system as complex as the working fluid of an i.c. engine are difficult to predict, Patterson recognized from Refs. 170 and 171 that, for many of the chemical species present, these relaxation times are of the order of 10^{-6} to 10^{-8} seconds at the temperatures and pressures existent during combustion. This lends support to our assumptions of chemical equilibrium during combustion.

During expansion, however, it has been shown by many workers[85,86] that the instantaneous concentrations of many of the chemical species present in the burnt mixture correspond to a state of non-equilibrium (see Section 2.2). This is due to several of the recombination reactions, which might be expected to take place during this stage of the cycle from equilibrium considerations, being kinetically limited owing to the temperatures, pressures and reaction rates being appreciably lower. In other words, the "time" for a change in state of the system is so short compared with the relaxation time that the gas is effectively "frozen" at a composition corresponding more to combustion temperature and pressure equilibrium values.

Even the assumption of a "frozen" composition is a poor criterion on which to base composition calculations during expansion since Newhall[86], in a kinetic analysis (see Section 2.2), has shown that a certain amount of recombination of certain species does in fact take place.

A condition between the two extremes of a "frozen" composition and an equilibrium composition is thus apparent.

The failure of the dissociated species to recombine during expansion is termed "equilibrium lag." Not all the recombination reactions lag the same amount and, for the complex system in an internal combustion engine, an eact analysis on this basis is difficult to make and apply (see Newhall [86]). For a further discussion on this subject, see Section 2.2.

The effects on engine performance of assuming equilibrium and non-equilibrium during expansion must now be considered. The assumption of chemical equilibrium during expansion increases the thermal efficiency and indicated mean effective pressure of the engine cycle because the recombination of dissociated species results in the reconversion of chemical energy to thermal energy which can be used to do work. On the other hand, if no recombination occurs at all during expansion so that the composition is considered "frozen" at a combustion temperature and pressure equilibrium value, the resulting temperatures and pressures are lower than they would be for an equivalent equilibrium expansion. Consequently, one would expect to obtain less useful work from such a system. As already stated, in reality, a condition somewhere between the two extremes of continuous equilibrium and "frozen" composition is attained. The former effect tends to overestimate and the latter to underestimate the engine performance.

In this context, it must be realized that the work outputs during expansion are significantly influenced by

the operating conditions under which the engine is run. In particular, by the air/fuel ratio and the compression ratio. The general effect of air/fuel ratio is shown in Fig. 6-1 which is taken from Starkman and Newhall's work[85]. Such behaviour results from fundamental differences between the chemical processes and temperatures in lean and rich mixtures. The influence of increasing compression ratio on expansion work (see Fig. 6-2 from Ref. 85) is attributed to the energy of dissociation becoming available at an earlier point in the expansion because of higher temperatures and flame speeds.

Since the rate of recombination of the dissociated species becomes lower as the pressure and temperature of the system are reduced, it is assumed in this work that there is a temperature below which this rate is so slow that for all practical purposes, no further reaction occurs and the equilibrium is "frozen." The difficulty in setting this temperature is that each particular recombination reaction has its own unique temperature at which the reaction effectively ceases. For example, Gaydon[172] recommends 1500° K for the reaction

$$CO = \tfrac{1}{2} CO_2 + \tfrac{1}{2} C_{solid}$$

and Hottel[173] suggests 1600° K for the water-gas reaction in Equation 2-2. The early work of Lovell and Boyd[174] gave 1600-1700° K as the temperature at which the equilibrium freezes in an internal combustion engine exhaust. In this study, 1600° K is the temperature used below which no further changes in composition occur (see also Appendix 1).

Charge Homogeneity.

It is well known that the mixture in an internal combustion engine is not entirely homogeneous. Such inhomogeneity arises during the induction process when the charge, consisting of air and both gaseous and liquid fuel, is inducted and mixed with the residual exhaust gas. Whether or not efficient mixing occurs depends largely on the design of the carburettor, manifold and inlet valve. Thus, the unburnt charge during combustion can be considered to consist of pockets of combustible material, some of which are richer and some leaner than the measured air/fuel ratio. Intermingled with these pockets are varying exhaust gas concentrations. The degree of the variations in air/fuel ratio and exhaust gas concentration between individual pockets of charge depends, of course, on the efficiency of the mixing. This assumes importance because if, for example, a stoichiometric mixture of fuel and air were burnt, one would expect to find evidence of products resulting from both rich and lean combustion in the exhaust gas.

The consequence of charge inhomogeneity is, therefore, incomplete and inefficient combustion. The assumption of complete charge homogeneity in this work, therefore, necessarily leads to predictions of thermal efficiencies and mean effective pressures which are higher than those actually attained in engines. The error in this idealization depends on the degree of homogeneity in the actual engine.

Flame propagation during combustion results in an additional inhomogeneity which is manifested as a continuous

stratification of the burnt products. This results in a temperature gradient being set up in the burnt combustion products during flame propagation in which the temperature of the burnt products is higher at the point of ignition than at the flame front (see Chapter 2). In the analytical model in this study, the temperature of the entire burnt charge is uniform throughout.

Flame Quenching at the Combustion Chamber Walls.

As stated in Chapter 2, studies of engine combustion processes have indicated that when the propagating flame approaches the relatively cool combustion chamber walls it is quenched. This occurs because the walls absorb the heat and chain carriers, one or both of which must be transported ahead of the flame to the unburnt charge to continue the propagation.

In the engine, this region near the wall has been found to be a layer a few thousandths of an inch thick around the inside of the entire combustion chamber[56]. Partially reacted combustion products such as hydrocarbons are formed in large quantities in this layer and the effect of these is to reduce the thermal efficiency and indicated mean effective pressure of an actual internal combustion engine. In our idealized system, such flame quenching is ignored so that the computer results will tend to overestimate the performance of the engine.

Concluding Remarks.

In conclusion, the assumptions made in this work that

a) the charge in the engine combustion chamber is completely

homogeneous and is all burnt.

b) no flame quenching occurs at the combustion chamber walls.

c) chemical equilibrium exists in the products of combustion at all temperatures above 1600°K during combustion and expansion.

will always produce calculated thermal efficiencies and mean effective pressures which are higher than those found if the exact condition of the working fluid was used. Such assumptions are necessary to circumvent the inherent difficulties of analysing a system with deviations from ideality.

6.2.2 THE CHEMICAL COMPOSITION AT EQUILIBRIUM

General.

The products of a hydrocarbon-air reaction consist of a number of atoms and molecules whose individual concentrations vary with changes in pressure and temperature according to the laws of chemical kinetics and subject to the condition that the mass of each basic atomic specie remains constant. When the condition of chemical equilibrium is imposed on the system, the amount of each constituent can be found by purely thermodynamic considerations.

In this work, the burnt combustion products are considered to consist of the 11 gaseous species:

Reactants	Products	Specie No.
Fuel: $C_m H_n$	CO_2	1
Air: O_2	CO	2
Air: N_2	N_2	3
	H_2O	4
	O_2	5

Products.	Specie No.
H_2	6
NO	7
OH	8
H	9
O	10
NO_2	11
N_2O	12
NH_3	13
HNO	14
N	15

To establish the amount of each of the 15 constituents in the system, 16 equations are necessarily required. Since most of these equations are non-linear, an explicit solution cannot be obtained and resort must be made to a trial and error solution of numerical methods. In a literature survey, many solution techniques were found to have been developed for such equations. These are generally of two types:

a) techniques aimed at specific solutions of equations for the combustion of a hydrocarbon fuel and air.

b) techniques which are quite general in scope and are capable of treating systems of arbitrary reactants with solid, liquid or gaseous products.

The specific type of solution is used by Goodenough and Felbeck[175] and Hershey et al.[1]. Huff and co-workers[176], on the other hand, proposed a general method of the form described in b) above. Vickland[177] analyzed a number of methods, both general and specific, finally adopting a combination of them both which was suitable for a computer solution. A summary and comparison of the most widely

used general methods is presented in Zeleznik[178]. In comparing the rate of convergence for these, it was found that no significant advantage was obtained using any one general method in preference to another.

Previous works in this field of computer simulations of combustion in spark ignition engines have tended to favour those methods which were explicitly developed to solve a set of equations arising in the combustion of a hydrocarbon fuel with air. Thus, Patterson[15] used the method based on the work of Ritter Von Stein[179] whilst Edson[14] and Phillipps and Orman[19] used Brinkley's general method[180] which was rearranged to be of a specific nature.

In this work, Brinkley's method is again used. Its adaptation to the combustion of a hydrocarbon fuel and air is presented in the following pages.

Computation of Homogeneous Gas Equilibrium.

A number of assumptions have been made or implied so far concerning the nature of the products of combustion. Briefly summarized, these are:

i) all constituents are in a state of chemical equilibrium.

ii) all the products are gaseous and can be treated as perfect gases.

iii) the system, comprising the products of combustion, is homogeneous and is maintained at constant temperature, pressure and volume.

iv) the fuel is a pure hydrocarbon of the form $C_m H_n$.

v) air is a mixture of O_2 and N_2 in the proportions stated in Appendix 1.

vi) the products consist of 15 species only.

vii) the mass of each basic atomic specie is known and remains constant.

The formal mathematical basis for Brinkley's method is described in Refs. 180 and 181. The method is completely general and is applicable to systems containing any number of chemical species coexisting at equilibrium in any number of phases. e.g. a single phase gaseous system or a single pure solid phase in contact with a gaseous phase. Only the single phase gaseous system need be considered in this work, however, since the 15 listed species present in the combustion products contain no solid constituent. The application of the method to such a problem is given in Ref. 181. A brief summary of this will now be given.

It consists essentially of two steps:

a) the derivation of the 16 working equations necessary to determine the concentrations of the individual species present in a given system.

b) their solution.

The equations are determined from a consideration of the following:

i) the conservation of mass.

ii) the law of mass action governing chemical equilibrium.

iii) the temperature, pressure and volume of the system.

To simplify the computation, the 15 listed species are allowed to remain unchanged both for varying air-fuel ratios and for the 3 individual fuels used in this work i.e. propane, iso-octane and benzene.

The calculation starts by choosing certain of the 15

listed species as independent components of the mixture. The remainder are then regarded as derived constituents. Certain restrictions are necessary, however, in the choice of these independent components:

a) they must fully define the overall system composition and must be equal in number to the chemical elements present in the system. For this problem, there are consequently four because the system contains four elements - carbon, hydrogen, oxygen and nitrogen.

b) it is necessary to pick as components those species which have the greatest probable concentrations at equilibrium subject to the following limitations:

   i) they must be stoichiometrically independent of one another.

   ii) all the chemical elements present in the system must also be present in the group of components selected.

This restriction ensures the speeding up of the numerical calculations.

Three of the four independent components required can obviously be CO_2, H_2O and N_2 as these undoubtedly compose the bulk of the equilibrium mixture at the temperature, pressure and air-fuel ratio conditions encountered in internal combustion engines. Experience with this method proved that great care must be exercised over the choice of the fourth component. Bearing in mind that the independent components should contain the species with the greatest probable concentrations at equilibrium, it was found that CO should be used as the fourth independent component for rich mixtures and O_2 for weak mixtures.

Thus, for rich and stoichiometric mixtures, the independent components are:

Specie.	Symbol.
CO_2	n_1
CO	n_2
N_2	n_3
H_2O	n_4

and the derived constituents are:

Specie.	Symbol.
O_2	n_5
H_2	n_6
NO	n_7
OH	n_8
H	n_9
O	n_{10}
NO_2	n_{11}
N_2O	n_{12}
NH_3	n_{13}
HNO	n_{14}
N	n_{15}

On the other hand, for weak mixtures, the independent components are:

Specie.	Symbol.
CO_2	c_1
O_2	c_2
N_2	c_3
H_2O	c_4

and the derived constituents are:

Specie.	Symbol.
CO	c_5
H_2	c_6

Specie.	Symbol.
NO	c_7
OH	c_8
H	c_9
O	c_{10}
NO_2	c_{11}
N_2O	c_{12}
NH_3	c_{13}
HNO	c_{14}
N	c_{15}

Consideration is first given to the derivation and solution of the working equations for the rich and stoichiometric mixtures. Subsequently, the same problems are considered in relation to the weak mixtures.

For rich and stoichiometric mixtures, the following chemical equations are constructed in consideration of the Law of Mass Action. A separate equation is obtained for each derived constituent and the participants in each reaction involve only the independent components and the corresponding derived constituents:

SERIES 6A

$$O_2 \rightleftharpoons 2CO_2 - 2CO$$

$$H_2 \rightleftharpoons H_2O + CO - CO_2$$

$$NO \rightleftharpoons \tfrac{1}{2} N_2 + CO_2 - CO$$

$$OH \rightleftharpoons \tfrac{1}{2} H_2O + \tfrac{1}{2} CO_2 - \tfrac{1}{2} CO$$

$$H \rightleftharpoons \tfrac{1}{2} H_2O + \tfrac{1}{2} CO - \tfrac{1}{2} CO_2$$

$$O \rightleftharpoons CO_2 - CO$$

$$NO_2 \rightleftharpoons \tfrac{1}{2} N_2 + 2CO_2 - 2CO$$

$$N_2O \rightleftharpoons N_2 + CO_2 - CO$$

$$NH_3 \rightleftharpoons \tfrac{1}{2} N_2 + \tfrac{3}{2} H_2O + \tfrac{3}{2} CO - \tfrac{3}{2} CO_2$$

$$HNO \rightleftharpoons \tfrac{1}{2} H_2O + \tfrac{1}{2} N_2 + \tfrac{1}{2} CO_2 - \tfrac{1}{2} CO$$
$$N \rightleftharpoons \tfrac{1}{2} N_2$$

It will be noted that there is only one possible equation by which any specific derived constituent can be formed from the independent components alone. For each of these equations in Series 6A, a mass-action (equilibrium) expression can be written. Using the symbols previously referred to for the product species in rich and stoichiometric mixtures, these expressions are:

SERIES 6B

$$n_5 = K_5 \cdot \left(\frac{P}{n_T}\right)^{-1} \cdot (n_1)^2 \cdot (n_2)^{-2}$$

$$n_6 = K_6 \cdot (n_1)^{-1} \cdot (n_2) \cdot (n_4)$$

$$n_7 = K_7 \cdot \left(\frac{P}{n_T}\right)^{-1/2} \cdot (n_1) \cdot (n_2)^{-1} \cdot (n_3)^{1/2}$$

$$n_8 = K_8 \cdot \left(\frac{P}{n_T}\right)^{-1/2} \cdot (n_1)^{1/2} \cdot (n_2)^{-1/2} \cdot (n_4)^{1/2}$$

$$n_9 = K_9 \cdot \left(\frac{P}{n_T}\right)^{-1/2} \cdot (n_1)^{-1/2} \cdot (n_2)^{1/2} \cdot (n_4)^{1/2}$$

$$n_{10} = K_{10} \cdot \left(\frac{P}{n_T}\right)^{-1} \cdot (n_1) \cdot (n_2)^{-1}$$

$$n_{11} = K_{11} \cdot \left(\frac{P}{n_T}\right)^{-1/2} \cdot (n_1)^2 \cdot (n_2)^{-2} \cdot (n_3)^{1/2}$$

$$n_{12} = K_{12} \cdot (n_1) \cdot (n_2)^{-1} \cdot (n_3)$$

$$n_{13} = K_{13} \cdot \left(\frac{P}{n_T}\right) \cdot (n_1)^{-1.5} \cdot (n_2)^{1.5} \cdot (n_3)^{0.5} \cdot (n_4)^{1.5}$$

$$n_{14} = K_{14} \cdot (n_1)^{0.5} \cdot (n_2)^{-0.5} \cdot (n_3)^{0.5} \cdot (n_4)^{0.5}$$

$$n_{15} = K_{15} \cdot \left(\frac{P}{n_T}\right)^{-0.5} \cdot n_3^{0.5}$$

In this series of equations,

P is the total pressure of the system (atmospheres).

n_T is the total number of moles of gas in the equilibrium mixture.

and K_5-K_{15} are the mass-action constants in partial pressure units. For a system obeying the perfect gas laws, these mass-action constants are equal to the corresponding thermodynamic equilibrium constants which are functions of temperature only. A more precise analysis would regard the mass-action constants as functions of temperature, pressure and the species concentrations and would calculate the equilibrium composition by an iterative procedure, improved values of K_5-K_{15} being used in each cycle. The extra complication is not considered to be worthwhile in this analysis.

The procedures used in calculating the equilibrium constants K_5-K_{15} in Series 6B are given in Appendix 6.

A further set of equations based on the Conservation of Mass (i.e. mass balances) of the independent components may also be written. For the rich and stoichiometric mixtures under consideration, these are:

$$\left.\begin{aligned}
n_1 &= q_1 - 2n_5 + n_6 - n_7 - \tfrac{1}{2}n_8 + \tfrac{1}{2}n_9 - n_{10} \\
&\quad - 2n_{11} - n_{12} + 1.5\, n_{13} - \tfrac{1}{2}\, n_{14} \\
n_2 &= q_2 + 2n_5 - n_6 + n_7 + \tfrac{1}{2}n_8 - \tfrac{1}{2}n_9 + n_{10} \\
&\quad + n_{12} - 1.5\, n_{13} + \tfrac{1}{2}\, n_{14} \\
n_3 &= q_3 - \tfrac{1}{2}\, n_7 - \tfrac{1}{2}\, n_{11} - n_{12} - \tfrac{3}{2}\, n_{13} - \tfrac{1}{2}\, n_{14} \\
n_4 &= q_4 - n_6 - \tfrac{1}{2}\, n_8 - \tfrac{1}{2}\, n_9 - 1.5\, n_{13} - \tfrac{3}{2}\, n_{14}
\end{aligned}\right\} \quad \text{SERIES 6C}$$

where q_1, q_2, q_3 and q_4 represent the number of moles of each independent component in the absence of all derived constituents. These values are easily calculated from the known composition of the unburnt fraction.

One additional equation is required before the actual calculations can be started - namely, a summation for n_T, the total number of moles of gas at equilibrium:

$$\left.\begin{aligned} n_T = {} & n_1 + n_2 + n_3 + n_4 + n_5 + n_6 + n_7 \\ & + n_8 + n_9 + n_{10} + n_{11} + n_{12} + n_{13} \\ & + n_{14} + n_{15} \end{aligned}\right\} \quad \text{---- 6-6}$$

The sixteen equations which constitute Series 6B, Series 6C and Equation 6-6, with numerical values substituted for the k's, q's and P, are the working equations. These can be solved simultaneously for the fifteen unknowns by the methods about to be described.

Firstly, the values of q_1 to q_4 are calculated from the unburnt fraction composition. These are easily determined from the following general equation for rich and stoichiometric mixtures of the reaction between a hydrocarbon fuel and air when no derived constituents are present:

$$C_m H_n + x\left(m + \frac{n}{4}\right) O_2 + 3.764\, x\left(m + \frac{n}{4}\right) N_2 = n\, H_2O$$

$$+ \left(m\,(2x-1) + \frac{n}{2}\,(x-1)\right) CO_2 + \left(2m(1-x) + \frac{n}{2}\,(1-x)\right) CO + 3.764\, x\left(m + \frac{n}{4}\right) N_2 \qquad \text{---- 6-7}$$

In this equation, x (≤ 1) is the fraction of chemically correct air entering the reaction. Thus,

$$q_1 = \left(m(2x-1) + \frac{n}{2}\,(x-1)\right)$$

$$q_2 = \left(2m(1-x) + \frac{n}{2}\,(1-x)\right)$$

$$q_3 = 3.764x\left(m + \frac{n}{4}\right)$$

and $q_4 = \frac{n}{2}$

Secondly, the values of the thermodynamic equilibrium constants K_5 to K_{15} are evaluated for the known temperature

of the mixture by methods described in Appendix 6.

A first estimate is then made of the number of moles of the independent components n_1, n_2, n_3 and n_4, and, also, of the total number of moles, n_T. From these estimated values, corresponding values of n_5 to n_{15} are calculated from the equations in Series 6B. If the initial estimates of n_T, n_1, n_2, n_3 and n_4 were correct, the resulting values of n_5 to n_{15} will satisfy the set of equations in Series 6C. If they do not, an improved set of values for n_T, n_1, n_2, n_3 and n_4 is obtained by application of a simple iteration technique. This general procedure is repeated until the required accuracy is achieved. In this work, this was considered to be when consecutive values of each of the mole fractions of the independent components differed by less than .01 per cent.

In the determination of the chemical composition at equilibrium for <u>weak mixtures</u>, exactly similar techniques are used except that O_2 replaces CO as an independent component. The chemical equations for such mixtures are now:

$$CO \rightleftharpoons CO_2 - \tfrac{1}{2} O_2$$
$$H_2 \rightleftharpoons H_2O - \tfrac{1}{2} O_2$$
$$NO \rightleftharpoons \tfrac{1}{2} N_2 + \tfrac{1}{2} O_2$$
$$OH \rightleftharpoons \tfrac{1}{2} H_2O + \tfrac{1}{4} O_2$$
$$H \rightleftharpoons \tfrac{1}{2} H_2O - \tfrac{1}{4} O_2$$
$$O \rightleftharpoons \tfrac{1}{2} O_2$$
$$NO_2 \rightleftharpoons \tfrac{1}{2} N_2 + O_2$$
$$N_2O \rightleftharpoons N_2 + \tfrac{1}{2} O_2$$
$$NH_3 \rightleftharpoons \tfrac{1}{2} N_2 + \tfrac{3}{2} H_2O - \tfrac{3}{4} O_2$$
$$HNO \rightleftharpoons \tfrac{1}{2} H_2O + \tfrac{1}{2} N_2 + \tfrac{1}{4} O_2$$
$$N \rightleftharpoons \tfrac{1}{2} N_2$$

SERIES 6D

and the corresponding mass action expressions (corresponding to those in Series 6B) are:

$$c_5 = G_6 . \left(\frac{P}{c_T}\right)^{-1/4} . (c_1) . (c_2)^{-1/2}$$

$$c_6 = G_6 . \left(\frac{P}{c_T}\right)^{-1/2} . (c_2)^{-1/2} . (c_4)$$

$$c_7 = G_7 . (c_2)^{1/2} . (c_3)^{1/2}$$

$$c_8 = G_8 . \left(\frac{P}{c_T}\right)^{-1/4} . (c_2)^{1/4} . (c_4)^{1/2}$$

$$c_9 = G_9 . \left(\frac{P}{c_T}\right)^{-3/4} . (c_1)^{-1/4} . (c_4)^{1/2}$$

$$c_{10} = G_{10} . \left(\frac{P}{c_T}\right)^{-1/2} . (c_2)^{1/2}$$

$$c_{11} = G_{11} . \left(\frac{P}{c_T}\right)^{1/2} . (c_2) . (c_3)^{1/2}$$

$$c_{12} = G_{12} . \left(\frac{P}{c_T}\right)^{1/2} . (c_2)^{1/2} . (c_3)$$

$$c_{13} = G_{13} . \left(\frac{P}{c_T}\right)^{1/4} . (c_2)^{-3/4} . (c_3)^{1/2} . (c_4)^{1.5}$$

$$c_{14} = G_{14} . \left(\frac{P}{c_T}\right)^{1/4} . (c_2)^{1/4} . (c_3)^{1/2} . (c_4)^{1/2}$$

$$c_{15} = G_{15} . \left(\frac{P}{c_T}\right)^{-1/2} . (c_3)^{1/2}$$

SERIES 6E.

In this set of equations, the symbols previously referred to for the product species in weak mixtures have been used and, in addition, G_5 to G_{15} are the mass action constants for the respective reactions in Series 6D. The term c_T is the total number of moles of gas in the equilibrium mixture.

The set of equations based on the Conservation of Mass for weak mixtures are:

$$c_1 = z_1 - c_5$$

$$c_2 = z_2 + \tfrac{1}{2} c_5 + \tfrac{1}{2} c_6 - \tfrac{1}{2} c_7 - \tfrac{1}{4} c_8 + \tfrac{1}{4} c_9 - \tfrac{1}{2} c_{10} - c_{11} - \tfrac{1}{2} c_{12} + \tfrac{3}{4} c_{13} - \tfrac{1}{4} c_{14}$$

$$c_3 = z_3 - \tfrac{1}{2} c_7 - \tfrac{1}{2} c_{11} - c_{12} - \tfrac{1}{2} c_{13} - \tfrac{1}{2} c_{14} - \tfrac{1}{2} c_{15}$$

$$c_4 = z_4 - c_6 - \tfrac{1}{2} c_8 - \tfrac{1}{2} c_9 - 1.5\, c_{13} - \tfrac{1}{2} c_{14}$$

SERIES 6F

in which z_1- z_4 are the number of moles of each independent component in the absence of all derived constituents.

The final equation, based on the summation of the total number of moles of gas at equilibrium is:

$$c_T = c_1 + c_2 + c_3 + c_4 + c_5 + c_6 + c_7 + c_8 + c_9 + c_{10} + c_{11} + c_{12} + c_{13} + c_{14} + c_{15} \qquad \text{----- 6-8}$$

The sixteen equations comprising Series 6E, Series 6F and Equation 6-8 constitute the working equations for weak mixtures. The values of z_1- z_4 are calculated from the unburnt fraction composition. As before, a general equation for the combustion of a hydrocarbon fuel in air is obtained for weak mixtures when no derived constituents are present. This is:

$$C_m H_n + x.\left(m + \frac{n}{4}\right) O_2 + 3.764\, x \left(m + \frac{n}{4}\right) N = m\, CO_2 + \frac{n}{2} H_2O + (x-1).\left(m + \frac{n}{4}\right) O_2 + 3.764\, x \left(m + \frac{n}{4}\right) N_2 \qquad \text{---- 6-9}$$

where x (>1) is the fraction of chemically correct air entering the reaction. Thus,

$$z_1 = m$$

$$z_2 = (x-1).\left(m + \frac{n}{4}\right)$$

$$z_3 = 3.764.\ x.\ \left(m + \frac{n}{4}\right)$$

$$z_4 = \frac{n}{2}$$

Solution methods are exactly the same as those described earlier for the rich and stoichiometric mixtures.

6.2.3. COMPUTER CALCULATIONS OF CHEMICAL EQUILIBRIUM COMPOSITIONS.

The sets of equations and solution techniques described above have been programmed on a digital computer for use in the analytical model. Some results from this dissociation work are plotted in Figs. 6-3 to 6-47.

Those plots in Figs. 6-3 to 6-17 refer to the combustion of Propane in air over the temperature range 2000-3250°K at equivalence ratios of 0.8, 1.0, 1.2 and 1.4, and at 10 ATM and 50 ATM pressure. The results in Figs. 6-18 to 6-32 are for iso-octane combustion and those in Figs. 6-33 to 6-47 are for the combustion of benzene over the same temperature range and at the seme equivalence ratios and pressures as stated above for Propane.

These results and plots are in excellent agreement with other relevant published calculations. e.g. Patterson[15], Vickland et all[177] and Ref.2102.

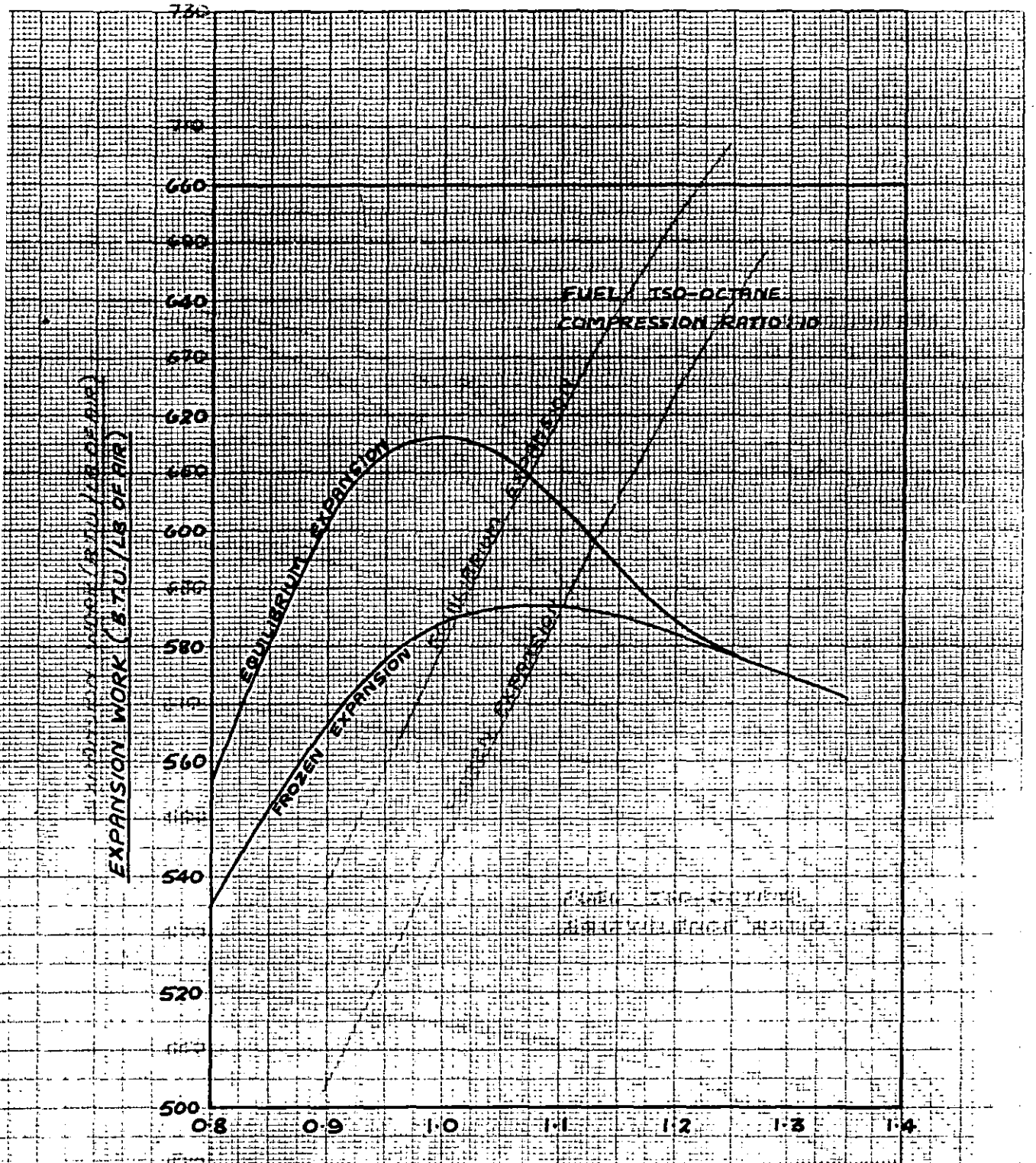

FIG. 6-1 — VARIATION OF EXPANSION WORK WITH AIR-FUEL RATIO FOR EQUILIBRIUM AND FROZEN EXPANSIONS (FROM STARKMAN AND NEWHALL[85])

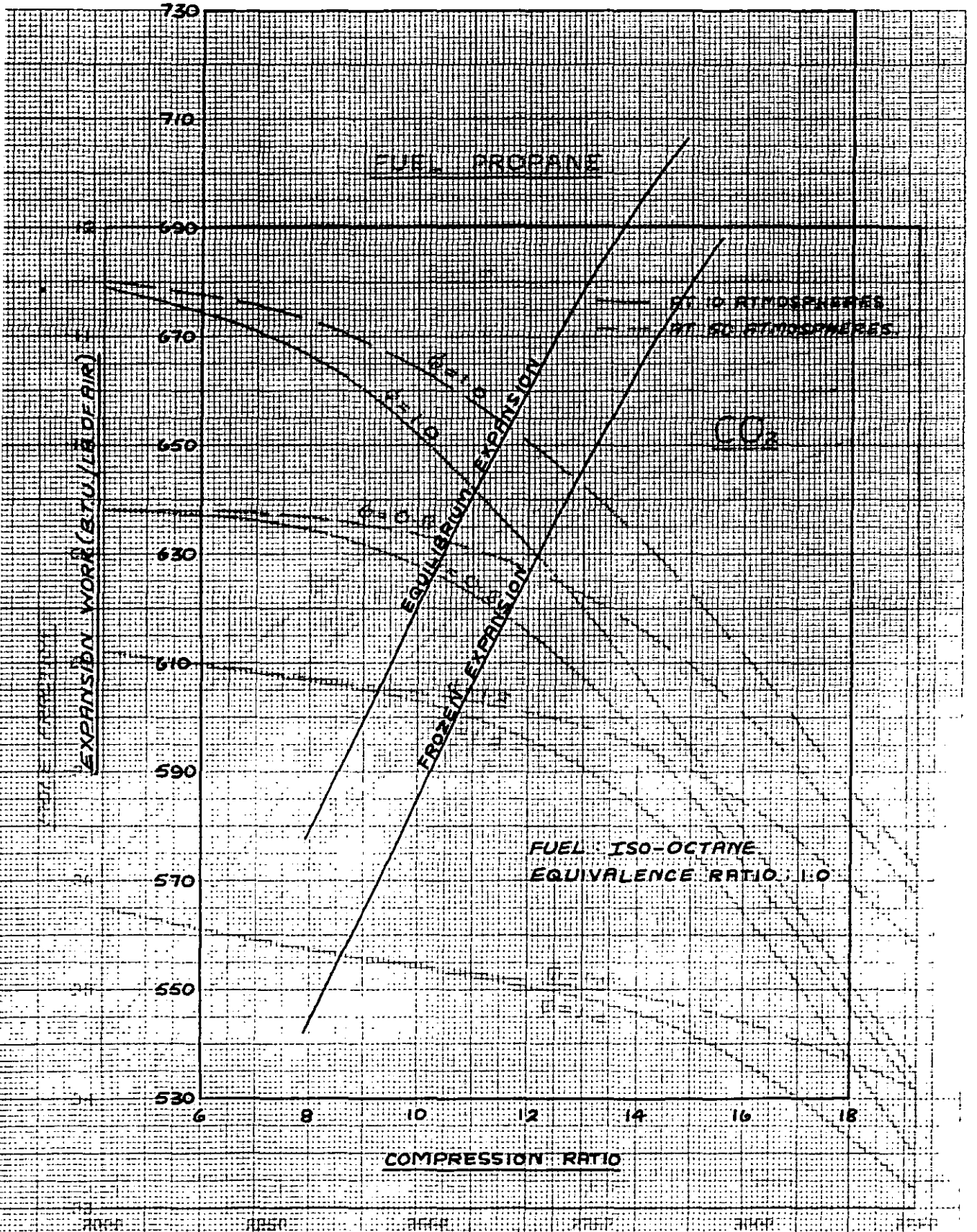

FIG 6-2 — COMPARISON OF EQUILIBRIUM AND FROZEN EXPANSIONS FOR VARIOUS COMPRESSION RATIOS (FROM STARKMAN AND NEWHALL[86]).

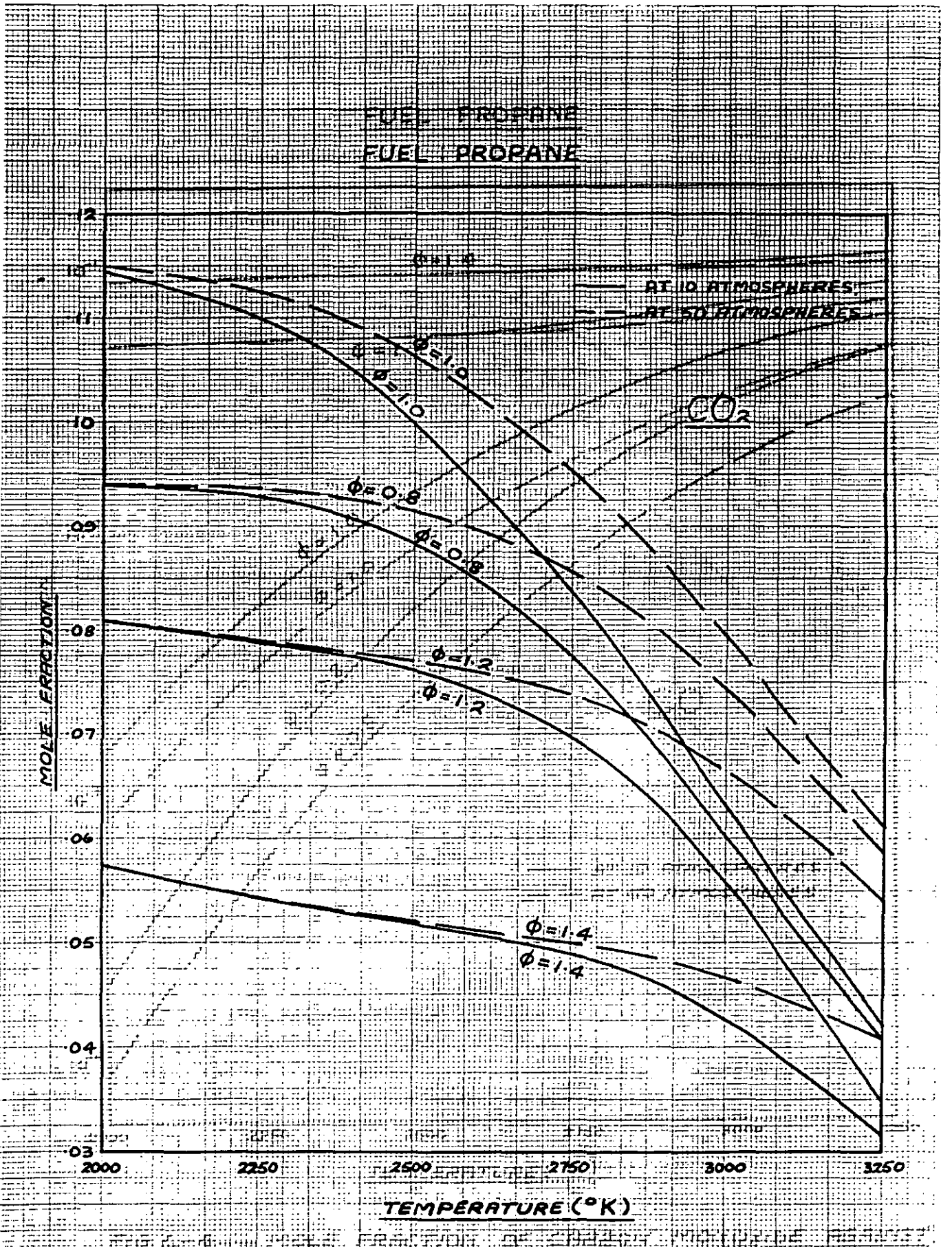

FIG. 6-3 —— MOLE FRACTION OF CARBON DIOXIDE AGAINST TEMPERATURE

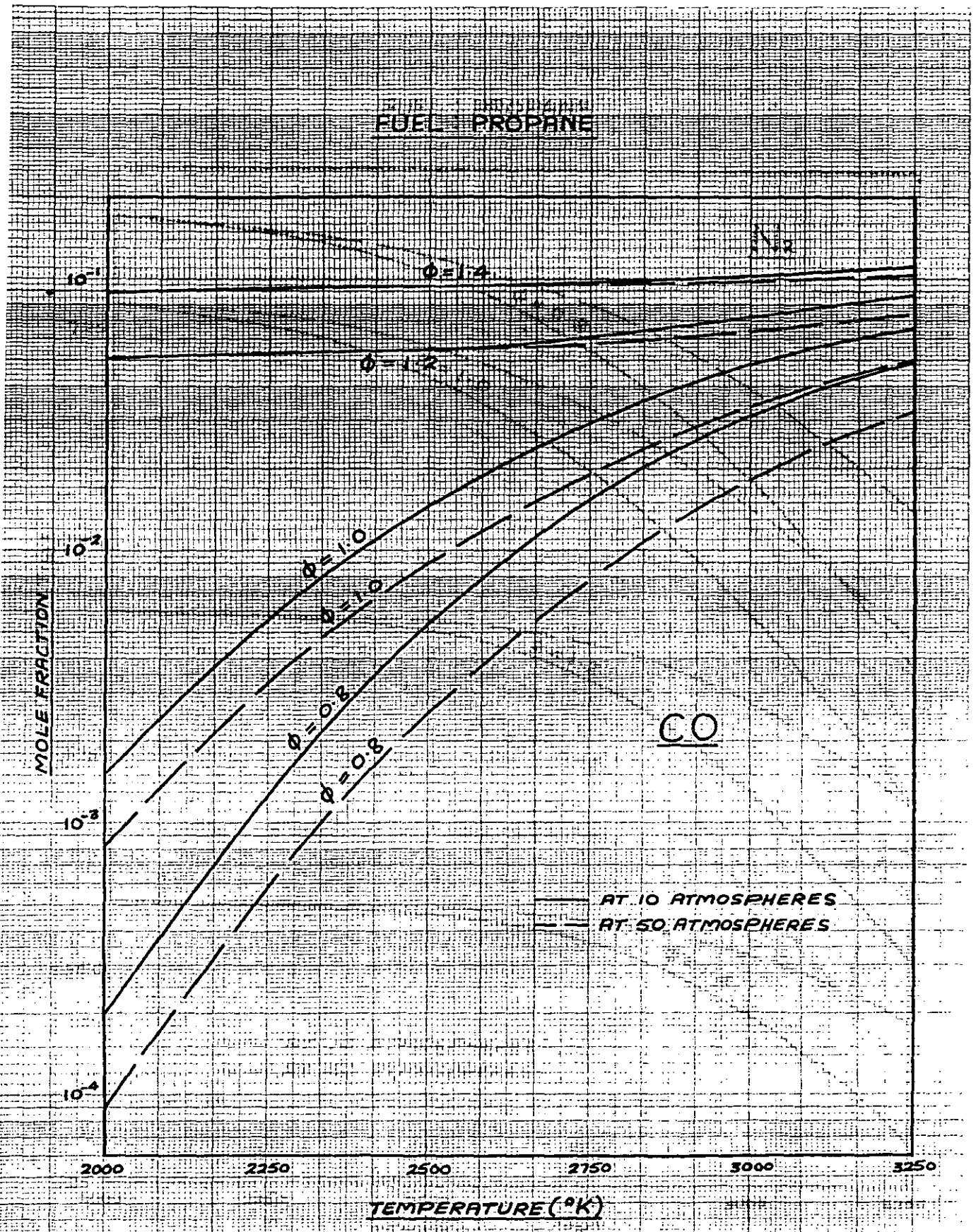

FIG. 6-4 — MOLE FRACTION OF CARBON MONOXIDE AGAINST TEMPERATURE

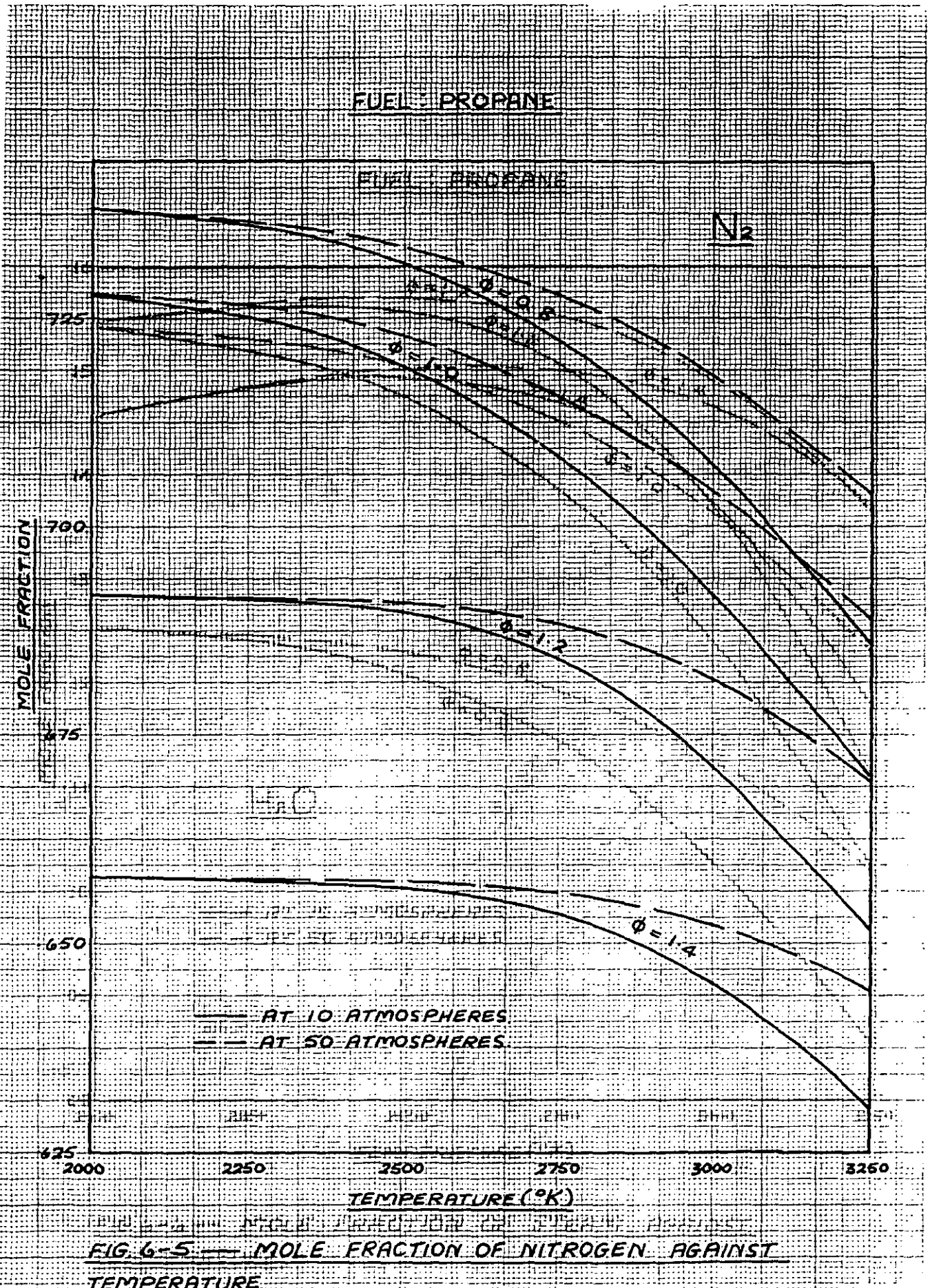

FIG. 6-5 —— MOLE FRACTION OF NITROGEN AGAINST TEMPERATURE.

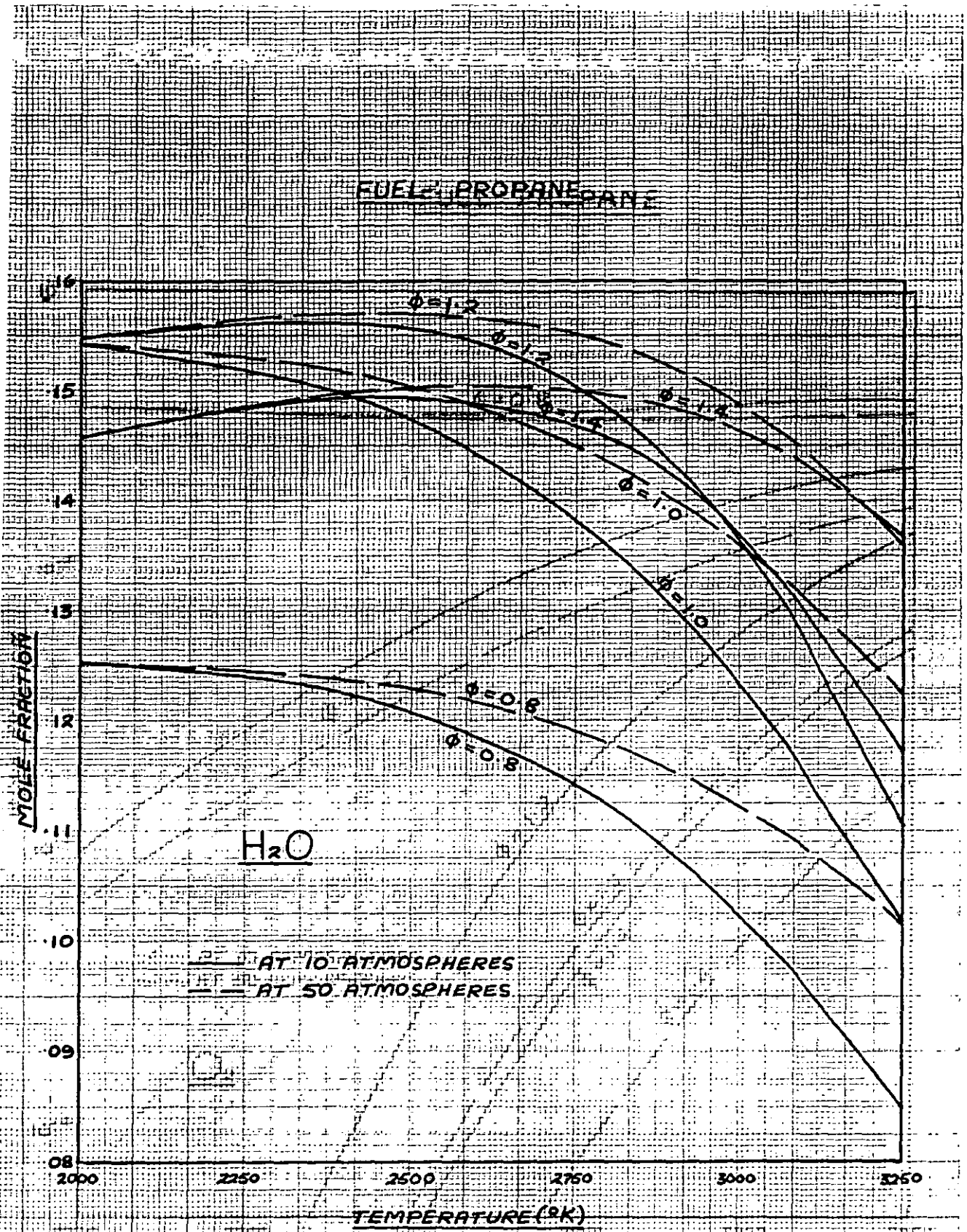

FIG. 6-6 — MOLE FRACTION OF STEAM AGAINST TEMPERATURE.

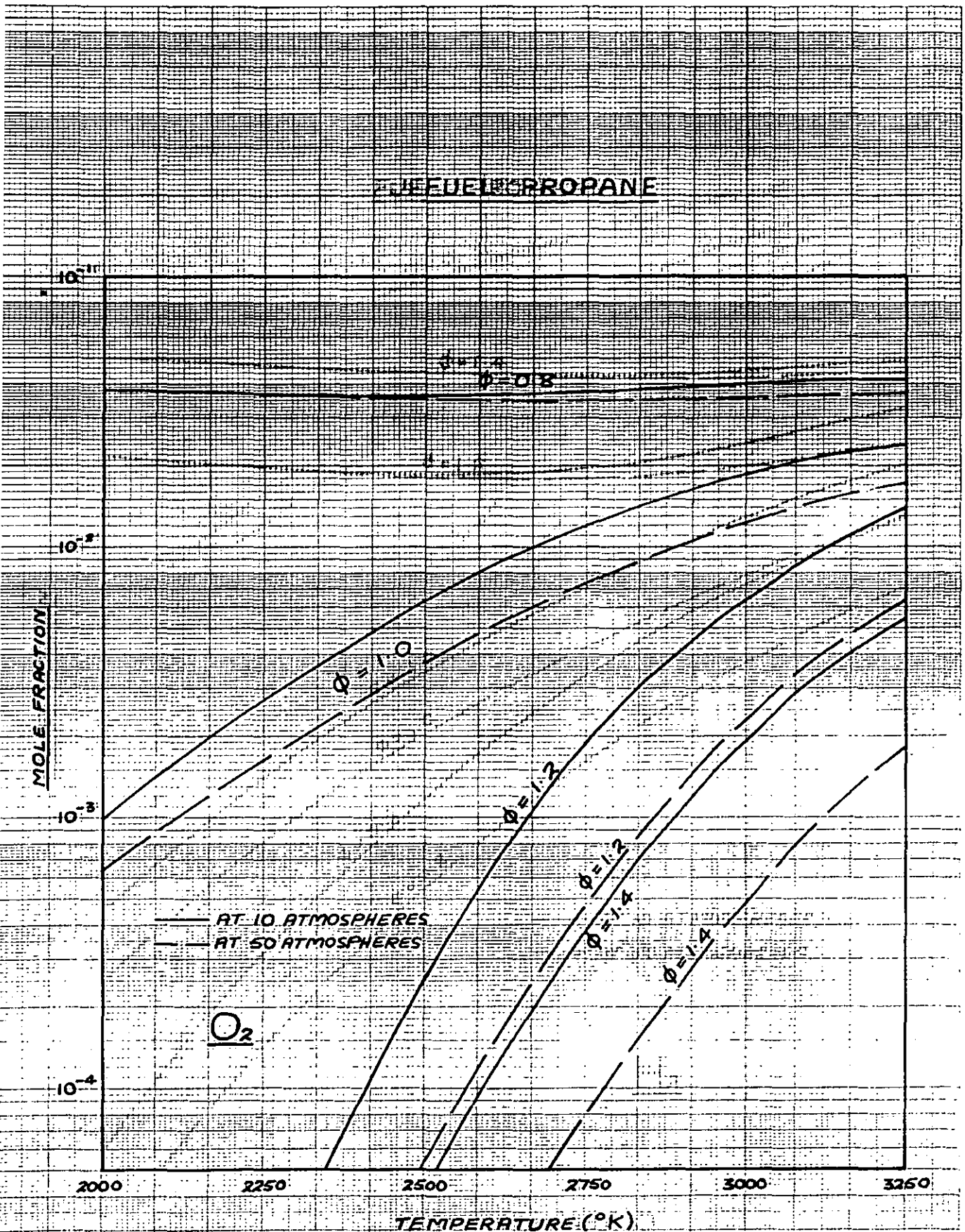

FIG. 6-7 —— MOLE FRACTION OF OXYGEN AGAINST TEMPERATURE

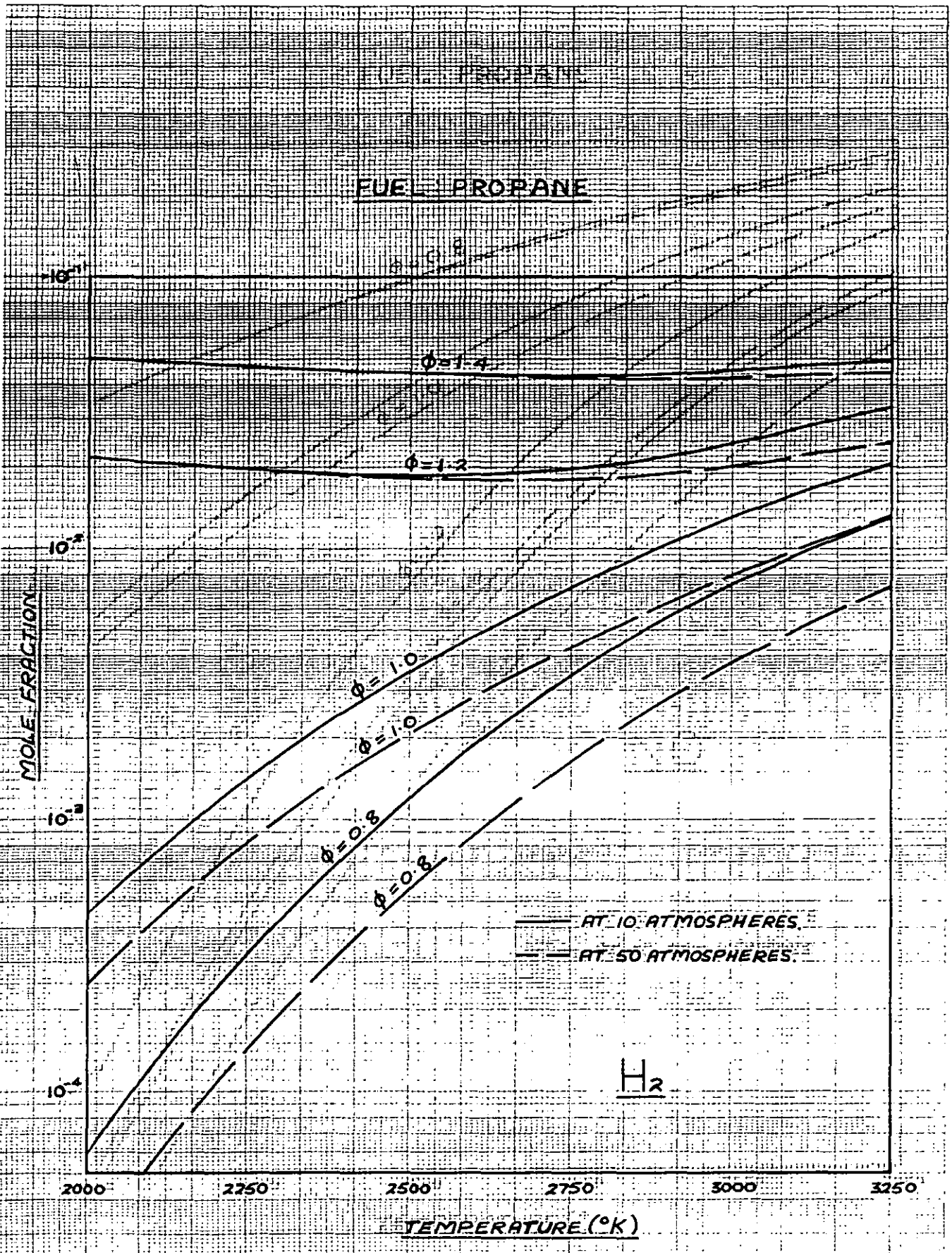

FIG. 6-8 —— MOLE FRACTION OF HYDROGEN AGAINST TEMPERATURE

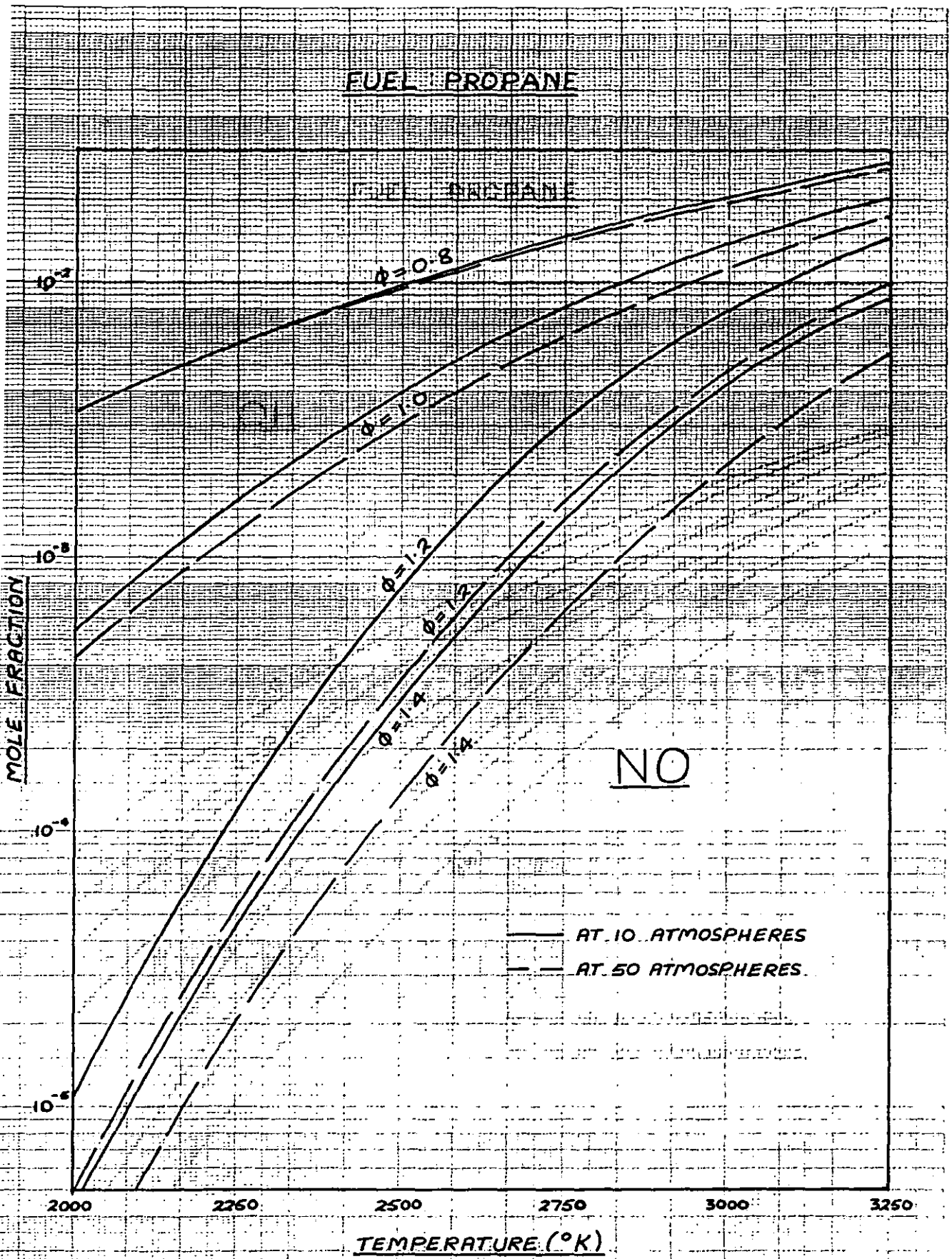

FIG. 6-9 — MOLE FRACTION OF NITRIC OXIDE AGAINST TEMPERATURE

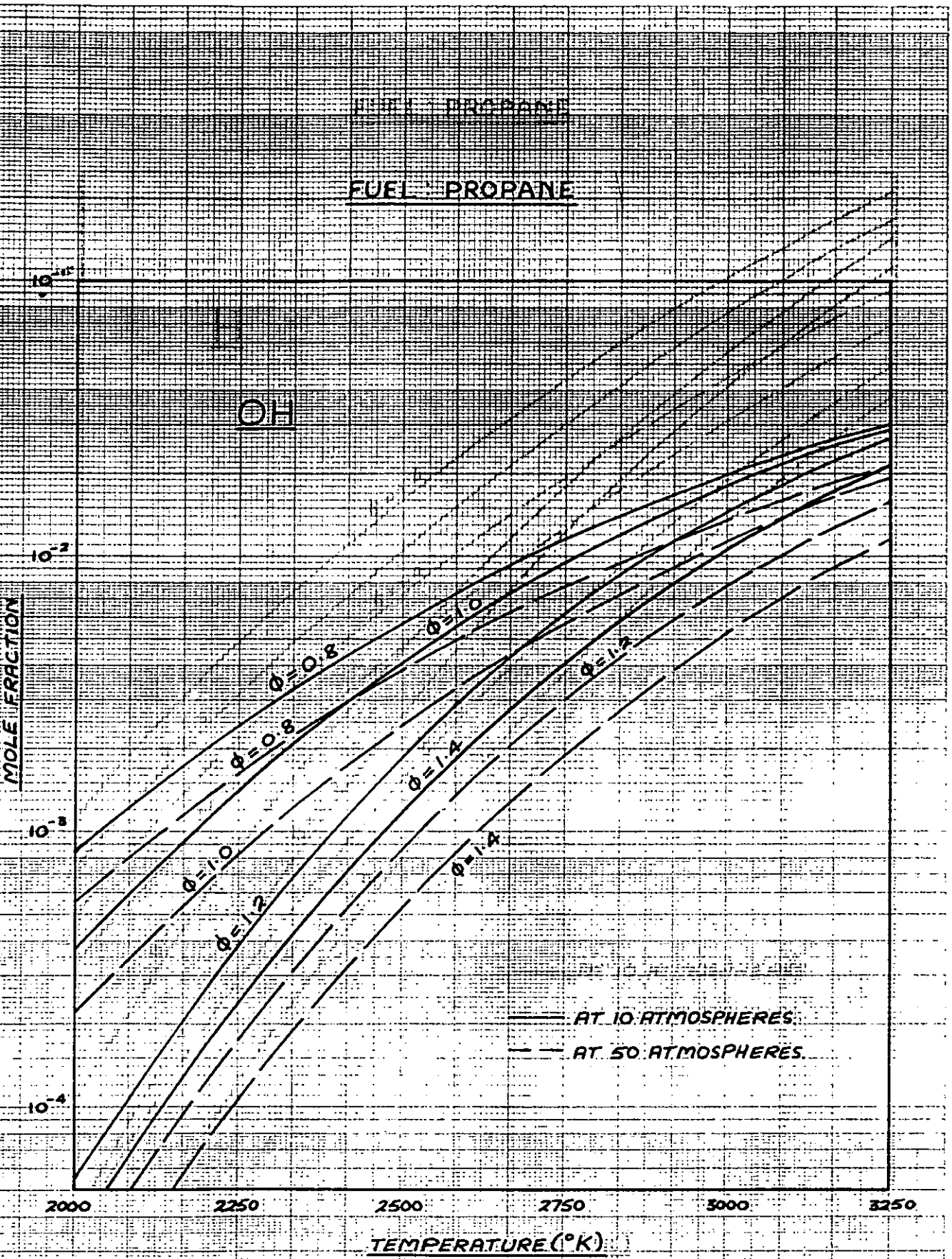

FIG. 6-10 —— MOLE FRACTION OF THE HYDROXYL RADICAL (OH) AGAINST TEMPERATURE

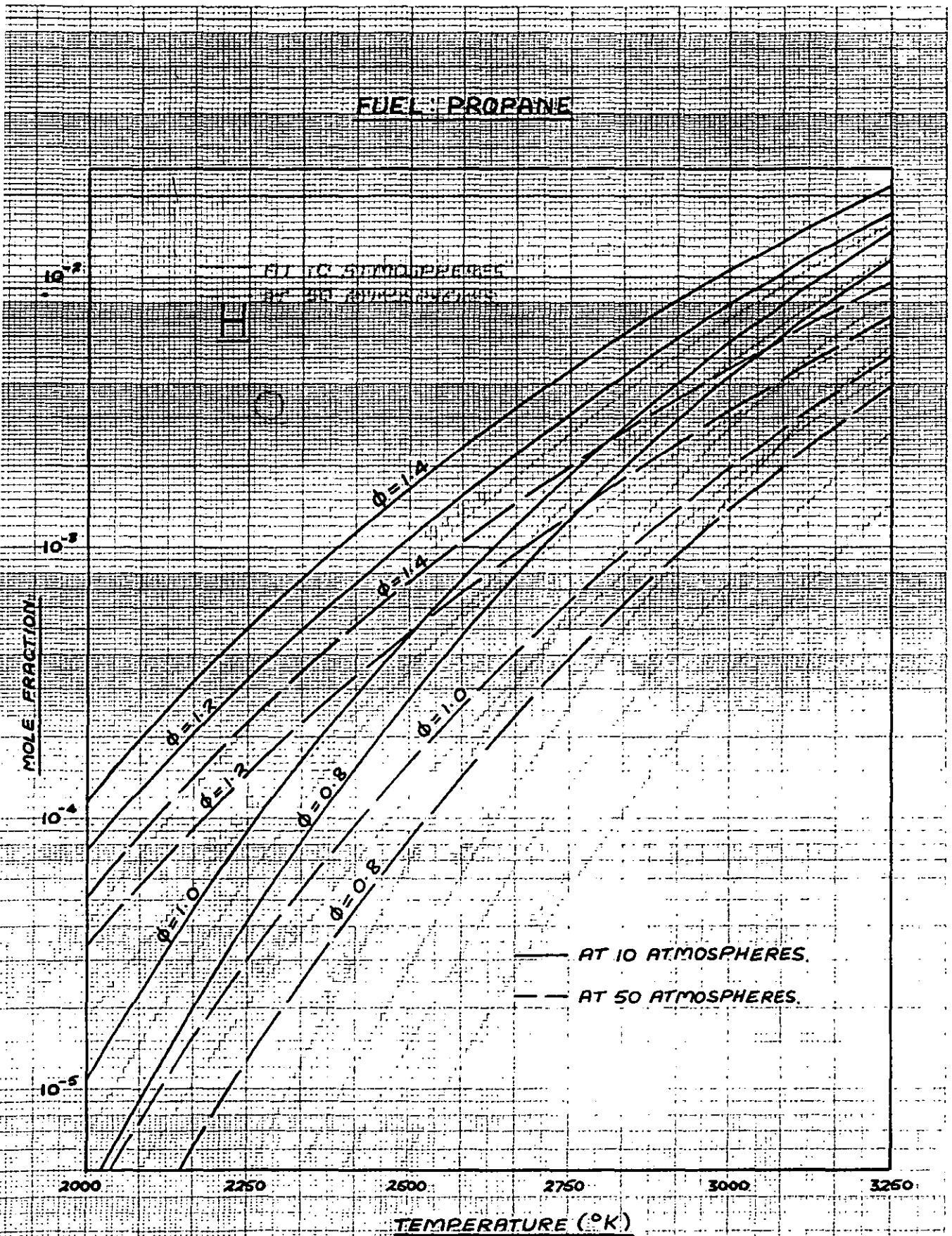

FIG. 6 – 11 —— MOLE FRACTION OF ATOMIC HYDROGEN (H) AGAINST TEMPERATURE.

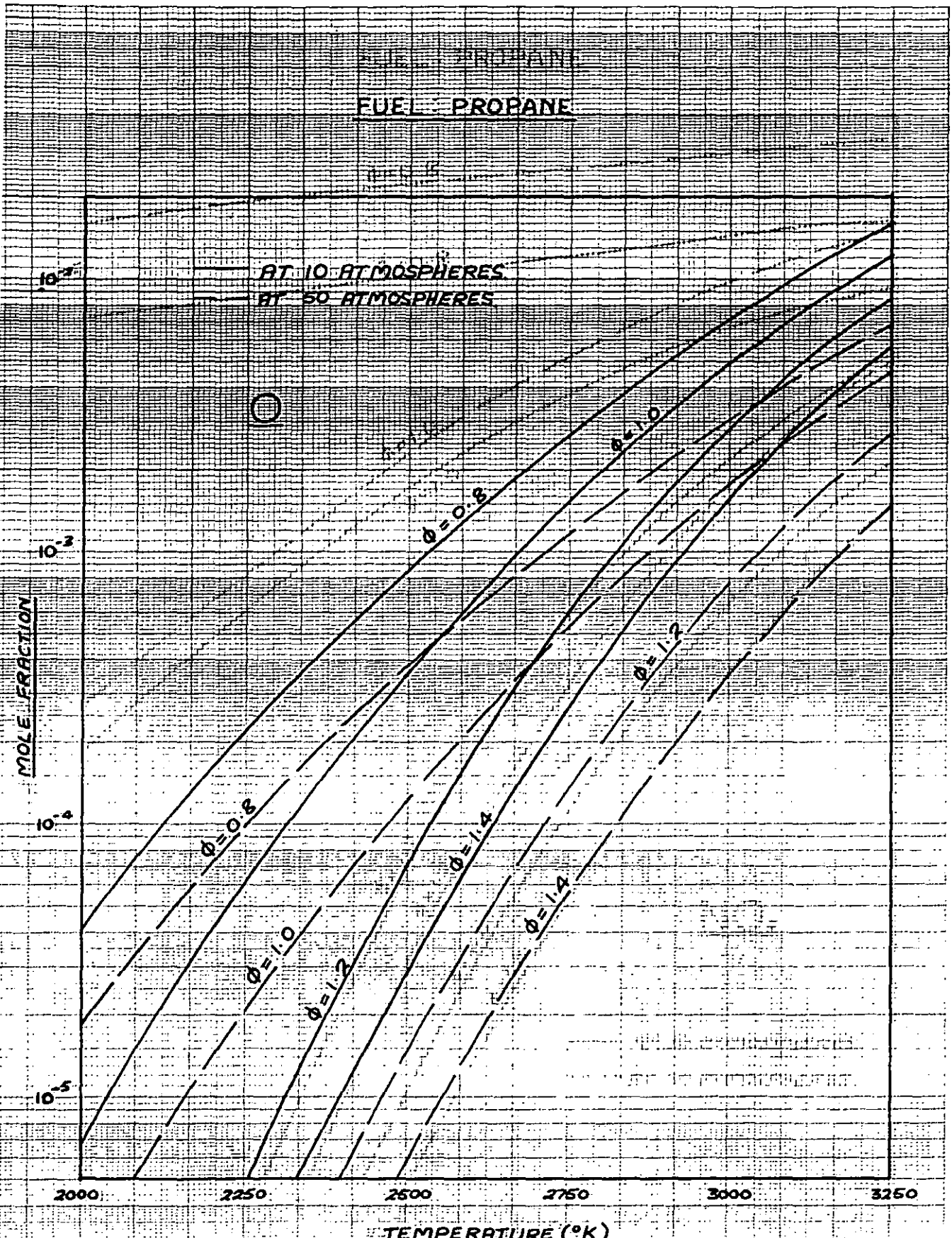

FIG. 6-12 —— MOLE FRACTION OF ATOMIC OXYGEN (O) AGAINST TEMPERATURE.

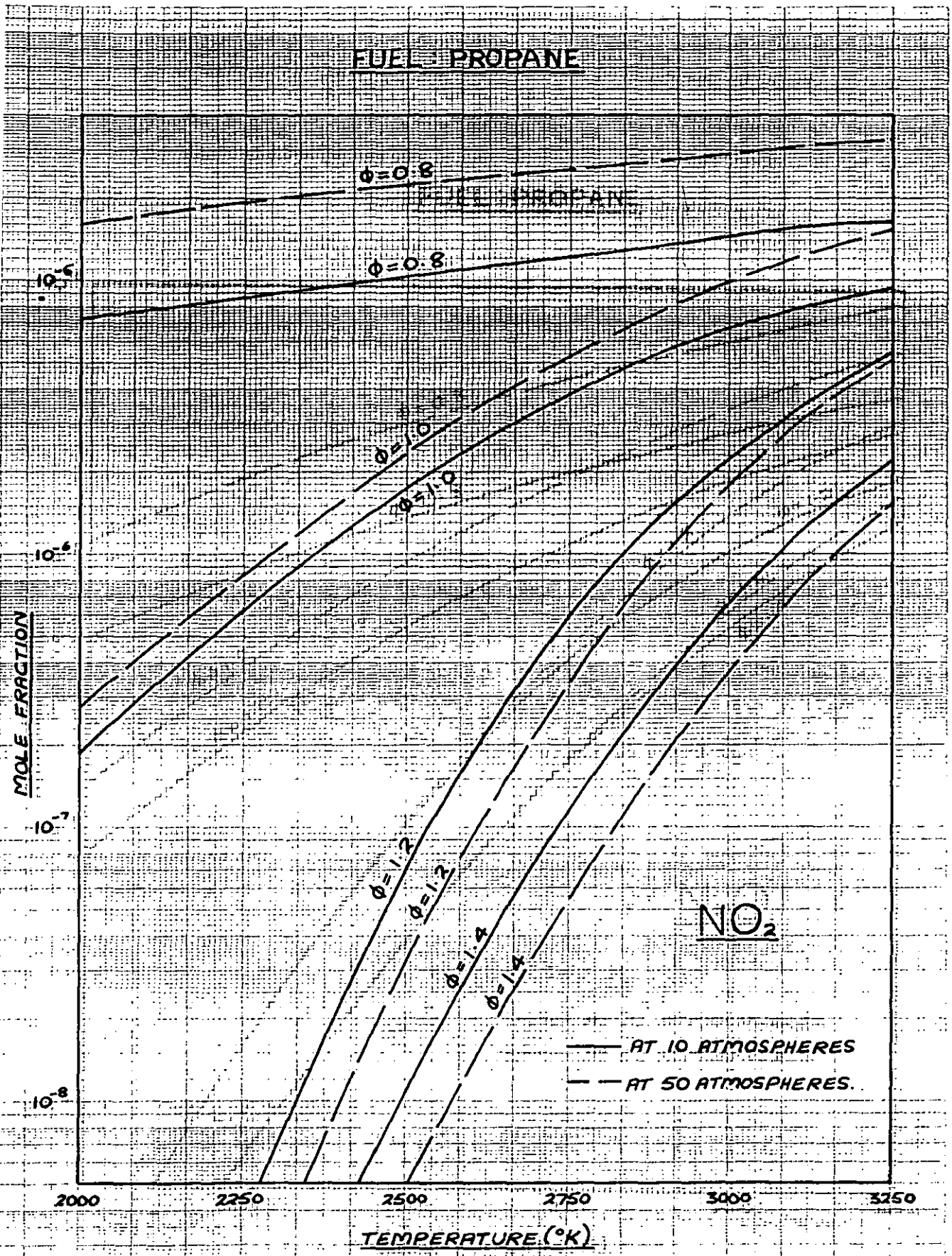

FIG. 6-13 —— MOLE FRACTION OF NITROGEN DIOXIDE (NO_2) AGAINST TEMPERATURE.

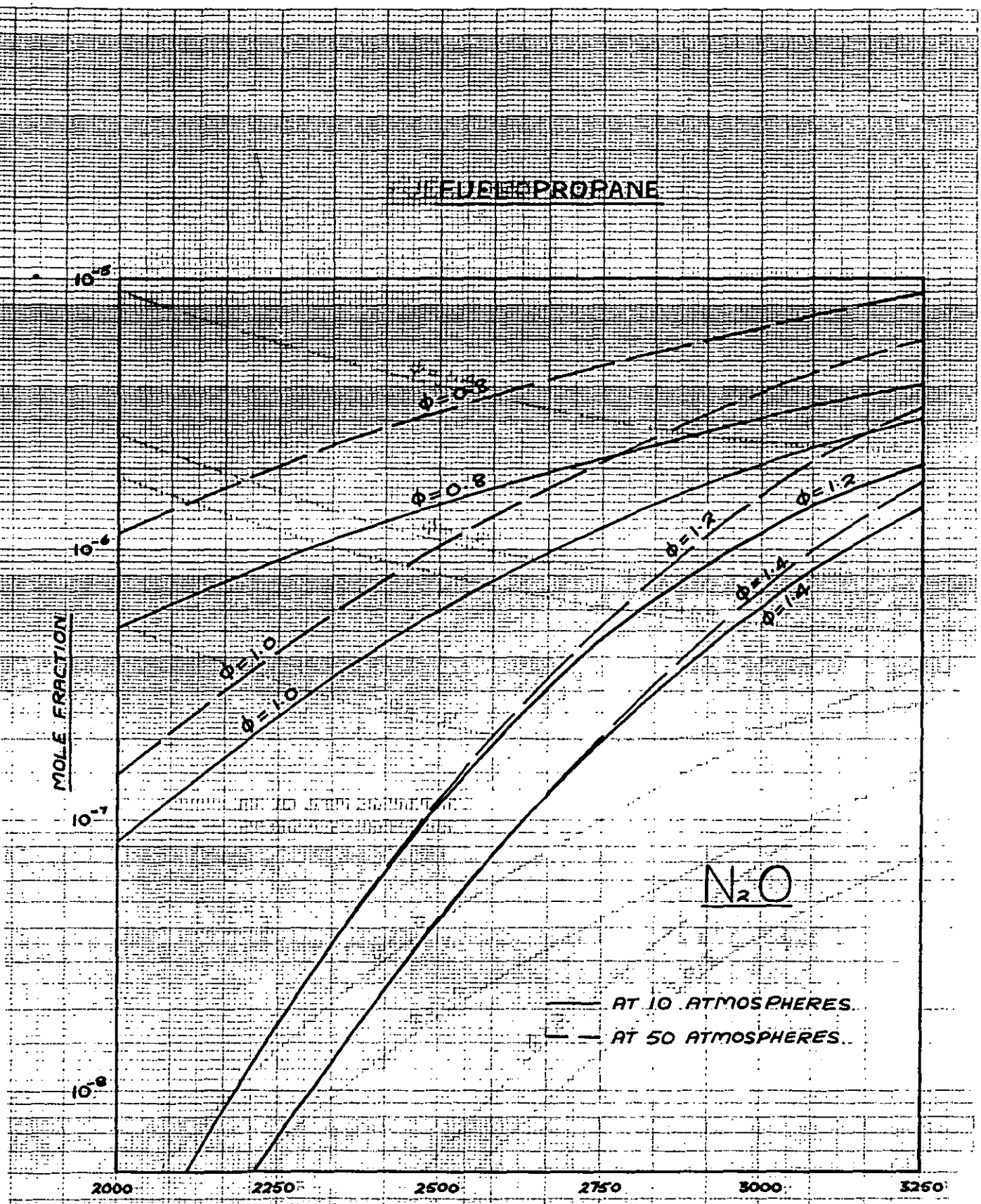

FIG. 6-14 — MOLE FRACTION OF NITROUS OXIDE (N_2O) AGAINST TEMPERATURE

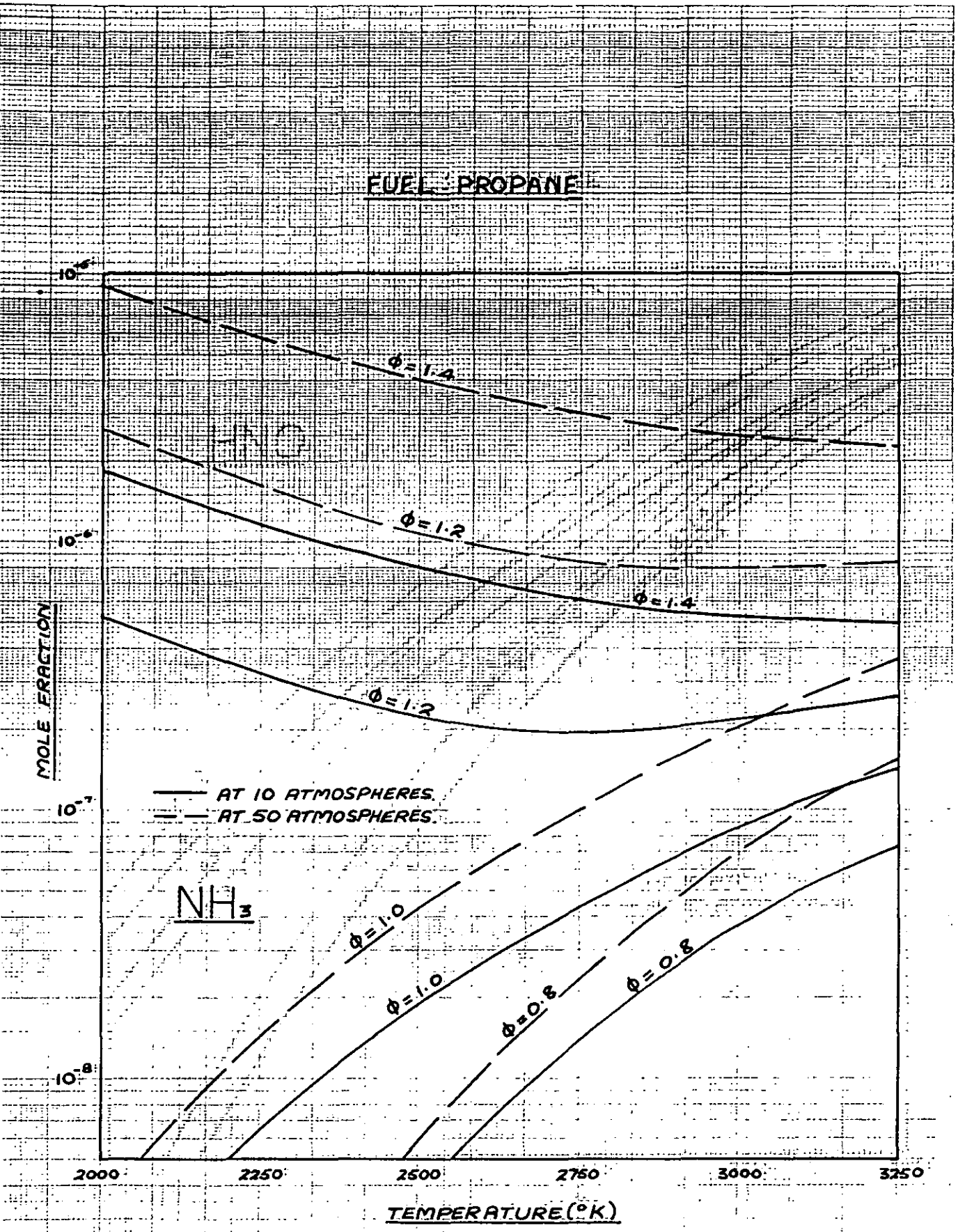

FIG. 6-15 —— MOLE FRACTION OF AMMONIA (NH_3) AGAINST TEMPERATURE

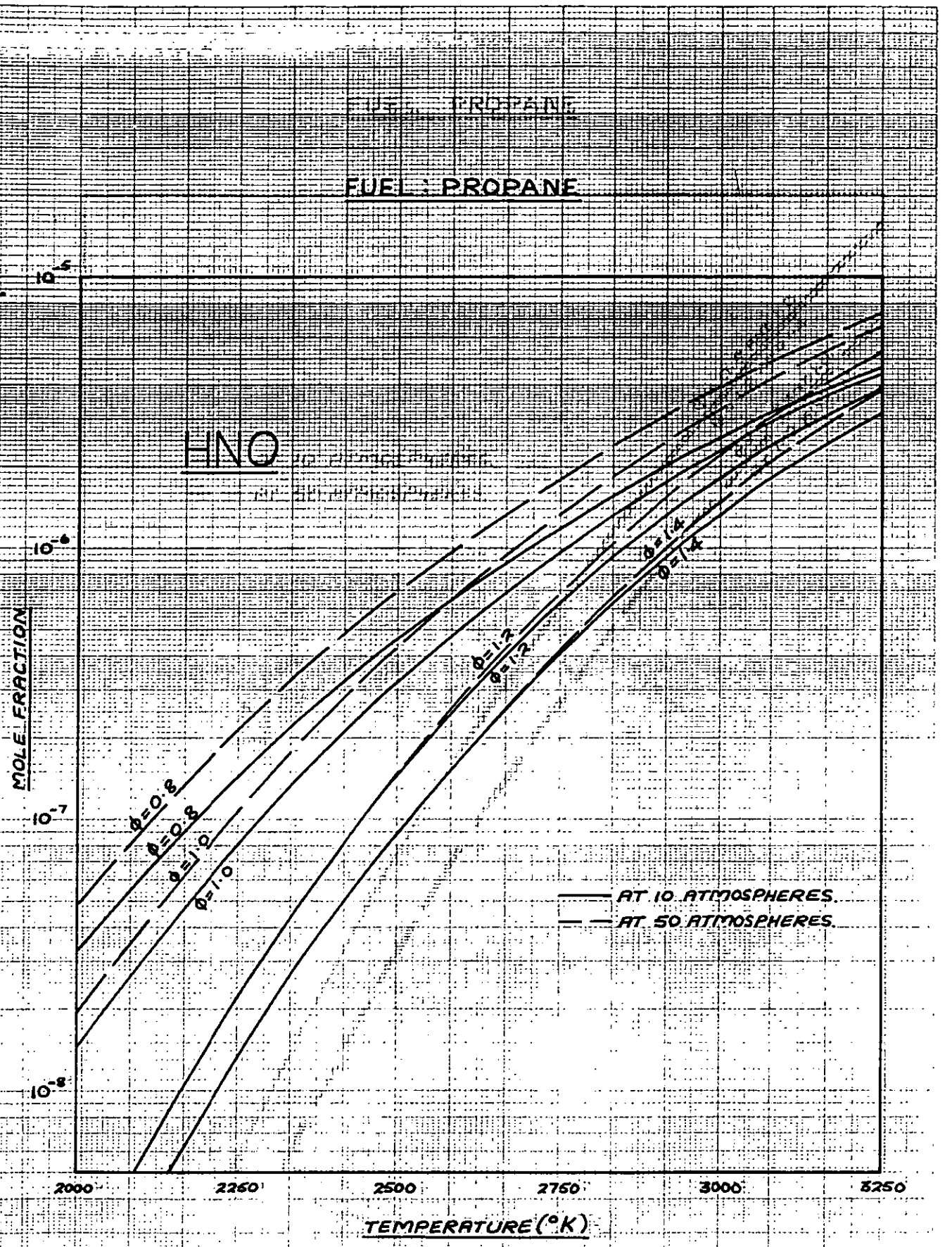

FIG. 6-16 —— MOLE FRACTION OF HNO AGAINST TEMPERATURE.

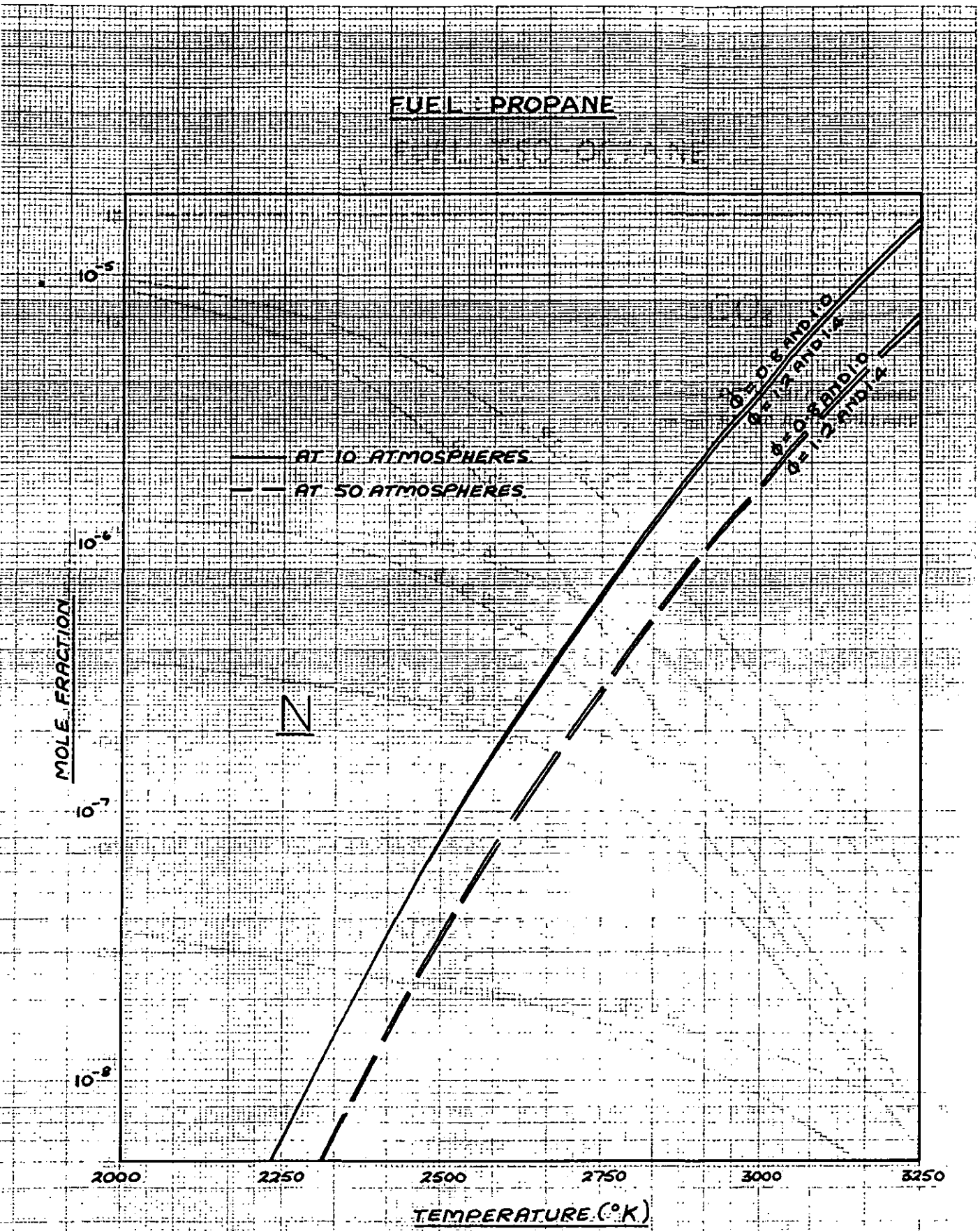

FIG. 6—17 —— MOLE FRACTION OF ATOMIC NITROGEN (N) AGAINST TEMPERATURE

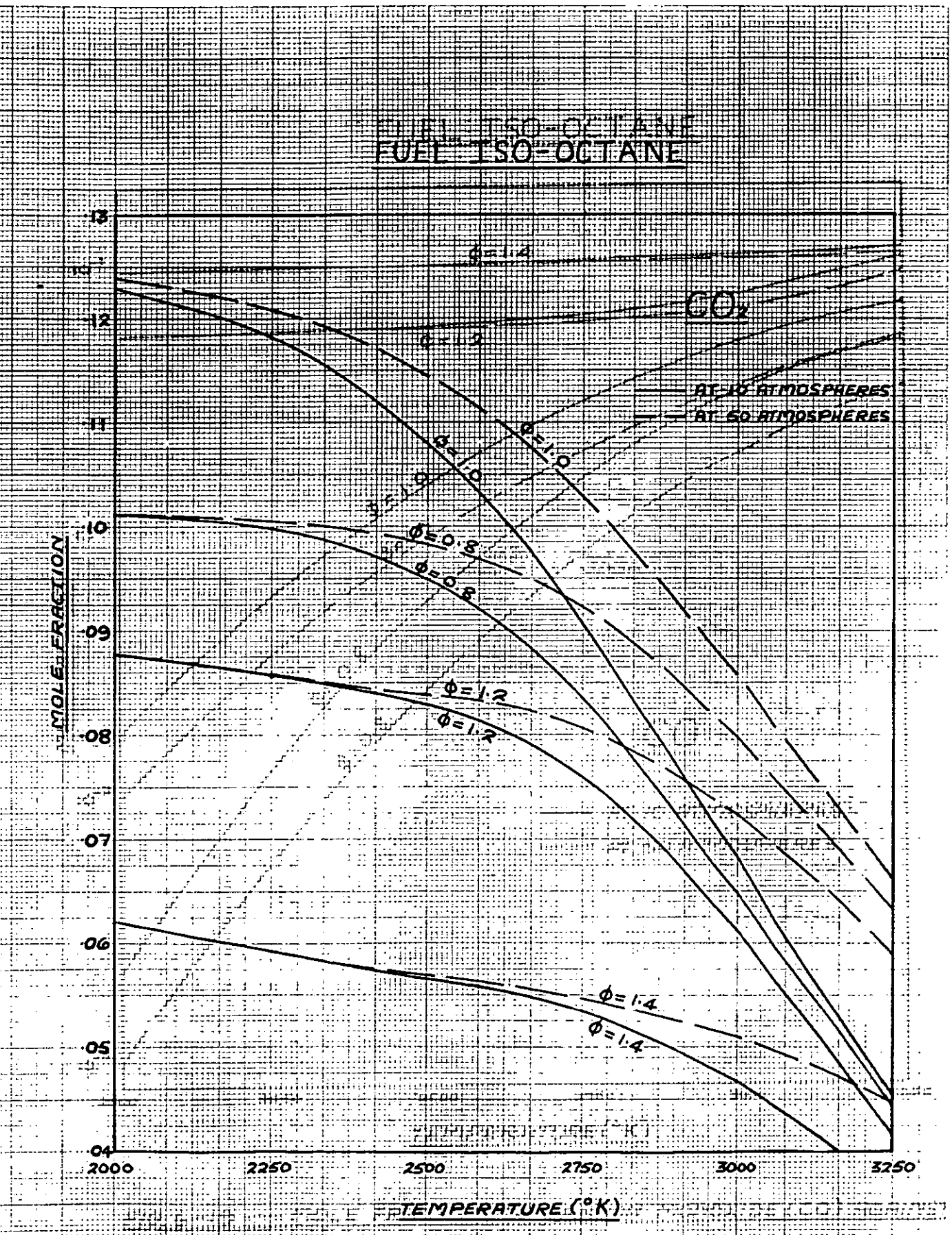

FIG. 6-18 — MOLE FRACTION OF CARBON DIOXIDE (CO_2) AGAINST TEMPERATURE

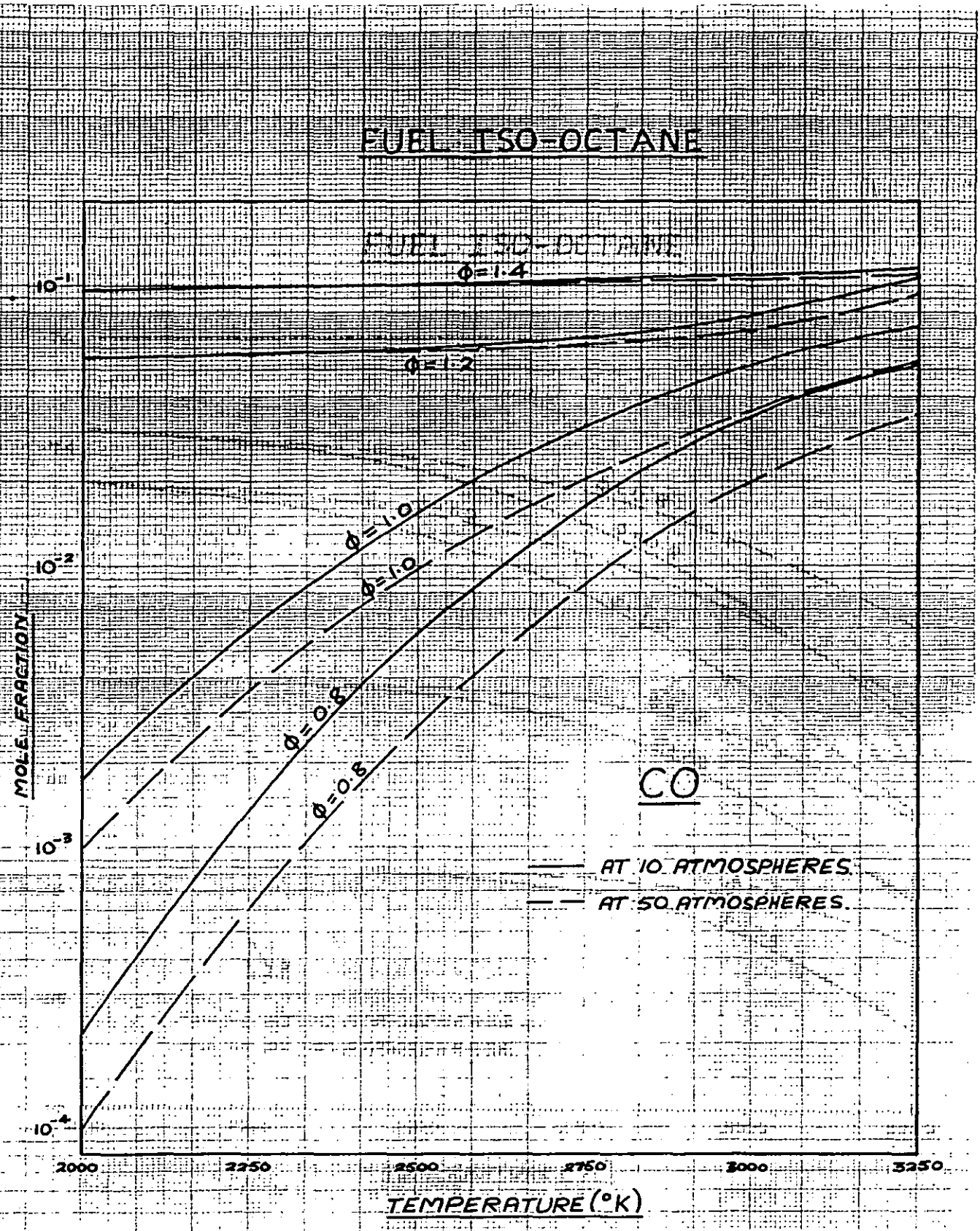

FIG. 6-19 — MOLE FRACTION OF CARBON MONOXIDE (CO) AGAINST TEMPERATURE

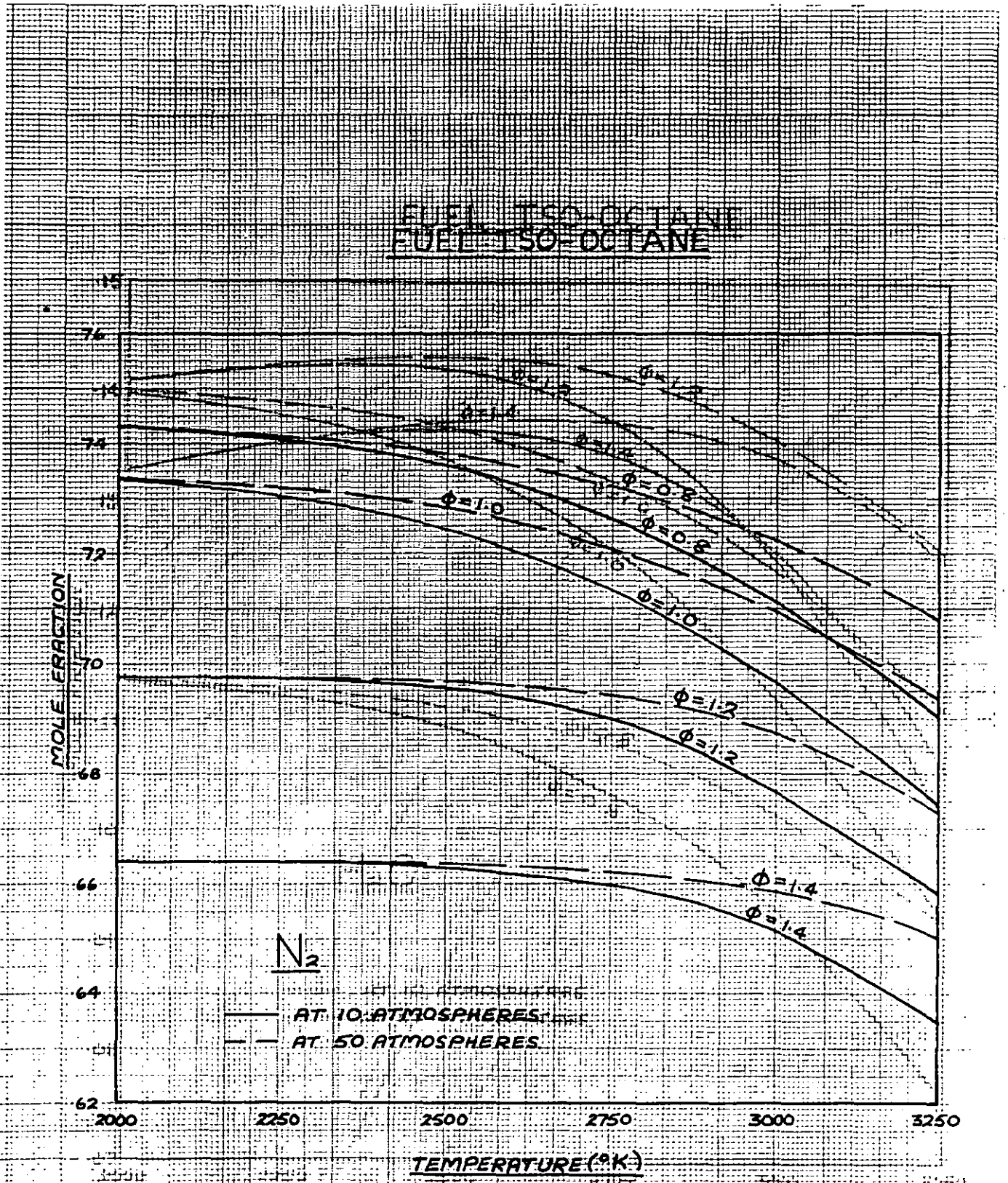

FIG. 6-20— MOLE FRACTION OF NITROGEN (N_2) AGAINST TEMPERATURE

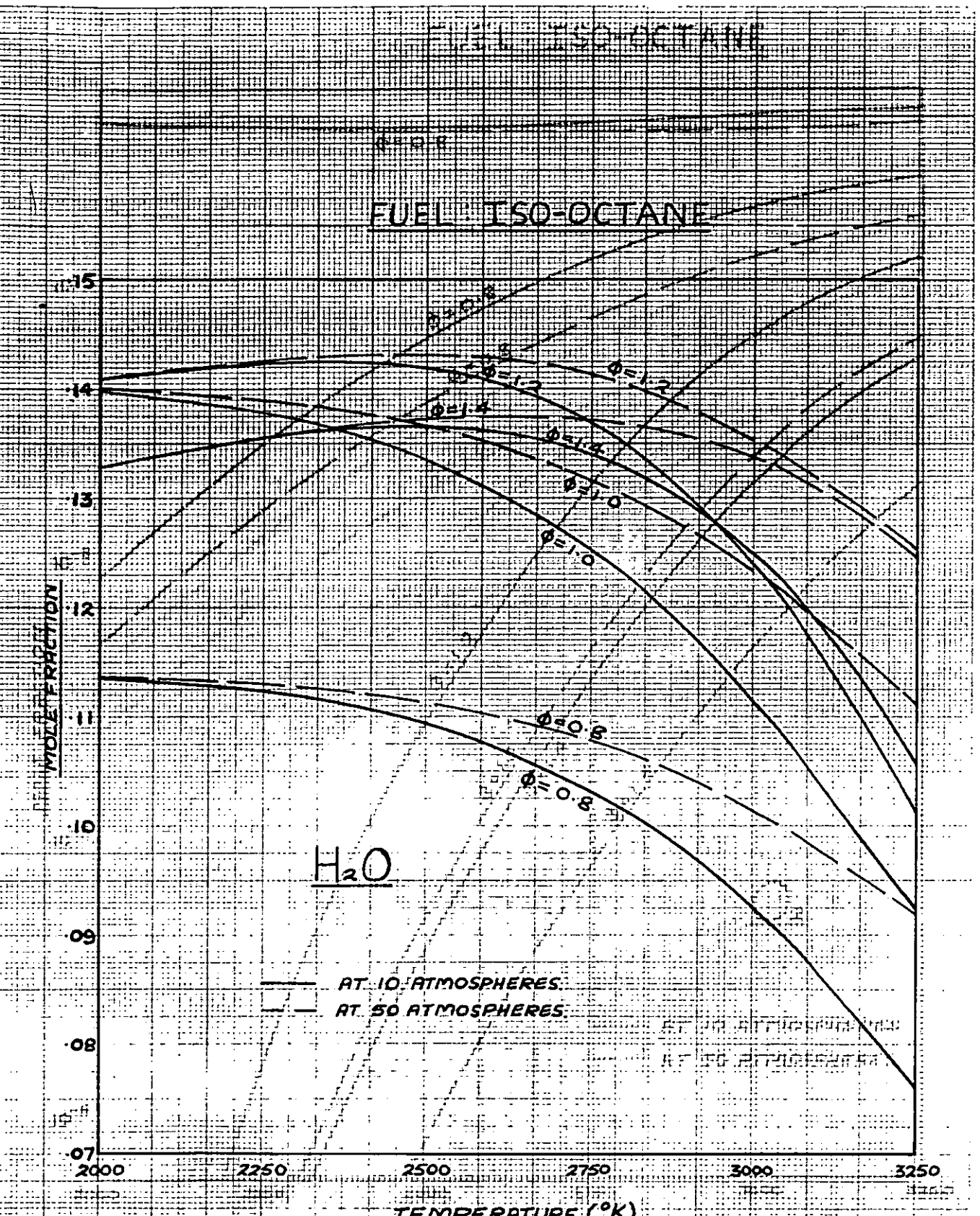

FIG. 6-21 — MOLE FRACTION OF STEAM (H_2O) AGAINST TEMPERATURE

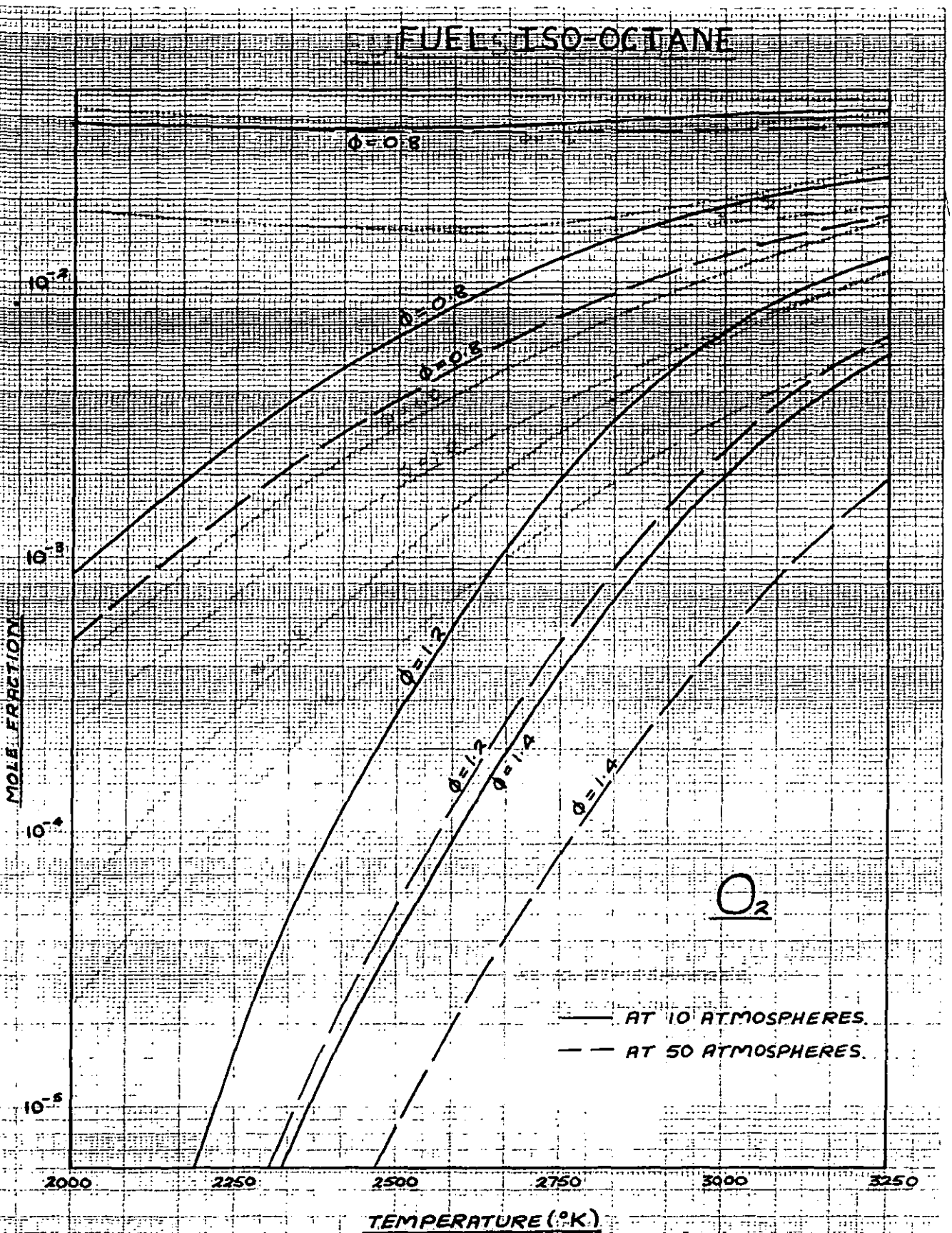

FIG. 6-22 — MOLE FRACTION OF OXYGEN (O_2) AGAINST TEMPERATURE

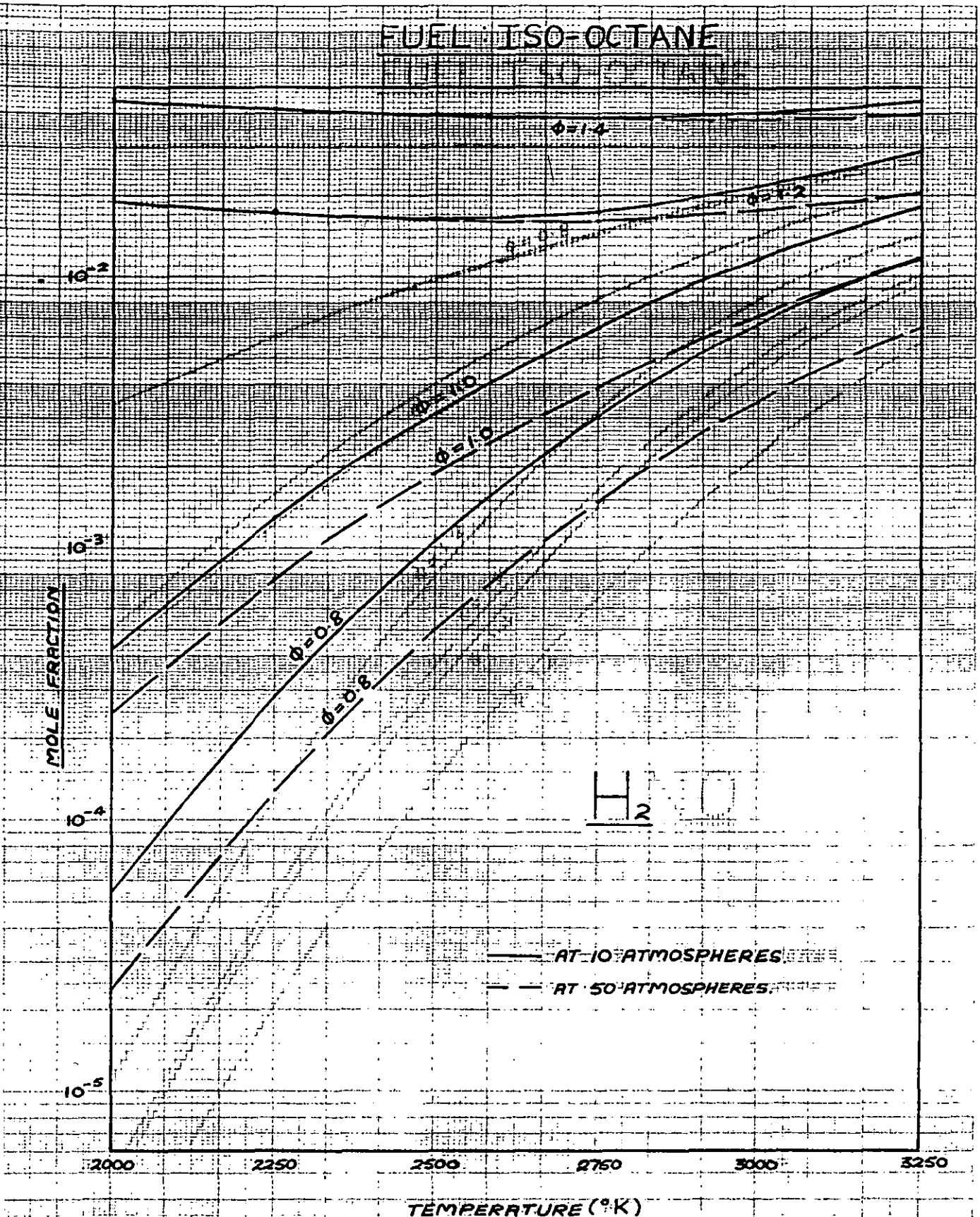

FIG. 6-23 — MOLE FRACTION OF HYDROGEN (H_2) AGAINST TEMPERATURE

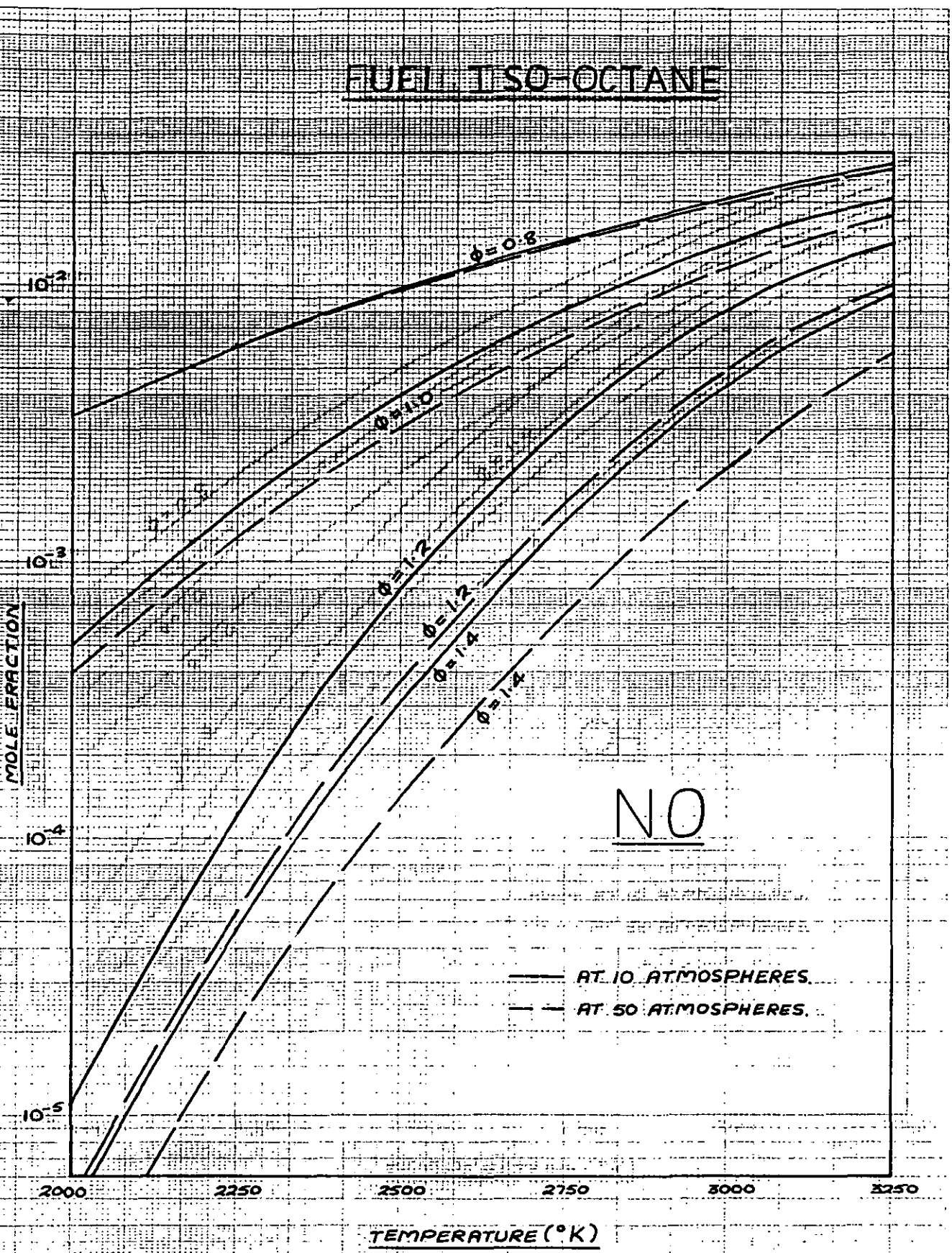

FIG. 6-24 —— MOLE FRACTION OF NITRIC OXIDE (NO) AGAINST TEMPERATURE

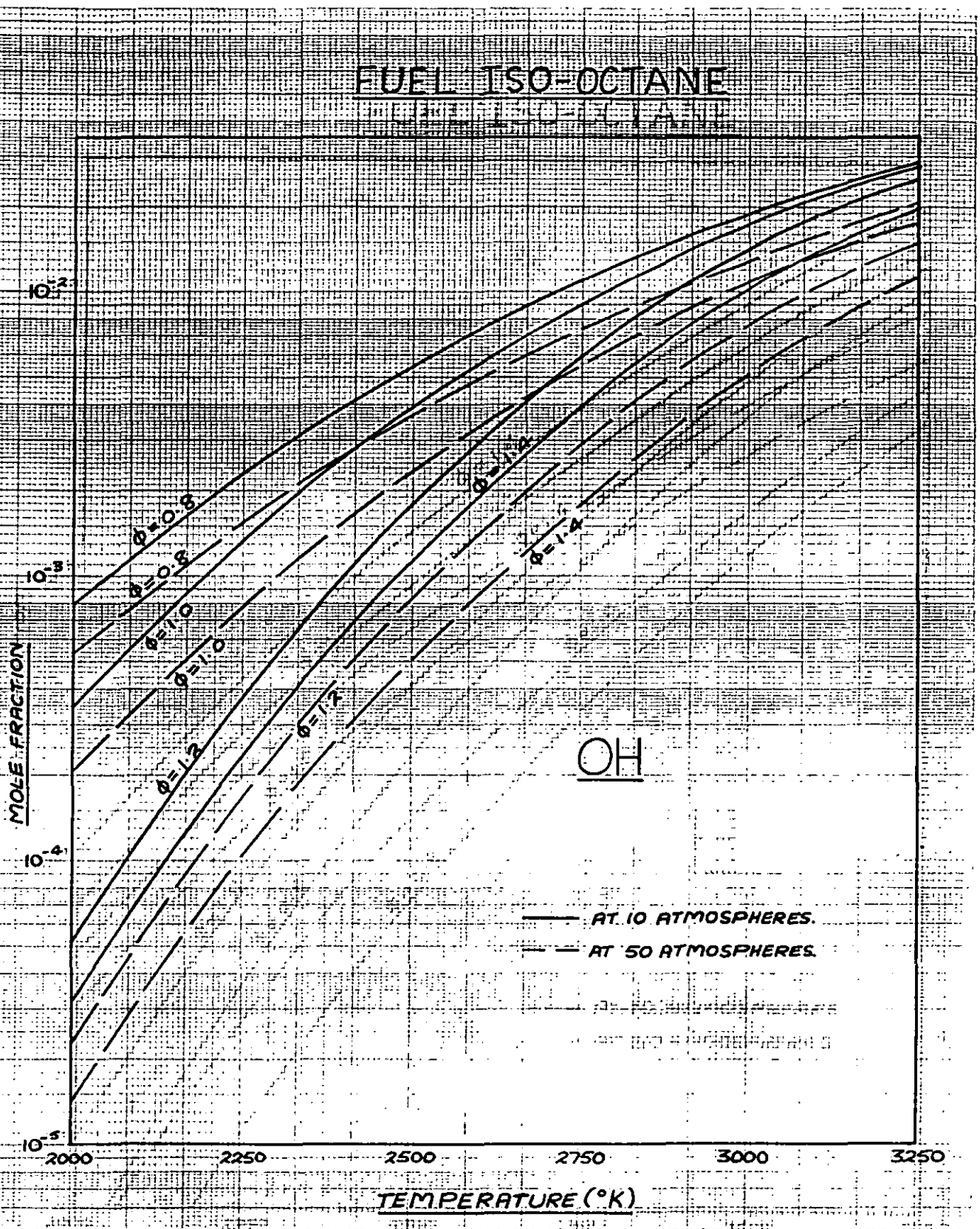

FIG. 6-25 — MOLE FRACTION OF THE HYDROXYL RADICAL (OH) AGAINST TEMPERATURE.

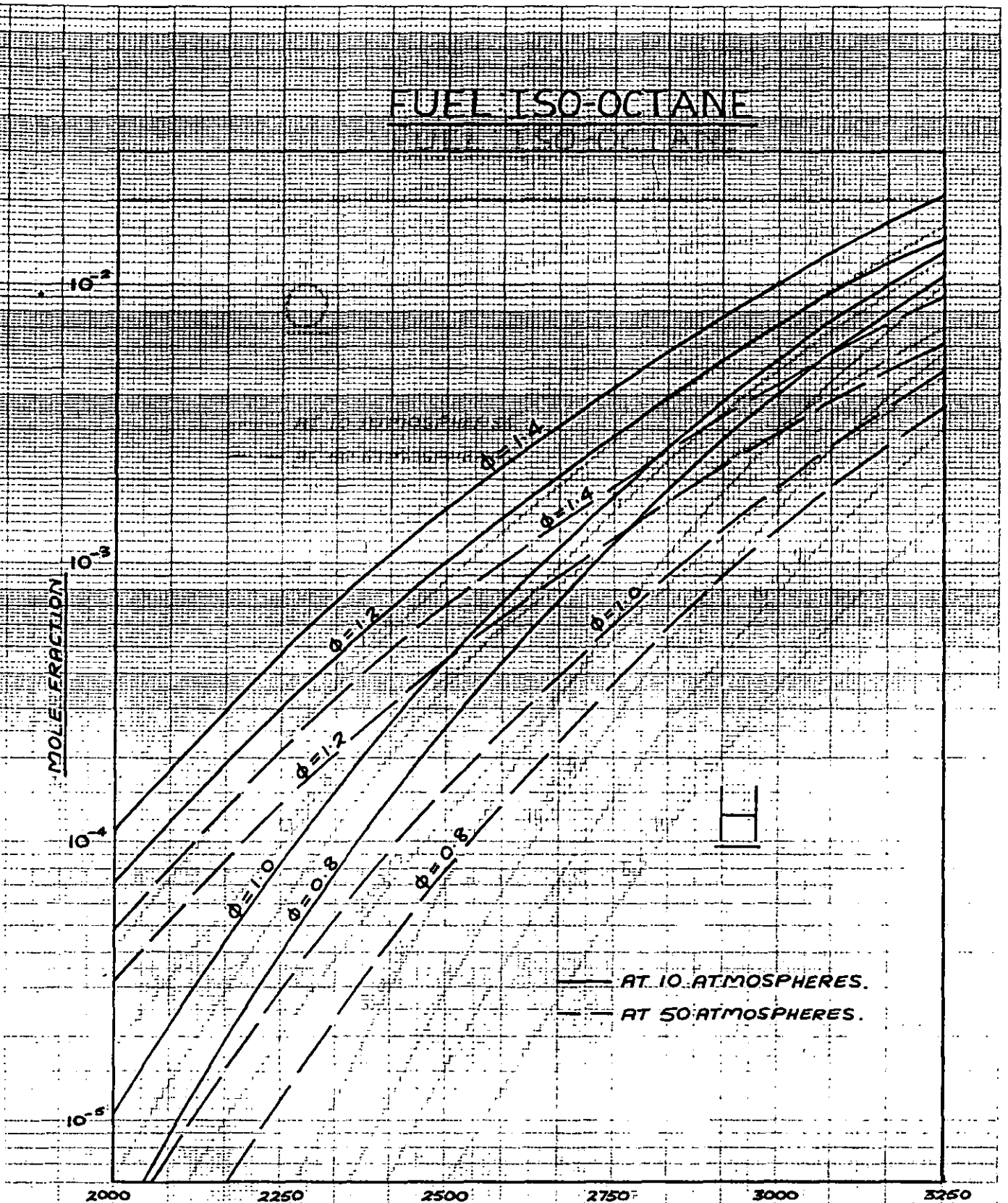

FIG 6-26 — MOLE FRACTION OF ATOMIC HYDROGEN (H) AGAINST TEMPERATURE.

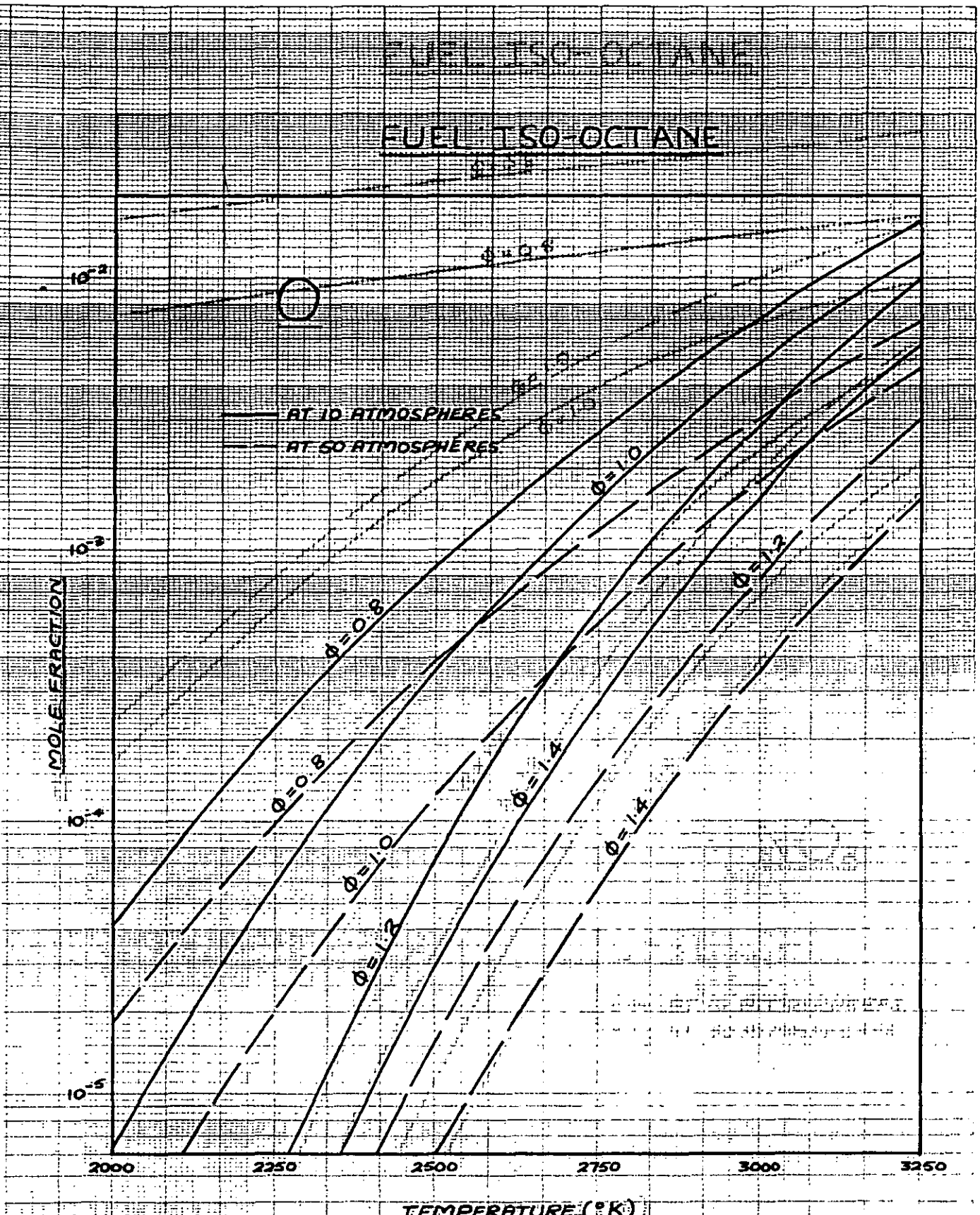

FIG. 6-27 — MOLE FRACTION OF ATOMIC OXYGEN (O) AGAINST TEMPERATURE.

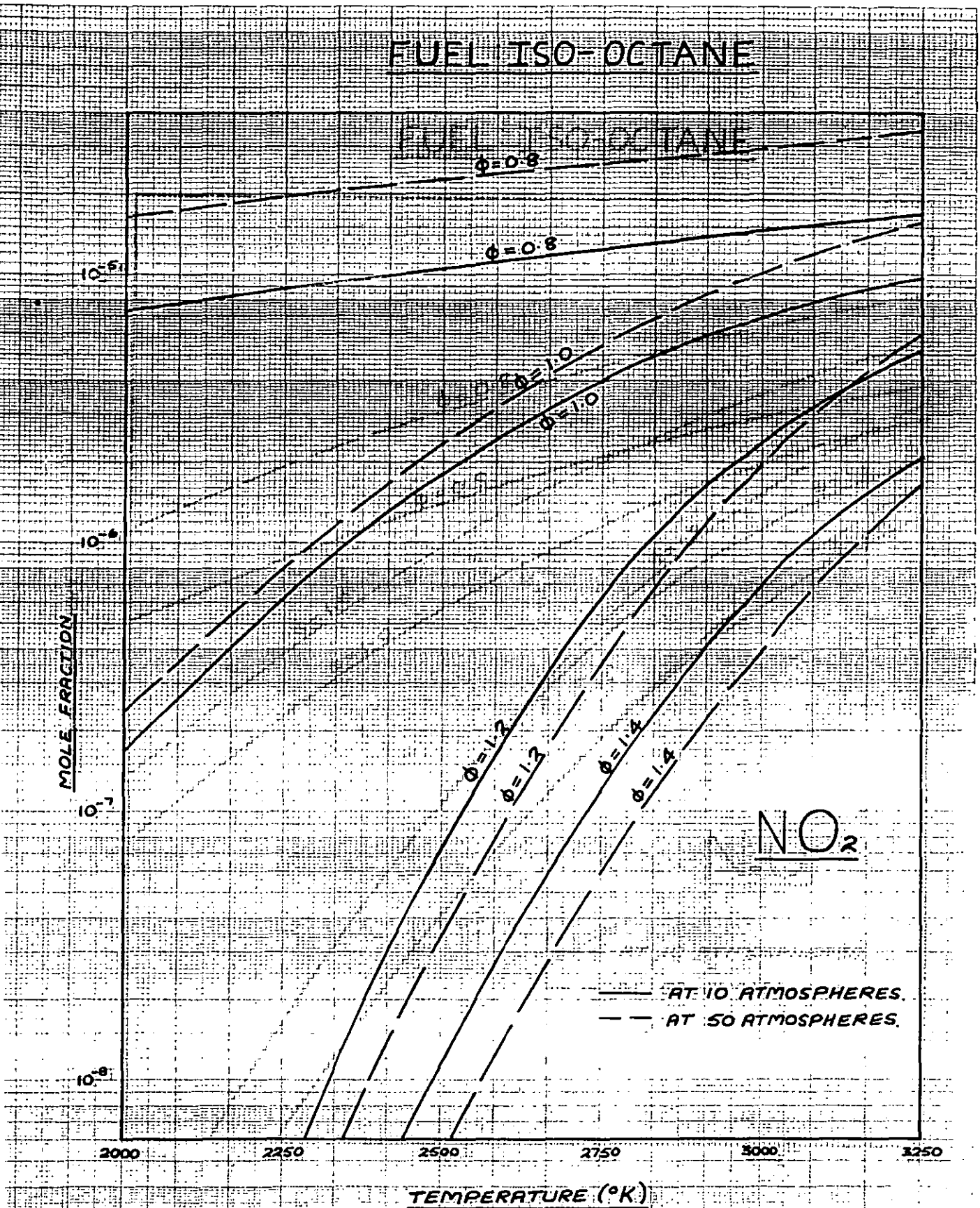

FIG. 6-28 — MOLE FRACTION OF NITROGEN DIOXIDE (NO_2) AGAINST TEMPERATURE.

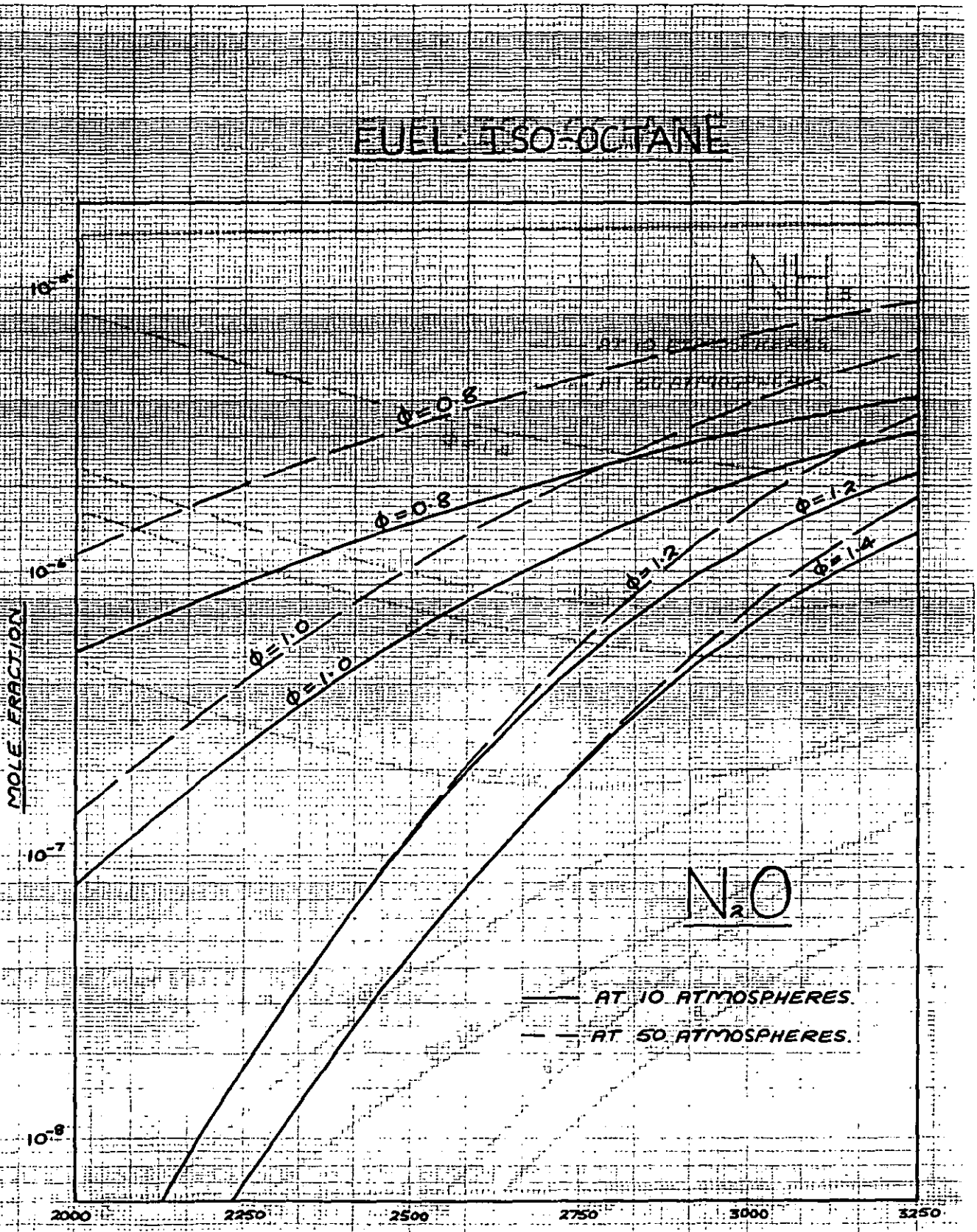

FIG. 6—29 — MOLE FRACTION OF NITROUS OXIDE (N_2O) AGAINST TEMPERATURE.

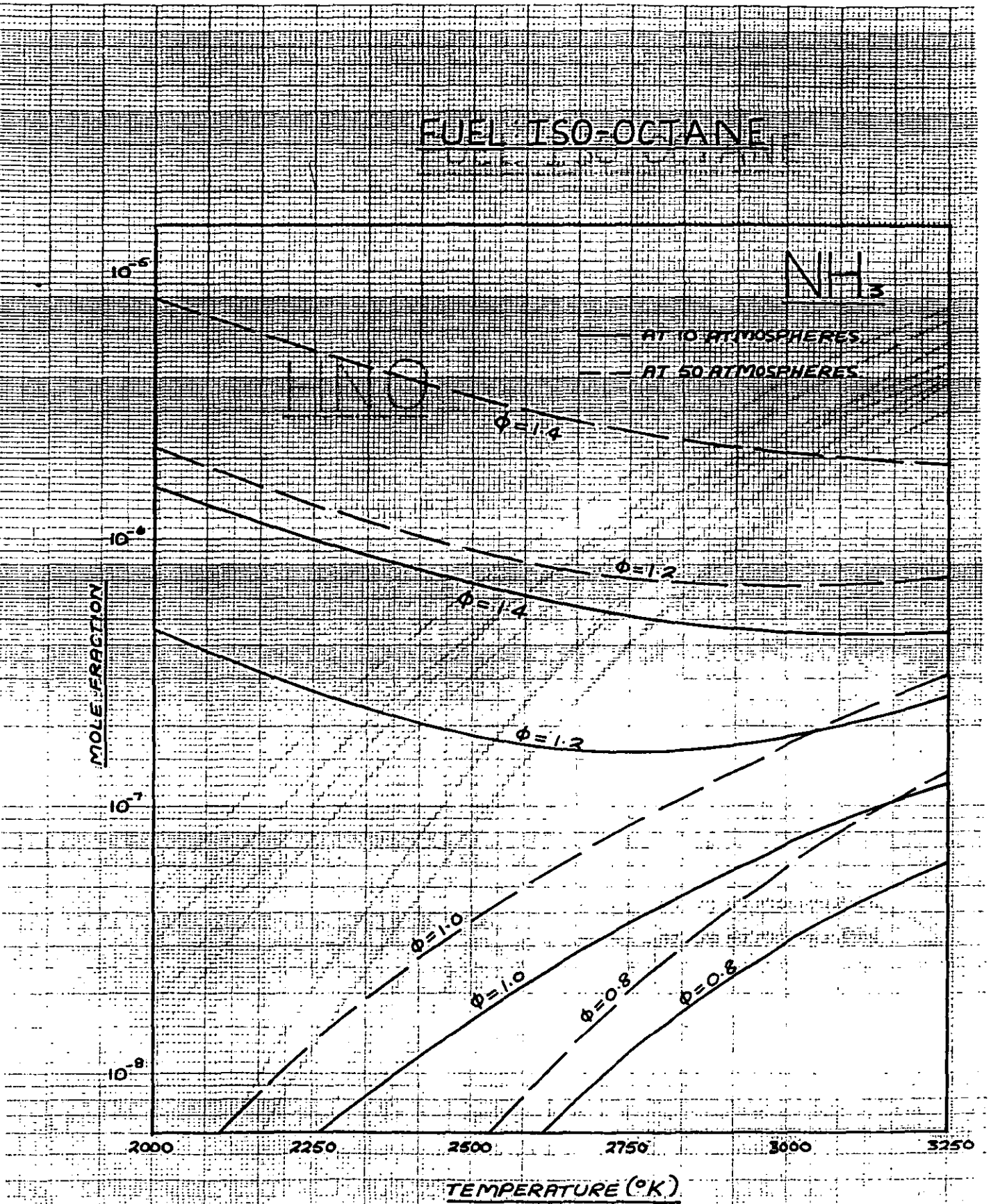

FIG. 6-30 —— MOLE FRACTION OF AMMONIA (NH_3) AGAINST TEMPERATURE

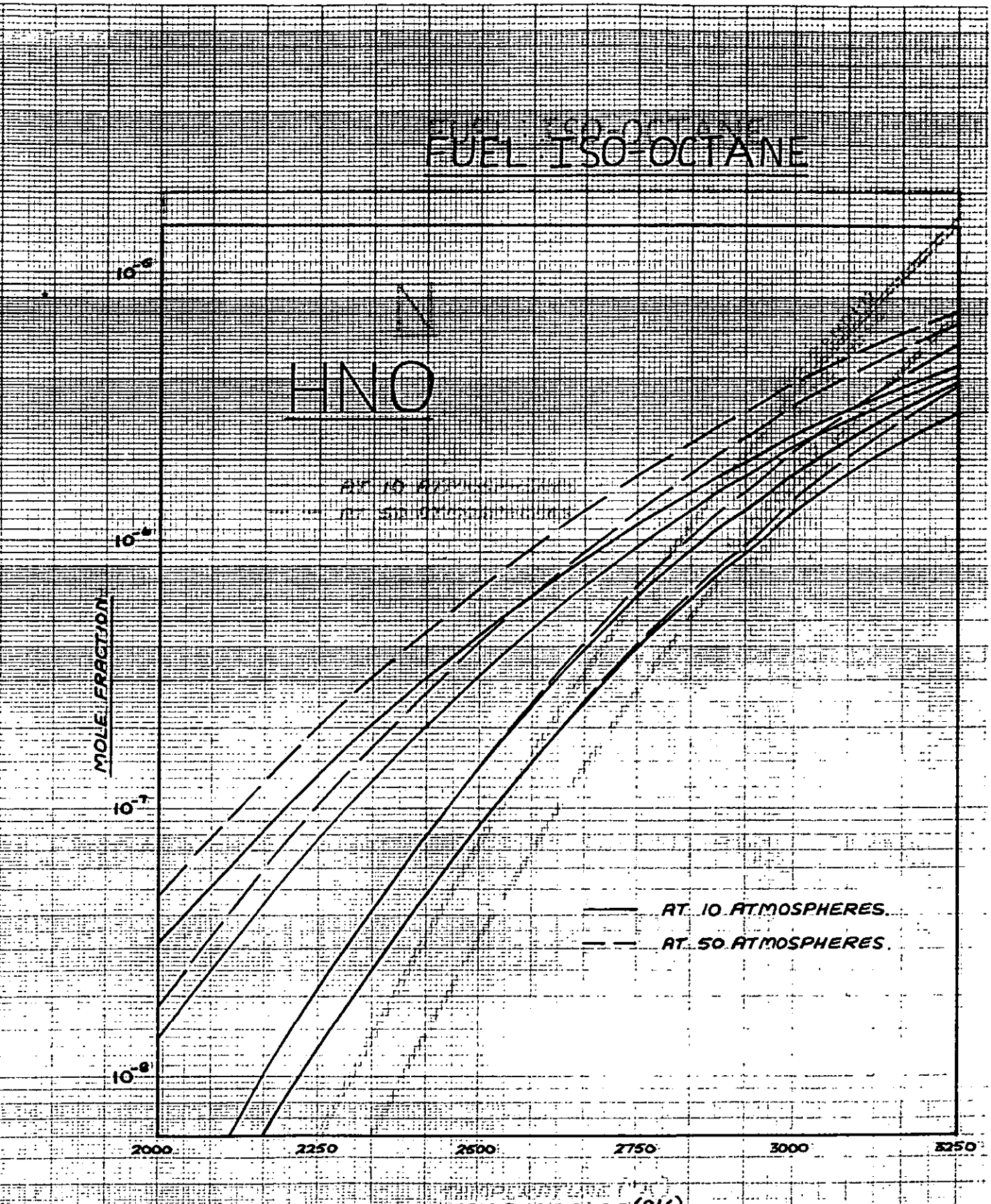

FIG. 6-31 —— MOLE FRACTION OF HNO AGAINST TEMPERATURE.

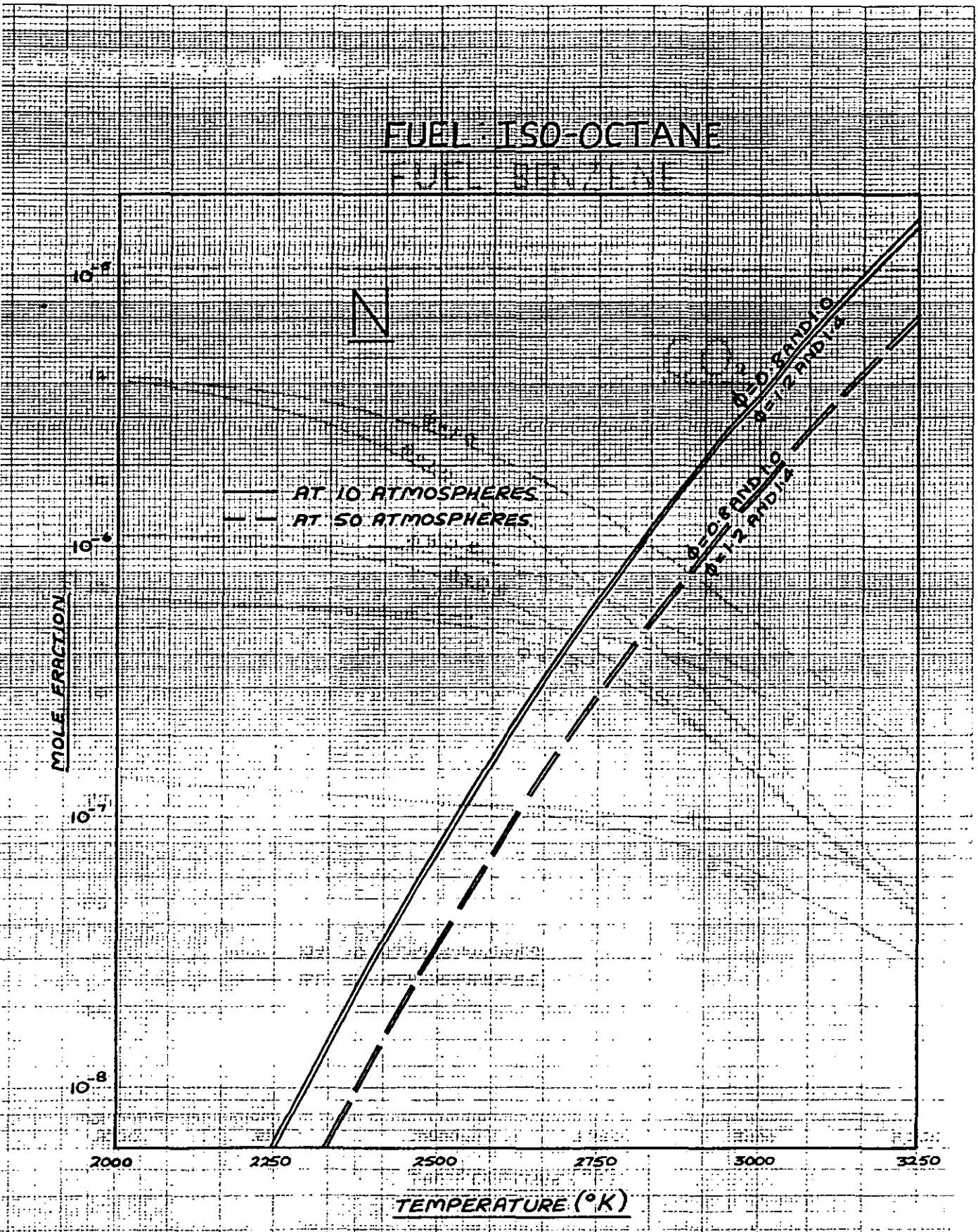

FIG. 6-32 — MOLE FRACTION OF ATOMIC NITROGEN (N) AGAINST TEMPERATURE.

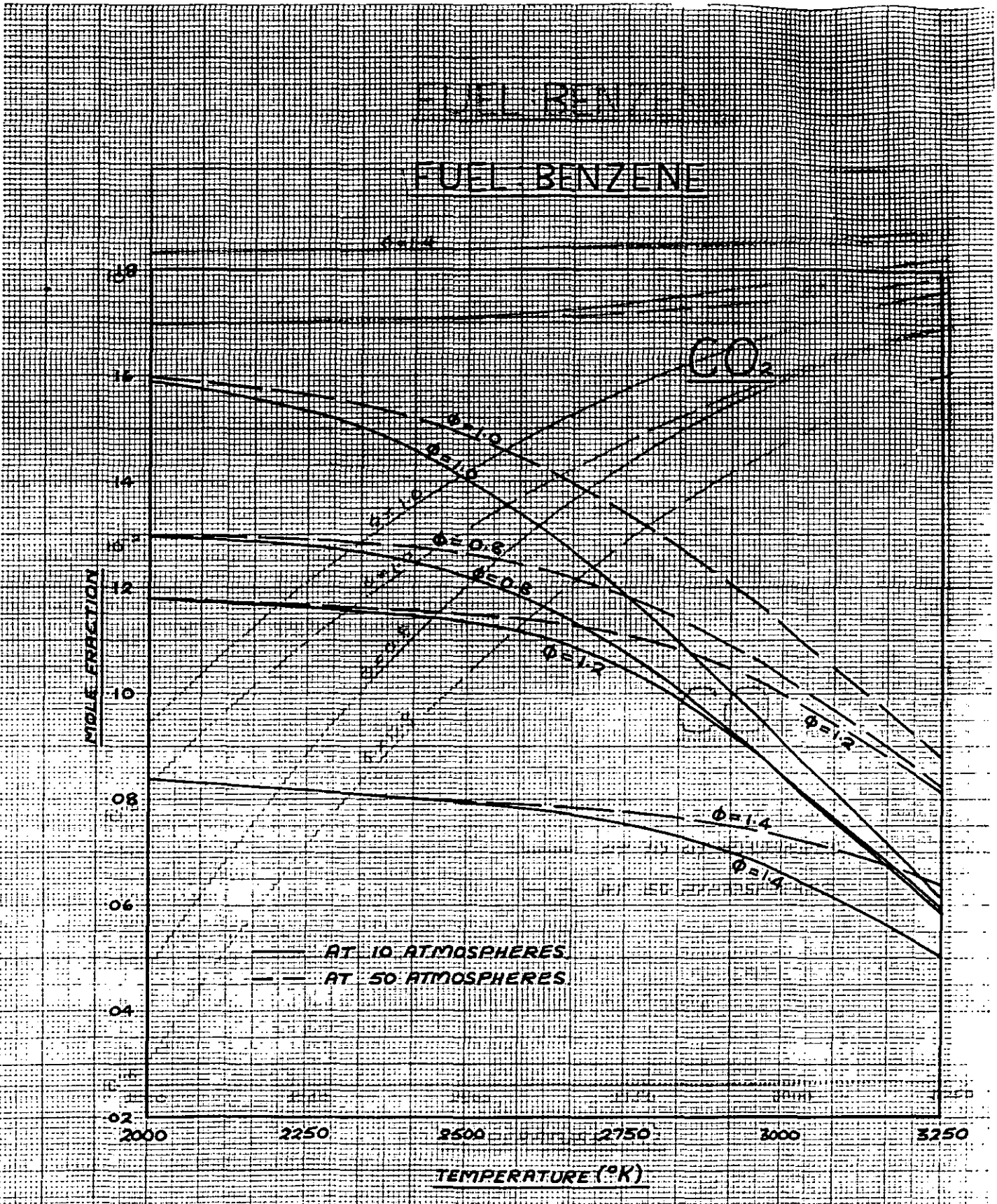

FIG 6-33 — MOLE FRACTION OF CARBON DIOXIDE (CO_2) AGAINST TEMPERATURE

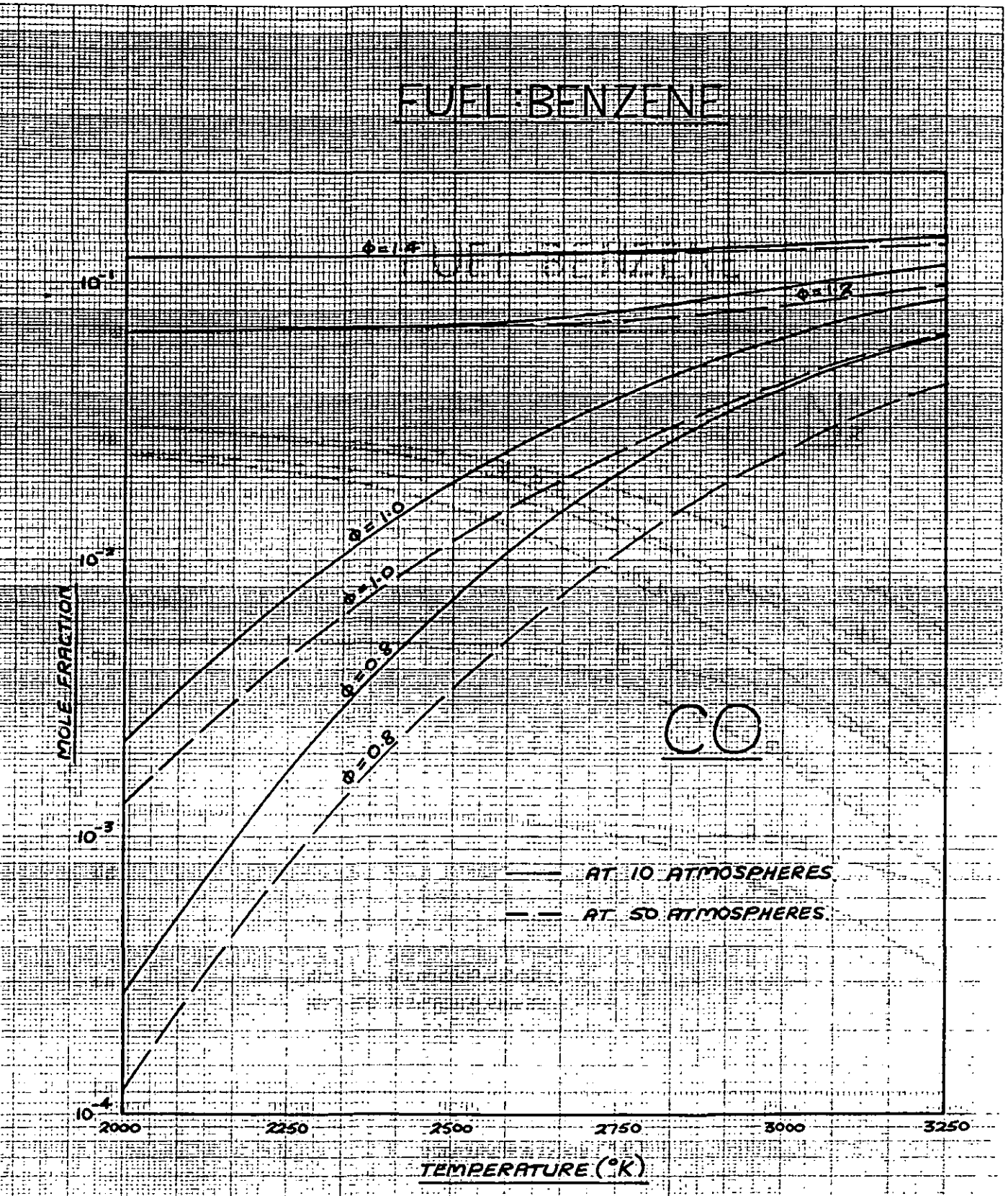

FIG. 6-34 — MOLE FRACTION OF CARBON MONOXIDE (CO) AGAINST TEMPERATURE.

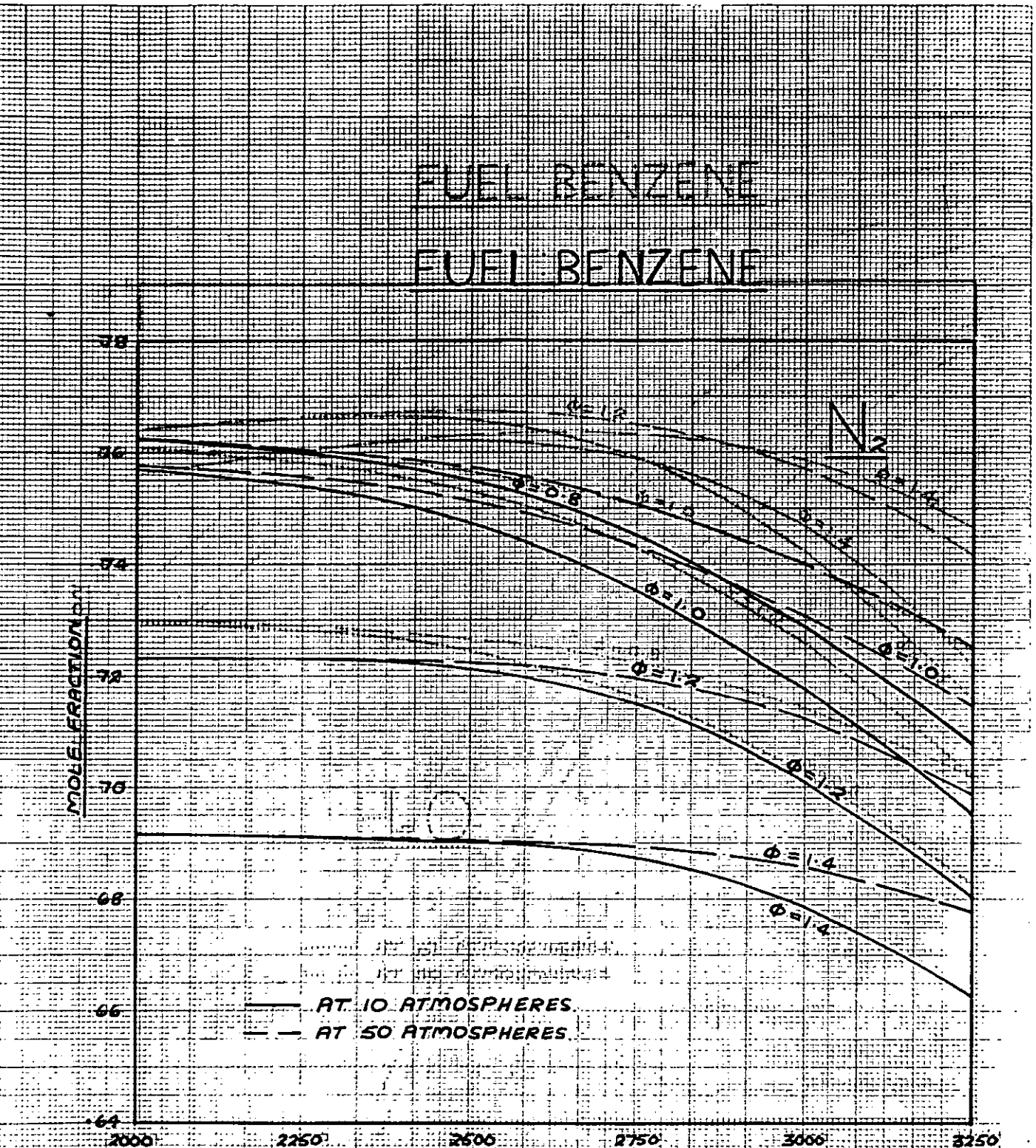

FIG. 6-35 — MOLE FRACTION OF NITROGEN (N_2) AGAINST TEMPERATURE

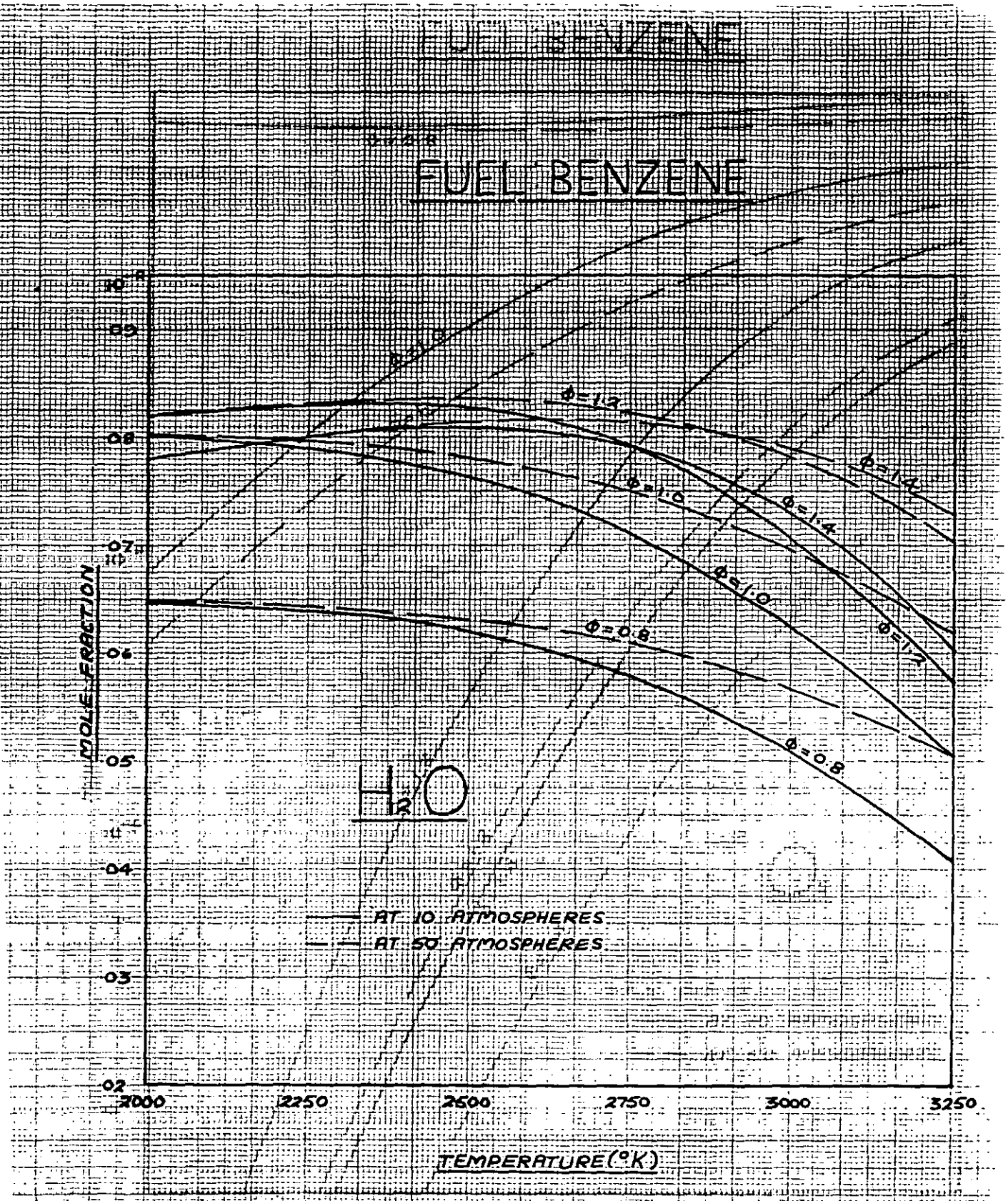

FIG. 6-36 —— MOLE FRACTION OF STEAM (H_2O) AGAINST TEMPERATURE

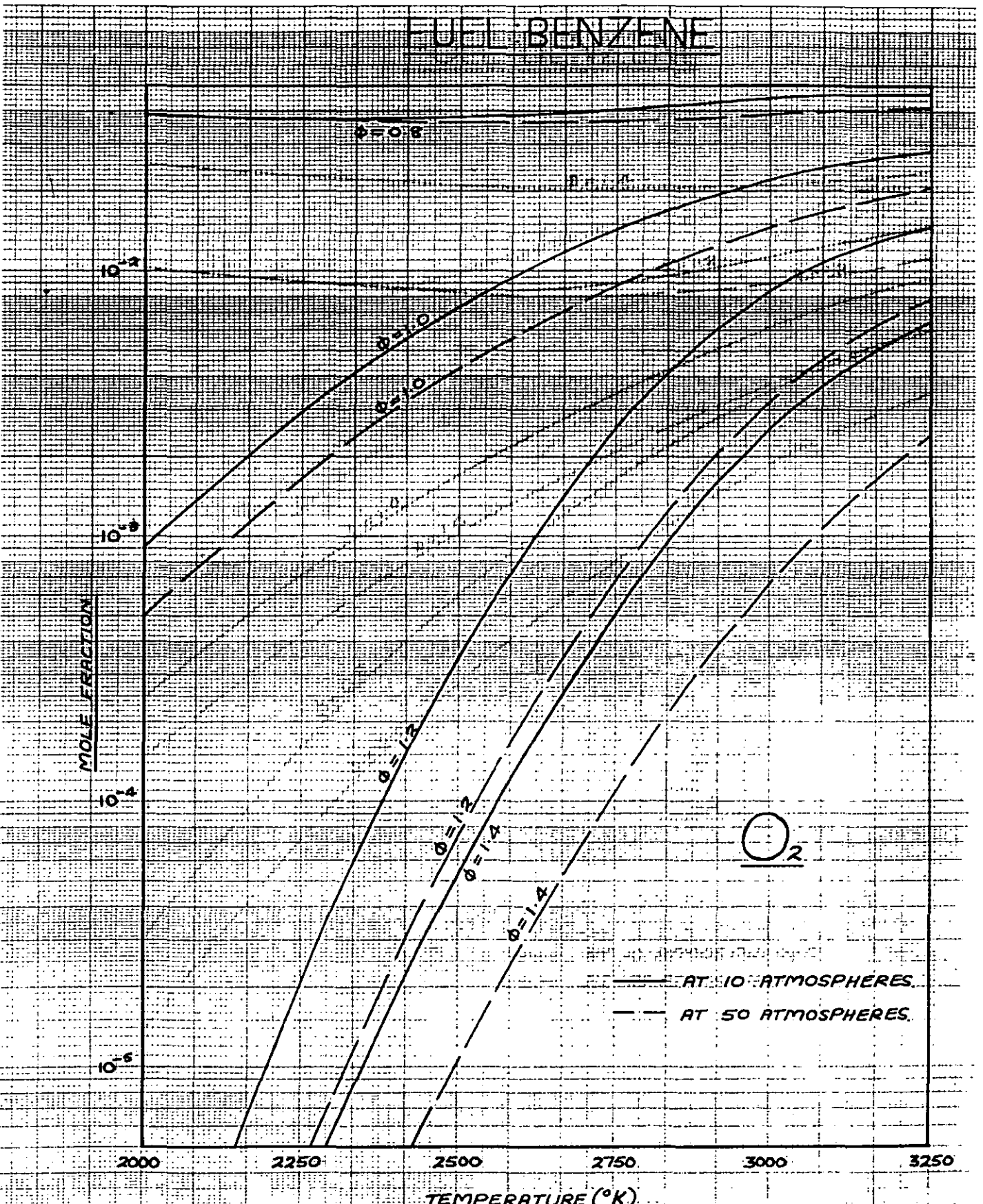

FIG. 6-37 —— MOLE FRACTION OF OXYGEN (O_2) AGAINST TEMPERATURE.

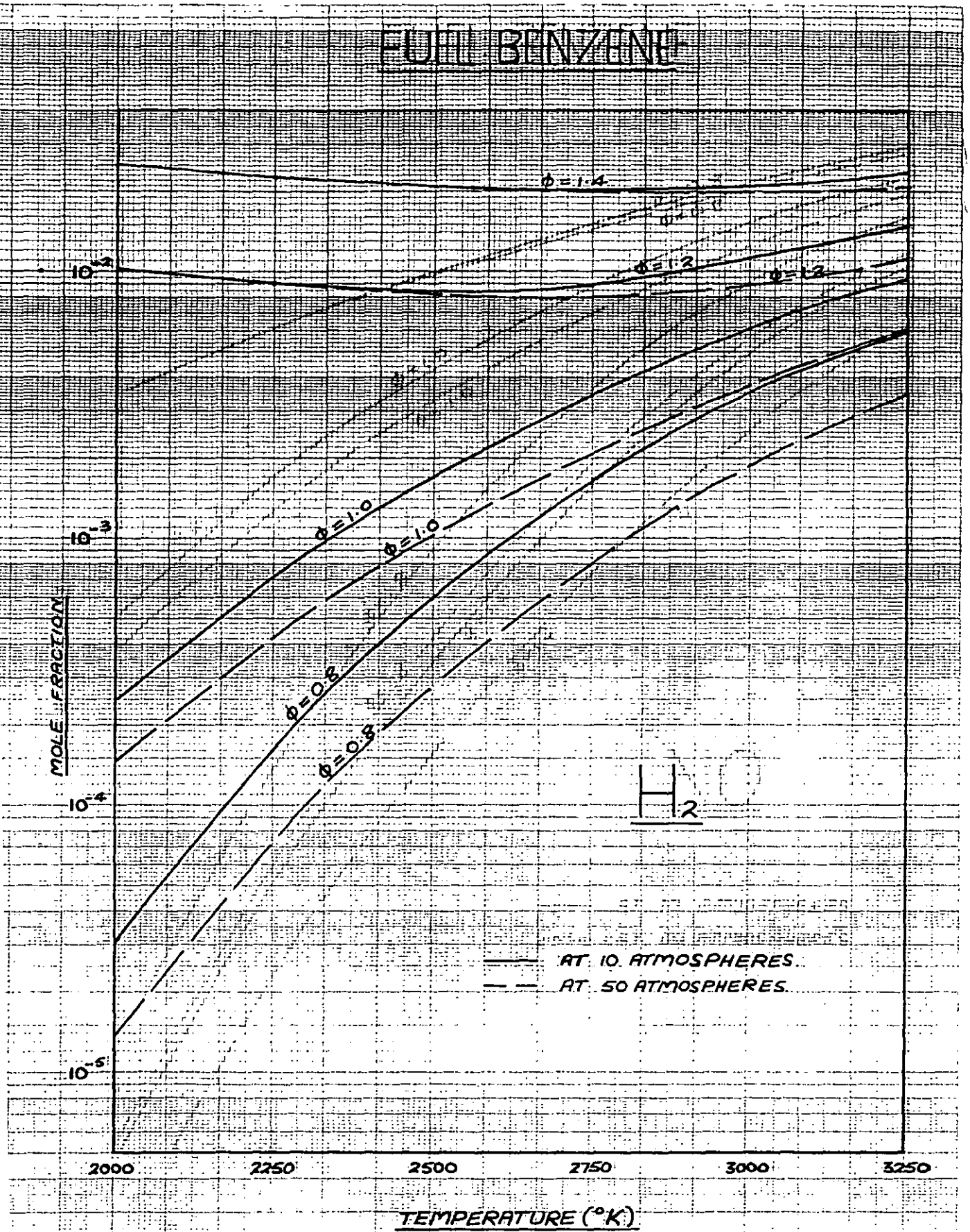

FIG. 6-38 — MOLE FRACTION OF HYDROGEN (H_2) AGAINST TEMPERATURE

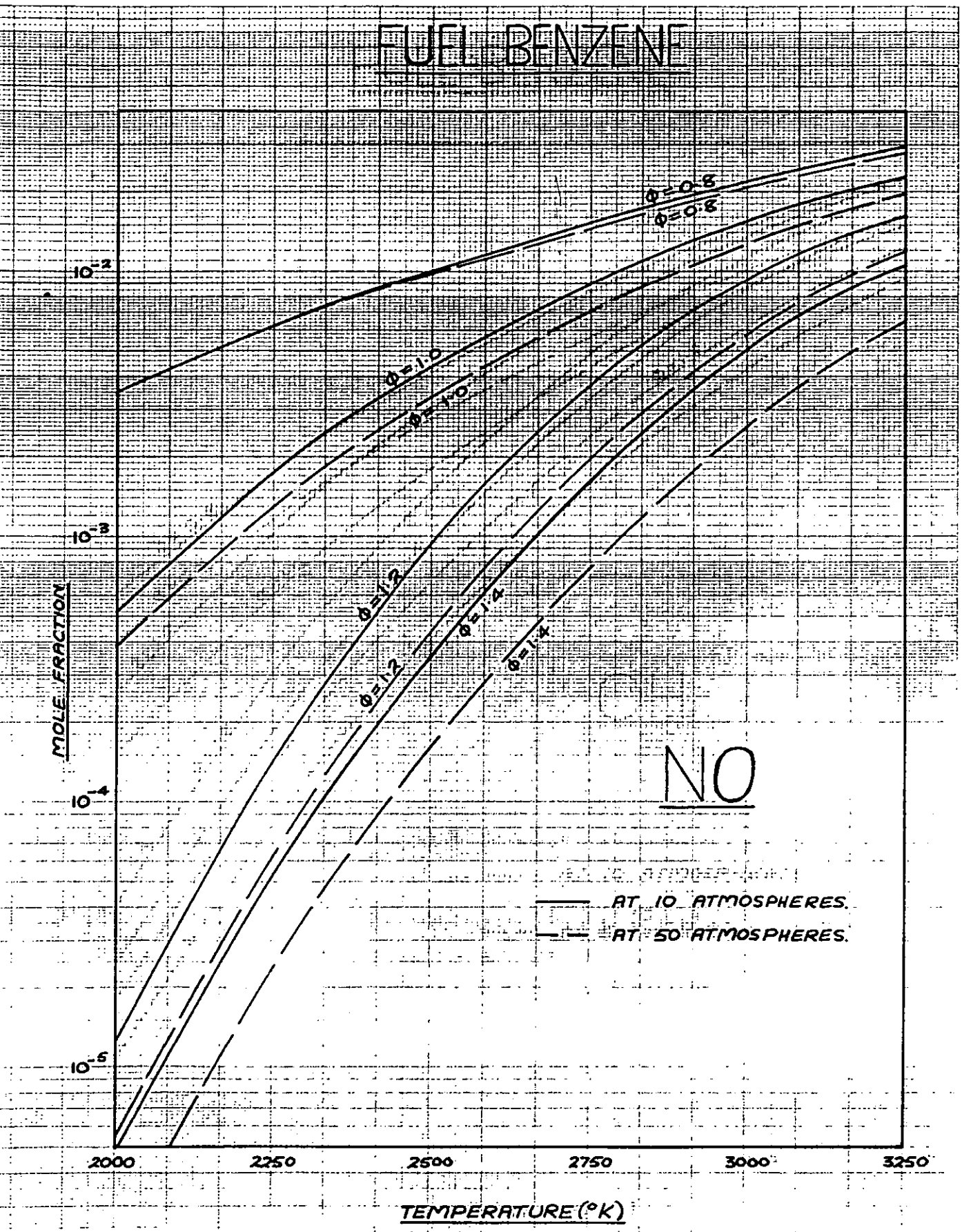

FIG 6-39 — MOLE FRACTION OF NITRIC OXIDE (NO) AGAINST TEMPERATURE

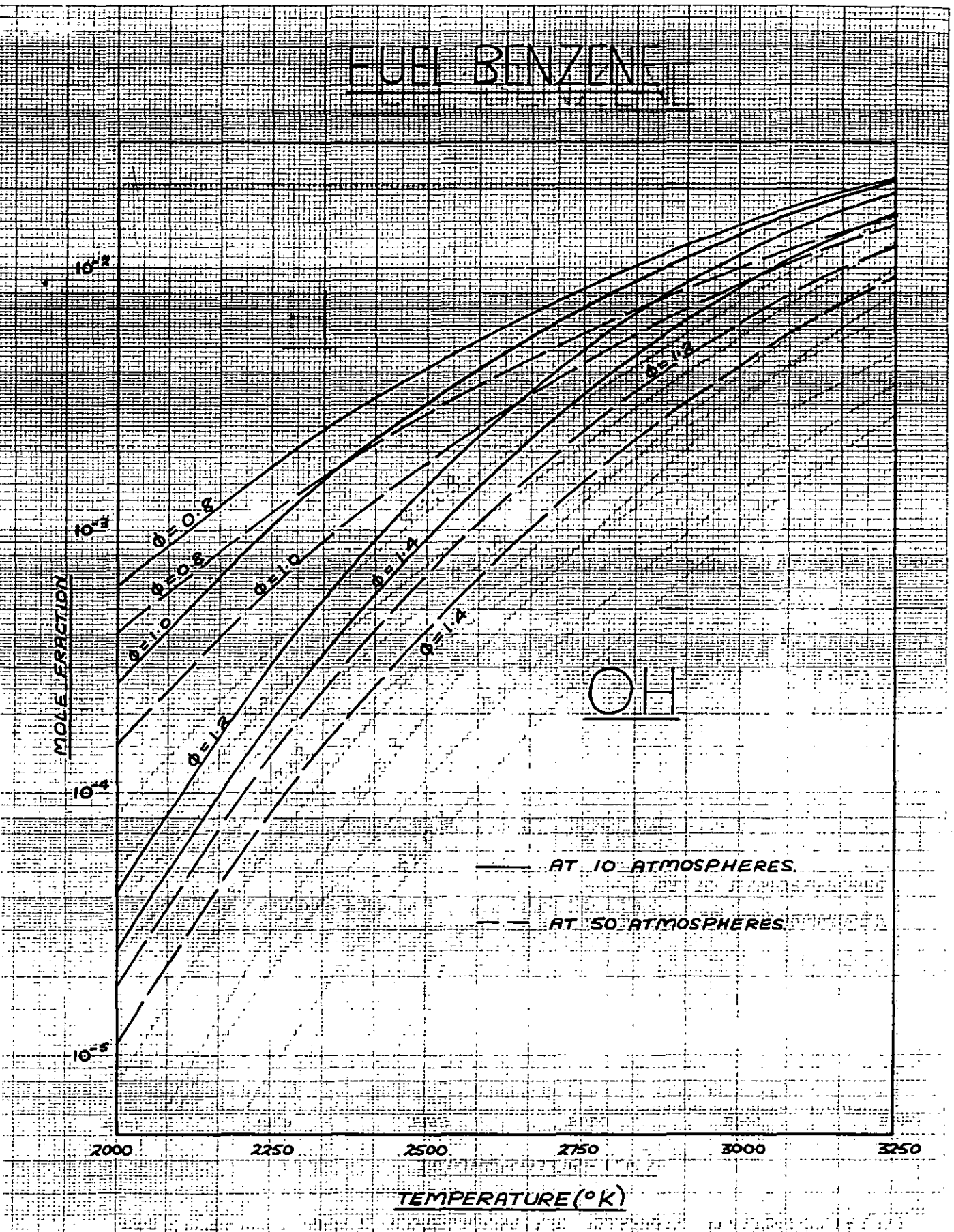

FIG. 6-40 — MOLE FRACTION OF THE HYDROXYL RADICAL (OH) AGAINST TEMPERATURE.

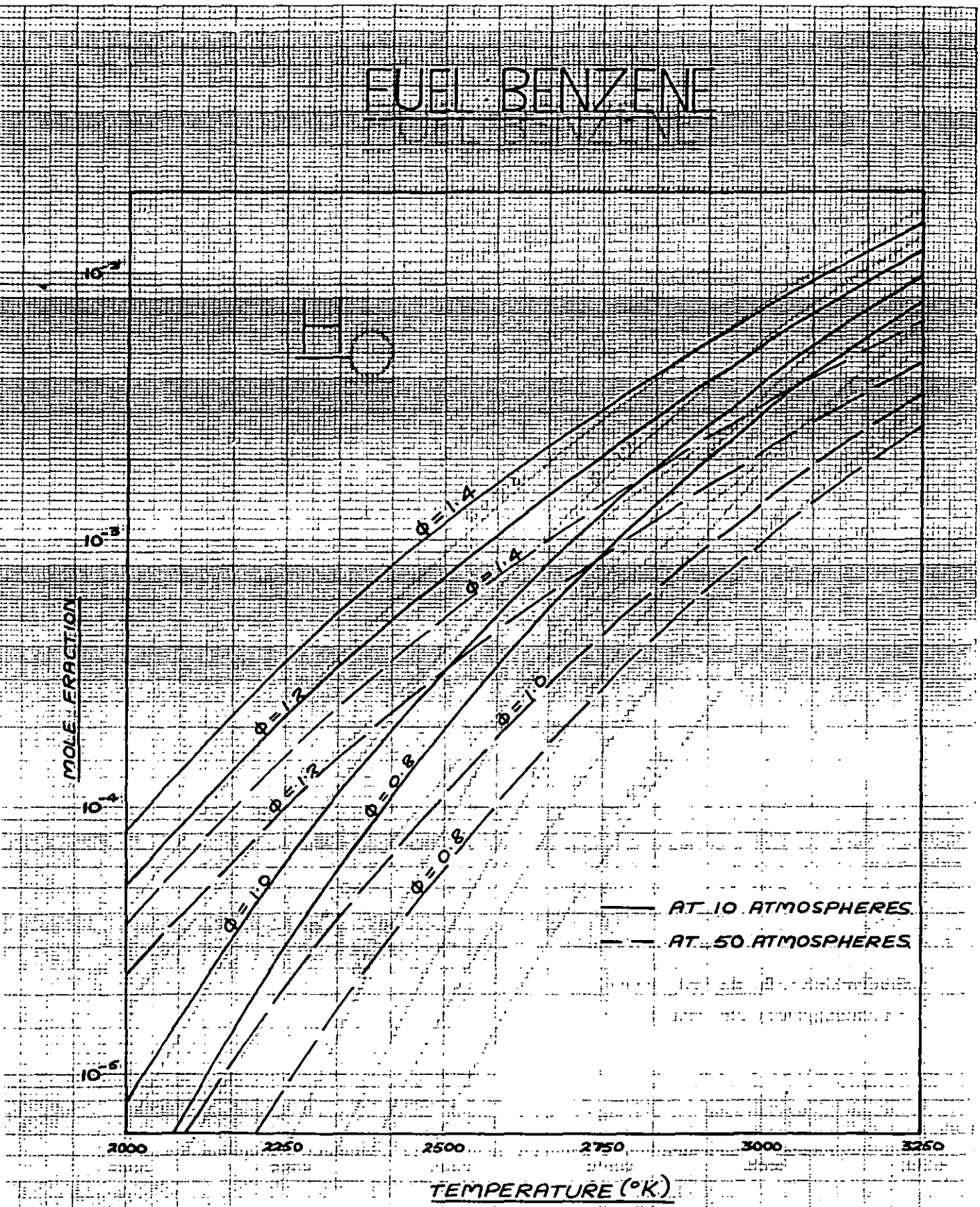

FIG.6-41 —— MOLE FRACTION OF ATOMIC HYDROGEN (H) AGAINST TEMPERATURE.

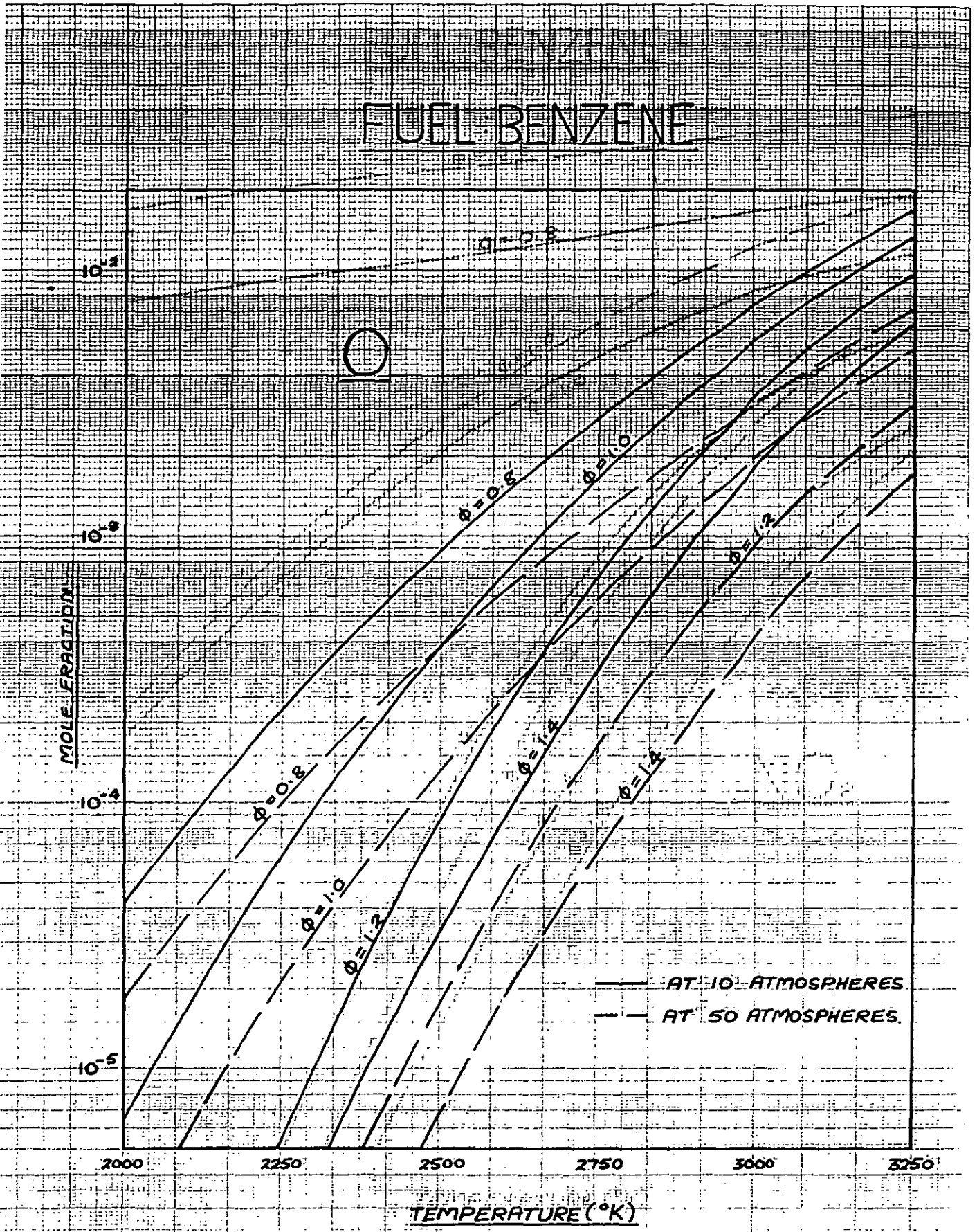

FIG. 6-42 — MOLE FRACTION OF ATOMIC OXYGEN (O) AGAINST TEMPERATURE.

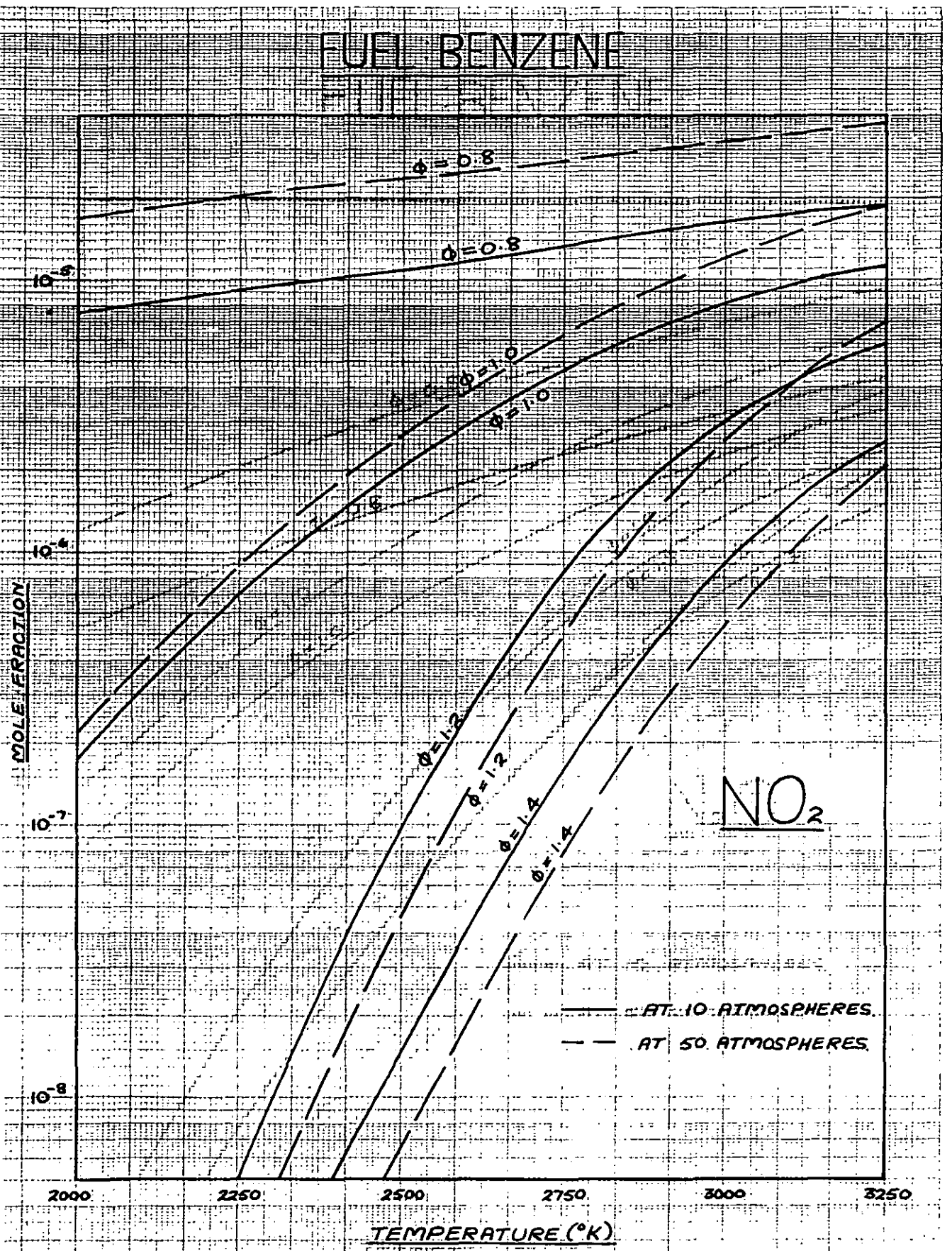

FIG. 6-43 — MOLE FRACTION OF NITROGEN DIOXIDE (NO_2) AGAINST TEMPERATURE.

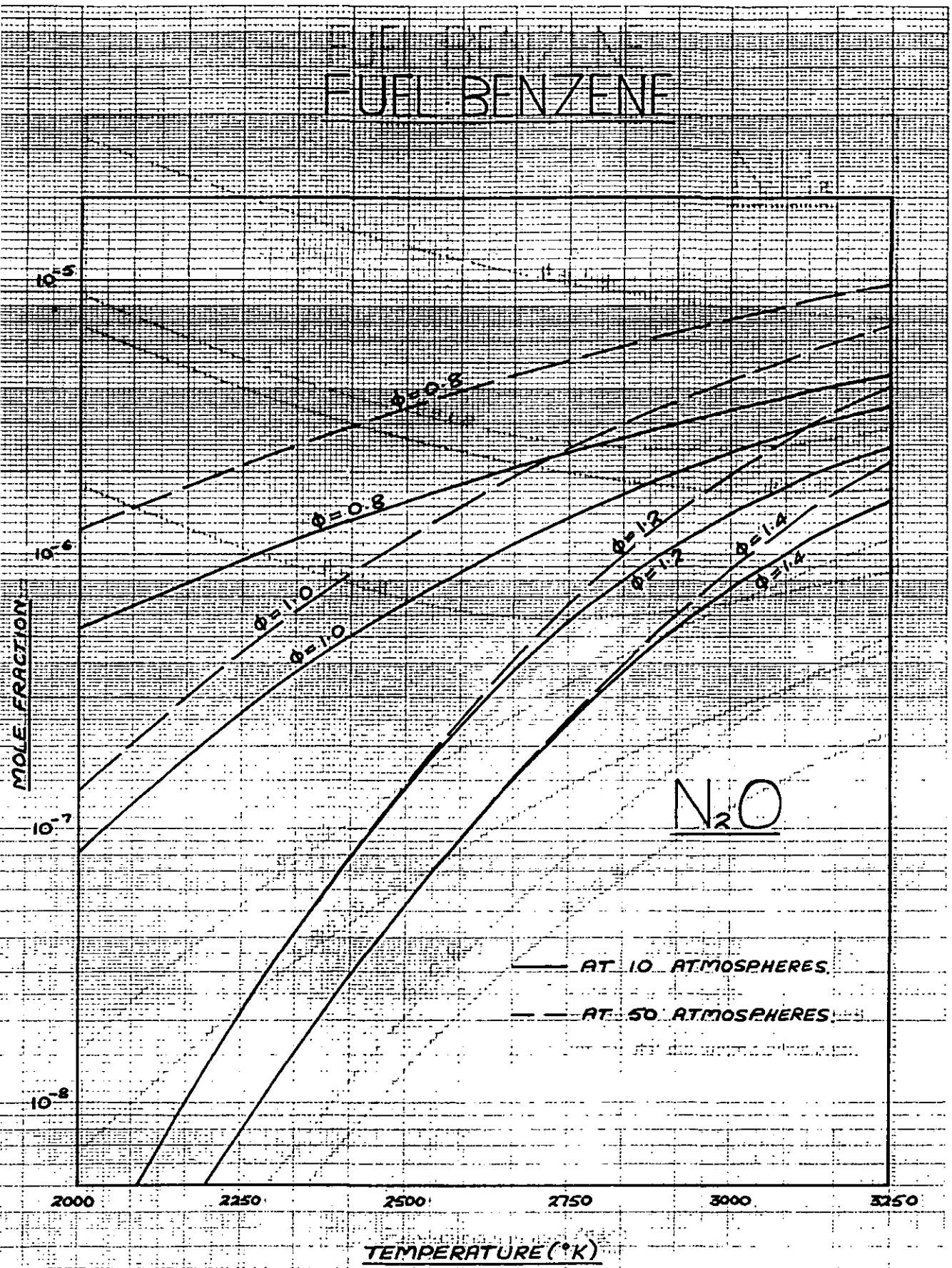

FIG. 6-44 — MOLE FRACTION OF NITROUS OXIDE (N_2O) AGAINST TEMPERATURE.

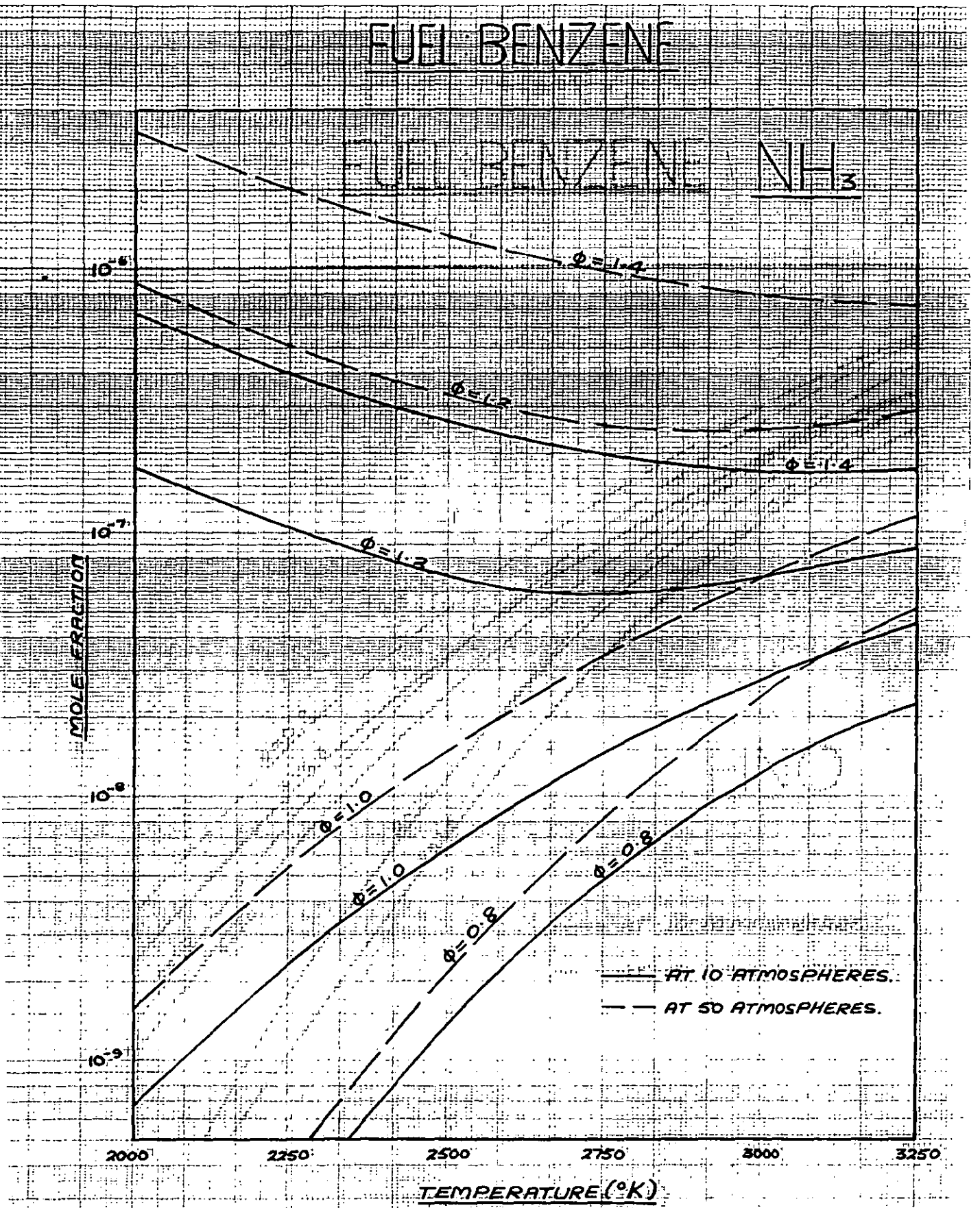

FIG. 6-45 —— MOLE FRACTION OF AMMONIA (NH_3) AGAINST TEMPERATURE.

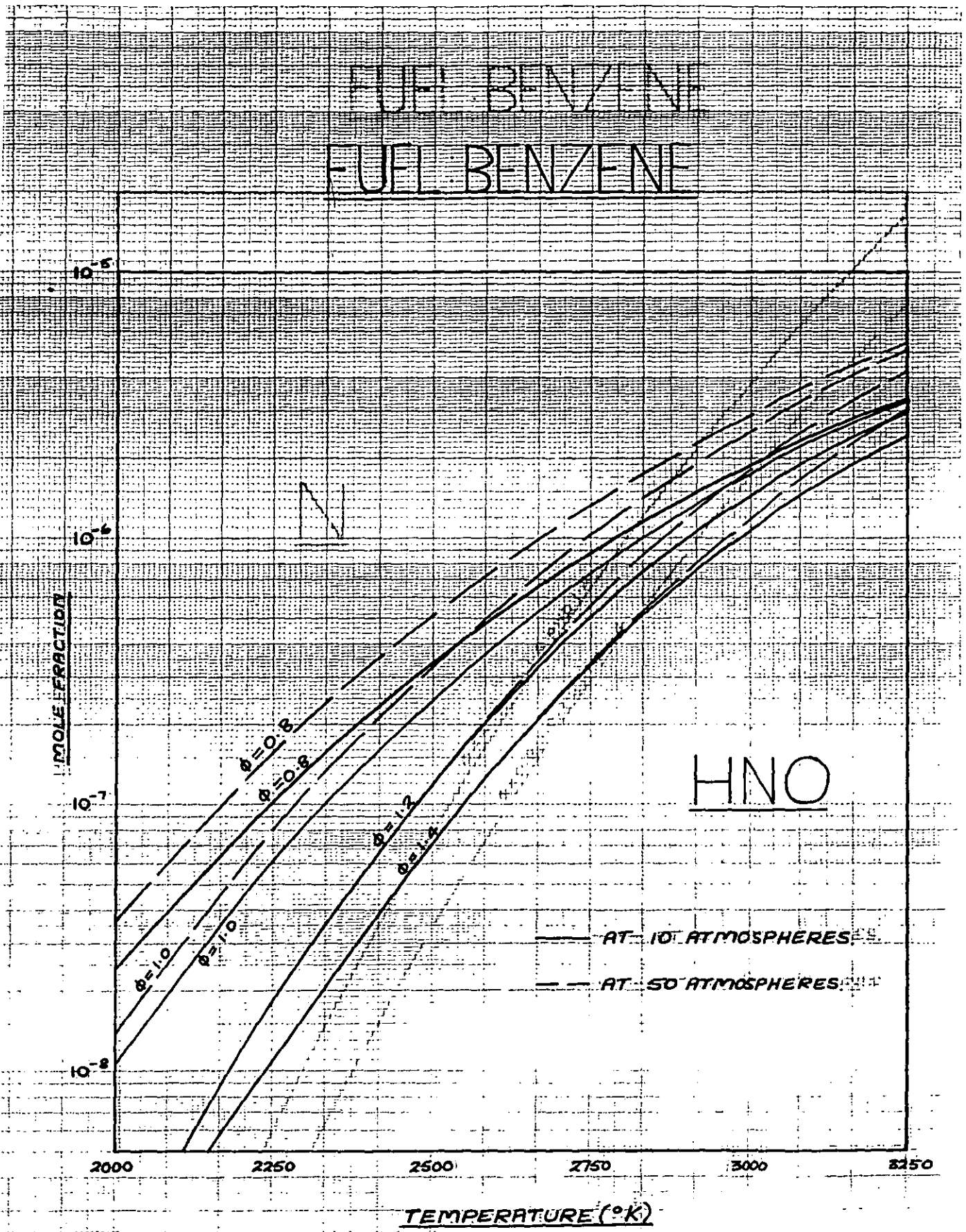

FIG. 6-46 —— MOLE FRACTION OF HNO AGAINST TEMPERATURE

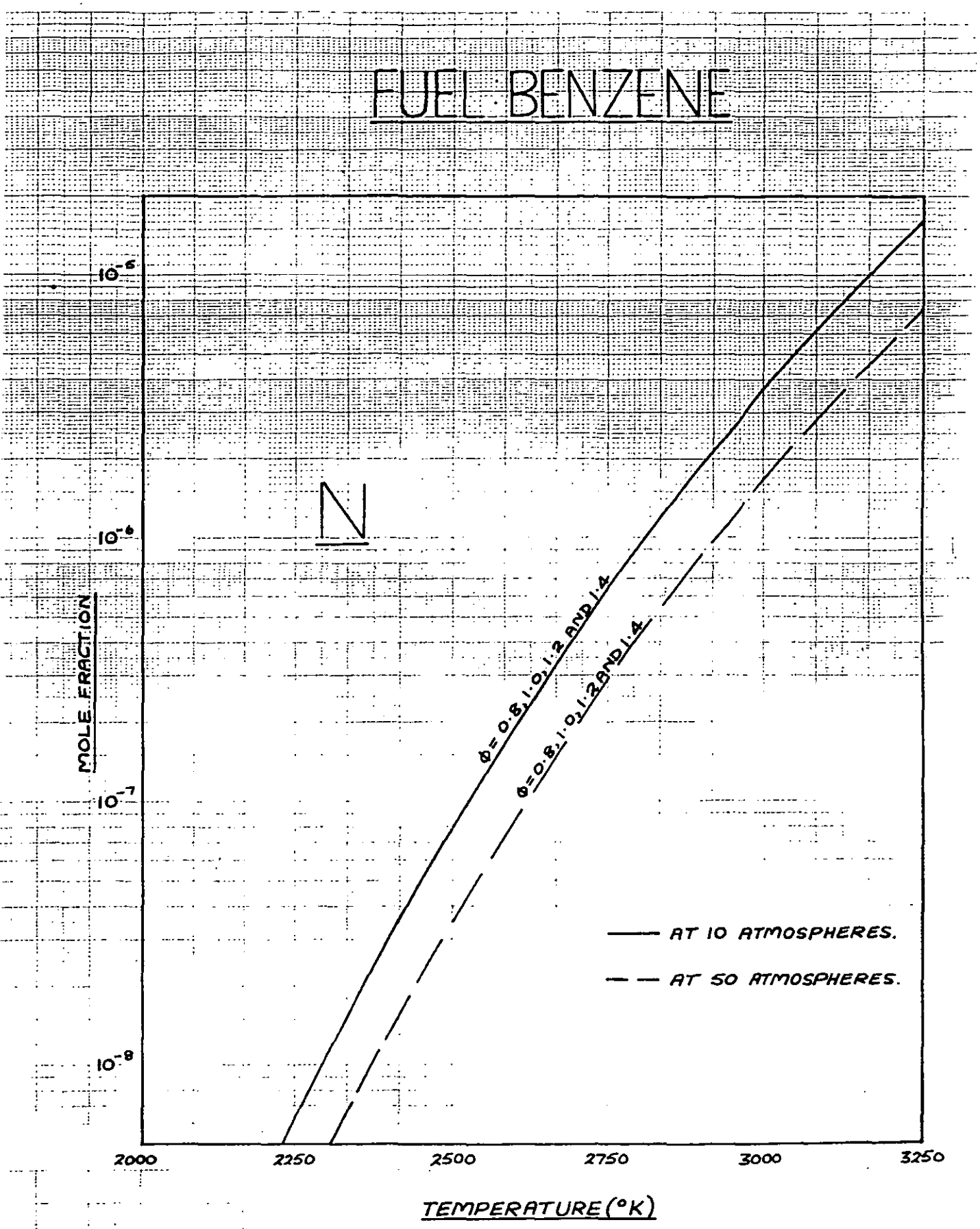

FIG. 6-47 — MOLE FRACTION OF ATOMIC NITROGEN (N) AGAINST TEMPERATURE.